

Alteration and Genesis of the Goldboro Meguma-Hosted Orogenic Gold Deposit, Goldboro, Nova Scotia, Canada

By Marko Szmihelsky

A Thesis submitted to the School of Graduate Studies in partial fulfillment of the
requirements for the degree of

Master of Science, Department of Earth Sciences

Memorial University of Newfoundland

May 2022

St. John's, Newfoundland and Labrador

Abstract

The Goldboro deposit (16,036,000 tonnes @ 3.78 g/t Indicated and Measured, 5,306,000 tonnes @ 4.68 g/t Inferred, 1,946,100 oz and 798,100 oz Au, respectively) is a Meguma-type orogenic gold deposit in Nova Scotia, Canada. Despite the economic importance of Meguma-type orogenic gold deposits, their origin, paragenesis, and hydrothermal footprint are not completely understood compared to other sediment-hosted orogenic gold districts (e.g., Victorian gold belt, Sukhoi Log). Deposits are hosted within folded metaturbidite successions that consist of repeating fining-upwards successions containing argillite and greywacke. Gold in the deposit is predominantly hosted within quartz veins that lie parallel to bedding, at the contacts between greywacke and mudstone. Four distinct vein generations exist at Goldboro: V1) foliated, bedding parallel, glassy quartz veins that are rich in sulfides, V2) foliated, bedding parallel and discordant milky white quartz veins with abundant arsenopyrite, V3) undeformed, tan, carbonate-rich veinlets, and V4) undeformed, albite+K-feldspar+chlorite+biotite+ilmenite veins. A broad halo of sericite alteration surrounds Goldboro (>100 m from the hinge line of the Upper Seal Harbour anticline) with more localized biotite, chlorite, and albite+sericite alteration. Biotite alteration occurs proximal to V1 and V4 veins (< 2 m), and albite+sericite and chlorite alteration are local to V4 veins (\leq 2 cm). V2 veins exhibit rare arsenopyrite alteration of the wall-rock, and V3 veins are not associated with any alteration. Lithogeochemistry and mineral chemistry were used to identify vectors

towards mineralization by demonstrating chemical changes within the wall-rock mudstones resulting from fluid-rock interactions during vein-stage mineralization: 1) K₂O and 3K/Al changes reflect the intensity of K-related mica alteration; 2) mass increases in Fe₂O₃ and MgO were found to correlate to biotite and chlorite alteration; 3) mass increases in Na₂O and CaO correspond to albite alteration; 4) Rb, Ba, and Cs were found to be proxies for K₂O; and 5) Sr was identified as a proxy for CaO, and can be used to identify carbonates in V3 veinlets. Gold mineralization is predominantly hosted within V1, V2, and V4 veins as free gold and as cores and inclusions in arsenopyrite. Petrographic textures and mineral assemblages suggest that V4 veins are potentially magmatic-hydrothermal in origin. Vein and mineral parageneses suggest two main mineralizing events, providing evidence for gold remobilization and refocusing, as has been suggested by previous researchers in the Meguma zone.

Acknowledgements

I would like to thank Dr. Stephen Piercey for his supervision, advice, guidance, eye for detail and, of course, sense of humour over the course of my time at Memorial University of Newfoundland. Steve's approach to supervision granted me a large amount of freedom and flexibility during my research which was greatly appreciated. I would also like to thank Dr. Graham Layne for being a part of my supervisory committee and for reviewing this manuscript and Dr. Wanda Aylward for her assistance and guidance using the SEM and EPMA. Finally, I would like to thank Mr. David Copeland from Anaconda Mining Inc.

for his feedback, support, and co-design of this research project. Dave and the rest of the Anaconda exploration team have been invaluable to completing this project and made me feel like a welcome part of the family over at Goldboro.

I cannot thank the members of the \$JP research group enough for their willingness to provide feedback, edits and to answer what seemed like a never-ending supply of questions. I would like to acknowledge Nikola Denisova and Matthew Manor specifically for providing edits to documents leading up to this manuscript. And above all else, the other members of 5016, Carly Mueller and Robert King, for an endless supply of antics, enthusiasm, conversation, and much-needed comic relief. I owe a huge thanks to Robert King, Amy Parkinson, Carly Mueller, Nikola Denisova, and Regan Jacobson, whom all became family in St. John's in this tumultuous time, as well as to my close friends Jarret Hamilton and Alex Hague for their support. I also thank my mother, Irene, and sister, Laryssa, for their constant encouragement throughout my academic career thus far. Regretfully, I cannot name every individual who has supported me during my degree in this short acknowledgement, but any and all who have helped in any magnitude have my sincere thanks.

Financial support for this Master's degree was provided by Anaconda Mining Inc., an NSERC Collaborative Research and Development Grant to Dr. Stephen Piercy, and a Research Fellowship from the School of Graduate Studies at MUN to myself. This project also benefitted from generous in-kind support from Anaconda Mining Inc.

Table of Contents

Abstract	ii
Acknowledgements.....	iii
Table of Contents	vi
List of Tables	ix
List of Figures	ix
List of Abbreviations	xi
Chapter 1: Introduction to the Goldboro Sediment-hosted Gold Deposit, Nova Scotia, Canada.....	14
1.1 History.....	14
1.2 Sediment-Hosted Orogenic Gold Deposits	15
1.3 Regional Geology of the Meguma Terrane.....	18
1.4 Local Geology.....	22
1.5 Thesis Objectives	25
1.6 Methods.....	26
1.6.1 Core Logging	26
1.6.2 Lithogeochemistry	27
1.6.3 Petrography, Scanning Electron Microscopy, and Electron Probe Micro-Analysis.....	29
1.7 Co-Authorship Statement.....	30
1.8 Presentation.....	30
1.9 References.....	32
Chapter 2: Lithogeochemistry and Genesis of a Meguma Terrane-Hosted Gold Deposit: Goldboro, Nova Scotia, Canada	46
2.1 Abstract	46
2.2 Introduction.....	48
2.3 Geological Setting.....	51
2.4 Deposit Geology	53
2.5 Mineralization and Alteration	53

2.5.1	Lithofacies, Lithostratigraphy, and Mineralization.....	53
2.5.2	Alteration	56
2.6	Paragenesis.....	58
2.6.1	Overview.....	58
2.6.2	Arsenopyrite.....	61
2.6.3	Gold.....	61
2.7	Geochemical and Mineralogical Methods	62
2.7.1	Lithogeochemistry	62
2.7.2	Petrography and Scanning Electron Microscopy	65
2.7.3	Electron Probe Microanalysis	65
2.8	Results.....	67
2.8.1	Principal Component Analysis	67
2.8.2	Lithogeochemistry	68
2.8.1.1	Immobile Elements and Provenance.....	69
2.8.1.2	Mobile Element Lithogeochemistry.....	71
2.8.1.4	Mass Change Calculations	72
2.8.3	Electron Probe Microanalysis	76
2.9	Discussion	78
2.9.1	Gold Paragenesis and Implications for Meguma-type Gold Deposits	78
2.9.2	Hydrothermal Alteration of the Goldboro Deposit	81
2.9.3	Vectors to Mineralization	88
2.9.4	Formation of the Goldboro Deposit.....	90
2.10	Conclusions.....	94
2.11	References.....	97
	Chapter 3: Summary and Future Research	140
3.1	Summary	140
3.2	Future Research	141
	Appendix A: Graphic Logs	144
	Appendix B: Whole-rock Geochemical Analysis Results	193
	Appendix C: Mass Change Results.....	203
	Appendix D: EPMA Results.....	229

Appendix E: Chlorite Geothermometry 353

List of Tables

Table 2.1: Vein Generations of the Goldboro Deposit

Table 2.2: Representative Geochemical Results

List of Figures

Chapter 1

Figure 1.1: Regional geologic map of the Meguma Terrane.

Figure 1.2: Regional stratigraphy of the Meguma Terrane.

Figure 1.3: Simplified local geology of the Goldboro deposit.

Figure 1.4: Representative cross-section of the Goldboro deposit.

Chapter 2

Figure 2.1: Regional geologic map of the Meguma Terrane.

Figure 2.2: Regional stratigraphy of the Meguma Terrane.

Figure 2.3: Simplified local geology of the Goldboro deposit.

Figure 2.4: Representative cross-section of the Goldboro deposit.

Figure 2.5: Stratigraphy and lithology of the Goldboro deposit.

Figure 2.6: Vein generations of the Goldboro deposit.

Figure 2.7: V4 vein mineralogy and textures at varying scales.

Figure 2.8: Alteration types of the Goldboro deposit.

Figure 2.9: Alteration at varying scales.

Figure 2.10: Paragenesis of the Goldboro deposit.

Figure 2.11: Arsenopyrite generations and gold morphology.

Figure 2.12: PCA results for geochemical data.

Figure 2.13: Immobile element pair diagrams.

Figure 2.14: Immobile element diagrams and REE diagram.

Figure 2.15: CIA (chemical index of alteration) plot and $\text{SiO}_2/\text{Al}_2\text{O}_3$ vs. K_2O sorting curve.

Figure 2.16: Downhole profile.

Figure 2.17: Mass change histograms.

Figure 2.18: EPMA results for chlorite.

Figure 2.19: EPMA results for biotite.

List of Abbreviations

ΔM	Mass Change
μm	Micrometer
$^{\circ}C$	Degrees Celsius
2D, 3D	Two-, and three-dimensional
Ab	Albite
Ant	Anatase
Ank	Ankerite
Apy	Arsenopyrite
arg	Argillite
Au	Gold
b.s.l.	Below sea level
Bt	Biotite
Bx	Breccia
CDR	Coupled dissolution-reprecipitation
CIA	Chemical index of alteration
CCFS	Cobequid-Chedabucto Fault System
CO_3	Carbonate
Ccp	Chalcopyrite
Chl	Chlorite
cm	Centimeter
CREAIT	Core Research Equipment and Instrument Training
EDX	Electron dispersive X-ray
EPMA	Electron probe micro-analysis
Fig(s).	Figure(s)
g/t	grams per ton
Gn	Galena
gw	Greywacke
HFSE	High Field Strength Elements

ICP-AES	Inductively coupled plasma atomic emission spectrometry
ICP-MS	Inductively coupled plasma mass spectrometry
Ilm	Ilmenite
Ksp, K-feldspar	Potassium feldspar
km	kilometer
kV	kilovolt
LA-ICP-MS	laser ablation inductively coupled plasma mass spectrometry
LMCE	Low melting-point chalcophile elements
LOI	Loss on ignition
LREE	Light rare earth elements
m	Meters
Ma	Mega annum
mm	Millimeter
ms	Millisecond
Mt	Megaton
nA	Nano amperes
PCA	Principal component analysis
PC	Principal component
ppb	Parts per billion
ppm	Parts per million
Py	Pyrite
QA/QC	Quality assurance and quality control
Qtz	Quartz
REE	Rare earth elements
SEM	Scanning electron microscope
ser	Sericite
SMB	South Mountain batholith
Sp	Sphalerite
t	tonne

T	Temperature
USHA	Upper Seal Harbour anticline
wt. %	Weight percent

Chapter 1: Introduction to the Goldboro Sediment-hosted Gold Deposit, Nova Scotia, Canada

1.1 History

The Goldboro deposit is one of the largest gold deposits in Nova Scotia in terms of historical production (16,036,000 tonnes @ 3.78 g/t Indicated and Measured, 5,306,000 tonnes @ 4.68 g/t Inferred, 1,946,100 oz and 798,100 oz Au, respectively; Kuntz et al., 2021) and is located in Guysborough County on the eastern shore of Nova Scotia (Fig. 1.1). Since its discovery, Goldboro has had a long history of exploration and acquisitions by different companies. In historical literature, the deposit is referred to as the Upper Seal Harbour gold district (e.g., Malcolm, 1929).

The property's history of gold exploration dates back to 1862 when Howard Richardson of the Geological Survey of Canada first discovered quartz veins within the Isaac's Harbour anticline. In 1892, Richardson subsequently discovered what is currently known as the Boston-Richardson belt and gold production began in 1893 by the Richardson Mining Company. During this time, the average reported grade was 13.03 g/t Au with recoveries between 50% and 60%. Production by the Richardson Mining Company continued until 1910, when milling results of new exploration shafts returned unsatisfactorily, and the mine was abandoned. The property underwent intermittent exploration, testing, and tailings reprocessing between 1910 and 1981. In 1981, Patino Mines Ltd.

completed a geophysical survey that led to the discovery of new mineralized zones (Malcolm, 1923). Orex Exploration Inc. subsequently acquired the property in 1988 and conducted exploration via exploration drilling, metallurgical testing, resource estimation programs, and economic assessments (Kuntz et al., 2021).

In March of 2017, Anaconda Mining Inc. acquired Orex Exploration as a subsidiary; Anaconda has had ownership of the property and continues exploration at the time of writing (Kuntz et al., 2021).

1.2 Sediment-Hosted Orogenic Gold Deposits

Orogenic gold deposits are the world's most geographically and temporally widespread type of metallic mineral deposit (Groves et al., 2019; Hedenquist et al., 2019). They are generally typified by having gold lodes hosted within quartz veins, and by their spatial and temporal association with metamorphism and orogenesis (Barley and Groves, 1992; Goldfarb et al., 1998; Groves et al., 1998). Generally, these deposits are grouped based on the time of their formation: Precambrian versus Phanerozoic. Precambrian gold deposits typically occur in greenstone belts, whereas Phanerozoic orogenic gold deposits are predominantly hosted within accreted oceanic sedimentary rocks with some greenstone-hosted deposits (e.g., Mother Lode District, CA; Baie Verte-Pointe Rousse, NL) (Goldfarb et al., 1998; Groves et al., 2019). The Phanerozoic sediment-hosted gold deposits include world-class gold districts of various ages, including the Otago Schist belt in New Zealand, the Lachlan (Victorian) fold belt in southeastern Australia, Sukhoi Log in Siberia, Muruntau in Uzbekistan, and the

Meguma gold district in Nova Scotia, Canada (Bierlein et al., 2004, Goldfarb et al., 2001; Groves et al., 2019).

Several models have been proposed to explain the genesis of sediment-hosted orogenic gold deposits: 1) syngenetic, exhalative deposition with seafloor sediments (Hutchinson, 1987); 2) magmatic-hydrothermal processes (Sillitoe and Bonham Jr., 1990; Spooner, 1993); and 3) processes related to metamorphism/metamorphic fluids (Kerrick, 1983; Phillips and Powell, 2010; Groves et al., 2019). The current paradigm favours the model that metamorphic fluids generated during the regional metamorphic breakdown of hydrous minerals play a key role in transporting and depositing gold (Groves et al., 2019). However, recent work argues that in some orogenic gold deposits associated with granitic intrusions, a mixture of metamorphic and magmatic-hydrothermal fluid was responsible for the ore mineralization (Kontak and Horne, 2010; Kontak et al., 2011). Some studies also suggest that orogenic gold deposits are locally upgraded by the dissolution and reprecipitation of gold (“remobilization”), which increases the grade of deposits by means of zone refinement (Large et al., 2009; Hastie et al., 2020, 2021; Gourcerol et al., 2020)

In the metamorphic model, ore-forming fluid travels along crustal-scale fault networks, ascending into the upper crust and depositing gold by reacting with wall-rock, or due to a decrease in temperature and/or pressure that provokes phase separation (Cox et al., 1991; Cox, 1999; Hagemann and Lüders, 2003; Weatherley and Henley, 2013). Recent experimental work (Weatherley and

Henley, 2013) identified abrupt, local depressurization as a possible mechanism of quartz vein formation. These pressure changes are caused by faults or flexural jogs and can account for episodic quartz vein formation over a region's tectonic history. Stress regimes required for flexural slip have been shown to be achievable at significant depths in the Earth's crust (>3 km b.s.l.)(Upton and Craw, 2014). These studies support suggestions that orogenic quartz veins develop during protracted tectonism and potentially at variable crustal levels (Morelli et al., 2005; Sangster and Smith, 2007; Zoheir et al., 2019).

The source of Au in orogenic deposits is still debated; the proposed origins of Au include metaintrusive, metasedimentary, or sub-crustal sources. Recently, the crustal conveyor model (Pitcairn et al., 2014) suggests that Au is sourced directly from the accreted metasediments over an extended period of time. In the crustal conveyor model, the authors show that the orogenic processing of metasediments to amphibolite facies can liberate significant Au and other metals from diagenetic sulfides. For example, Pitcairn et al. (2014) show that over 1127 t of Au, 10.1 Mt of As, 47,000 Mt of Hg, and 560,000 t Sb were mobilized in the Southern Alps of New Zealand. Recent work by Hastie et al. (2020, 2021) has provided evidence for the remobilization of gold in the Abitibi greenstone belt through nanomelting of auriferous pyrite, suggesting gold was entirely hosted within refractory phases before the main remobilization event. Evidence has been presented for similar processes in the Meguma Terrane by Gourcerol et al. (2020).

1.3 Regional Geology of the Meguma Terrane

The Appalachian orogen of North America comprises five tectonostratigraphic zones: the Humber, Dunnage, Gander, Avalon, and Meguma zones (Fig. 1.1)(Williams, 1979). The Humber zone is composed of metaclastic remnants of the Laurentian continental margin. The Dunnage zone consists of continental and oceanic arc terranes that formed in the Iapetus Ocean and were subsequently accreted. The Gander, Avalon, and Meguma Terranes were peri-Gondwanan microcontinents that were accreted onto Laurentia during the Salinic, Acadian, and Neoacadian orogenies (Williams et al., 1999; van Staal, 2007).

The Meguma Terrane is the easternmost of the accreted terranes in the Canadian Appalachian orogen. Despite only outcropping on land in Nova Scotia, the regional extent of the Meguma Terrane is much broader; the Meguma Terrane has been identified offshore, extending from the Grand Banks of Newfoundland to Cape Cod (van Staal and Barr, 2012). The accretion of the Meguma Terrane was largely accommodated by the Cobéquid-Chedabucto Fault System (CCFS), which bounds the Meguma Terrane in northern Nova Scotia, separating it from its neighbouring Avalon Terrane (White, 2010; van Staal and Barr, 2012).

Two main lithologies define the Meguma Terrane: the thick (>12 km) Early Cambrian to Early Ordovician (537–475 Ma) Meguma Supergroup and the mid-Devonian to Early Carboniferous South Mountain Batholith and its associated plutons (Kontak and Reynolds, 1994; Waldron et al., 2009; White, 2010; Gingras et al., 2011; van Staal and Barr, 2012). Following its accretion, the

Meguma Terrane underwent periodic, intense orogenesis between 400–320 Ma, during which the terrane was regionally folded and metamorphosed to greenschist facies and locally to amphibolite facies. The South Mountain Batholith and its satellite plutons were emplaced during this period of orogenesis, ca. 375 Ma (Hicks et al., 1999; Sangster and Smith, 2007; van Staal and Barr, 2012).

The Meguma Supergroup is divided into the metagreywacke-dominated Goldenville Group and the overlying, mudstone-dominated Halifax Group (Fig. 2)(Horne and Pelley, 2007; White, 2010). The Goldenville Group comprises a series of fining-upwards successions of medium grey to light grey greywacke-dominated metaturbidite, fining upwards into medium grey to dark grey mudstones. Locally, mudstone is metamorphosed into shale or phyllite. However, these mudstones are not always preserved due to the erosive nature of the basal contacts of turbidite flows (Mulder and Alexander, 2001). In contrast to the underlying Goldenville Group, the Halifax Group is composed mainly of turbiditic metapelites and has few gold deposits (Horne and Pelley, 2007; Sangster and Smith, 2007; White, 2010; van Staal and Barr, 2012). Individual formations have been mapped in the Halifax Group (Glenbrook, Cunard, Beaverbrook formations) and Goldenville Group (Taylors Head, Tangier, Moose River formations)(Horne and Pelley, 2007).

Gold mineralization occurs throughout the Goldenville Group. Gold in the Meguma Terrane is typically hosted in quartz veins with localized occurrences of disseminated wall-rock mineralization (e.g., Tangier, Moose River, and North

Brookfield deposits)(Sangster and Smith, 2007). Veins commonly occur at the crests of anticlinal domes and at lithologic contacts along the limbs of the anticline, typically at sharp greywacke-mudstone contacts, or, in some locations, extend within both lithologies (Ryan and Smith, 1998; Sangster and Smith, 2007). Common minerals associated with free gold include arsenopyrite, pyrite, pyrrhotite, sphalerite, and galena. Although uncommon, scheelite has been documented in some deposits in the Meguma Terrane (Dostal et al., 2009).

The vein-proximal alteration assemblage of most Meguma-type gold deposits commonly includes biotite, chlorite, anatase, and carbonate (Kontak et al., 1993; Bierlein and Smith, 2003). The breakdown of metamorphic chlorite, introduction of carbonate phases, and albite alteration results in visible bleaching of sandstone units local to certain veins (Bierlein and Smith, 2003). Biotite and chlorite laths typically accompany near-ubiquitous sericite alteration of host mudstones (Bierlein and Smith, 2003). The spatial extent of alteration and its relationship to gold remains unclear (Kontak and Smith, 1993).

The genesis of Meguma-type gold deposits is still debated, with several models proposed. Currently, hypotheses exist explaining the formation of gold-bearing veins in Meguma-type deposits by: 1) hydrothermal venting on the paleo seafloor (Hunt, 1868; Hind, 1869, 1870, 1872; McBride 1978; Haynes, 1987); 2) deposition from fluids of diverse origins early in the tectonothermal history of the terrane; and 3) deposition from magmatic or deep crustal hydrothermal fluids, post-peak metamorphism (Sangster and Smith, 2007; Groves et al., 2019).

Syngenetic deposition on the seafloor was proposed by McBride (1978) and Haynes (1987). However, the field observations and documentation of structural features in the deposits in the Meguma Terrane by other workers (Mawer, 1987; Henderson et al., 1990; Williams and Hy, 1990) are not consistent with the syngenetic model.

An early syntectonic depositional model was suggested, wherein the deposition of structurally controlled gold-bearing quartz veins occurs before or during folding, but predating granite emplacement in the region. This model also suggests that vein material was more proximally sourced from the enclosing host rock, transported by normal metamorphic fluids (Graves and Zentilli, 1982; Henderson and Henderson, 1986; Henderson et al., 1986; Sangster, 1990, 1992). There is compelling geochemical and isotopic evidence that fluids are of a deep crustal origin, which is inconsistent with this model (Kontak and Kerrich, 1995; Kontak and Jackson, 1999; Kontak and Archibald, 2002).

The late syntectonic models describe vein genesis as a function of hydrothermal processes related to coupled regional plutonism and orogenesis, thus incorporating attributes of intrusion-related gold deposit models (Kontak et al., 2011b). Granitic or mafic magmas, the lower crust, or surrounding wall-rock are suggested as sources of the magmatic or deep metamorphic fluids responsible for the vein formation. Recent work suggests a variant of the metamorphic model, reflecting a mixing between magmatic-hydrothermal and metamorphic fluids (Kontak and Horne, 2010; Kontak et al., 2011b, 2011a).

The absolute timing of vein formation is unclear, but geochronological studies imply at least two main metallogenic events in the Meguma Terrane. Reported $^{40}\text{Ar}/^{39}\text{Ar}$ dates of hydrothermal biotite and amphibole range between 380 and 362 Ma (Kontak et al., 1990, 1993, 1998; Kontak and Archibald, 2002), suggesting vein formation during Acadian and Neoacadian magmatism and orogenesis. These results are consistent with suggestions made by Henderson et al. (1986), who suggested episodic generations of vein formation. However, Re-Os dates of arsenopyrite formation at the Ovens and Dufferin deposits suggest ages of ca. 408 Ma and ca. 380 Ma, respectively (Morelli et al., 2005). Morelli et al. (2005) suggest that mineralization occurred over a long period or as widely spaced multiple events (Sangster and Smith, 2007). More recent work using $^{39}\text{Ar}/^{40}\text{Ar}$ dating supports this idea and reports that there were two thermal events which reset biotite and amphibole ages at similar times; one event at ca. 408 Ma and another ca. 380 Ma, corresponding to regional deformation and emplacement of large granitic batholiths, respectively (Kontak and Horne, 2010; Kontak et al., 2011).

1.4 Local Geology

Located on the eastern shore of Nova Scotia, the Goldboro sediment-hosted orogenic gold deposit is approximately 5 km northeast of the town of Goldboro (Fig. 1.3). The deposit is hosted by the metagreywacke-dominated Goldenville Group, entirely hosted by thin (≤ 10 m) fining-upwards successions of sandstone to mudstone. These successions are largely unmetamorphosed but are

locally metamorphosed to greenschist facies (van Staal, 2007; White, 2010) The stratigraphy of the Goldboro area is folded into the upright, east-west trending shallowly east plunging fold, the Upper Seal Harbour anticline. The area is cut by at least three regional brittle faults that dip steeply and strike to the NE and S. Detailed structural measurements are described by Kuntz et al. (2021).

Mineralization at Goldboro occurs within quartz veins or veinlets and is locally disseminated in vein-adjacent wall-rock. There are at least four generations of veining: an early generation (V1) of foliated veins that contain colourless, transparent quartz, and are bedding-parallel and sulfide-rich; second-generation (V2) foliated and non-foliated veins that contain near-opaque, milky-white quartz and commonly have crack-seal structures; third-generation (V3) veinlets that are non-foliated, tan, and carbonate-rich; and fourth-generation (V4) veins that are non-foliated, are rich in albite, K-feldspar, chlorite, biotite, and can contain fluorapatite and ilmenite. Gold mineralization is hosted in V1, V2, and V4 veins, with the highest gold grades associated with V4 veins.

V1 and V2 veins occur as angular veins, leg reefs, and saddle reefs along the Upper Seal Harbour anticline, with V2 veins also forming non-foliated veins during regional extension. Saddle reefs occur in the fold hinges, reaching thicknesses of up to tens of meters, and pinch out along the fold limbs to form leg reefs. Both saddle and leg reefs are formed in space accommodated by flexural slip (Ryan and Smith, 1998; Weatherley and Henley, 2013); slip occurs at mudstone-sandstone boundaries and is interpreted to have formed due to

lubrication of these contacts by fluid (Horne and Culshaw, 2001). In some cases, leg reefs occur without saddle reefs present along the same stratigraphic horizon or are discontinuous (Sangster and Smith, 2007). Late extension veins of both V1 and V2 generations are regionally present throughout the Meguma Terrane and consist of quartz infilling late extensional joints (Williams and Hy, 1990). At Goldboro, these late extension veins range from a few centimeters to decimeters in thickness. Late extension veins cross-cut bedding and have variable thickness. V3 and V4 veins are non-foliated and occurred after compression. V3 veinlets commonly infill brecciation and cleavage. V4 veins infill fractures in V1 and V2 veins and are at high angles to bedding.

Previous work has defined high-grade gold occurrences within three broad zones: the Boston-Richardson (BR), the East Goldbrook (EG), and the West Goldbrook (WG) zones, referred to as Gold Systems in industry reports (Ryan and Smith, 1998; Kuntz et al., 2021). These zones are defined based on their geographic, structural, and stratigraphic positions (Figs. 1.3 and 1.4). The Boston-Richardson and the East Goldbrook are separated by a thick (20 m-60 m), massive greywacke unit that is generally devoid of mineralization or quartz veins. A fault cutting through the Goldboro deposit separates these two mineralized belts from the West Goldbrook zone.

Alteration associated with quartz veins and gold mineralization is variable. Carbonate alteration at Goldboro is very rare and is only present in greywacke beds; carbonate alteration at Goldboro is very rare compared to what is observed

in many orogenic gold deposits. The most distinct alteration type is a broad halo of sericite that extends outwards for >100 m from the hinge line of the Upper Seal Harbour anticline. Biotite and chlorite alteration are the second most dominant alteration types; the intensity of this alteration varies between mudstone units but increases in proximity to V1 and V4 veins. V4 veins exhibit local albite+sericite+anatase alteration in mudstones extending up to 3 cm from V4 vein margins and broad albite+sericite alteration in greywacke.

1.5 Thesis Objectives

This study aims to describe the stratigraphy, alteration, and lithogeochemistry of the Goldboro deposit, contributing to enhancing our understanding of the alteration processes and genesis of deposits in the greater Meguma Terrane. The main detailed objectives are as follows: 1) document the geological and stratigraphic setting of mineralization and the vein and alteration mineral paragenesis; 2) document the alteration assemblages and their spatial distribution with respect to veins and lithologies through using drill core observations, petrography, and lithogeochemistry; 3) use lithogeochemistry to characterize and assess chemostratigraphy and mudstone alteration at Goldboro (this information will be used to calculate mass changes and to quantify the elemental gains and losses with respect to different alteration types and their spatial relationships); 4) determine compositional variations in micas using electron probe micro-analysis (EPMA) to understand mineral-scale chemical changes throughout the deposit, 5) quantify the elemental, mineralogical, and

mineral chemical vectors to mineralization and create custom alteration indexes; and 6) to integrate the above information to understand the geochemical controls on alteration and mineralization and the physico-chemical conditions of gold formation so as to enhance our understanding of the genesis and alteration footprint of mineralization at Goldboro and its implication for other Meguma-type gold deposits in Nova Scotia and globally.

1.6 Methods

The thesis objectives mentioned above were addressed using the following methods: 1) documenting the stratigraphy, quartz vein distribution, and alteration through core logging; 2) identification of micro-scale alteration textures and mineral assemblages through petrography and scanning-electron microscopy (SEM); and 3) quantification of chemical and mineralogical changes associated with alteration using lithogeochemistry and mineral chemistry (via EPMA). The synthesis goal of this study was to integrate the results from the above methods to create models for the genesis and alteration of the Goldboro deposit.

1.6.1 Core Logging

Core logging was undertaken in October-November 2019 and August 2020 at the Goldboro core warehouse. A total of 17 drillholes consisting of approximately 4850 m of drill core from across the property was logged, allowing for complete coverage of the stratigraphy and alteration from the West Goldbrook, Boston-Richardson, and East Goldbrook Gold Systems. Lithology, alteration, and mineralization were documented in these drill logs, including

detailed notes and photographs. Hand-drawn graphic logs were digitized using Adobe Illustrator (Appendix A). A total of 381 samples were selected from the drillholes based on their alteration, lithology, and/or mineral assemblages.

1.6.2 Lithogeochemistry

A total of 109 mudstone samples were analyzed at ALS Minerals Laboratories in Sudbury, Ontario, for major and trace elements. All samples were quartered or halved core. Before shipment, all samples were trimmed of any non-representative contaminants using a water-cooled Dewalt tile saw in the CREATL Lapidary and Saw facility at Memorial University of Newfoundland, washed in order to mitigate contamination from the rock saw and bagged in individual polyurethane bags. At ALS, all samples were crushed using an agate mill to a size where 70% of grains passed through a 2 mm sieve; 250 g was then riffle split to mitigate potential nugget effects of gold. Samples were analyzed using the complete characterization package CCP-PKG01. Major element analysis was conducted using lithium metaborate fusion followed by an acid finish and subsequent analysis using inductively coupled plasma atomic emission spectroscopy (ICP-AES). Total carbon and sulfur were analyzed via combustion using Leco methods and inorganic carbon was analyzed using perchloric (HClO_4) acid digestion and analysis by CO_2 coulometer (analysis package C-GAS05). Some metals (Cd, Co, Cu, Li, Mo, Ni, Pb, Sc, Ag and Zn) were determined using four-acid digestion and an inductively coupled plasma mass spectrometer (ICP-MS) finish. Volatile elements and semi-metals (viz., As, Bi, Hg, In, Re Sb, Se, Te,

and Tl) were determined by aqua regia digestion and ICP-MS finish. Trace elements, including high field strength elements (HFSE), low field strength elements (LFSE), and rare earth elements (REE), were analyzed using lithium borate fusion, followed by four-acid digestion and an ICP-MS finish. Gold was analyzed using fire assay pre-preparation and an ICP-AES (AuICP21) finish; samples with over-limit values (above upper detection limits) were re-determined by gravimetric methods. Quality assurance and quality control (QA/QC) was evaluated by using included CMIC-1 internal reference material, which was included with the samples using the method described in Piercey (2014). CMIC-1 was chosen because the matrix is similar to the host rocks at Goldboro and ALS internal standards. The measure of precision (%RSD; high values correspond to low precision) for the mudstone standard was <4% for major elements except for MnO and P₂O₅, which were below the limit of quantification (LOQ); MnO and P₂O₅ returned %RSD <7%. The %RSD of trace elements above the limit of quantification (LOQ) was <10%, except for elements As, Li, Mo, and Au (83%, 19%, 32%, and 167%, respectively). The measure of accuracy (%RD; high values mean low accuracy) was <5% for all elements above the LOQ except for Ga, Ta, Tm, As, Tl, Li, Mo, Pb, and Au (13%, 13%, 7%, 1163%, 26%, 8%, 18%, 7%, and 88%, respectively). The especially high %RSD and %RD for As and Au were determined to be a result of cross-contamination and carry-over, respectively. Samples with inflated As concentrations due to cross-contamination were noted, and high-Au samples with carry-over were ignored. The high %RD values for

other elements were determined to be a result of heterogeneity in the samples or, in the case of Li, due to contamination during Li-borate fusion.

1.6.3 Petrography, Scanning Electron Microscopy, and Electron Probe

Micro-Analysis

A total of 110 polished thin sections were prepared at Vancouver Petrographics. Thin sections were polished to 30 µm thickness for standard petrography, whereas double-polished thin sections were polished to 100 and 150 µm thickness for fluid inclusion analysis. Detailed petrographic descriptions were completed to establish micro-scale paragenetic relationships, as well as to characterize ore and alteration mineralogy and textures.

Scanning electron microscopy (SEM) and energy dispersive X-ray (EDX) analyses were conducted on carbon-coated thin sections at the CREAT Hibernia Electron Beam Facility at Memorial University using a JEOL JSM 7100 F microscope for micro- to nanoscale textures and semi-quantitative analysis of minerals and textures.

Electron probe micro-analysis (EPMA) was conducted using a JEOL JXA 8230 electron microprobe at the CREAT Hibernia Electron Beam Facility at Memorial University to analyze major and minor element chemical variations in muscovite, chlorite, and biotite between proximal and distal alteration zones and between stratigraphic zones.

1.7 Co-Authorship Statement

This research project was designed by Dr. Stephen J. Piercey from Memorial University of Newfoundland and Mr. David Copeland from Anaconda Mining Inc. This project greatly benefitted from conversations with Tanya Tettelaar, Michelle English, and Alana Haysom from Anaconda Mining. The primary editor of this paper is Dr. Stephen J. Piercey with secondary editing by Dr. Graham Layne.

1.8 Presentation

This thesis is presented as three chapters and supplementary appendices. Chapter 1 is an introductory chapter that describes the purpose of the study by providing background information about Goldboro, including historical, global, regional, and local geological context and presenting the methods used in this study.

Chapter 2 is written as a publication-style manuscript and is the main body of this thesis. This chapter is intended to be submitted for publication in a peer-reviewed journal (e.g., Economic Geology or similar journal). Presented in Chapter 2 are descriptions of the lithology, alteration assemblages, and lithogeochemical results. This chapter also presents models for the formation of the alteration associated with the Goldboro deposit using geochemical, petrographic, and statistical analyses. Additionally, in Chapter 2, we present possible regional implications for the wider Meguma Terrane and other Meguma-type gold deposits.

Chapter 3 provides a summary of the conclusions drawn in Chapter 2 and the appendices. Here are outlined some direction for future research and outstanding questions that would benefit our understanding of the Goldboro deposit and other Meguma-type gold deposits.

The appendices provide supplementary data, figures, and drill logs that were not included in Chapter 2 but were used to reach conclusions outlined there. The appendices contain the complete geochemical datasets, QA/QC results, digitized drill logs, and a compilation of electron probe microanalysis results.

1.9 References

- Kuntz, G., Robinson, J., Jundis, R., Raponi, T., Kirchner, T., Pumphrey, S., McIsaac, R., Parks, J., Betts, A., Harkonen, H., 2021, Goldboro gold project resource update phase 2 Guysborough County, Nova Scotia. NI 43-101 Technical Report and Mineral Resource Estimate no. 20048-02, 237 p.
- Barley, M.E., and Groves, D.I., 1992, Supercontinent cycles and the distribution of metal deposits through time: *Geology*, v. 20, p. 291–294.
- Bierlein, F.P., Fuller, T., Stuwe, K., Arne, D.C., and Keays, R.R., 1998, Wallrock alteration associated with turbidite-hosted gold deposits. Examples from the Palaeozoic Lachlan Fold Belt in central Victoria, Australia: *Ore Geology Reviews*, v. 13, p. 345-380.
- Bierlein, F.P., Christie, A.B., and Smith, P.K., 2004, A comparison of orogenic gold mineralisation in central Victoria (AUS), western South Island (NZ) and Nova Scotia (CAN): implications for variations in the endowment of Palaeozoic metamorphic terrains: *Ore Geology Reviews*, v. 25, p. 125–168.
- Bierlein, F.P., and Smith, P.K., 2003, The Touquoy Zone deposit: An example of “unusual” orogenic gold mineralisation in the Meguma Terrane, Nova Scotia, Canada: *Canadian Journal of Earth Sciences*, v. 40, p. 447–466.

Cox, S.F., Wall, V.J., Etheridge, M.A., and Potter, T.F., 1991, Deformational and metamorphic processes in the formation of mesothermal vein-hosted gold deposits - examples from the Lachlan Fold Belt in central Victoria, Australia: *Ore Geology Reviews*, v. 6, p. 391–423.

Cox, S.F., 1999, Deformational controls on the dynamics of fluid flow in mesothermal gold systems: Geological Society of London, Special Publication, v. 155, p. 123–140.

Dostal, J., Kontak, D.J., and Chatterjee, A.K., 2009, Trace element geochemistry of scheelite and rutile from metaturbidite-hosted quartz vein gold deposits, Meguma Terrane, Nova Scotia, Canada: Genetic implications: *Mineralogy and Petrology*, v. 97, p. 95–109.

Gingras, M.K., Waldron, J.W.F., White, C.E., and Barr, S.M., 2011, The evolutionary significance of a Lower Cambrian trace-fossil assemblage from the Meguma terrane, Nova Scotia: *Canadian Journal of Earth Sciences*, v. 48, p. 71–85.

Goldfarb, R.J., Groves, D.I., and Gardoll, S., 2001, Orogenic gold and geologic time: A global synthesis: *Ore Geology Reviews*, v. 18, p. 1–75.

Goldfarb, R.J., and Groves, D.I., 2015, Orogenic gold: Common or evolving fluid and metal sources through time: *Lithos*, v. 233, p. 2–26.

Graves, M.C., and Zentilli, M., 1982, A review of the geology of gold in Nova Scotia, *in* Hodder, R.W. and Petruk, W. eds., Geology of Canadian Gold Deposits: Canadian Institute of Mining and Metallurgy, Special Volume 24, p. 233–242.

Groves, D.I., Goldfarb, R.J., Gebre-Mariam, M., Hagemann, S.G., and Robert, F., 1998, Orogenic gold deposits: A proposed classification in the context of their crustal distribution and relationship to other gold deposit types: *Ore Geology Reviews*, v. 13, p. 7–27.

Groves, D.I., Santosh, M., Deng, J., Wang, Q., Yang, L., and Zhang, L., 2019, A holistic model for the origin of orogenic gold deposits and its implications for exploration: *Mineralium Deposita*, v. 55, p. 275-292.

Hagemann, S.G., and Lüders, V., 2003, P-T-X conditions of hydrothermal fluids and precipitation mechanism of stibnite-gold mineralization at the Wiluna lode-gold deposits, Western Australia: Conventional and infrared microthermometric constraints: *Mineralium Deposita*, v. 38, p. 936–952.

Hastie, E.C.G., Schindler, M., Kontak, D., Lafrance, B., 2021, Transport and coarsening of gold nanoparticles in an orogenic deposit by dissolution-reprecipitation and Ostwald ripening: *Communications Earth & Environment*, v. 2, p. 1-9.

Hastie, E.C.G., Kontak, D.J., and Lafrance, B., 2020, Gold Remobilization: Insights from Gold Deposits in the Archean Swayze Greenstone Belt, Abitibi Subprovince, Canada: *Economic Geology*, v. 115, p. 241–277.

Haynes, S.J., 1987, Classification of quartz veins in turbidite-hosted gold deposits, greenschist facies, eastern Nova Scotia.: Canadian Mining & Metallurgical Bulletin, v. 80, p. 37–51.

Hedenquist, J.W., Thompson, J.F.H., Goldfarb, R.J., Richards, J.P., Kerrich, R., Goldfarb, R.J., and Richards, J.P.R., 2019, Metallogenic Provinces in an Evolving Geodynamic Framework: Economic Geology One Hundredth Anniversary Volume, p. 1097–1136.

Henderson, J.R., Henderson, M.N., and Wright, T.O., 1990, Water-sill hypothesis for the origin of certain veins in the Meguma Group, Nova Scotia, Canada: Geology, v. 18, p. 654–657.

Henderson, J.R., Wright, T.O., and Henderson, M.N., 1986, A history of cleavage and folding: An example from the Goldenville Formation, Nova Scotia: Geological Society of America Bulletin, v. 97, p. 1354–1366.

Henderson, M.N., and Henderson, J.R., 1986, Constraints on the origin of gold in the Meguma zone, Ecum Secum area, Nova Scotia: Contributions to the Geology of the Meguma Terrane, Nova Scotia: Maritime Sediments and Atlantic Geology, v. 22, p. 1–14.

Hicks, R.J., Jamieson, R.A., and Reynolds, P.H., 1999, Detrital and metamorphic $^{40}\text{Ar}/^{39}\text{Ar}$ ages from muscovite and whole-rock samples, Meguma

Supergroup, southern Nova Scotia: Canadian Journal of Earth Sciences, v. 36, p. 23–32.

Horne, R., and Culshaw, N., 2001, Flexural-slip folding in the Meguma Group, Nova Scotia, Canada: Journal of Structural Geology, v. 23, p. 1631–1652.

Horne, R.J., and Pelley, D., 2007, Geological Transect of the Meguma Terrane from Centre Musquodoboit to Tangier: NS Mineral Resources Branch, Report of Activities, v. ME 2007-1, p. 71–89.

Hutchinson, R.W., 1987, Metallogeny of Precambrian gold deposits: Space and time relationships: Economic Geology, v. 82, p. 1993–2007.

Kerrich, R., 1983, Geochemistry of gold deposits in the Abitibi Greenstone Belt: Canadian Institute of Mining and Metallurgy, Special Paper 27.

Kontak, D.J., Horne, R.J., Sandeman, H., Archibald, D., and Lee, J.K.W., 1998, $^{40}\text{Ar}/^{39}\text{Ar}$ dating of ribbon-textured veins and wall-rock material from Meguma lode gold deposits, Nova Scotia: Implications for timing and duration of vein formation in slate-belt hosted vein gold deposits: Canadian Journal of Earth Sciences, v. 35, p. 746–761.

Kontak, D.J., and Kerrich, R., 1995, Geological and geochemical studies of a metaturbidite-hosted lode gold deposit: the Beaver Dam deposit, Nova Scotia: II. Isotopic studies: Economic Geology, v. 90, p. 885–901.

- Kontak, D.J., Smith, P.K., and Reynolds, P.H., 1993, Geology and $^{40}\text{Ar}/^{39}\text{Ar}$ geochronology of the Beaver Dam gold deposit, Meguma Terrane, Nova Scotia, Canada: evidence for mineralization at 370 Ma: *Economic Geology*, v. 88, p. 139–170.
- Kontak, D.J., Smith, P.K., Reynolds, P., and Taylor, K., 1990, Geological and $^{40}\text{Ar}/^{39}\text{Ar}$ geochronological constraints on the timing of quartz vein formation in Meguma Group lode-gold deposits, Nova Scotia: *Atlantic Geology*, v. 26, p. 201–227.
- Kontak, D.J., and Archibald, D.A., 2002, $^{40}\text{Ar}/^{39}\text{Ar}$ dating of hydrothermal biotite from high-grade gold ore, Tangier gold deposit, Nova Scotia: Further evidence for 370 Ma gold metallogeny in the Meguma Terrane: *Economic Geology*, v. 97, p. 619–628.
- Kontak, D.J., and Horne, R.J., 2010, A multi-stage origin for the Meguma lode gold deposits, Nova Scotia, Canada: a possible global model for slate belt-hosted gold mineralization, *in* Deb, M. and Goldfarb, R.J. eds., *Gold metallogeny: India and beyond*, Oxford, Alpha Science International Ltd., p. 58–82.
- Kontak, D.J., Horne, R.J., Creaser, R.A., Petrus, J.A. Archibald, D., 2013, A petrological and geochronological study of a 360 Ma metallogenic event in Maritime Canada with implications for lithophile-metal mineralization in the Canadian Appalachians: *Canadian Journal of Earth Sciences*, v. 50, p. 1147–1163.

Kontak, D.J., Horne, R.J., and Kyser, K., 2011, An oxygen isotope study of two contrasting orogenic vein gold systems in the Meguma Terrane, Nova Scotia, Canada, with implications for fluid sources and genetic models: Mineralium Deposita, v. 46, p. 289–304.

Kontak, D.J., and Jackson, S.J., 1999, Documentation of variable trace- and rare-earth-element abundances in carbonates from auriferous quartz veins in Meguma lode-gold deposits, Nova Scotia: Canadian Mineralogist, v. 37, p. 469–488.

Kontak, D.J., and Kyser, K., 2011, A fluid inclusion and isotopic study of an intrusion-related gold deposit (IRGD) setting in the 380 Ma South Mountain Batholith, Nova Scotia, Canada: Evidence for multiple fluid reservoirs: Mineralium Deposita, v. 46, p. 337–363.

Malcolm, W., 1929, Gold fields of Nova Scotia, *in* Geological Survey of Canada, Memoir 158, p. 253.

Mawer, C.K., 1987, Mechanics of formation of gold-bearing quartz veins, Nova Scotia, Canada: Tectonophysics, v. 135, p. 99–119.

Morelli, R.M., Creaser, R.A., Selby, D., Kontak, D.J., and Horne, R.J., 2005, Rhenium-osmium geochronology of arsenopyrite in Meguma group gold deposits, Meguma terrane, Nova Scotia, Canada: Evidence for multiple gold-mineralizing events: Economic Geology, v. 100, p. 1229–1242.

Mulder, T., and Alexander, J., 2001, The physical character of subaqueous sedimentary density flow and their deposits: *Sedimentology*, v. 48, p. 269–299.

Phillips, G.N., and Powell, R., 2010, Formation of gold deposits: A metamorphic devolatilization model: *Journal of Metamorphic Geology*, v. 28, p. 689–718.

Piercey, S.J., 2014, Modern analytical facilities 2. A review of quality assurance and quality control (QA/QC) procedures for lithogeochemical data: *Geoscience Canada*, v. 41, p. 75–88.

Ryan, R.J., and Smith, P.K., 1998, A review of the mesothermal gold deposits of the Meguma Group, Nova Scotia, Canada: *Ore Geology Reviews*, v. 13, p. 153–183.

Sangster, A.L., 1992, Light stable isotope evidence for a metamorphogenic origin for bedding-parallel, gold-bearing veins in Cambrian flysch, Meguma Group, Nova Scotia: *Exploration and Mining Geology*, v. 1, p. 69–79.

Sangster, A.L., 1990, Metallogeny of the Meguma Terrane, Nova Scotia, *in* Sangster, A.L. ed., *Mineral Deposit Studies in Nova Scotia: Volume 1, Geological Survey of Canada*, p. 115–162.

Sangster, A.L., and Smith, P.K., 2007, Summary of the Meguma Gold Deposits, Nova Scotia, *in* Goodfellow, W.D. ed., *Mineral Deposits of Canada: A Synthesis of Major Deposit-Types, District Metallogeny, the Evolution of Geological*

Provinces, and Exploration Methods, Geological Association of Canada, Mineral Deposits Division, p. 727–732.

Sillitoe, R.H., and Bonham Jr., H.F., 1990, Sediment-hosted gold deposits: Distal products of magmatic-hydrothermal systems: Geology, v. 18, p. 157–161.

Spooner, E.T.C., 1993, Magmatic sulphide/volatile interaction as a mechanism for producing chalcophile element enriched, Archean Au-quartz, epithermal Au-Ag and Au skarn hydrothermal ore fluids: Ore Geology Reviews, v. 7, p. 359–379.

van Staal, C.R., 2007, Pre-Carboniferous metallogeny of the Canadian Appalachians., *in* Goodfellow, W.D. ed., Mineral Deposits of Canada: A Synthesis of Major Deposit Types, District Metallogeny, the Evolution of Geological Provinces, and Exploration Methods., Geological Association of Canada, Mineral Deposits Division, Special Publication no. 5, p. 793–818.

van Staal, C.R., and Barr, S.M., 2012, Lithospheric architecture and tectonic evolution of the Canadian Appalachians and associated Atlantic margin: Tectonic Styles in Canada: the LITHOPROBE Perspective, Geological Association of Canada Special Paper, v.49, p. 41–95.

Upton, P., and Craw, D., 2014, Extension and gold mineralisation in the hanging walls of active convergent continental shear zones: Journal of Structural Geology, v. 64, p. 135–148.

Waldron, J.W.F., White, C.E., Barr, S.M., Simonetti, A., and Heaman, L.M., 2009,
Provenance of the Meguma terrane, Nova Scotia: Rifted margin of early
Paleozoic Gondwana: Canadian Journal of Earth Sciences, v. 46, p. 1–8.

Weatherley, D.K., and Henley, R.W., 2013, Flash vaporization during earthquakes
evidenced by gold deposits: Nature Geoscience, v. 6, p. 294–298.

White, C.E., 2010, Stratigraphy of the Lower Paleozoic Goldenville and Halifax groups
in the western part of southern Nova Scotia: Atlantic Geology, v. 46, p. 136–154.

Williams, H., Dehler, S.A., Grant, A.C., and Oakey, G.N., 1999, Tectonics of Atlantic
Canada: Geoscience Canada, v. 26, p. 51–70.

Williams, P.F., and Hy, C., 1990, Origin and Deformational and Metamorphic History of
Gold-Bearing Quartz Veins on the eastern Shore of Nova Scotia, in Sangster, A.L.
ed., Mineral Deposit Studies in Nova Scotia: Volume 1, Geological Survey of
Canada, p. 169–194.

Zoheir, B., Steele-MacInnis, M., and Garbe-Schönberg, D., 2019, Orogenic gold
formation in an evolving, decompressing hydrothermal system: Genesis of the
Samut gold deposit, Eastern Desert, Egypt: Ore Geology Reviews, v. 105, p. 236–
257

Chapter 1 Figures

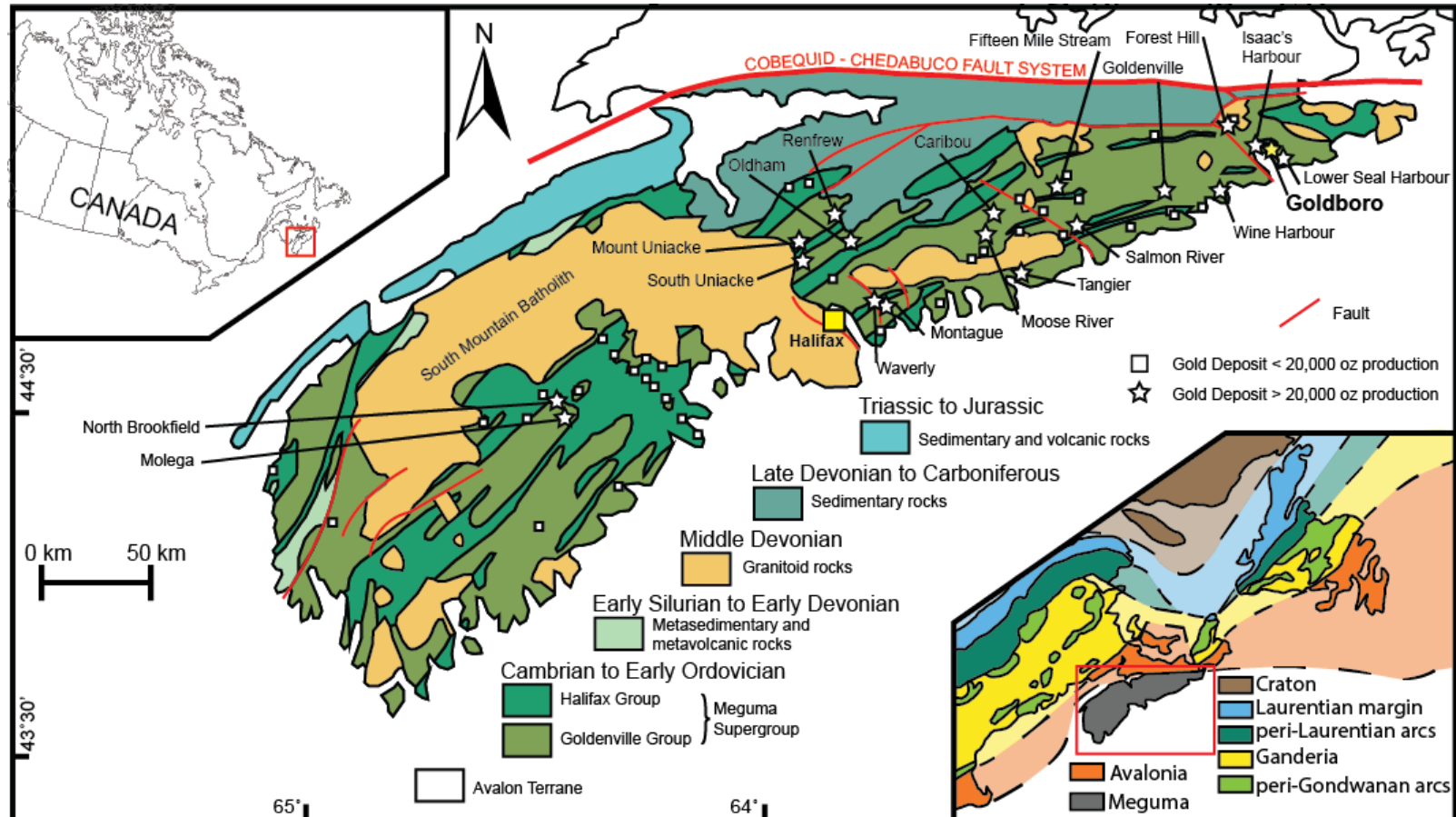


Figure 1.1: Regional map of the Meguma Terrane and its major gold deposits. Gold production data from Sangster and Smith (2007), modified from Kontak et al. (2013)

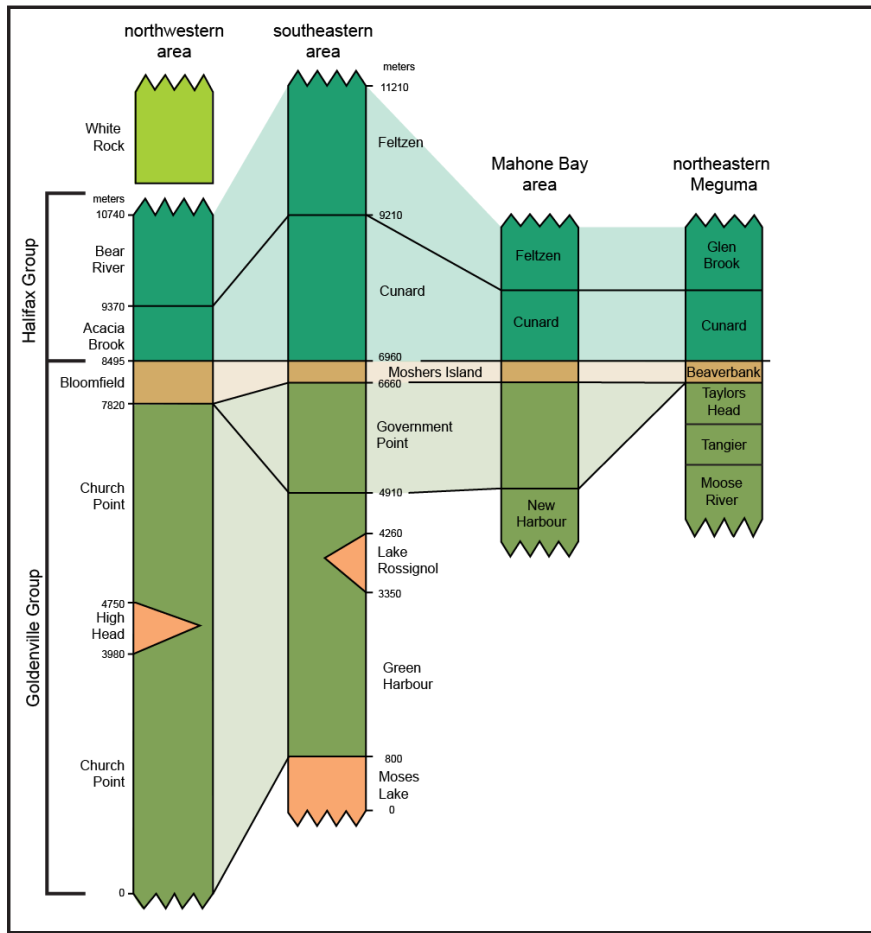


Figure 1.2: Regional stratigraphy of the Meguma Terrane, including regionally mapped formations. For these sections, no stratigraphic thickness is implied. Modified from White (2010).

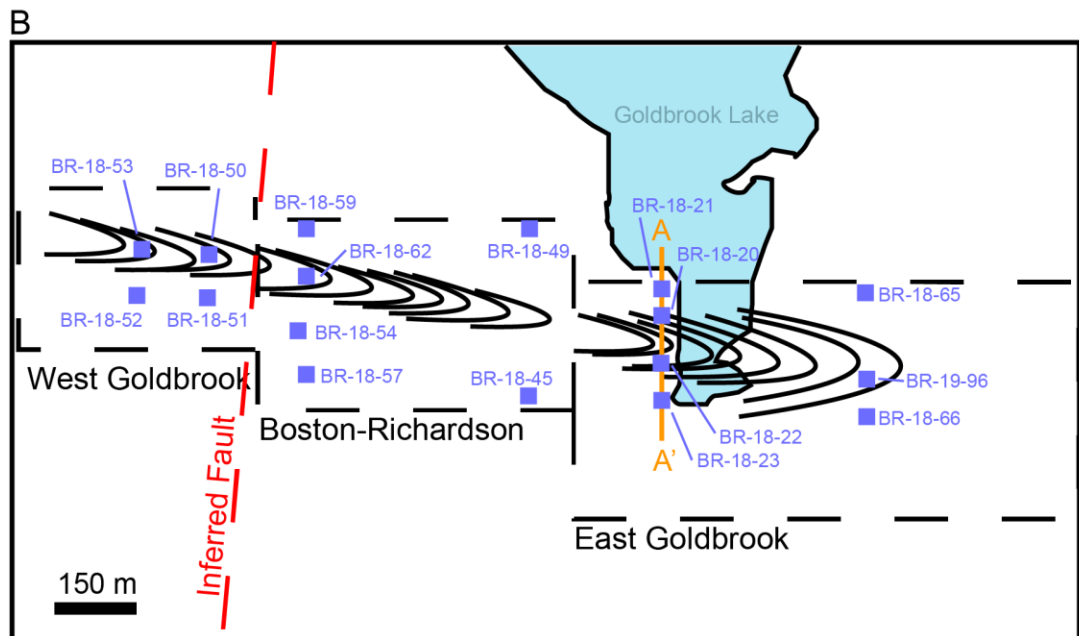
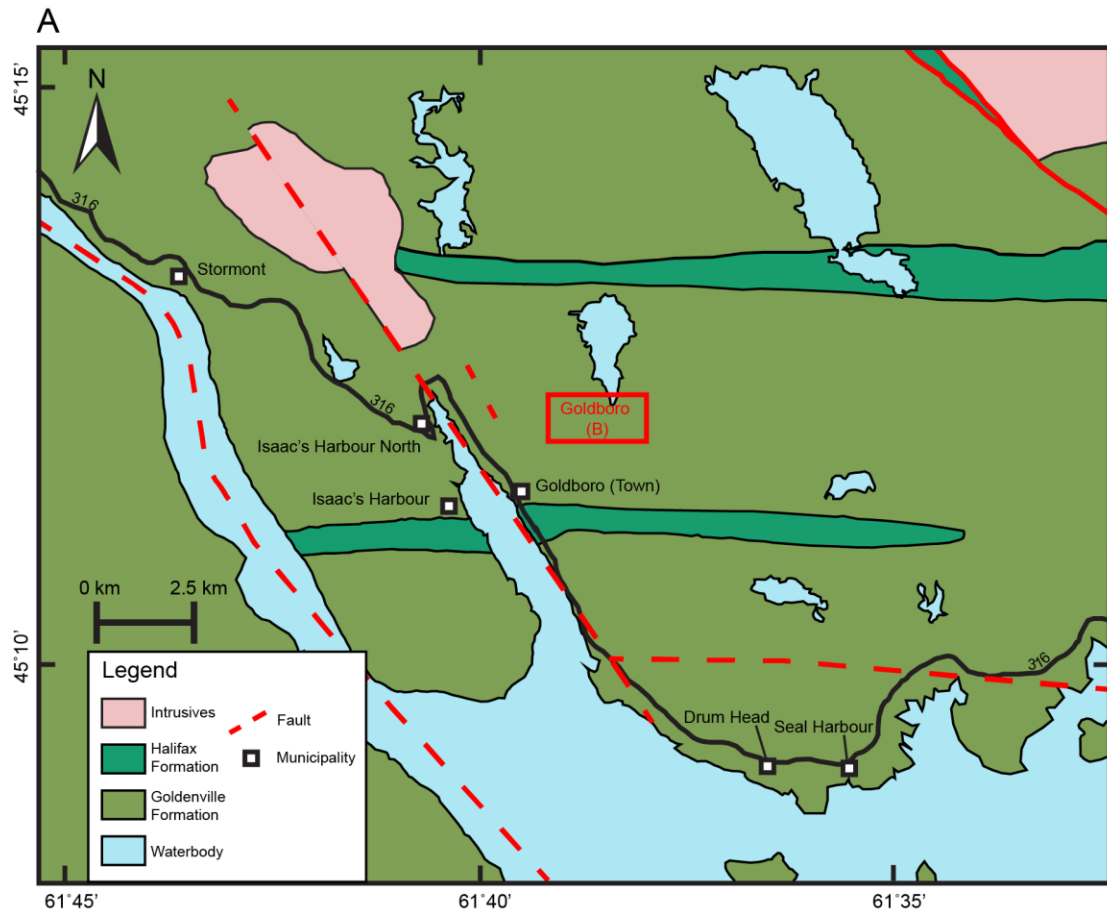


Figure 1.3: a)
Simplified local geological map of the Goldboro deposit, Nova Scotia (modified from Ryan and Smith, 1998). b) Plan view of the Goldboro property, depicting the stratigraphic belts and drillholes logged in this study. The fault shown here separated the BR zone from the WG zone. The line A-A' in b) denotes the cross section shown in Figure 1.4.

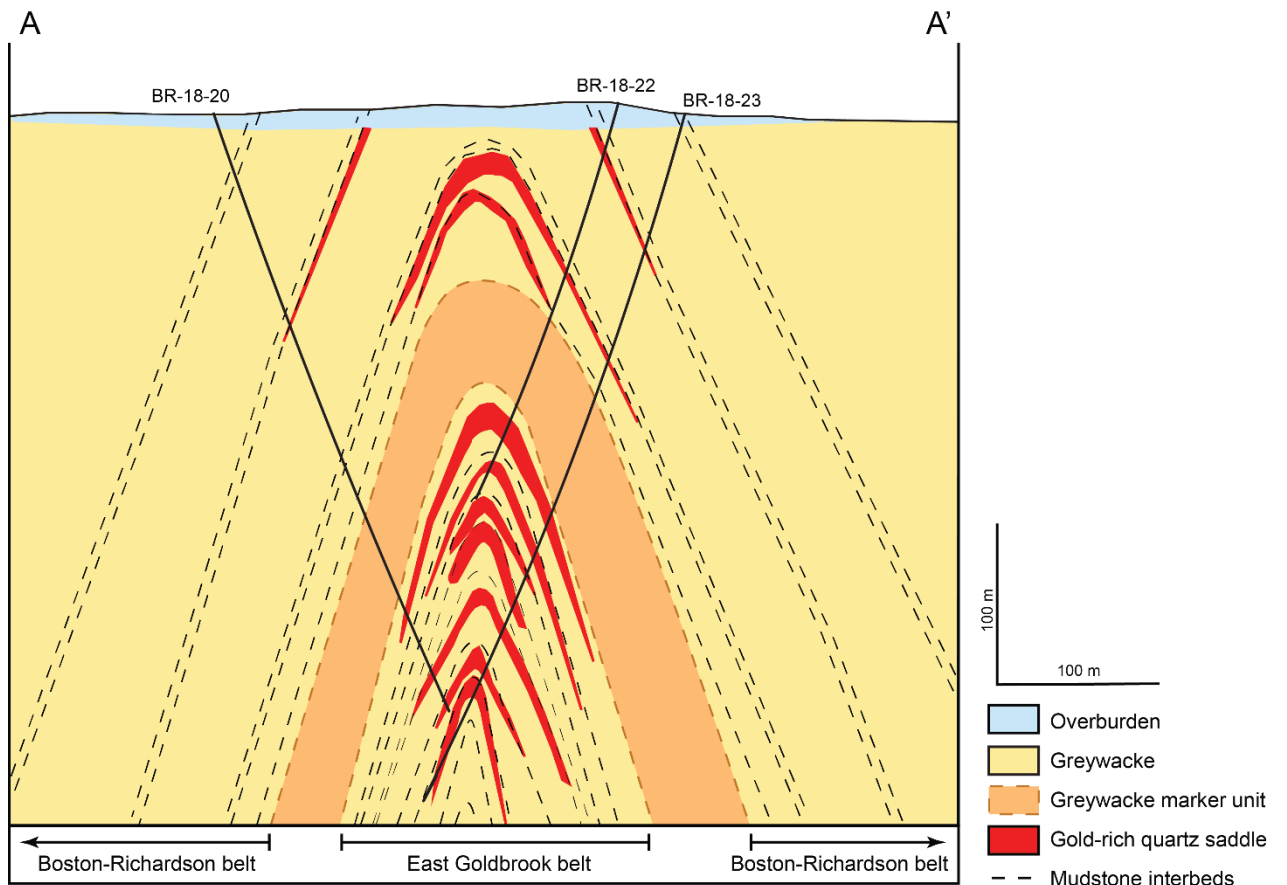


Figure 2.4: Cross-section of the Goldboro deposit (facing East), the line A-A' is shown in the inset of Figure 2.3 (modified from Kuntz et al., 2021). Shown are the East Goldbrook and the underlying Boston-Richardson belts, separated by a thick, massive greywacke unit used as a stratigraphic marker. Shown here is the higher density of mudstone interbeds and quartz saddles in the Boston-Richardson relative to the East Goldbrook.

Chapter 2: Lithogeochemistry and Genesis of a Meguma Terrane-Hosted Gold Deposit: Goldboro, Nova Scotia, Canada

2.1 Abstract

The Goldboro sediment-hosted orogenic gold deposit (16,036,000 tonnes @ 3.78 g/t Indicated and Measured, 5,306,000 tonnes @ 4.68 g/t Inferred; 1,946,100 oz and 798,100 oz Au, respectively), Nova Scotia, Canada, is hosted in the Goldenville Group of the Meguma Terrane. Mineralization at Goldboro is primarily hosted within stratiform quartz saddle and leg reefs along the Upper Seal Harbour anticline and locally within discordant veins and disseminated in wall-rock. The wall-rock at Goldboro is composed of repeating, graded turbidite successions that fine upwards from fine-grained greywacke to mudstone. The primary purpose of this study is to document alteration assemblages, paragenesis, understand fluid-rock interaction, and provide insight into the genesis of the Goldboro deposit. Detailed lithogeochemical studies of this kind have not been conducted on deposits hosted in the Meguma Terrane, and this study provides valuable insight into the alteration systematics of the Goldboro deposit.

The Goldboro deposit consists of four stages of quartz vein mineralization: V1) foliated, bedding-parallel, glassy quartz veins that are rich in arsenopyrite, chalcopyrite, pyrrhotite, and sphalerite; V2) foliated, bedding-parallel, milky white quartz veins that only contain arsenopyrite; V3) non-foliated, tan,

carbonate-rich veinlets that infill brecciation and fractures within wall-rock, and; V4) non-foliated albite+K-feldspar+chlorite+biotite+quartz+carbonate (\pm ilmenite, fluorapatite, gold) pegmatitic veins. The latter veins (V4) are interpreted to be magmatic-hydrothermal in origin and suggest potential magmatic-hydrothermal inputs into the Goldboro orogenic gold deposit; this insight has significant implications regarding the genesis of other Meguma-type gold deposits, suggesting late magmatism may play a role in gold upgrading, regionally.

The veins and associated mineralization are associated with distinct alteration footprints. Sericite alteration of mudstones is the broadest, most easily recognized hydrothermal footprint and extends >100 m from the hinge of the Upper Seal Harbour anticline. V1 veins exhibit biotite alteration of the wall-rock, and V4 veins exhibit albite+sericite, biotite, and chlorite alteration of the mudstone, and sericite+albite alteration of greywacke. Biotite and chlorite alteration halos of both vein types span multiple meters from their respective source vein and the Mn, Fe, and Mg contents of the micas are distinct between vein generations. Albite+sericite alteration extends \leq 3 cm from V4 veins in mudstones. Oblloid quartz+biotite+K-feldspar (\pm pyrrhotite, arsenopyrite) blebs (3-5 mm) are observed near-ubiquitously in mudstone at Goldboro and are interpreted to represent relic features of diagenetic pyrite.

Mass change calculations and principal component analysis (PCA) demonstrate that all mudstones have increased SiO₂ due to quartz veinlets, whereas mudstone samples with biotite and chlorite alteration exhibit increased

Fe_2O_3 and MgO . Sericite altered rocks exhibit losses in K_2O , CaO , and Na_2O . Albite alteration exhibits gains in CaO , and Na_2O and losses in Fe_2O_3 and MgO . Certain quartz saddle-proximal mudstone beds exhibit a gain in Sb , but this gain is not ubiquitous throughout the deposit. Large-ion lithophile elements (LILE; viz., Rb , Ba , Cs) share similar patterns to K_2O , with the exception of Sr , which mimics the pattern of CaO . The concentration of As varies widely due to the heterogeneous distribution of arsenopyrite in the mudstones. The chemical trends mentioned above were used to construct an alteration framework for vectoring towards alteration.

2.2 Introduction

Since sparking the first Canadian gold rush in 1861, orogenic gold deposits of the Meguma Terrane have historically been significant contributors to the economy of eastern Canada (Malcolm, 1929). Despite their economic significance both in the Meguma Terrane and globally, their origin, and that of orogenic gold deposits in general, remains debated (Sangster and Smith, 2007; Goldfarb and Groves, 2015; Groves et al., 2019). In the Meguma Terrane there are fundamental questions that remain unanswered, including (after Sangster and Smith, 2007): 1) what is(are) the mechanism(s) of gold deposition for Meguma-type gold deposits?; 2) what is the hydrothermal footprint of Meguma-type gold deposits and how do they compare to other sediment-hosted orogenic gold districts globally?; and 3) what are the genetic relationships between regional orogenesis, magmatism, and gold deposition in the Meguma Terrane?

Metamorphic devolatilization has been commonly invoked as a driver for orogenic gold mineralization in sediment-hosted orogenic gold deposits (Groves et al., 2019). In this model, mineralizing fluids are derived from the regional metamorphic devolatilization of the crust where there is the breakdown of chlorite to amphibole generates hydrothermal fluid and the breakdown of pyrite leads to release of metals, including Au, and H₂S needed for the transport and deposition of Au (Pitcairn et al., 2010). However, in orogenic gold deposits that are spatially and temporally associated with granitic intrusions, like Meguma-type deposits, a mixture of metamorphic and magmatic-hydrothermal fluid are involved in the formation of some deposits, although the mechanism by which is unclear (Kontak and Horne, 2010; Kontak et al., 2011). Recent work has demonstrated that orogenic gold deposits can be upgraded by the local dissolution and reprecipitation of Au, leading to increased Au grades via zone refinement, with these systems effectively being open systems that are continuously refined and upgraded during polyphase orogenesis (Hastie et al., 2020, 2021; Gourcerol et al., 2020).

The metamorphic model has been invoked to explain many world-class sediment-hosted orogenic gold deposits, such as in the Victorian gold belt, Otago schist belt, and at Sukhoi Log (Groves et al., 2019). These deposits are known to have been upgraded via aseismic refinement, where gold is upgraded by means of pressure dissolution of quartz and carbonate and the deposition of gold along pressure solution surfaces (Voisey et al., 2020). Deposits hosted in the Meguma

Terrane are often lumped into this “metamorphic” category, but evidence of a mineralization age coinciding with regional igneous activity suggests that this model does not fully explain the formation of Meguma-type deposits. A number of studies suggest that gold mineralization occurred during two events in the Meguma Terrane: an initial event during the onset of metamorphism, and a later event that is temporally associated with regional plutonism (Kontak et al., 1990, 1993, 1998; Kontak and Archibalt, 2002; Morelli et al., 2005; Kontak et al., 2011). The deposition of gold during the time period of regional emplacement of plutonism raises the possibility that these plutons played a key role in the metallogeny of the Meguma Terrane.

In addition to uncertainties in the genetic model for Meguma-type deposits there is also minimal recent research on hydrothermal alteration and lithogeochemistry of Meguma-type orogenic gold deposits compared to other sediment-hosted orogenic gold districts (e.g., Dugdale et al., 2007, 2009; Rusinov et al., 2008; Hamisi et al., 2017), with very little known about the types and extent of hydrothermal alteration and its spatial relationship to gold mineralization. This impacts not only our understanding of ore formation, but also our exploration approach.

The Goldboro deposit (also Upper Seal Harbour deposit) is one of the largest orogenic gold deposits in the Meguma Terrane (16,036,000 tonnes @ 3.78 g/t Indicated and Measured, 5,306,000 tonnes @ 4.68 g/t Inferred, 1,946,100 oz and 798,100 oz Au, respectively)(Ryan and Smith, 1998; Sangster and Smith,

2007, Kuntz et al., 2021). The deposit has well-defined stratigraphy and structure and an extensive library of drill core from recent exploration, making it an ideal natural laboratory for resolving and testing the questions cited above. The stratigraphic and structural framework established during previous exploration (Kuntz et al., 2021), allows this study to provide deeper insight into the ore mineral and vein paragenesis, lithogeochemistry and mineralogy of host stratigraphy and wall-rock alteration, nature of fluid-rock interaction, and genesis of the deposit.

This study documents the geology and stratigraphy of mineralization, wall-rock alteration assemblages and their distribution, and the lithogeochemistry and mineral chemistry of host rocks and alteration assemblages. These are used to understand both chemostratigraphy and the hydrothermal footprint, the latter having the potential to provide chemical and mineral/mineral chemical vectors to gold mineralization. This work will provide insight into the processes responsible for gold formation at Goldboro but also has implications other deposits in the Meguma Terrane and sediment-associated orogenic gold deposits globally.

2.3 Geological Setting

The Appalachian orogen in eastern Canada is composed of five tectonostratigraphic belts: the Humber, Dunnage, Gander, Avalon, and Meguma zones (Fig. 2.1)(Williams, 1979). The Meguma zone, which hosts the Goldboro deposit, was a peri-Gondwanan microcontinent that was accreted onto composite Laurentia during the Neoacadian orogeny in the Early Devonian to the Early

Carboniferous (van Staal, 2007; van Staal et al., 2009). Despite only outcropping in Nova Scotia, the regional extent of the Meguma Terrane is much larger; it has been identified offshore, extending from the Grand Banks of Newfoundland to Cape Cod, Massachusetts (van Staal and Barr, 2012). The accretion of the Meguma Terrane to composite Laurentia was accommodated by the Cobequid-Chedabucto fault system (CCFS), which separates the Meguma Terrane from the neighbouring Avalon Terrane to the North (White, 2010; van Staal and Barr, 2012).

The Meguma Terrane is defined by two main units: the thick (>12 km) Early Cambrian to Early Ordovician (537-475 Ma) Meguma Supergroup and the mid-Devonian to Early Carboniferous South Mountain Batholith (SMB) and its associated plutons (Kontak and Reynolds, 1994; Waldron et al., 2009; White, 2010; Gingras et al., 2011; van Staal and Barr, 2012). Following its accretion to composite Laurentia, the Meguma Terrane underwent periodic, intense orogenesis between 395-320 Ma, during which the terrane was regionally folded and metamorphosed to greenschist facies and, locally, to amphibolite facies (Sangster and Smith, 2007; van Staal and Barr, 2012). The SMB and its satellite plutons were emplaced during this period of orogenesis at ca. 375 Ma (Hicks et al., 1999; Sangster and Smith, 2007; van Staal and Barr, 2012).

The Meguma Supergroup is divided into the lower metagraywacke-dominated Goldenville Group and the overlying mudstone-dominated Halifax Group (Fig. 2.2)(Horne and Pelley, 2007). Both groups have been further

subdivided into individual formations (Fig. 2.2). Sediment-hosted gold mineralization, including the Goldboro deposit, occurs throughout the Goldenville Group. In contrast, the Halifax Group contains fewer gold deposits, albeit the Halifax Group covers a much smaller area of the Meguma Supergroup (Horne and Pelley, 2007; Sangster and Smith, 2007; White, 2010; van Staal and Barr, 2012).

2.4 Deposit Geology

The Goldboro deposit is located on the eastern shore of Nova Scotia, approximately 5 km northeast of the town of Goldboro (Fig. 2.3). The deposit is hosted in the greywacke and mudstone of the Goldenville Group, within repeating, thin (cm-scale to 10s of meters) fining-upwards successions of sandstone to mudstone. These successions contain some local areas of sedimentary rocks metamorphosed to the lower greenschist facies. The stratigraphy at Goldboro is folded into the Upper Seal Harbour anticline, an upright, east-west trending shallowly east plunging antiformal anticline. The property is cut by at least three regional brittle faults that dip steeply and strike to the northeast and south.

2.5 Mineralization and Alteration

2.5.1 Lithofacies, Lithostratigraphy, and Mineralization

The deposit contains three previously defined zones (Ryan and Smith, 1998; Kuntz et al., 2021): the Boston-Richardson, the East Goldbrook, and the West Goldbrook Gold Systems. These zones are separated based on their geographic position relative to historical mine workings, as well as their

lithostratigraphic positions (see inset on Figure 2.3). The Boston-Richardson and East Goldbrook are separated by a thick (20-60m), massive greywacke marker unit that is generally barren of mineralization. A fault cutting through the property separates these two Gold Systems from the West Goldbrook; the latter is stratigraphically equivalent to the Boston-Richardson. A cross-section showing the stratigraphy of the Goldboro deposit is shown in Figure 2.4. Unless specified, the West Goldbrook is considered equivalent to the Boston-Richardson herein.

The lithology of the Boston-Richardson and the East Goldbrook Gold Systems are very similar, the two zones differ mainly in the thicknesses of the turbiditic successions that host quartz veins (Fig. 2.4, 2.5). Specifically, the East Goldbrook contains thick fining-upwards successions (≤ 20 m) that are dominated by massive greywacke. In contrast, the units that make up the Boston-Richardson zone are thinner (≤ 15 m) and contain a higher proportion of mudstone (Fig. 2.5). Flexural slip folding has been identified as a main mechanism for quartz vein formation throughout the Meguma Group, primarily along mudstone-greywacke contacts and within mudstone units (Horne and Culshaw, 2001). The competency contrast between mudstone and greywacke units has also been identified as an important factor in quartz vein development in sediment-hosted orogenic gold deposits worldwide (Bierlein et al., 2004). Flexural slip in the Goldboro deposit was facilitated by the high abundance of mudstone units in the Boston-Richardson, resulting in thicker and more abundant quartz veins relative to the East Goldbrook.

Gold mineralization at Goldboro occurs in quartz veins or veinlets and is locally disseminated in wall-rock. At least four vein generations (V1 to V4) are present based on cross-cutting relationships and mineral assemblages (Fig. 2.6; Table 2.1). Two generations of bedding-parallel quartz veins occur and are interpreted to be syn-foliation: V1, the earliest stage of veining, and V2, the second stage of veining. V1 and V2 are linked to the main period of folding and cleavage development, as they are all foliated parallel to bedding. V1 veins are glassy, bedding-parallel quartz veins ranging from <1 cm-30 cm that contain pyrrhotite, chalcopyrite, sphalerite, and galena. Biotite wall-rock alteration is found proximal to V1 veins extending up to 5 m from the veins. V2 veins are thick (30 cm-5 m), milky-white (bull quartz) quartz veins that commonly contain euhedral arsenopyrite up to 10 cm in diameter; arsenopyrite alteration of the wall-rock is locally present and extends up to 5 cm from vein margins. Regional, late extensional A-C joints are also included in the V2 vein generation, and lie orthogonal to the fold hinge. Gold is reported to occur within V1 and V2 veins in saddle and leg reefs (Kuntz et al., 2021). V1 and V2 veins make up the vast majority of veins in Goldboro.

V3 and V4 are undeformed and cross-cut V1 and V2 veins; V3 and V4 tend to form preferentially along axial planar fractures. V3 veins are thin (\leq 5 mm) veinlets that commonly infill wall-rock fragments and cleavage in the wall-rock, and are tan coloured due to the presence of Fe-dolomite and ankerite; V3 veins do not have enveloping wall-rock alteration. V4 veins are \leq 5 cm thick, and are distinguished from the V3 veins by a different characteristic mineral assemblage,

including K-feldspar, albite, biotite, chlorite, apatite, ilmenite, and gold. V4 veins are the only vein generation that contain feldspars and are rich in feldspar, biotite and chlorite ($\geq 30\%$, modally). The V3 and V4 veins cross-cut one another in different locations and are interpreted to have been emplaced synchronously and/or cyclically. Gold is most commonly observed within V4 veins where they cross-cut V1-V2 veins. Albite, sericite, biotite/chlorite, and anatase alteration are closely associated with V4 veins in adjacent wall-rock and extend up to 20 m from V4 veins in the hinge of the Upper Seal Harbour anticline. V4 veins make up a very small proportion of quartz veins in Goldboro (~1 % by volume) but represent high-grade gold mineralization and overprinting by V4 veins may explain the distribution of high gold concentrations within V1 and V2 veins.

In contrast to the other vein types, V4 veins are particularly distinct due to their mineral composition and textures (Fig. 2.7). In addition to the vein mineralogy described above, V4 veins exhibit granophyric intergrowths (Barker, 1970) of quartz and K-feldspar, which is unique to this Goldboro vein generation (Fig. 2.7d-f).

2.5.2 Alteration

Alteration associated with quartz veins and gold mineralization is variable but is most intense and widespread in mudstones, rather than greywackes, and is particularly intense in the Boston-Richardson zone (Fig. 2.8, 2.9). Biotite and chlorite alteration are the most dominant alteration types and increase in intensity proximal to V1 and V4 veins (<5 m from vein margins)(Fig. 2.8, 2.9). Biotite and

chlorite alteration is patchy, and forms biotite and chlorite laths within mudstone. Biotite and chlorite also form rims around quartz-feldspathic blebs, which are discussed in the following paragraph. Sericite alteration is widespread and occurs throughout the stratigraphy, and was observed in the most distal samples from the hinge of the Upper Seal Harbour anticline (>150 m from the hinge). Sericite alteration is pervasive, increasing in intensity within 1 m of V4 veins in the limbs of the fold, and within 20 m of V4 veins in the hinge of the fold. V4 veins are associated with visible bleaching, a combination of albite alteration and sericite alteration. Visible bleaching is highly localized, extending \leq 1 cm from V4 veins. Widespread bleaching also occurs in greywacke units, but there is no spatial association between greywacke bleaching and V4 veins; it is not known definitively which vein stage is responsible for greywacke bleaching. In contrast to most orogenic gold deposits, carbonate alteration at Goldboro is low-intensity in the surrounding wall-rock, but carbonates are common vein components.

A common feature of the Goldboro mudstones is abundant 3-5 mm obloid blebs that consist of quartz+biotite+K-feldspar+chlorite+pyrrhotite+apatite (\pm ilmenite, chalcopyrite, and sphalerite) in variable proportions (Fig. 2.8e,f). These blebs are common features proximal to and within Meguma gold deposits, but their origin is not well understood (Kontak and Smith, 1993; Sutton, 2007). Melvin (1987) described them as mineral lineations but they were later recognized as biotite-rich mineral aggregates (Kontak and Smith, 1993; MacDonald, 1998). A number of suggestions have been made regarding the origin of the blebs:

retrograde metamorphosed andalusite; replaced cordierite; a replacement feature of sulfides; and isolated microliths of metasiltstone (Kontak et al., 1993; Sutton, 2007). Sutton (2007) refined the possible origins of the blebs to: 1) a relict feature of replaced sulfides; or 2) microliths of metasiltstone. Furthermore, Sutton (2007) suggests that neither process is singularly responsible for bleb formation on a regional scale. In Goldboro, these blebs are biotite-dominated proximal to V1 and V4 veins and contain arsenopyrite cores with biotite or chlorite rims proximal to V2 veins; there are no blebs proximal to V3 veins. The blebs ubiquitously contain pyrrhotite, arsenopyrite, and chalcopyrite in varying amounts. Due to the high sulfide (viz. pyrrhotite, arsenopyrite, sphalerite, and chalcopyrite) content within blebs, we suggest that the blebs were likely formed by the replacement of early (diagenetic?) sulfides, such as arsenian pyrite, in the host mudstones at Goldboro.

2.6 Paragenesis

2.6.1 Overview

The paragenesis of mineralization and vein development at Goldboro is divided into six stages: primary/diagenetic; pre-vein; V1; V2; V3; and V4 (Fig. 2.10). The paragenesis was determined by cross-cutting vein relationships and mineral textures derived from fieldwork, petrography, and scanning electron microscopy (SEM).

The earliest stage of mineralization at Goldboro is the primary/diagenetic stage. These minerals include pyrite, pyrrhotite, and ilmenite, and occur along bedding planes and laminations and/or are found within diagenetic cement (e.g.,

quartz/calcite). These minerals are interpreted to have been deposited as detrital grains (e.g., ilmenite) or formed shortly after deposition during burial and diagenesis (e.g., diagenetic pyrite and pyrrhotite). The diagenetic pyrite is only observed as cores within arsenopyrite and was largely replaced during later mineralization stages. Pyrrhotite is commonly visible in hand-sample; in thin section and SEM, pyrrhotite contains inclusions of quartz. Ilmenite is much finer-grained and is only visible through petrography, occurring as small ($\leq 100 \mu\text{m}$) anhedral nodules.

The pre-vein stage of mineralization describes minerals in the wall-rock that appear to predate vein formation, but there lacks sufficient evidence to consider them primary or diagenetic. Pre-vein minerals include an early generation of euhedral arsenopyrite that contain framboidal pyrite cores; these phases are typically found in quartz-biotite blebs, but their paragenetic timing is uncertain.

V1 veins ($\leq 30 \text{ cm}$) are bedding-parallel, foliated, and contain euhedral quartz, arsenopyrite, chalcopyrite, sphalerite, and galena as in-vein minerals, and patchy or bladed biotite, chlorite, and sericite as wall-rock alteration (Fig. 2.5a). The V1 stage is interpreted to have formed during compression, as the foliation of V1 veins is continuous with host-rock deformation.

Compared to V1 veins, V2 veins ($\leq 5 \text{ m}$) are relatively barren, containing largely quartz and coarse ($\leq 10 \text{ cm}$) euhedral arsenopyrite. V2 veins rarely exhibit arsenopyrite mineralization of the wall-rock proximal to veins (Fig. 2.5b). As V2

veins are also foliated and form the majority of saddle reefs in the deposit, the V2 stage is also interpreted to have occurred during compression. V3-stage mineralization consists of thin (≤ 5 mm), tan, carbonate-rich veinlets that are undeformed, cross-cut bedding, and infill breccia of the wall-rock and pre-existing quartz veins. Quartz, pyrite, and Fe-dolomite are typical phases within the veinlets and they do not have significant wall-rock alteration associated with their margins (Fig. 2.5c). Like V3 veins, V4 veins are undeformed, cross-cut bedding and are thinner than V1 and V2 veins, but up to 5 cm in thickness. V4 veins are most commonly observed within earlier vein types, occurring as infills of fractures and microfractures. Standalone V4 veins are uncommon compared to other vein generations. The mineral assemblage of V4 veins is very distinct compared to the other vein generations and contains K-feldspar, albite, quartz, muscovite, ilmenite, chalcopyrite, sphalerite, galena, arsenopyrite, fluorapatite, biotite, chlorite and gold (Figure 2.6d; Fig. 2.7).

Wall-rock alteration assemblages are distinct for each vein generation (Fig. 2.5; Fig. 2.10). V1 veins commonly exhibit biotite and chlorite alteration of their vein margins, extending up to 1 cm into the country rock (Fig. 2.8, 2.9). V2 exhibits occasional arsenopyrite alteration of the wall-rock, but lacks the biotite and chlorite alteration associated with V1 veins. V3 does not exhibit any discernable alteration. V4-stage wall-rock alteration minerals include anatase/rutile, albite, sericite, and chlorite extend up to 5 cm from V4 vein margins (Fig. 2.8; Fig. 2.9).

2.6.2 Arsenopyrite

Arsenopyrite is commonly associated with gold in Meguma-type gold deposits and other orogenic gold districts globally (Ryan and Smith, 1998; Bierlein et al., 2004; Sangster and Smith, 2007). There are two generations of arsenopyrite at Goldboro (Fig. 2.11a).

Arsenopyrite 1 is a pre-vein stage of arsenopyrite and is formed by the replacement of pyrite with arsenopyrite (Fig. 2.11b). This generation of arsenopyrite is typically bedding-parallel or disseminated in the wall-rock and is fine-grained (≤ 5 mm) relative to arsenopyrite 2. Arsenopyrite 1 commonly hosts abundant chalcopyrite, pyrrhotite, galena, sphalerite, and rarely native gold, as inclusions. It can also display a “porous” texture of unfilled voids. Occasionally, chalcopyrite, pyrrhotite, galena, and sphalerite partially replace arsenopyrite 1; arsenopyrite 1 is commonly replaced by arsenopyrite 2 (Fig. 2.11a). In contrast, arsenopyrite 2 forms as a vein-stage mineral during V1, V2, and V4 events and is coarser-grained than arsenopyrite 1 (≥ 5 mm). Arsenopyrite 2 hosts very few inclusions in comparison to arsenopyrite 1, occasionally containing galena. Arsenopyrite 2 is also more closely related to gold mineralization, containing gold inclusions, cores, and wires along fractures.

2.6.3 Gold

At Goldboro, historically it has been interpreted that gold is largely hosted in V1 and V2 quartz saddles along the Upper Seal Harbour anticline (Ryan and Smith, 1998; Kuntz et al., 2021). Whereas most gold mineralization is hosted in

quartz saddles, on a smaller scale gold is closely associated with V4 veins that cross-cut bedding-parallel veins. Thus, gold mineralization or gold remobilization occurred later in the paragenesis at Goldboro than previously thought. Gold has two main morphologies at Goldboro: 1) as free gold in veins; and 2) in close association with arsenopyrite 1 and 2 as cores, inclusions, and wires along fractures (Fig. 2.11c,d). Gold inclusions occur in arsenopyrite 1 and are commonly associated with sphalerite, chalcopyrite, galena, and pyrrhotite inclusions. In contrast, gold inclusions, cores, and wires occur alone in arsenopyrite 2, or locally associated with galena (Fig. 2.11a,c,d).

2.7 Geochemical and Mineralogical Methods

2.7.1 Lithogeochemistry

A total of 109 drill core samples of mudstone were analyzed for whole-rock geochemistry to understand primary geochemistry of the sedimentary rocks and superimposed alteration. Mudstone was preferentially sampled and analyzed as it is more homogenous than greywacke, is found intimately associated with orogenic Au mineralization, and displayed more pervasive alteration than the greywacke units. Samples were spatially selected to achieve coverage across the Upper Seal Harbour anticline, between the East Goldbrook, Boston-Richardson, and West Goldbrook zones, and to obtain downhole alteration profiles. Alteration is most intense in the hinge of the Upper Seal Harbour anticline proximal to mineralization, so samples distal to the hinge were selected to provide a background of least altered samples for mass-balance calculations.

All samples were half or quartered drill core, roughly 15 cm in length. All samples were trimmed of any non-representative contaminants, such as quartz veins, using a water-cooled Dewalt tile saw in the CREAT Lapidary and Saw Facility at Memorial University of Newfoundland, then washed in order to mitigate contamination from the rock saw, and individually bagged in labelled polyurethane bags. The samples were sent to ALS Minerals Laboratories in Sudbury, Ontario, for further preparation and analysis. At ALS, all samples were crushed using an agate mill to minimize contamination of the sediment and then split. The samples were then analyzed for various elements using the complete characterization package (CCP-PKG01; all analytical codes refer to those of the ALS website). Major elements were analyzed using lithium metaborate fusion and subsequent dissolution of the fusion bead in acid and analyzed with an inductively coupled plasma atomic emission spectrometer (ICP-AES) finish. Total carbon and sulfur were analyzed using Leco; inorganic carbon was analyzed using perchloric (HClO_4) acid digestion and analysis by CO_2 coulometer (analysis package C-GAS05). Some metals (Ag, Cd, Co, Cu, Li, Mo, Ni, Pb, Sc, and Zn) were determined using four-acid digestion and an inductively coupled plasma mass spectrometer (ICP-MS) finish. Volatile elements and metalloids (As, Bi, Hg, In, Re Sb, Se, Te, and Tl) were determined by aqua regia digestion and ICP-MS finish. Lithophile trace elements, including high field strength elements (HFSE), low field strength elements (LFSE), and rare earth elements (REE), were analyzed using lithium borate fusion, followed by four-acid digestion and an ICP-MS finish. Gold was analyzed using fire assay and an ICP-AES (AuICP21) finish;

samples with detection overlimits were re-determined by gravimetric methods. Quality assurance and quality control (QA/QC) was evaluated by using CMIC-1, an internal Au-bearing mudstone reference material, which was included with the samples in the method described in Piercey (2014), in addition to ALS internal standards. The standard was shaken for a minimum of 30 seconds prior to sampling to ensure the homogenous distribution of heavy minerals that would normally settle to the bottom of the container. The measure of precision (%RSD) for the mudstone standard was <4% for major elements except for MnO and P₂O₅, which were below the limit of quantification (LOQ); MnO and P₂O₅ returned %RSD <7%. The %RSD of trace elements above the limit of quantification (LOQ) was <10%, except for elements As, Li, Mo, and Au (83%, 19%, 32%, and 167%, respectively. The measure of accuracy (%RD) was <5% for all elements above the LOQ except for Ga, Ta, Tm, As, Tl, Li, Mo, Pb, and Au (13%, 13%, 7%, 1163%, 26%, 8%, 18%, 7%, and 88%, respectively). The notably high %RSD and %RD for As and Au were determined to be a result of cross-contamination and carry-over during analysis, respectively. This was determined by anomalously high As and Au concentrations in the interspersed standard. High As was random, but standards with high (carry-over) Au values occurred in the next analytical position following a sample with definably high Au. The high %RD values for other elements did not occur in the standard and were therefore determined to be a result of heterogeneity in the samples or, in the case of Li, due to contamination during Li-borate fusion.

2.7.2 Petrography and Scanning Electron Microscopy

A total of 110 thin sections were prepared at Vancouver Petrographics. Thin sections were polished to 30 µm thickness for standard petrography. Scanning electron microscopy (SEM) and energy dispersive X-ray (EDX) analysis were conducted on carbon-coated thin sections at the CREATIT Hibernia Electron Beam Facility at Memorial University of Newfoundland using a JEOL JSM 7100 F microscope for micro- to nanoscale textures and semi-quantitative analysis of minerals and textures. Thin sections were all carbon-coated before analysis to minimize surface charging. Petrography and SEM imaging were undertaken to establish alteration mineral assemblages, textural relationships, mineral assemblages, and micro-scale paragenetic relationships.

2.7.3 Electron Probe Microanalysis

A set of wall-rock and in-vein biotite (n=104) and chlorite (n=57) samples were analyzed by electron probe microanalysis (EPMA). Biotite and chlorite were chosen for analysis as they are widespread and are associated with both V1 and V4 veins. EPMA was somewhat exploratory, with the goal of these analyses being to determine if these micas were chemically distinct between the two vein generations and their proximity to veins. A total of 12 thin sections from across the Goldboro deposit were picked for analysis. These thin sections were chosen because they either exhibited chlorite or biotite alteration or they contained in-vein biotite or chlorite. The chosen sample set included thin sections from proximal and distal alteration zones, veins, and a least-altered sample. Because

biotite and chlorite alteration are localized to veins, a least-altered sample was chosen on the basis of it being distal from any known veins and it not exhibiting any alteration that could be identified using petrography. Analyses were conducted using a JEOL JXA 8230 electron EPMA with a W filament and five wavelength dispersive spectrometers (WDS) at the CREATIT Hibernia Electron Beam Facility at Memorial University of Newfoundland. Biotite grains were analyzed for elements Si, Al, Fe, Mg, Mn, Ca, Na, K, Ti, Zn, Ba, Sr, F, and Cl; chlorites were analyzed for these same elements as well as for Cr and V. The analyses were carried out with a spot diameter of 3 μm , electron beam current of 20 nA and an accelerating voltage of 15 kV. The X-ray takeoff angle was 40°, and the count time was 10-60 seconds depending on the element being analyzed, with off-peak (background) count times equal to half the peak count time. LIFL, LIFH, LDE1, PETL, and TAP crystals were used to determine concentrations of appropriate elements. A combination of natural and synthetic minerals were used as calibration standards at the start and end of each analytical session. Astimex biotite and chlorite were used as secondary standards and were analyzed at the beginning and end of each analytical session and every 30 unknown analytical points to check precision and accuracy. The results from EPMA analysis are compiled and presented in Appendix D. Stoichiometric calculations were conducted to determine the atoms per formula unit (APFU) for mineral identification and geothermometry. All analyses yielded results consistent with the stoichiometry of biotite and chlorite.

Chlorite (n=57) geothermometry was undertaken to provide estimates for the temperature of chlorite formation at Goldboro. Four geothermometers were tested (Kranidiotis and MacLean, 1987; Cathelineau, 1988; Zang and Fyfe, 1995; Xie et al., 1997), but only the temperatures calculated using the Cathelineau (1988) geothermometer were consistent with reported fluid inclusion homogenization temperatures (350-400°C) in Meguma deposits in Nova Scotia (Kontak and Smith, 1989, 1993; Kontak et al., 1990, 1996). The Cathelineau (1988) equation is $T(^{\circ}\text{C}) = -61.92 + (321.98 * \text{Al}^{\text{IV}})$.

2.8 Results

2.8.1 Principal Component Analysis

Principal component analysis (PCA) of the whole-rock geochemical data was undertaken using Reflex ioGAS 7.2 software for initial exploratory data analysis using a correlation matrix to: 1) determine the elemental variability in the data; 2) identify correlations between variables; and 3) to group those variables into principal components.

Before statistical analysis, the whole-rock data were corrected using a centered log-ratio transformation to correct for non-normality common in lithogeochemical data (e.g., Aitchison, 1986). The scree plot and eigenvalues of the dataset demonstrate that there are five principal components (PC), defined by having eigenvalues >1 (Fig. 2.12a). PC1, PC2, and PC3 were chosen to create biplots, explaining 37%, 14.3%, and 8.5% of the variation, respectively, and 59.8% cumulatively. The following processes and mineral assemblages were

determined to produce clusters that affect the principal components in PC1-PC2 and PC1-PC3 plots: 1) detrital feldspar, chlorite, ilmenite, and rutile (K_2O , Cr_2O_3 , TiO_2 , BaO , and Al_2O_3); 2) sulfides (viz. pyrrhotite, pyrite, and sphalerite); 3) biotite alteration (Fe_2O_3 , MgO , Ni , Zn); 4) zircon and manganese nodules (Zr , MnO); 5) quartz+carbonate veinlets and albite alteration (SiO_2 , CO_2 , CaO , Na_2O , SrO); 6) apatite (P_2O_5 , MnO); 7) and arsenopyrite, zircon, and galena (As , Pb , and Zr)(Fig. 2.12b,c). In PC1-PC2, the data disperses laterally in a way that correlates with sericite alteration, with the K_2O vector on the left and the $Na_2O+CaO-CO_3-Sr$ vectors on the right.

2.8.2 Lithogeochemistry

Representative lithogeochemical analyses for the Goldboro mudstone samples are presented in Table 2.2 and the entire dataset can be found in Appendices B (raw data) and D (mass balance). All samples from the Goldboro deposit are hydrothermally altered to some degree, and thus a limited list of elements can be used to understand the primary processes and primary chemostratigraphy. Immobile elements are typically utilized to see through alteration processes and infer information about primary lithogeochemistry and sediment provenance, whereas mobile elements characterize the hydrothermal processes that form the alteration footprint associated with mineralization (MacLean, 1990; McLennan et al., 2003). The combination of mobile and immobile elements is utilized in mass balance calculations, where elemental gains

and losses are calculated relative to examples of unaltered sediments or from projections from least altered examples (see discussion below) (MacLean, 1990).

2.8.1.1 Immobile Elements and Provenance

Immobile elements are especially useful for assessing primary processes, as they are not typically affected by hydrothermal alteration (Morton and Hallsworth, 1994; McLennan et al., 2003). Elements such as Al, Ti, Fe, Mn, Zr, Hf, Nb, Sn, Cr, Ni, V, Co, and the REE are typically highly compatible and are not released into solution (Taylor and McLennan, 1985; McLennan et al., 2003). However, some elements that are commonly accepted as immobile, such as Zr, Hf, Ti, Ni, V, and the REE, are highly enriched in certain mineral phases (e.g., apatite, monazite, zircon) that can be preferentially enriched by processes of sedimentary sorting and diagenesis (McLennan et al., 1993, 2003; Morton and Johnsson, 1993; Morton and Hallsworth, 1994; McLennan, 2001)

Following the procedure set by Kranidiotis and MacLean (1987), the immobility and homogeneity of the above elements can be evaluated (Fig. 2.13). When evaluated this way, Al_2O_3 and TiO_2 were determined to be immobile and homogenous (Fig. 2.13a,b). K_2O also appears to be immobile in these plots, however, there appears to be minor K^+ mobility as discussed below. Zr and Hf were non-linear (Fig. 2.13c,d) due to varying amounts of Zr- and Hf-bearing minerals (e.g., zircon) in the mudstones (McLennan et al., 1993, 2003). Additionally, immobile element pairs (i.e., Al_2O_3 and TiO_2) will plot along a straight line passing through the origin when plotted against one another.

Conversely, if the samples have multiple sources, they will plot along multiple trendlines (MacLean and Kranidiotis, 1987; MacLean, 1990; MacLean and Barrett, 1993). When plotting TiO_2 and K_2O vs. Al_2O_3 (Fig. 2.13a,b), the Goldboro mudstones plot along a single trendline, indicating they were derived from a single sediment provenance source.

Zr , Th , Cr , Sc , Y , Ni , and V are particularly useful for evaluating the provenance of mudstones because of their tendency to become enriched in certain mineral phases. The elements Th and Zr , when normalized to Sc , are beneficial for assessing provenance as both Th/Sc and Zr/Sc typically increase with igneous differentiation and maturity of crust (e.g., higher in continental vs oceanic crust), and Zr/Sc increases independently of Th/Sc during sediment recycling, reflecting accumulation of heavy minerals like zircon (McLennan et al., 2003). As shown in Figure 2.14a, the Goldboro shales plot close to the upper continental crust (UCC) with elevated Zr/Sc . These values are consistent with a passive continental margin, where sediments are subjected to recycling and are more enriched in heavier minerals. Cr/V vs. Y/Ni (Fig. 2.14b) provides insight into the ophiolitic and mafic sedimentary components; Y/Ni increases with mafic input (monitors general ferromagnesian trace elements like Ni against a proxy for HREE, Y), and Cr/V (chromite) increases with ophiolitic input (McLennan, 2003). As shown in Figure 2.14b, the Goldboro mudstones have both low Y/Ni and Cr/V , consistent with an UCC source and minimal input from juvenile (mafic/ultramafic) sources. Upper crust-normalized REE plots of host rock analyses were used to determine

whether the gold systems at Goldboro were chemically distinct from one another (Fig. 2.14c). The average REE patterns for the East Goldbrook are slightly more enriched than the Boston-Richardson, but the REE values do not differentiate the zones.

2.8.1.2 Mobile Element Lithogeochemistry

All mudstones at Goldboro have been altered to some extent and show a chemical index of alteration (CIA; CIA=(Al₂O₃/(Al₂O₃+CaO*+Na₂O+K₂O))*100) between 55 and 72. The data show a linear trend on a CIA ternary plot of CIA components (Nesbitt and Young, 1984) (Fig. 2.15), with a trend from the most unaltered mudstones towards increasing depletion in CaO*+Na₂O with increasing Al₂O₃. This linear trend spans from plagioclase towards decreasing Na₂O+CaO* and likely reflects different intensities of sericite, biotite, and chlorite alteration of mudstones, although biotite alteration is more explicitly evident using the 3K/Al alteration index.

A challenge when choosing a least altered sample in sedimentary rocks is that the composition of mudstone-greywacke successions can vary over distances as small as a few centimeters, possibly masking changes in K₂O and other oxides during alteration (Lickley et al., 1987). However, by using SiO₂/Al₂O₃ sorting curves, it is possible to estimate the original, pre-alteration K₂O content of altered samples. Consequently, the least altered samples can be distinguished, as they lie closely along a hyperbolic curve (Fig. 2.15b), whereas the altered samples exhibit

an elevated $\text{SiO}_2/\text{Al}_2\text{O}_3$ relative to the curve; the least-altered sample (385095,

Table 2.2) lies along this hyperbolic curve.

The alteration index $3\text{K}/\text{Al}$ represents K-mica alteration and is used here to describe sericite and biotite alteration. Values approaching the maximum value of 1.0 indicate that all of the available Al is held in K-mica (Christie and Braithwaite, 2003). As shown in Figure 2.16, K-mica alteration is ubiquitous throughout the Goldboro mudstones, with $3\text{K}/\text{Al}$ ranging between 0.6 and 1. More intense K-mica alteration is attributed to biotite alteration, which, when present, heavily affects this alteration index. $3\text{K}/\text{Al}$ approaches 1.0 proximal to large quartz saddles, where abundant biotite is present (Fig. 2.16). Additionally, the alteration index Na/Al , used to describe the intensity of albite alteration (Christie and Braithwaite, 2003), ranges from 0.0 to 0.2. Similar to $3\text{K}/\text{Al}$, Na/Al mirrors the pattern of Na in Figure 2.16, indicating that this alteration index can be used as a proxy for Na_2O .

2.8.1.4 Mass Change Calculations

In contrast to raw lithogeochemical data, mass change calculations estimate absolute gains and losses of elements during alteration, while considering volume and mass changes (Gresens, 1967; Grant, 1986; MacLean, 1990; MacLean and Barrett, 1993). Determining which elements are immobile is an essential reference for accurate mass balance calculations and evaluating primary processes, as immobile elements are not added nor removed during weathering and alteration.

Given the immobile element diagrams mentioned previously (Fig. 2.13a,b), samples from Goldboro can be modelled as originating from a single homogeneous precursor and the single precursor method of MacLean (1990) is utilized herein, where mass changes are determined by calculating the relative change from a uniform precursor rock composition. Al_2O_3 was determined to be highly immobile (Fig. 2.13a,b) and because it has a high concentration in the mudstones, Al_2O_3 was chosen as a basis to calculate enrichment factors (EF) for each sample.

The least-altered sample (Table 2.2, Appendices A, B – sample 385095) was chosen based on its position on the hyperbolic curve shown in Figure 2.15b, its low CIA, low content of alteration minerals, its distal location from the hinge of the Upper Seal Harbour anticline, as well as its low concentration of SiO_2 (55 wt. %) relative to other samples, indicating little to no SiO_2 contamination by quartz veins or silica alteration. Results for mass change calculations are discussed below. There is insufficient data density for a 3D alteration model that is compatible with field observations, but some of the data are presented in 2D as downhole profiles in Figure 2.16. Mass change histograms are shown in Figure 2.17.

SiO_2 : Mass changes in SiO_2 account for most mass gains and losses in the Goldboro mudstones and have the most pronounced mass changes of the major elements. Mass changes in SiO_2 range from -20% to >+100% (Fig. 2.17a, Appendix C); the highest mass gains of SiO_2 are found along the hinge of the

anticline, exemplified in Figure 2.16, where BR-18-62 is a downhole profile along the axial plane; this is attributed to extensive V1 and V2 veining in saddles, as well as V3 and V4 veining infilling fractures and breccia.

K₂O: K₂O exhibits both mass increases and mass losses, ranging from -2 wt.% to +1 wt.% (Fig. 2.17b). Mass loss in K₂O is attributed to sericite alteration of pre-existing detrital feldspar, whereas mass gains are likely due to a small degree of K⁺ addition via biotite alteration and K-feldspar mineralization. Given that the mudstone is composed of varying components of clay and silt/sand, there is a large amount of variability of K₂O in the precursor, and therefore mass changes in K₂O are not sufficient to systematically bias the initial heterogeneity of K₂O in the precursor. K-related alteration is therefore better evaluated using molar ratios and mass changes in other elements. In particular, the alteration index 3K/Al more specifically describes the intensity of K-mica alteration, which includes both biotite and sericite alteration, and mass gains in Fe₂O₃ and MgO are better tools to identify biotite alteration. Sericite alteration was observed petrographically in all samples, therefore defining a halo that extends >150 m from the hinge of the Upper Seal Harbour anticline.

Na₂O+CaO: The elements Na and Ca show similar mass change trends (Fig. 2.17c,d). There is a general mass gain for both elements common to all samples. However, the process attributed to these enrichments differs. For CaO, the mass gain is associated with the presence of V3 veinlets, which contain Ca-bearing carbonate minerals as a primary phase. In contrast, Na₂O enrichment is a

consequence of albite alteration of the wall-rock proximal to V4 veins. Both CaO and Na₂O share the same pattern as the Na/Al alteration index, indicating that albite is the dominant Na+Ca phase associated with high values of Ca. Both Na₂O and CaO exhibit mass gains within approximately 20 m of quartz saddles that contain a V4 component (Fig. 2.16). However, in intensely biotite-altered mudstones (evidenced by K₂O mass gains or 3K/Al approaching 1.0), Na₂O and CaO decrease sharply.

Fe₂O₃+MgO: The Goldboro mudstones exhibit mass loss and mass gain in Fe₂O₃ (Fig. 2.17e). These changes represent Fe-leaching during V4-stage alteration of ilmenite to anatase, and a Fe-gain that corresponds to biotite and chlorite alteration. Fe-Mg mass changes attributed to biotite and chlorite alteration are local to V1 and V4 veins, increasing sharply <3 m of these veins (Fig. 2.16). However, the thickness (i.e., volume) of mudstone units is commonly a limiting factor in the extent of biotite and chlorite alteration.

As: Due to the presence of large crystals of arsenopyrite, there is a considerable variation in the As content, ranging from 20 ppm to >250 ppm (upper limit of detection); these high concentrations reflect common arsenopyrite throughout the Goldboro mudstones.

Au: There is a ubiquitous nominal mass loss of Au in the Goldboro mudstones relative to the precursor, ranging from 0-1 ppm. However, given the analytical reproducibility of Au, the significance of this is within the range of

analytical error. Proximal to large quartz saddles, two samples exhibited mass gains of 2.5 ppm and 4.8 ppm (2.5 ppm gain is shown in Figure 2.16).

Sb: Although Sb typically has low concentrations, the mudstones exhibit a mass gain proximal to large quartz saddles (e.g., Fig. 2.16). Proximal (≤ 1 m) to certain quartz saddles mudstone exhibited mass gains of up to 55 ppm (Fig. 2.17f).

Rb, Sr, Ba, and Cs: With the exception of Sr, the large-ion lithophile elements (LILE: Rb, Ba, Cs) share similar patterns to K₂O in a downhole profile (Fig. 2.16) and likely reflect K-related alteration (i.e., biotite, chlorite, and sericite alteration). Rb mass change ranges from -75 ppm to +75 ppm, Ba from -1000 ppm to +250 ppm, and Cs from -4 ppm to +6.5 ppm (Fig. 2.17g-i). In contrast, Sr mirrors the downhole profile of CaO (Fig. 2.16); the systematics of Sr are likely a proxy for carbonate mineralization (i.e., V3 veins) as Sr²⁺ readily substitutes for Ca²⁺ in carbonates. Mass changes of Sr range from -100 ppm to +400 ppm (Fig. 2.17j).

2.8.3 Electron Probe Microanalysis

Compiled EPMA data for chlorite and biotite are presented in Appendices E (raw data) and F (chlorite geothermometry). Chemical data for chlorite and biotite are shown in Figures 2.18 and 2.19, respectively. Chlorite was not observed in the least-altered sample. As such, it is assumed that biotite is both primary (detrital) and secondary (formed through alteration or mineralization) in nature, whereas chlorite is solely secondary.

The chlorites analyzed are all diabantite with a slight variation in $\text{Fe}/(\text{Fe}+\text{Mg})$ ranging from 0.4-0.5. Chlorites yield formation temperatures of 303-397 °C using the Cathelineau (1988) equation and 108-211 °C using the Kranidiotis and MacLean (1987) equation (Fig. 2.18b; Appendix E). Chlorites from different vein generations have variable Mn-Mg-Fe systematics, V1 stage chlorites are more Mn-rich compared to V4, whereas the V4 chlorites show two distinct trends: in-vein chlorite follows a line where $\text{Mg}/(\text{Mg}+\text{Fe})$ increases with Mn, whereas alteration product chlorite exhibits decreasing $\text{Mg}/(\text{Mg}+\text{Fe})$ with increasing Mn (Fig. 2.18c).

Chemical data for biotite is summarized in Figure 2.19. Like chlorite, biotite exhibits variation in Fe, Mn, and Mg depending on vein generation and whether it formed as a product of wall-rock alteration or as a vein component (Fig. 2.19b). When compared to the least-altered sample, V1-stage biotite is enriched in Mn, whereas V4-stage biotite is depleted in Mn. When comparing zones, the Boston-Richardson samples primarily contain V4-stage biotite, whereas samples from the East Goldbrook and West Goldbrook are primarily composed of V1-stage biotites. However, because the sample set used for EPMA was limited and small scale, it may not fully capture the distribution of V1 and V4 micas between zones, as stated in the captions of Figures 2.18 and 2.19.

As quartz-feldspathic blebs are near-ubiquitous in mudstone at Goldboro, all analyzed thin sections included biotite and chlorite that compose the rims. The analysis of blebs yielded signatures that were indistinguishable from surrounding

V1 and V4 micas, and therefore it is suggested that bleb development must have commenced during the V1 stage.

2.9 Discussion

2.9.1 Gold Paragenesis and Implications for Meguma-type Gold Deposits

In sediment-hosted orogenic gold deposits, it is thought that the fluids that transport Au are sourced during regional metamorphic devolatilization due to the breakdown of chlorite (Groves et al., 1998, 2003; Goldfarb and Groves, 2015). Au is then typically transported in bisulfide complexes ($\text{Au}(\text{HS})_2^-$), which are thought to be destabilized by rapid decompression-driven vapour production during flexural slip (Robb, 2004; Williams-Jones et al., 2009; Weatherley and Henley, 2013). This mechanism of Au transport and deposition describes gold deposits that adhere to the metamorphic model. Contrasting models suggest that gold formation is a result of regional magmatism and magmatic-hydrothermal processes (Sillitoe and Bonham Jr., 1990; Spooner, 1993). Geochronological studies have established two main temporal windows for Meguma Au deposits: ca. 408 Ma and ca. 375 Ma, both supported by Re-Os mineralization dates of vein-stage arsenopyrite, as well as $^{40}\text{Ar}/^{39}\text{Ar}$ dates corresponding to the regional thermal resetting of biotite (379-408 Ma)(Kontak et al., 1993, 1998; Kontak and Kerrich, 1995; Morelli et al., 2005; Kontak and Horne, 2010). Broadly, these dates correspond to the onset of orogenesis and to the emplacement of the South Mountain Batholith (SMB) and its satellite plutons, respectively.

The vein generations at Goldboro can be separated into two temporal groups based on their physical structure: 1) pre- or syn-deformational veins that are foliated and bedding-parallel (V1 and V2), and 2) post-compression veins that are hosted in breccias and fractures (V3 and V4). Although we cannot provide absolute age estimates, these vein generations may correspond to the regional mineralizing and thermal events: V1 and V2 veins corresponding to the compressional stage of orogenesis, and V3 and V4 veins corresponding to regional plutonism. Gold is hosted within V1, V2, and V4 veins; the distribution of gold within post-compression V4 veins suggests that gold metallogeny may not be simply the result of compressional orogenesis. The granite-like mineralogy of these veins, specifically coexisting K-feldspar, quartz, albite, apatite, ilmenite, and chlorite, as well as the presence of granophytic intergrowth of K-feldspar and quartz (Fig. 2.7) suggest that V4 veins are magmatic-hydrothermal in origin, providing evidence that plutonism played a role in the gold metallogeny at Goldboro.

Partial melting of the Meguma Supergroup and high-grade metamorphism are suggested to have been complementary processes in the development of both the Liscomb complex in Nova Scotia, as well as the wider Meguma terrane (Dostal et al., 2006; Shellnut and Dostal, 2015). This model introduces two possible fluid sources that may relate to gold mineralization: 1) metamorphic fluids derived from high-grade metamorphism, and 2) fluids exsolving from the magmas directly. Although the former is not discounted in this study, it is likely

that the fluid that formed V4 veins is magmatic in origin, potentially as a late-stage pegmatitic exsolution based on the presence of granophytic intergrowths of K-feldspar and quartz (Fig. 2.7), which is a texture unique to late phase crystallization in vapour-rich granitoid intrusions (Barker, 1970). Despite the clear spatial association between V4 veins and gold, their genetic relationship remains unclear. Although gold is hosted within V4 veins, it is more specifically associated with or hosted within pre-existing arsenopyrite 2 that is in contact with V4 veins (Fig. 2.11). Gourcerol et al. (2020) show that arsenopyrite in the Meguma Terrane sedimentary rocks hosts significant amounts of Au (<100 ppm,) as invisible gold or nanoparticles and so we argue that the source of gold may have been from early sulfides, presumably early pyrite and arsenopyrite and later remobilized during V4-stage veining via similar processes as presented by Hastie et al. (2020, 2021).

The magmatic nature of the V4 veins in this study directly links gold mineralization in Meguma-type orogenic gold deposits to fluids of a magmatic-hydrothermal origin, generated from the regional emplacement of granitic plutons. This argument is consistent with recent studies that advocate for a multi-stage origin of gold in the Meguma Terrane (Morelli et al., 2005; Kontak and Horne, 2010; Hastie et al., 2020, 2021; Gourcerol et al., 2020), and studies that provide evidence for both magmatic and metamorphic hydrothermal fluids in Meguma-type gold deposits (Kontak and Horne, 2010; Kontak et al., 2011). The presence of magmatic veins and their apparent role in zone refinement has important

implications regarding the depositional model of Meguma-type gold deposits: 1) that magmatic fluids drive a crucial stage in the gold metallogeny, and hence 2) that potentially, the Meguma terrane may not completely adhere to the metamorphic model of orogenic gold deposit formation, and that plutonism may play a key role in regional gold metallogeny.

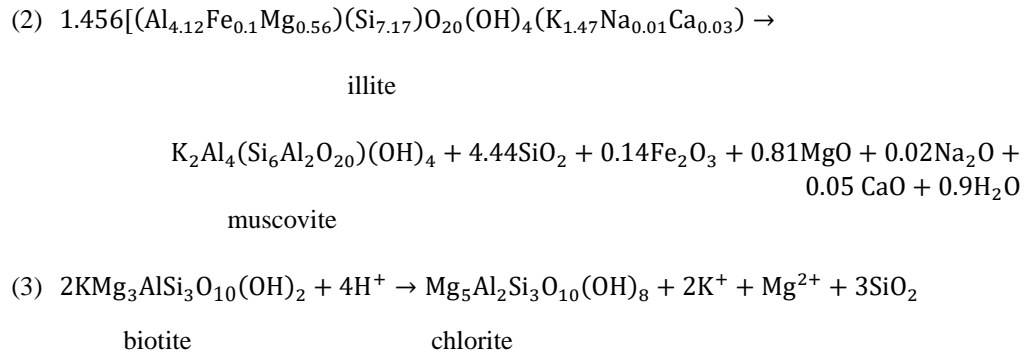
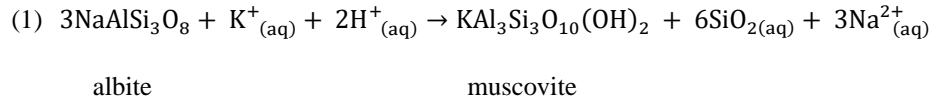
2.9.2 Hydrothermal Alteration of the Goldboro Deposit

Mineralization in sediment-hosted orogenic gold deposits is spatially linked to hydrothermal wall-rock alteration (Gao and Kwak, 1995, 1997; Ramsay et al., 1998; Phillips and Powell, 2010; Goldfarb and Groves, 2015; Groves et al., 2019b). The interaction between hydrothermal fluids and wall-rock during mineralization results in characteristic alteration assemblages that can be used to vector towards mineralization (Mikucki, 1998; Ridley and Diamond, 2000). In Goldboro, gold mineralization is predominantly within quartz veins and locally disseminated in wall-rock. The vein paragenesis at Goldboro contains four distinct stages, which have alteration assemblages unique to each stage (Fig. 2.7-2.9). Identifying these alteration types is imperative to understanding vein distribution during mineral exploration, as it allows alteration to be used as a vector towards gold-bearing veins. The mass changes of specific elements can be related to the alteration assemblages of certain vein types, and describe their spatial extent.

The mass losses of Na₂O, CaO, and K₂O are attributed to: 1) the alteration of minor detrital feldspars in the wall-rock; 2) the sericite alteration of illite; and 3) the chlorite alteration of pre-existing detrital or alteration biotite. These

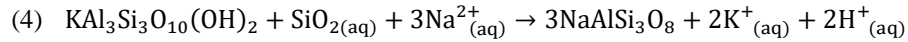
changes are accommodated through one or more of the following reactions

(Riverin and Hodgson, 1980; Parry and Downey, 1982; van de Kamp, 2008):



The above reactions (1) and (2) result in the loss of Na^+ and Mg^{2+} , and SiO_2 by the alteration of plagioclase and illite to muscovite-sericite. These elemental changes can be used to map the broad sericite alteration of the Goldboro deposit that spans >150 m from the hinge of the Upper Seal Harbour anticline. In particular, the loss of Na_2O and CaO by reaction (2) results in samples plotting along a line that becomes progressively $\text{Na}_2\text{O}+\text{CaO}^*$ -poor on the CIA diagram in Figure 2.17, and explains the widespread sericite alteration surrounding Goldboro. Reaction (3) explains the transition of biotite to chlorite, with a small loss of K^+ and Mg^{2+} .

The net gains in Na₂O result from the albite alteration of the wall-rock proximal to V4 veins. Albite alteration is a result of the inverse of reaction (1):



muscovite

albite

Visible bleaching caused by albite and sericite alteration proximal to V4 veins is very localized in mudstones, ≤ 3 cm from the margin of V4 veins, but has a much larger halo when examined using mass change results (Fig. 2.16). Mass gains in Na₂O and CaO are observed up to 20 m from quartz saddles with a V4 component in the hinge (BR-18-62, Fig. 2.16) but this effect is significantly more localized along the limbs of the Upper Seal Harbour anticline (≤ 1 m; BR-18-23, Fig. 2.16), spanning only a few meters. The more pervasive nature of albite alteration in the hinge is likely a result of V4 fluid concentrating at the hinge, which was likely the most robust fluid pathway for V4 fluids. The brecciation of mudstone and fracturing of quartz veins is also abundant in the hinge of the anticline, and this probably facilitated the upward and possibly lateral flow of fluid along the Upper Seal Harbour Anticline hinge zone. Although the relationship between bleaching in greywackes and V4 veins was not confirmed in this study, sandstone units are nominally more permeable and facilitate fluid migration. Thus, future mapping of albite and sericite alteration in greywacke units and brecciation in both mudstone and greywacke units may be useful in delineating the fluid pathways of mineralizing fluids.

The albitization process in reaction (4) may also explain the close association of anatase alteration with albite-altered zones proximal to V4 veins; the alteration of ilmenite requires acidic to slightly acidic conditions, which would have coincided with the release of H⁺ into solution by reaction (4), leading to the

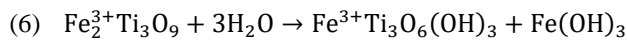
conversion of ilmenite to anatase (Grey and Reid, 1975; Mücke and Bhadra

Chaudhuri, 1991):

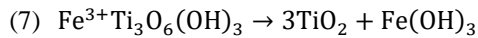


ilmenite

pseudorutile



pseudorutile



rutile/anatase

Mücke and Bhadra Chaudhuri (1991) also state that ilmenite alteration can occur in both oxidizing and reducing environments, but when these reactions occur in reducing conditions the alteration products will be overgrown with hematite. Therefore, at Goldboro, these reactions must have been driven by an acidic to lightly acidic oxidizing fluid given the absence of hematite in the alteration assemblages at Goldboro.

The presence of an acidic fluid may also explain why Goldboro lacks the distinctive carbonate alteration halo that is considered a classic feature of turbidite-hosted gold deposits (e.g., Kerrich and Wyman; Groves and Phillips, 1987; Nesbitt et al., 1989; Kontak and Smith, 1993; Gao and Kwak, 1997; Goldfarb et al., 1998; Li et al., 1998; Bierlein et al., 2004; Rusinov et al., 2008; Dugdale et al., 2009). Carbonates (e.g., ankerite and Fe-dolomite) are only

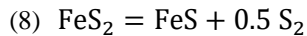
observed in V3 and V4 veins, not as alteration products. The lack of carbonate alteration suggests that either there was insufficient open space required to precipitate carbonates in the wall-rock, a CO₂-rich fluid was not responsible for mineralization at Goldboro, or that carbonate spots formed during the initial stage of veining (viz., V1 and V2) and were subsequently destroyed or overprinted during later mineralization (V3 and V4). Vein-hosted carbonates are a common late-stage phase at Goldboro, discounting the possibility that CO₂ was not available during mineralization, and CO₂-bearing fluids were identified by Kerr et al. (2021) as likely being responsible for mineralization in nearby deposits. It is also generally accepted that carbonate spots are a product of replacement of pre-existing minerals (e.g., Gao and Kwak, 1997, Dugdale et al., 2009), mitigating the requirement for open space for mineralization. Further, carbonate spots are present in other Meguma-type deposits (e.g., Touquoy, Beaver Dam, and Fifteen Mile Stream; Kerr et al., 2021). Therefore, it is likely that early carbonate alteration was destroyed by late-stage (V3 and V4) mineralizing fluids.

Net gains present in Fe₂O₃ and MgO (Fig. 2.16, Fig. 2.17) are primarily attributed to biotite and chlorite alteration that extends multiple meters from V1 and V4 veins, increasing in intensity proximal to these veins. Figures 2.19 and 2.20 demonstrate there were two stages of both biotite and chlorite alteration; the Mn content of the micas in these two stages varies with respect to Mg and Fe. V1-stage biotite and chlorite are enriched in Mn compared to V4-stage micas. As the biotite samples are also enriched in Mn relative to the least-altered sample, this

enrichment is inferred to be the result of the introduction of Mn into the system during the V1 stage. In contrast, V4 micas are depleted in Mn relative to earlier generations. Because the V4-stage micas represent re-equilibration of earlier phases, this is attributed to the release of Mn during the V4 alteration process.

Biotite and chlorite alteration are observed up to 2 m from the margins of V1 and V4 veins, but are usually limited by the thickness of the mudstone bed.

The composition of biotite and chlorite in mica-rimmed blebs is indistinguishable from the surrounding micas, indicating that bleb formation must have commenced during V1 or earlier, later overprinted by V1 biotite, and again during V4. Because the non-sulfide mineralogy of the blebs is very similar to V4 veins (i.e., K-feldspar+quartz+apatite+ilmenite), this process must have also continued during the V4 stage. The earliest sulfides in the paragenesis of Goldboro are pyrrhotite and arsenopyrite 1, with rare occurrences of early pyrite cores within arsenopyrite 1. Additionally, pyrrhotite is present within most blebs. It is, therefore, possible that early pyrite was entirely replaced by pyrrhotite during metamorphism, resulting in a bleb-shaped replacement texture via the following reaction (Toulmin and Barton, 1964):



pyrite pyrrhotite

Arsenopyrite, sphalerite, chalcopyrite, and galena might also be produced if As, Zn, Cu, and Pb are released by pyrite breakdown. Although the metamorphic grade at Goldboro is relatively low for sediment-hosted orogenic gold deposits, it

has been suggested that reaction (8) can precede chlorite devolatilization and that the pyrite-pyrrhotite transition is much wider than previously thought (Pitcairn et al., 2010; Zhong et al., 2015; Finch and Tompkins, 2017). Reaction (8) could explain the presence of arsenopyrite, chalcopyrite, galena, and sphalerite within blebs by means of releasing Zn, Cu, Pb, and As from pyrite, but does not explain the presence of other phases (i.e., K-feldspar+quartz+apatite+ilmenite). The mineral assemblage closely resembles that of V4 veins, suggesting that the replacement process continues during the V4 phase, tentatively by means of coupled dissolution-reprecipitation (CDR) as proposed by Hastie et al. (2020, 2021). Pyrite has been suggested to be a key source for As and Au in orogenic gold systems (Large et al., 2011; Thomas et al., 2011; Hastie et al., 2020, 2021), and the presence of blebs on a regional scale may represent a missing piece of metallogeny throughout the Meguma Supergroup. As mentioned earlier, Sutton (2007) presents the possibility that the blebs could also reflect microlithic components within mudstone. Although this study does not discount this possibility, it is unlikely that microlithic K-feldspar was ubiquitously preserved in the blebs with no signs of sericitization, whereas the biotite and chlorite components of the blebs are clearly similar to hydrothermal alteration products associated with veining, and the blebs are hosted in sericite-altered rocks. (Fig. 2.17b, Fig. 2.18b). Therefore, we suggest that the blebs in the Goldboro deposit are dominantly a replacement texture of pre-vein sulfides during V4 mineralization.

2.9.3 Vectors to Mineralization

The Goldboro deposit reflects complex processes at differing scales that are reflected in the rocks, alteration, lithogeochemistry, and mineral chemistry of the deposit. Key vectors to mineralization include:

Distance from the hinge of the Upper Seal Harbour anticline: the majority of gold mineralization at Goldboro is hosted in the quartz saddle and leg reefs that straddle the hinge of the anticline. These saddles vary in thickness, but their thickness sharply decreases past 20 m of the axial plane. Thus, exploration should target areas within 20 m North and South of the axial plane for optimal results.

V4 vein distribution: gold is closely associated with V4 veins. Although V1 and V2 quartz contain gold (e.g., as shown in Figure 2.4), high-grade gold occurrences are restricted to V4 veins. Because V4 veins represent a very small proportion of veins (~1 volume %), they represent small-scale, high-grade targets within larger quartz veins. Exploration should therefore focus on identifying V4 veins within V1 and V2 veins.

Chemical vectors and alteration: the hydrothermal footprint at Goldboro can be recognized at various scales using lithogeochemistry. A higher chemical index of alteration (CIA) and 3K/Al can be used to delineate sericite alteration, and are more reliable tools than mass gains in K₂O. Mass gains in Fe₂O₃ and MgO can be used to identify V1 and V4 veins up to 5 m away, as these mass gains reflect biotite alteration. Mass losses in Fe₂O₃ and K₂O combined with mass gains in Na₂O and CaO is specific to V4 alteration, up to 20 m from the vein along the

hinge of the anticline, and within 1 m along the limbs. The alteration index Na/Al can also be used to identify V4-associated albite alteration on the same scale. Enrichments in As may be used as arsenopyrite is associated with Au. However, this method should be used with caution as arsenopyrite creates a nugget effect for As and is widespread throughout the deposit. Elements Cs, Ba, and Rb can be used as proxies for K₂O, as they substitute readily for K⁺ and mimic the pattern of K₂O in a downhole profile, and Sr has the same effect for CaO. Sb can be used as a vector as it is enriched in certain mudstone beds that are proximal to quartz saddles (Fig. 2.16), although this effect is not ubiquitous throughout all mudstones Hg.

Bleaching of greywacke: given that bleaching is associated with V4 veins, the bleaching of greywacke is a potential vector towards these veins. Due to the higher permeability of greywacke units compared to mudstone units, bleaching of greywacke may represent fluid pathways that would be integral in understanding the distribution of V4 veins throughout Goldboro. Due to the significantly higher permeability of greywacke compared to mudstones, fluids would easily percolate upwards through these units without the need for fluid-focusing features such as fractures. However, because this study focused on mudstone units, this vector requires further testing.

Mineral chemistry and mineral assemblages: The distribution of V4 alteration is evident in the compositions of biotite and chlorite. Mn-poor biotite and chlorite can be used to establish the extent of V4 alteration where it is cryptic and not visible using field observations or petrography alone. Further, V4 veins

have a unique mineral assemblage that includes K-feldspar + albite + chlorite + biotite > 30% modally, with accessory apatite and ilmenite; this assemblage in veins would suggest higher prospectivity for Au mineralization than other assemblages in this region.

2.9.4 Formation of the Goldboro Deposit

The detailed model for formation of sediment-hosted orogenic gold deposits remains contentious. Most published research favours the metamorphic devolatilization model (Kerrich, 1983; Phillips and Powell, 2010; Groves et al., 2019), but other work argues that metamorphic fluids cannot be solely responsible for mineralization (Kontak and Horne, 2010; Kontak et al., 2011). The metamorphic model is consistent with the regional metamorphic grade for most sediment-hosted orogenic gold districts (Victorian gold belt, Sukhoi Log, Otago schist) and largely explains their formation (Bierlein et al., 2004; Pitcairn et al., 2010; Wilson et al., 2013; Cave et al., 2017). Based on its metamorphic grade and mineralization styles (e.g., quartz saddles), the Meguma Terrane looks like a conventional sediment-hosted orogenic gold district in a broad sense. However, there are variations between Meguma-type gold deposits and other Phanerozoic orogenic gold deposits in terms of alteration and mineral assemblages that suggest Meguma-type deposits represent a hybrid deposit with inputs from both metamorphic and igneous fluid sources.

Quartz veins in Goldboro represent two temporal groups: veins associated with a pre- or syn-compression event (bedding-parallel V1 and V2 veins), a

common feature of metamorphic orogenic gold deposits, and a later event (undeformed V3 and V4 veins) that suggests mineralization and gold deposition continued after the main stage of compression. V1 and V2 veins are interpreted to have formed via metamorphic devolatilization of the lower Meguma Supergroup, during flexural slip (Horne and Culshaw, 2001), resulting in precipitation of V1 and V2 veins through rapid, local decompression (e.g., Weatherley and Henley, 2013). The mineral assemblages in V3 and V4 veins are drastically different from those of V1 and V2 veins, with V4 veins having an assemblage that closely resembles that of granite. Further, granophytic intergrowths of feldspar and quartz (Fig. 2.7) in V4 veins are consistent with an igneous-derived fluid (Barker, 1970). We argue that the presence of igneous-like assemblages, was a result of the combination of metamorphic devolatilization and magmatic exsolution, facilitated by fluid flow through permeable greywacke units and existing/evolving fracture networks. The onset of high-grade metamorphism and partial melting in the lower Meguma Supergroup (Dostal et al., 2006; Shellnut and Dostal, 2015) potentially triggered the V4 stage of mineralization. These fluids were likely acidic and oxidizing, resulting in albite, sericite, and anatase/rutile alteration, as well as the second stage of biotite and chlorite alteration. We tentatively suggest that V1 and V2 veins correspond to the onset of metamorphism in the Meguma Terrane at ca. 380 Ma, whereas the later V3 and V4 veins were formed during regional magmatism between 380-362 Ma (Kontak et al., 1990, 1993, 1998; Kontak and Archibald, 2008; Morelli et al., 2005; Kontak and Horne, 2010; Kontak et al., 2011). It is acknowledged that without robust geochronological constraints, the

age assignments for veining events are conjectural; however, they are consistent with regional metallogenic models for the Meguma Terrane and can be readily tested through Re-Os dating of arsenopyrite 1 and 2, and $^{40}\text{Ar}/^{39}\text{Ar}$ dating of V1 and V4 biotite.

Typically, in purely “metamorphic” sediment-hosted orogenic gold deposits, high-grade gold is hosted in bedding-parallel quartz saddles along the hinge of anticlines. Although gold is hosted within V1 and V2 vein at Goldboro, the highest gold grades are found within and proximal to V4 veins within V1 and V2 veins. In an LA-ICP-MS study of arsenopyrite in the Meguma Terrane, Gourcerol et al. (2020) recognized that gold deposition occurred in two events: 1) an initial event, occurring as invisible gold in arsenopyrite, and 2) a subsequent upgrading event manifesting visible gold. Zone refinement is commonly invoked as an upgrading process in orogenic gold deposits, although different mechanisms have been proposed. Aseismic refinement has been suggested to be the dominant mechanism in the Victorian gold belt, where gold is deposited along pressure solution seams in quartz and microscale fractures (Voisey et al., 2020). The lack of these gold textures or pressure solution seams in Goldboro suggests that aseismic refinement was not a dominant upgrading mechanism in Goldboro. In other orogenic gold deposits, particularly the Abitibi greenstone belt, gold remobilization is primarily driven by coupled pressure dissolution-reprecipitation (CDR) reactions (Hastie et al., 2020, 2021), where Au is remobilized from auriferous pyrite or arsenopyrite by means of partial melting, yielding porous

residual textures in the interiors of sulfide grains (e.g., porous cores and less porous rims). In CDR systems, melting is triggered by the introduction of low melting point chalcophile elements (LMCE), where the melt is transported a short distance and deposited. This mechanism results in gold closely associated with arsenopyrite grains as inclusions, cores, and wires along fractures in pyrite (Hastie et al., 2020, 2021). Characteristic porous textures in arsenopyrite are abundant in Goldboro, particularly dominant in arsenopyrite 1 crystals, in which inclusions of gold are present alongside sphalerite, chalcopyrite, galena, and pyrrhotite. In subsequent arsenopyrite 2, gold occurs as cores and wires along fractures. The similarities in texture of arsenopyrite and gold to those of the Abitibi greenstone belt suggest that CDR reactions were likely responsible for the upgrading of the Goldboro deposit. If this is the case, Au was initially refractory in arsenopyrite 1, and the introduction of LMCE during the infiltration of V4-forming fluids may have been the catalyst for the remobilization and deposition of gold. The morphology of native gold likely reflects the degree of which arsenopyrite 1 was subjected to CDR. As described by Hastie et al. (2020, 2021), gold first deposits as inclusions, progressing to wires and free gold as the degree of CDR increases. The texture of pyrite also changes, transitioning from porous to completely cleared of inclusions as CDR continues; in Goldboro, these textures correspond to what is observed in arsenopyrite 1 and arsenopyrite 2, respectively. The Goldboro deposit is particularly interesting because although it closely resembles other sediment-hosted orogenic gold deposits, it contains elements of both orogenic and magmatic-hydrothermal mineralization coupled with zone refining. The interplay

between these processes led to high-grade gold mineralization within a metasedimentary belt, and Goldboro represents a hybrid between metamorphic and magmatic gold deposition.

2.10 Conclusions

The conclusions of this study are:

1. There are four distinct quartz vein generations at Goldboro:
 - a. V1 veins that are bedding-parallel and sulfide-rich.
 - b. V2 veins that are bedding-parallel and contain arsenopyrite as the only sulfide.
 - c. V3 veinlets infill brecciation and fractures that are tan and carbonate-rich.
 - d. V4 veins infill fractures and contain K-feldspar, albite, chlorite, biotite, fluorapatite, ilmenite, and gold.

Veining can be separated into two events: 1) pre- or syn-deformational veins that are foliated (V1 and V2), and 2) post-compression veins that are possibly related to regional plutonism (V3 and V4). Gold is hosted in V1 and V4 veins, with high-grade gold occurrences in V1 and V2 veins that contain a high density of V4 veins. V4 veins are interpreted to be magmatic-hydrothermal in origin, linking igneous activity to gold metallogeny in Meguma.

2. This study established vein, alteration, mineral chemical, and geochemical vectors towards gold mineralization. Gold-proximal quartz veins can be vectored towards by a sharp increase in biotite and chlorite alteration within 3 m of vein margins, and the identification of V4 veins within larger V1 and V2 can be used to find high-grade gold occurrences. Mass balance results show that mass changes in K₂O, Na₂O, CaO, Fe₂O₃, and MgO can be used to identify alteration types, mass changes in Rb, Ba, and Cs can be used as proxies for K₂O, and Sr can be used to identify intensity of V3 veining. Electron probe micro-analysis (EPMA) results show that V1-stage biotite and chlorite is enriched in Mn relative to unaltered samples, and V4-stage biotite and chlorite are Mn-depleted. Identification of biotite and chlorite alteration can be used to vector towards V1 and V4 veins, using biotite mineral chemistry to distinguish between these generations, and albite alteration can be used as a vector towards areas with a high density of V4 veins.

3. Hydrothermal alteration at Goldboro can be classified as follows:

- a. V4-stage albite alteration that is recorded by mass changes of Na₂O+CaO up to 20 m from quartz saddles at the hinge of the Upper Seal Harbour anticline. In the limbs of the anticline, these changes are much more localized to veins (≤ 1 m).

- b. Sericite alteration is present in all samples, resulting in an alteration halo >150 m from the hinge of the Upper Seal Harbour anticline.
 - c. Biotite and chlorite alteration are widespread, but sharply increase in intensity <3 m from V1 and V4 vein margins. However, the thickness of mudstone units is commonly less than 3 m, limiting the alteration halo to the thickness of the respective unit.
4. The quartzo-feldspathic blebs that are common features in Meguma-type gold deposits likely represent relict features of early sulfides that were altered and replaced during the V1 and V4 stages.
5. Gold deposition occurred in two temporal events at Goldboro. An initial stage where gold is deposited as a refractory phase in arsenopyrite 1, and a later remobilization via coupled dissolution-reprecipitation reactions (CDR) during V4 development. Remobilization via CDR caused native gold inclusions and wires in arsenopyrite 2, as well as free gold within V4 veins.
6. Goldboro is a hybrid between the classic “metamorphic” and a magmatic-hydrothermal sediment-hosted orogenic gold deposit. The initial stages of veining (V1 and V2) are well explained by flexural slip and the formation of metamorphic fluids via the breakdown of hydrous silicates during greenschist-amphibolite metamorphism in the lower crust. During the compressional phase of orogenesis, early pyrite transitioned to pyrrhotite and likely arsenopyrite, sphalerite, chalcopyrite, and galena, with gold as a

refractory phase in arsenopyrite 1. Later veining of magmatic-hydrothermal origin (V4) had a zone refinement effect on the deposit, remobilizing gold from arsenopyrite 1 via CDR and concentrating native gold along V4 veins and as inclusions and wires in arsenopyrite 2. This later stage of veining may correspond to the partial melting of the lower crust during orogenic collapse and regional magmatism in the Meguma Terrane.

2.11 References

- Aitchison, J., 1986, The Statistical Analysis of Compositional Data. Chapman and Hall, London, UK, 416 pages.
- Kuntz, G., Robinson, J., Jundis, R., Raponi, T., Kirchner, T., Pumphrey, S., McIsaac, R., Parks, J., Betts, A., Harkonen, H., 2021, Goldboro gold project resource update phase 2 Guysborough County, Nova Scotia. NI 43-101 Technical Report and Mineral Resource Estimate no. 20048-02, 237 p.
- Barker, D.S., 1970, Compositions of granophyre, myrmekite, and graphic granite: Geological Society of America Bulletin, v. 81, p. 3339–3350.
- Bierlein, F.P., Christie, A.B., and Smith, P.K., 2004, A comparison of orogenic gold mineralisation in central Victoria (AUS), western South Island (NZ) and Nova Scotia (CAN): implications for variations in the endowment of Palaeozoic metamorphic terrains: Ore Geology Reviews, v. 25, p. 125–168.

Binns, R.A., and Eames, J.C., 1989, Geochemistry of wall rocks at the Clunes gold deposit, Victoria, *in* The Geology of Gold Deposits: The Perspective in 1988, Economic Geology Monograph Series, v. 6, p. 310–319.

Cave, B.J., Pitcairn, I.K., Craw, D., Large, R.R., Thompson, J.M., Johnson, S.C., 2017, A metamorphic mineral source for tungsten in the turbidite-hosted orogenic gold deposits of the Otago Schist, New Zealand; Mineralium Deposita, v. 52, p. 515–537.

Dostal, J., Keppie, D.J., Jutras, P., Miller, B.V., Murphy, B.J., 2006, Evidence for the granulite-granite connection: penecontemporaneous high-grade metamorphism, granitic magmatism, and core complex development in the Liscomb Complex, Nova Scotia, Canada: Lithos, v. 86, p. 77-90.

Dugdale, A.L., Wilson, C.J.L., Leader, L.D., Robinson, J.A., and Dugdale, L.J., 2009, Carbonate spots: understanding the relationship to gold mineralization in Central Victoria, southeastern Australia: Mineralium Deposita, v. 44, p. 205–219.

Finch, E.G., and Tomkins, A.G., 2017, Pyrite-pyrrhotite stability in a metamorphic aureole: Implications for orogenic gold genesis: Economic Geology, v. 112, p. 661–674.

Gao, Z.L., and Kwak, T.A.P., 1995, Turbidite-Hosted Gold Deposits in the Bendigo-Ballarat and Melbourne Zones, Australia. II. Nature of Ore Fluids: International Geology Review, v. 37, p. 1007–1038.

Gao, Z.L., and Kwak, T.A.P., 1997, The geochemistry of wall rock alteration in turbidite-hosted gold vein deposits, central Victoria, Australia: *Journal of Geochemical Exploration*, v. 59, p. 259–274.

Gingras, M.K., Waldron, J.W.F., White, C.E., and Barr, S.M., 2011, The evolutionary significance of a Lower Cambrian trace-fossil assemblage from the Meguma terrane, Nova Scotia: *Canadian Journal of Earth Sciences*, v. 48, p. 71–85.

Goldfarb, R.J., Phillips, G.N., and Nokleberg, W.J., 1998, Tectonic setting of synorogenic gold deposits of the Pacific Rim: *Ore Geology Reviews*, v. 13, p. 185–218.

Goldfarb, R.J., and Groves, D.I., 2015, Orogenic gold: common or evolving fluid and metal sources through time: *Lithos*, v. 233, p. 2–26.

Gourcerol, B., Kontak, D.J., Petrus, J.A., and Thurston, P.C., 2020, Application of LA ICP-MS analysis of arsenopyrite to gold metallogeny of the Meguma Terrane, Nova Scotia, Canada: *Gondwana Research*, v. 81, p. 265–290.

Gresens, R.L., 1967, Composition-volume relationships of metasomatism: *Chemical Geology*, v. 2, p. 47–65.

Grey, I.E., and Reid, A.F., 1975, The structure of pseudorutile and its role in the natural alteration of ilmenite: *The American Mineralogist*, v. 60, p. 898–906.

Groves, D.I., Goldfarb, R.J., Gebre-Mariam, M., Hagemann, S.G., and Robert, F., 1998, Orogenic gold deposits: A proposed classification in the context of their crustal distribution and relationship to other gold deposit types: *Ore Geology Reviews*, v. 13, p. 7–27.

Groves, D.I., Goldfarb, R.J., Robert, F., and Hart, C.J.R., 2003, Gold deposits in metamorphic belts: overview of current understanding, outstanding problems, future research, and exploration significance: *Economic Geology*, v. 98, p. 1–29.

Groves, D.I., and Phillips, G.N., 1987, The genesis and tectonic control on archaean gold deposits of the Western Australian Shield - a metamorphic replacement model: *Ore Geology Reviews*, v. 2, p. 287–322.

Groves, D.I., Santosh, M., Deng, J., Wang, Q., Yang, L., and Zhang, L., 2019, A holistic model for the origin of orogenic gold deposits and its implications for exploration: *Mineralium Deposita*, v. 55, p. 275–292.

Hastie, E.C.G., Schindler, M., Kontak, D., Lafrance, B., 2021, Transport and coarsening of gold nanoparticles in an orogenic deposit by dissolution-reprecipitation and Ostwald ripening: *Communications Earth & Environment*, v. 2, p. 1-9.

Hastie, E.C.G., Kontak, D.J., and Lafrance, B., 2020, Gold remobilization: insights from gold deposits in the Archean Swayze greenstone Belt, Abitibi subprovince, Canada: *Economic Geology*, v. 115, p. 241–277.

Hey, M.H., 1954, A new review of the chlorites: Mineralogical Magazine and Journal of the Mineralogical Society, v. 30, p. 277–292.

Hicks, R.J., Jamieson, R.A., and Reynolds, P.H., 1999, Detrital and metamorphic $^{40}\text{Ar}/^{39}\text{Ar}$ ages from muscovite and whole-rock samples, Meguma Supergroup, southern Nova Scotia: Canadian Journal of Earth Sciences, v. 36, p. 23–32.

Hind, H.Y., 1869, Notes on the structure and of the Nova Scotia gold district: Transactions of the Nova Scotia Institute of National Science, v. 2, p. 102-109.

Hind H.Y., 1870, On two gneissoid series in Nova Scotia and New Brunswick, supposed to be the equivalents of the Huronian (Cambrian) and Laurentian: Geological Society of London, v. 16, p. 468-479.

Hind, H.Y., 1872, Report on the Mt. Uniacke, Oldham, and Renfrew gold mining districts with plans and sections: Canadian Institute for Historical Microreproductions Microfiche Series no. 64772, 136 p.

Horne, R.J., and Culshaw, N., 2001, Flexural-slip folding in the Meguma Group, Nova Scotia, Canada: Journal of Structural Geology, v. 23, p. 1631-1652.

Horne, R.J., and Pelley, D., 2007, Geological Transect of the Meguma Terrane from Centre Musquodoboit to Tangier: NS Mineral Resources Branch, Report of Activities, v. ME 2007-1, p. 71–89.

Hunt, T.S., 1868, Report of Dr. T. Sterry Hunt, F.R.S., On the gold region of Nova

Scotia: Geological Survey of Canada, Separate Report 404, 48 p.

Kamber, B.S., Greig, A., and Collerson, K.D., 2005, A new estimate for the composition of weathered young upper continental crust from alluvial sediments, Queensland, Australia: *Geochimica et Cosmochimica Acta*, v. 69, p. 1041–1058.

van de Kamp, P., 2008, Smectite-illite-muscovite transformations, quartz dissolution, and silica release in shales: *Clay and Clay Minerals*, v. 56, p. 66-81.

Kerr, M., Hanley, J., Kontak, D.J., 2021, Application of bulk fluid volatile chemistry to exploration for metasedimentary rock-hosted orogenic gold deposits: An example from the Meguma terrane, Nova Scotia, Canada: *Journal of Geochemical Exploration*, v. 226, p. 1-20.

Kerrick, R., 1983, Geochemistry of gold deposits in the Abitibi Greenstone Belt: Canadian Institute of Mining and Metallurgy, Special Paper 27, 75 p.

Kerrick, R., and Wyman, D., 1990, Geodynamic setting of mesothermal gold deposits: An association with accretionary tectonic regimes: *Geology*, v. 18, p. 882–885.

Kontak, D.J., Horne, R.J., Sandeman, H., Archibald, D., and Lee, J.K.W., 1998, $^{40}\text{Ar}/^{39}\text{Ar}$ dating of ribbon-textured veins and wall-rock material from Meguma lode gold deposits, Nova Scotia: Implications for timing and duration of vein formation in

slate-belt hosted vein gold deposits: Canadian Journal of Earth Sciences, v. 35, p. 746–761.

Kontak, D.J., and Kerrich, R., 1995, Geological and geochemical studies of a metaturbidite-hosted lode gold deposit: the Beaver Dam deposit, Nova Scotia: II. Isotopic studies: Economic Geology, v. 90, p. 885–901.

Kontak, D.J., and Reynolds, P.H., 1994, $^{40}\text{Ar}/^{39}\text{Ar}$ dating of metamorphic and igneous rocks of the Liscomb Complex, Meguma Terrane, southern Nova Scotia, Canada: Canadian Journal of Earth Sciences, v. 31, p. 1643–1653.

Kontak, D.J., and Smith, P.K., 1989, Sulphur isotopic composition of sulphides from the Beaver Dam and other Meguma-Group-hosted gold deposits, Nova Scotia: implications for genetic models: Canadian Journal of Earth Sciences, v. 26, p. 1617–1629.

Kontak, D.J., and Smith, P.K., 1993, A metaturbidite-hosted lode gold deposit: the Beaver Dam deposit, Nova Scotia. I. Vein paragenesis and mineral chemistry: Canadian Mineralogist, v. 31, p. 471–522.

Kontak, D.J., Smith, P.K., and Reynolds, P.H., 1993, Geology and $^{40}\text{Ar}/^{39}\text{Ar}$ geochronology of the Beaver Dam gold deposit, Meguma Terrane, Nova Scotia, Canada: evidence for mineralization at 370 Ma: Economic Geology, v. 88, p. 139–170.

Kontak, D.J., Smith, P.K., Reynolds, P., and Taylor, K., 1990, Geological and $^{40}\text{Ar}/^{39}\text{Ar}$ geochronological constraints on the timing of quartz vein formation in Meguma Group lode-gold deposits, Nova Scotia: Atlantic Geology, v. 26, p. 201–227.

Kontak, D.J., and Horne, R.J., 2010, A multi-stage origin for the Meguma lode gold deposits, Nova Scotia, Canada: a possible global model for slate belt-hosted gold mineralization, *in* Deb, M. and Goldfarb, R.J. eds., Gold Metallogeny: India and Beyond, Oxford, Alpha Science International Ltd., p. 58–82.

Kontak, D.J., Horne, R.J., and Kyser, K., 2011, An oxygen isotope study of two contrasting orogenic vein gold systems in the Meguma Terrane, Nova Scotia, Canada, with implications for fluid sources and genetic models: Mineralium Deposita, v. 46, p. 289–304.

Kontak, D.J., Horne, R.J., and Smith, P.K., 1996, Hydrothermal characterization of the West Gore Sb-Au deposit, Meguma Terrane, Nova Scotia, Canada: Economic Geology, v. 91, p. 1239–1262.

Kontak, D.J., and Kyser, K., 2011, A fluid inclusion and isotopic study of an intrusion-related gold deposit (IRGD) setting in the 380 Ma South Mountain Batholith, Nova Scotia, Canada: Evidence for multiple fluid reservoirs: Mineralium Deposita, v. 46, p. 337–363.

Kranidiotis, P., and MacLean, W.H., 1987, Systematics of chlorite alteration at the Phelps Dodge massive sulfide deposit, Matagami, Quebec: Economic Geology, v. 82, p. 1898–1911.

Large, R.R., Bull, S.W., and Maslennikov, V. V., 2011, A carbonaceous sedimentary source-rock model for carlin-type and orogenic gold deposits: Economic Geology, v. 106, p. 331–358.

Large, R.R., Danyushevsky, L., Hollit, C., Maslennikov, V., Meffre, S., Gilbert, S., Bull, S., Scott, R., Emsbo, P., Thomas, H., Singh, B., and Foster, J., 2009, Gold and trace element zonation in pyrite using a laser imaging technique: implications for the timing of gold in orogenic and carlin-style sediment-hosted deposits: Economic Geology, v. 104, p. 635–668.

Large, R.R., Gregory, D.D., Steadman, J.A., Tomkins, A.G., Lounejeva, E., Danyushevsky, L.V., Halpin, J.A., Maslennikov, V., Sack, P.J., Mukherjee, I., Berry, R., and Hickman, A., 2015, Gold in the oceans through time: Earth and Planetary Science Letters, v. 428, p. 139–150.

Large, R.R., Halpin, J.A., Danyushevky, L.V., Maslennikov, V.V., Bull, S.W., Long, J.A., Gregory, D.D., Lounejeva, E.L., Lyons, T.W., Sack, P.J., McGoldrick, P.J., and Calver, C.R., 2014, Trace element content of sedimentary pyrite as a new proxy for deep-time ocean-atmosphere evolution: Earth and Planetary Science Letters, v. 389, p. 209–220.

Li, X., Kwak, T.A.P., and Brown, R.W., 1998, Wallrock alteration in the Bendigo gold ore field, Victoria, Australia: uses in exploration: *Ore Geology Reviews*, v. 13, p. 381–406.

Lickley, W.P., Whitehead, R.E., and Davies, J.F., 1987, The use of sorting curves in studying K₂O alteration in interbedded greywacke and argillite: *Journal of Geochemical Exploration*, v. 27, p. 299–309.

MacDonald, L.A., 1998, Carbonate in the Oldham Gold Deposit, Nova Scotia. Unpublished B.Sc. Honours Thesis: Dalhousie University, Halifax, Nova Scotia, 91 p..

MacLean, W.H., 1990, Mass change calculations in altered rock series: *Mineralium Deposita*, v. 49, p. 44–49.

Maclean, W.H., and Barrett, T.J., 1993, Lithogeochemical techniques using immobile elements: *Journal of Geochemical Exploration*, v. 48, p. 109–133.

Maclean, W.H., and Kranidiotis, P., 1987, Immobile elements as monitors of mass transfer in hydrothermal alteration: Phelps Dodge massive sulfide deposit, Matagami, Quebec (Canada).: *Economic Geology*, v. 82, p. 951–962.

Malcolm, W., 1929, Gold fields of Nova Scotia, *in Geological Survey of Canada, Memoir 158*, p. 253.

McLennan, S.M., 2001, Relationships between the trace element composition of sedimentary rocks and upper continental crust: *Geochemistry, Geophysics, Geosystems*, v. 2, 24 p.

McLennan, S.M., 1989, Rare earth elements in sedimentary rocks: Influence of provenance and sedimentary processes, *Reviews in Mineralogy*, v. 21, p.169–200.

McLennan, S.M., Bock, B., Hemming, S.R., Hurowitz, J.A., Lev, S.M., and McDaniel, D.K., 2003, The roles of provenance and sedimentary processes in the geochemistry of sedimentary rocks, *in* Lentz, D.R. ed., *Geochemistry of Sediments & Sedimentary Rocks: Evolutionary Considerations to Mineral Deposit-Forming Environments*, Geological Association of Canada, GeoText, v. 4, p. 7–38.

McLennan, S.M., Hemming, S.R., McDaniel, D.K., and Hanson, G.N., 1993, Geochemical Approached to Sedimentation, Provenance and Tectonics, *in* Johnsson, M.J. and Basu, A. eds., *Processes Controlling the Composition of Clastic Sediments*, Geologic Association of America, Special Paper, v.284, p. 21–40.

Melvin, A.E., 1987, Vein-host rock relationships in the Mooseland gold district of the Meguma group, Nova Scotia. Unpublished B.Sc. Honours Thesis: Saint Francis Xavier University, Antigonish, Nova Scotia, 86 p.

Mikucki, E.J., 1998, Hydrothermal transport and depositional processes in Archean lode-gold systems: A review: *Ore Geology Reviews*, v. 13, p. 307–321.

Morelli, R.M., Creaser, R.A., Selby, D., Kontak, D.J., and Horne, R.J., 2005, Rhenium-osmium geochronology of arsenopyrite in Meguma Group gold deposits, Meguma terrane, Nova Scotia, Canada: evidence for multiple gold-mineralizing events: *Economic Geology*, v. 100, p. 1229–1242.

Morton, A.C., and Hallsworth, C., 1994, Identifying provenance-specific features of detrital heavy mineral assemblages in sandstones: *Sedimentary Geology*, v. 90, p. 241–256.

Mücke, A., and Bhadra Chaudhuri, J.N., 1991, The continuous alteration of ilmenite through pseudorutile to leucoxene: *Ore Geology Reviews*, v. 6, p. 25–44.

Nesbitt, B.E., Muehlenbachs, K., and Murowchick, J.B., 1989, Genetic implications of stable isotope characteristics of mesothermal Au deposits and related Sb and Hg deposits in the Canadian Cordillera: *Economic Geology*, v. 84, p. 1489–1506.

Nesbitt, H.W., and Young, G.M., 1984, Prediction of some weathering trends of plutonic and volcanic rocks based on thermodynamic and kinetic considerations: *Geochimica et Cosmochimica Acta*, v. 48, p. 1523–1534.

Nesbitt, H.W., and Young, G.M., 1996, Petrogenesis of sediments in the absence of chemical weathering: Effects of abrasion and sorting on bulk composition and mineralogy: *Sedimentology*, v. 43, p. 341–358.

Parry, W.T., and Downey, L.M., 1982, Geochemistry of hydrothermal chlorite replacing igneous biotite: *Clays and Clay Minerals*, v. 30, p. 81-90.

Phillips, G.N., and Powell, R., 2010, Formation of gold deposits: a metamorphic devolatilization model: *Journal of Metamorphic Geology*, v. 28, p. 689–718.

Pitcairn, I.K., Olivo, G.R., Damon, A.H., Craw, D., 2010, Sulfide evolution during prograde metamorphism of the Otago and Alpine schists, New Zealand: The Canadian Mineralogist, v. 48, p. 1267-1295.

Ramsay, W.R.H., Bierlein, F.P., Arne, D.C., and Vandenberg, A.H.M., 1998, Turbidite-hosted gold deposits of Central Victoria, Australia: their regional setting, mineralising styles, and some genetic constraints: *Ore Geology Reviews*, v. 13, p. 131-151.

Ridley, J., and Diamond, L., 2000, Fluid chemistry of orogenic lode gold deposits and implications for genetic models, *Reviews in Economic Geology*, v. 13, p. 141–162.

Robb, L., 2004, Introduction to ore-forming processes: Oxford, Wiley-Blackwell, 386 p.

Rusinov, V.L., Rusinova, O. V., Kryazhev, S.G., Shchegol'kov, Y. V., Alysheva, E.I., and Borisovsky, S.E., 2008, Wall-rock metasomatism of carbonaceous terrigenous rocks in the Lena gold district: *Geology of Ore Deposits*, v. 50, p. 1–40.

Ryan, R.J., and Smith, P.K., 1998, A review of the mesothermal gold deposits of the Meguma Group, Nova Scotia, Canada: *Ore Geology Reviews*, v. 13, p. 153–183.

Sangster, A.L., and Smith, P.K., 2007, Summary of the Meguma Gold Deposits, Nova Scotia, *in* Goodfellow, W.D. ed., *Mineral Deposits of Canada: A Synthesis of Major Deposit-Types, District Metallogeny, the Evolution of Geological Provinces, and Exploration Methods*, Geological Association of Canada, Mineral Deposits Division, Special Publication no. 5, p. 727–732.

Shellnut, J.G., Dostal, J., 2015, Granodiorites of the South Mountain batholith (Nova Scotia, Canada) derived by partial melting of Avalonia granulite rocks beneath the Meguma terrane: Implications for the heat source of the Late Devonian granites of the Northern Appalachians: *Tectonophysics*, v. 655, p. 206–212.

van Staal, C.R., 2007, Pre-Carboniferous metallogeny of the Canadian Appalachians., *in* Goodfellow, W.D. ed., *Mineral Deposits of Canada: A Synthesis of Major Deposit Types, District Metallogeny, the Evolution of Geological Provinces, and Exploration Methods*, Geological Association of Canada, Mineral Deposits Division, Special Publication no. 5, p. 793–818.

van Staal, C.R., and Barr, S.M., 2012, Lithospheric architecture and tectonic evolution of the Canadian Appalachians and associated Atlantic margin, *in* Tectonic Styles in Canada: the LITHOPROBE Perspective, Geological Association of Canada, Special Paper 49, p. 41–95.

van Staal, C.R., Whalen, J.B., Valverde-Vaquero, P., Zagorevski, A., and Rogers, N., 2009, Pre-Carboniferous, episodic accretion-related, orogenesis along the Laurentian margin of the northern Appalachians: Geological Society, London, Special Publications, v. 327, p. 271–316.

Sutton, K., 2007, Nature and origin of oikocrysts in the Meguma group gold districts, Nova Scotia. Unpublished B.Sc. Honours Thesis: Dalhousie University, Halifax, Nova Scotia, 89 p..

Taylor, S.R., and McLennan, S.M., 1981, The composition and evolution of the continental crust: rare-earth element evidence from sedimentary rocks: Philosophical Transactions of the Royal Society of London, v. 301, p. 381–399.

Taylor, S.R., and McLennan, S.M., 1985, The continental crust: its composition and evolution: Oxford, Blackwell, 312 p.

Thomas, H.V., Large, R.R., Bull, S.W., Maslennikov, V., Berry, R.F., Fraser, R., Froud, S., Moye, R., 2011, Pyrite and pyrrhotite textures and composition in sediments, laminated quartz veins, and reefs at Bendigo gold mine, Australia: Insights for ore genesis: Economic Geology, v. 106, p. 1-31.

- Tomkins, A.G., 2010, Windows of metamorphic sulfur liberation in the crust: Implications for gold deposit genesis: *Geochimica et Cosmochimica Acta*, v. 74, p. 3246–3259.
- Toulmin, P., and Barton, P.B., 1964, A thermodynamic study of pyrite and pyrrhotite: *Geochimica et Cosmochimica Acta*, v. 28, p. 641–671.
- Voisey, C.R., Willis, D., Tomkins, A.G., Wilson, C.J.L., Micklethwaite, S., Salvemini, F., Bougoure, J., Rickard, W.D.A., 2020, Aseismic refinement of orogenic gold systems: *Economic Geology*, v. 115, p. 33–50.
- Weatherley, D.K., and Henley, R.W., 2013, Flash vaporization during earthquakes evidenced by gold deposits: *Nature Geoscience*, v. 6, p. 294–298.
- White, C.E., 2010, Stratigraphy of the Lower Paleozoic Goldenville and Halifax groups in the western part of southern Nova Scotia: *Atlantic Geology*, v. 46, p. 136–154.
- Williams, H., 1979, Appalachian Orogen in Canada: *Canadian Journal of Earth Sciences*, v. 16, p. 792–807.
- Williams-Jones, A.E., Bowell, R.J., and Migdisov, A.A., 2009, Gold in solution: *Elements*, v. 5, p. 281–287.
- Xie, X., Byerly, G.R., and Ferrell, R.E., 1997, IIb trioctahedral chlorite from the Barberton greenstone belt: crystal structure and rock composition constraints with

implications to geothermometry: Contributions to Mineralogy and Petrology, v. 126, p. 275–291.

Zang, W., and Fyfe, W.S., 1995, Chloritization of the hydrothermally altered bedrock at the Igarapé Bahia gold deposit, Carajás, Brazil: Mineralium Deposita, v. 30, p. 30–38.

Zhong, R., Brugger, J., Tomkins, A.G., Chen, Y., and Li, W., 2015, Fate of gold and base metals during metamorphic devolatilization of a pelite: Geochimica et Cosmochimica Acta, v. 171, p. 338–352.

Table 2.1 Vein Generations of the Goldboro Deposit

Vein	Vein	Mineralogy	Wall-rock	Distinguishing
Generation	Morphology		Alteration	Features
V1	Bedding-parallel, foliated	Quartz Biotite Chalcopyrite Sphalerite Pyrrhotite	Biotite	Glassy quartz, sulfide-rich
V2	Bedding-parallel, foliated, angular	Quartz Arsenopyrite	Arsenopyrite	Milky quartz, arsenopyrite-rich
V3	Breccia veinlets	Quartz Fe-dolomite Pyrite	None	Tan, carbonate-rich veinlets
V4	Angular veins and veinlets	Quartz Chlorite Plagioclase K-feldspar Fe-dolomite Ilmenite Gold (± biotite, pyrrhotite, sphalerite)	Bleaching (albite+sericite)	Plagioclase, K-feldspar, and chlorite-rich.

Table 2.2 Representative Whole-Rock Geochemical Results
of Mudstones

SAMPLE		385004	385095	385157	385218	385288	385330
Drillhole		BR-18-23	BR-18-59	BR-18-21	BR-18-51	BR-18-96	BR-18-66
Depth	m	57.42	205.6	119.2	236.57	15.7	183
Belt		East Goldbrook	Boston Richardson	East Goldbrook	Boston Richardson	East Goldbrook	Boston Richardson
SiO₂	wt. %	49.1	55.3	57	50.5	57.1	46.1
Al₂O₃	wt. %	23.8	22.5	21.1	23.8	21	26.2
Fe₂O₃	wt. %	9.61	6.91	6.99	8.55	6	7.22
CaO	wt. %	0.68	1.02	0.93	0.63	0.55	1.6
MgO	wt. %	3.3	2.93	2.75	3.42	2.55	3.17
Na₂O	wt. %	0.81	1.26	1.54	0.99	0.77	1.28
K₂O	wt. %	7.89	6.53	5.98	7.78	6.23	8.15
Cr₂O₃	wt. %	0.018	0.016	0.015	0.016	0.014	0.018
TiO₂	wt. %	0.98	0.86	0.88	0.89	0.85	1.14
MnO	wt. %	0.12	0.11	0.1	0.08	0.06	0.13
P₂O₅	wt. %	0.13	0.2	0.16	0.16	0.16	0.15
SrO	wt. %	0.02	0.02	0.02	0.01	0.01	0.03
BaO	wt. %	0.14	0.15	0.13	0.15	0.13	0.18
LOI	wt. %	3.02	2.8	2.26	3.96	3.29	3.51

Total	wt. %	99.62	100.61	99.86	100.94	98.71	98.88
C	wt. %	0.03	0.06	0.11	0.6	0.03	0.26
S	wt. %	0.28	0.53	0.02	0.69	0.03	0.23
Ba	ppm	1260	1350	1170	1415	1250	1635
Ce	ppm	87.4	94.7	83.3	92.1	72.4	109
Cr	ppm	120	110	100	120	110	130
Cs	ppm	11.75	8.49	10.7	10.45	7.97	13.9
Dy	ppm	5.95	6.49	6.24	6.39	5.74	6.45
Er	ppm	3.42	3.59	3.63	3.82	3.51	3.57
Eu	ppm	1.5	1.63	1.39	1.56	1.32	1.9
Ga	ppm	36.3	33.6	31.1	36.8	34.9	40.7
Gd	ppm	5.97	7.26	5.77	6.58	5.61	6.8
Ge	ppm	<5	<5	<5	<5	<5	<5
Hf	ppm	5.4	4.6	5	4.7	4.3	6.3
Ho	ppm	1.07	1.15	1.08	1.28	1.14	1.33
La	ppm	41.8	47.9	40.2	46.7	35.5	54.4
Lu	ppm	0.49	0.46	0.46	0.55	0.5	0.57
Nb	ppm	16	16.4	14.8	16.4	15.1	20.4
Nd	ppm	37.2	43.1	36	40.3	32.2	48.1
Pr	ppm	9.68	11	9.58	11.05	8.58	12.9
Rb	ppm	258	206	196	272	223	287
Sm	ppm	7.28	8.95	7	8.08	6.28	9.05
Sn	ppm	3	3	3	4	3	4
Sr	ppm	129.5	147	151	125.5	90	238
Ta	ppm	1	1	1.1	1.2	1.1	1.3

Tb	ppm	0.79	0.94	0.98	0.99	0.89	1.12
Th	ppm	13.05	11.65	11.5	12.85	12.2	14.85
Tm	ppm	0.5	0.47	0.43	0.56	0.5	0.58
U	ppm	2.57	2.31	2.52	2.72	2.44	3.13
V	ppm	126	127	129	157	143	166
W	ppm	15	13	9	13	11	14
Y	ppm	29.8	31.9	31.1	34.9	30.5	33.3
Yb	ppm	3.32	3.2	3.33	3.62	3.33	3.63
Zr	ppm	183	163	184	164	170	240
As	ppm	>250	>250	63.9	>250	168	>250
Bi	ppm	0.13	0.35	0.63	0.62	0.07	0.1
Hg	ppm	<0.005	<0.005	0.006	<0.005	0.007	<0.005
In	ppm	0.023	0.016	0.028	0.019	0.01	0.014
Re	ppm	<0.001	<0.001	<0.001	0.001	0.001	0.001
Sb	ppm	0.89	1.28	0.39	1.34	0.44	0.47
Se	ppm	<0.2	<0.2	<0.2	<0.2	<0.2	<0.2
Te	ppm	<0.01	0.02	0.08	0.2	0.01	0.05
Tl	ppm	0.7	0.57	0.67	0.82	0.27	0.69
Ag	ppm	<0.5	<0.5	<0.5	<0.5	<0.5	<0.5
Cd	ppm	1.5	<0.5	<0.5	1	<0.5	<0.5
Co	ppm	25	16	32	25	20	21
Cu	ppm	66	60	101	44	12	33
Li	ppm	90	80	70	80	70	90
Mo	ppm	1	<1	1	1	<1	<1
Ni	ppm	68	43	58	52	54	60

Pb	ppm	22	22	36	43	21	23
Sc	ppm	17	19	18	20	17	20
Zn	ppm	154	120	106	135	116	125
C	wt. %	<0.05	<0.05	<0.05	<0.05	<0.2	<0.05
CO₂	wt. %	<0.2	<0.2	<0.2	<0.2	<0.05	<0.2
Au	ppm	0.016	0.973	0.084	0.228	0.029	0.059

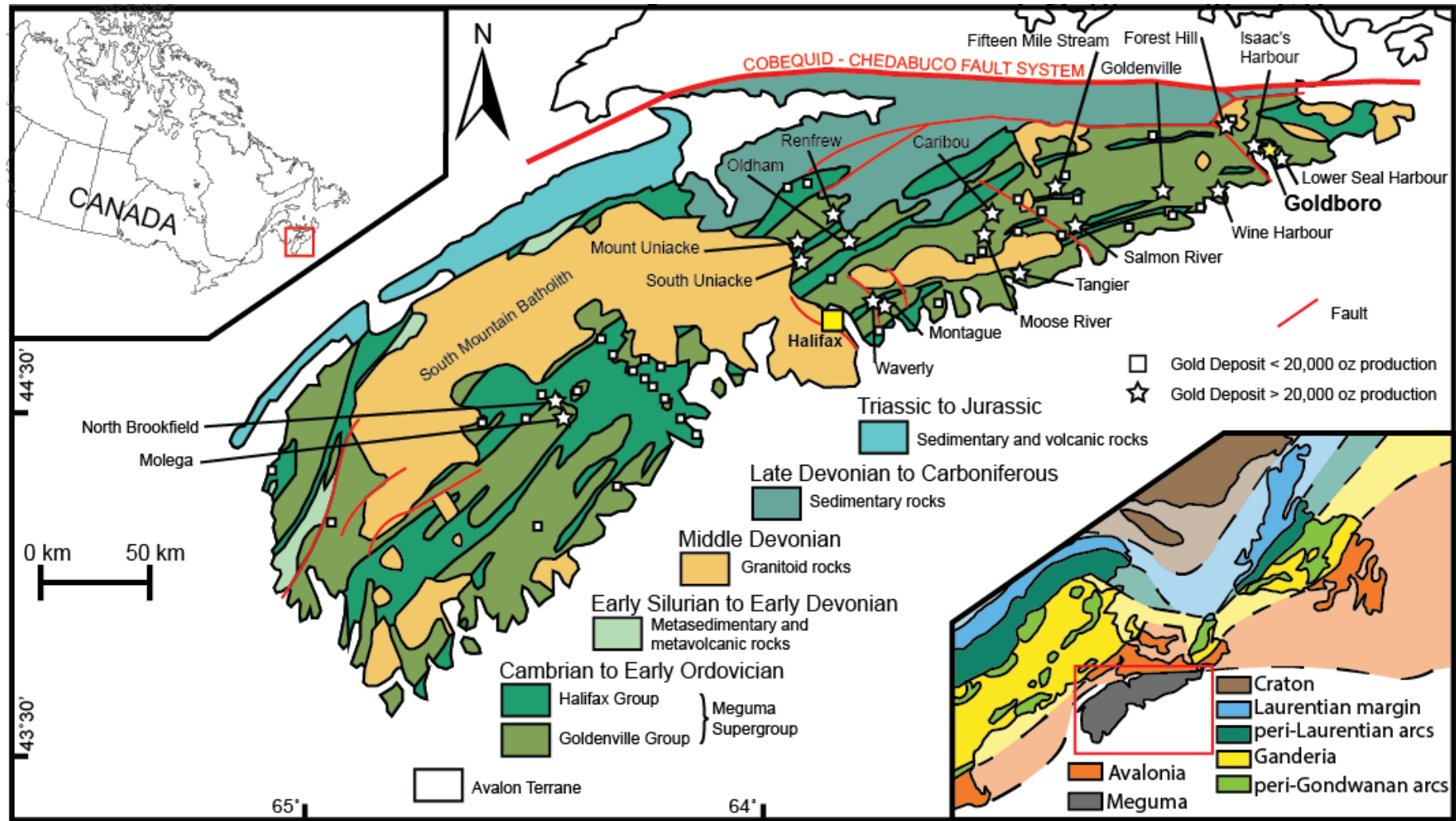


Figure 2.1: Regional map of the Meguma Terrane and its major gold deposits. Gold production data from Sangster and Smith (2007), modified from Kontak et al. (2003).

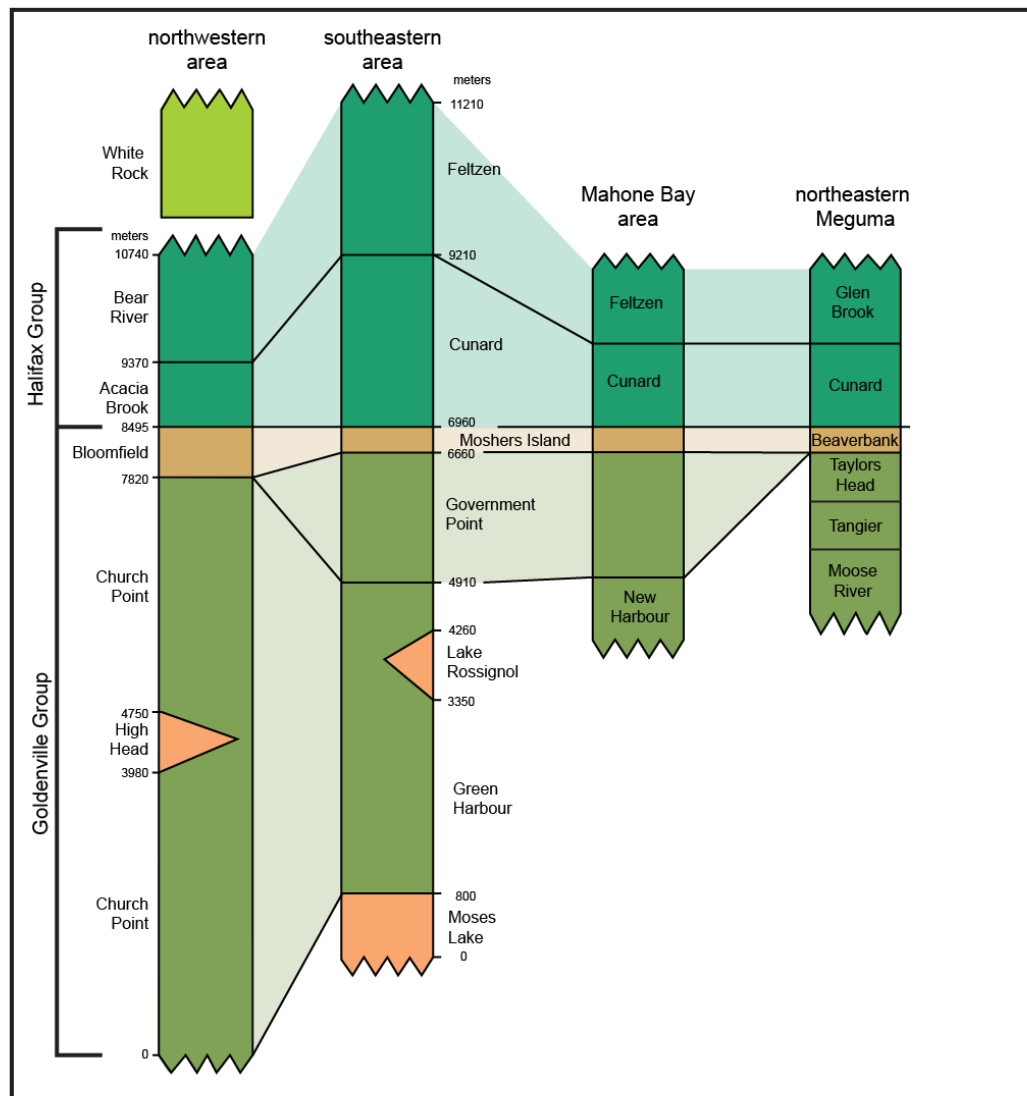


Figure 2.2: Regional stratigraphy of the Meguma Terrane, including regionally mapped formations. For these sections, no stratigraphic thickness is implied (modified from White, 2010).

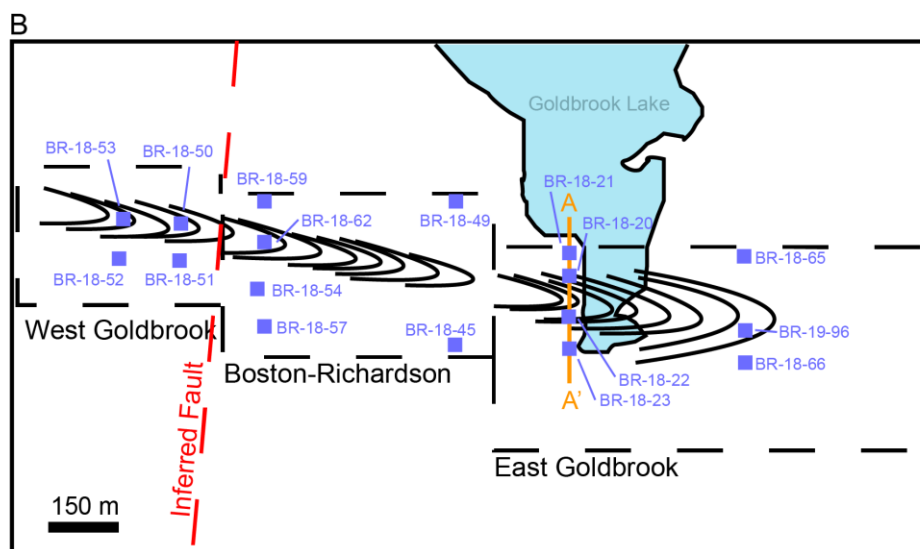
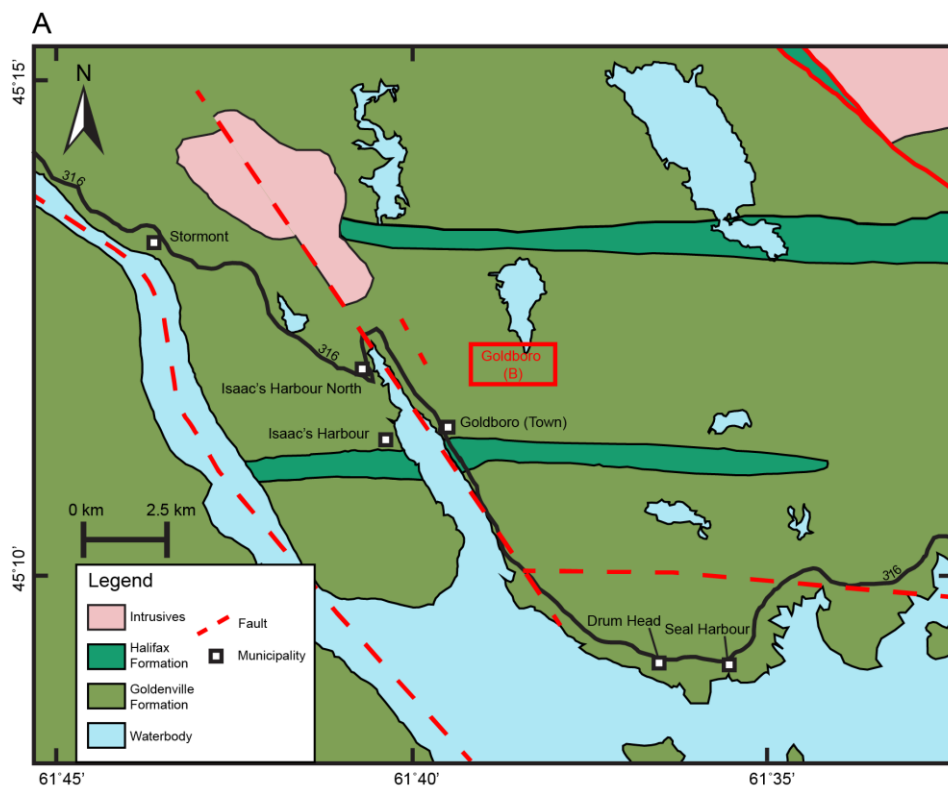


Figure 2.3: a) Simplified local geological map of the Goldboro deposit, Nova Scotia, modified from Ryan and Smith (1998). b) Plan view of the Goldboro property, depicting the stratigraphic belts and drillholes logged in this study. The line A-A' in b) denotes the cross section shown in Figure 2.4.

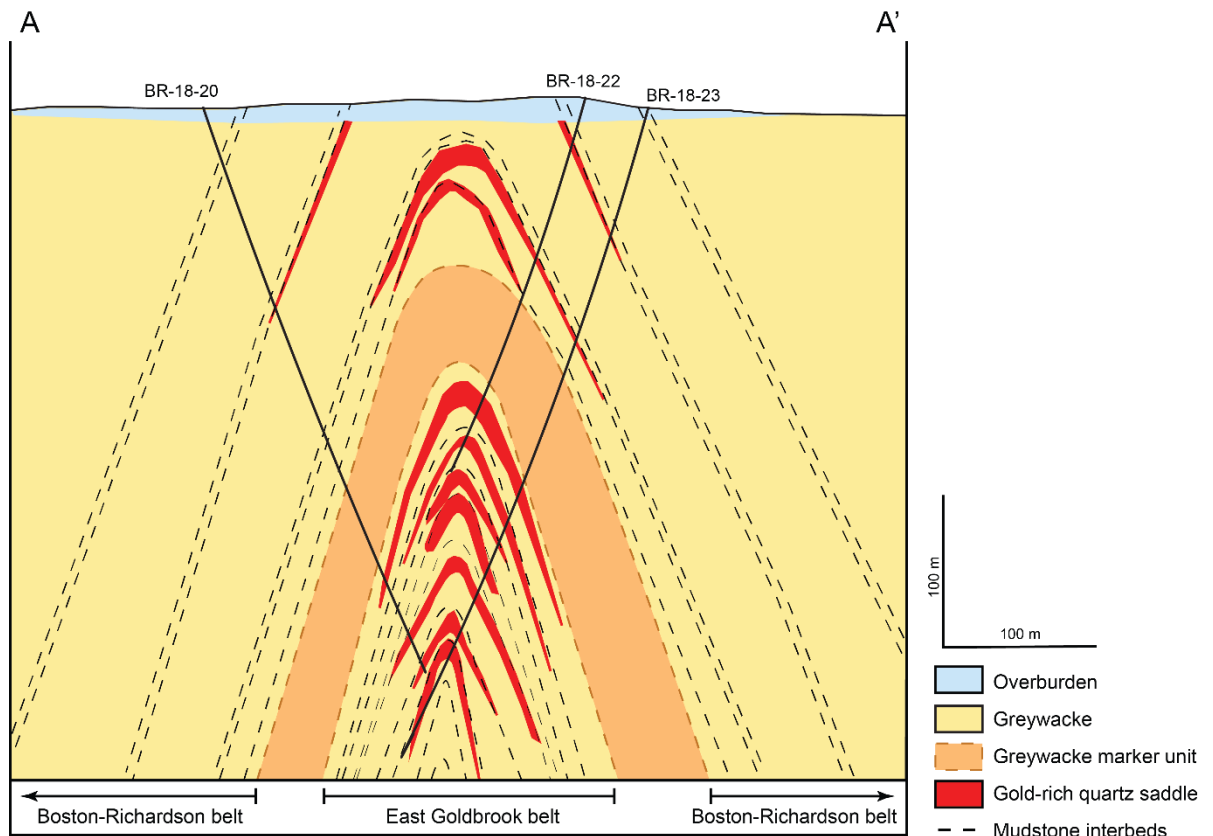


Figure 2.4: Cross-section of the Goldboro deposit (facing East), the line A-A' is shown in the inset of Figure 2.3 (modified from Kuntz et al., 2021). Shown are the East Goldbrook and the underlying Boston-Richardson belts, separated by a thick, massive greywacke unit used as a stratigraphic marker. Shown here is the higher density of mudstone interbeds and quartz saddles in the Boston-Richardson relative to the East Goldbrook.

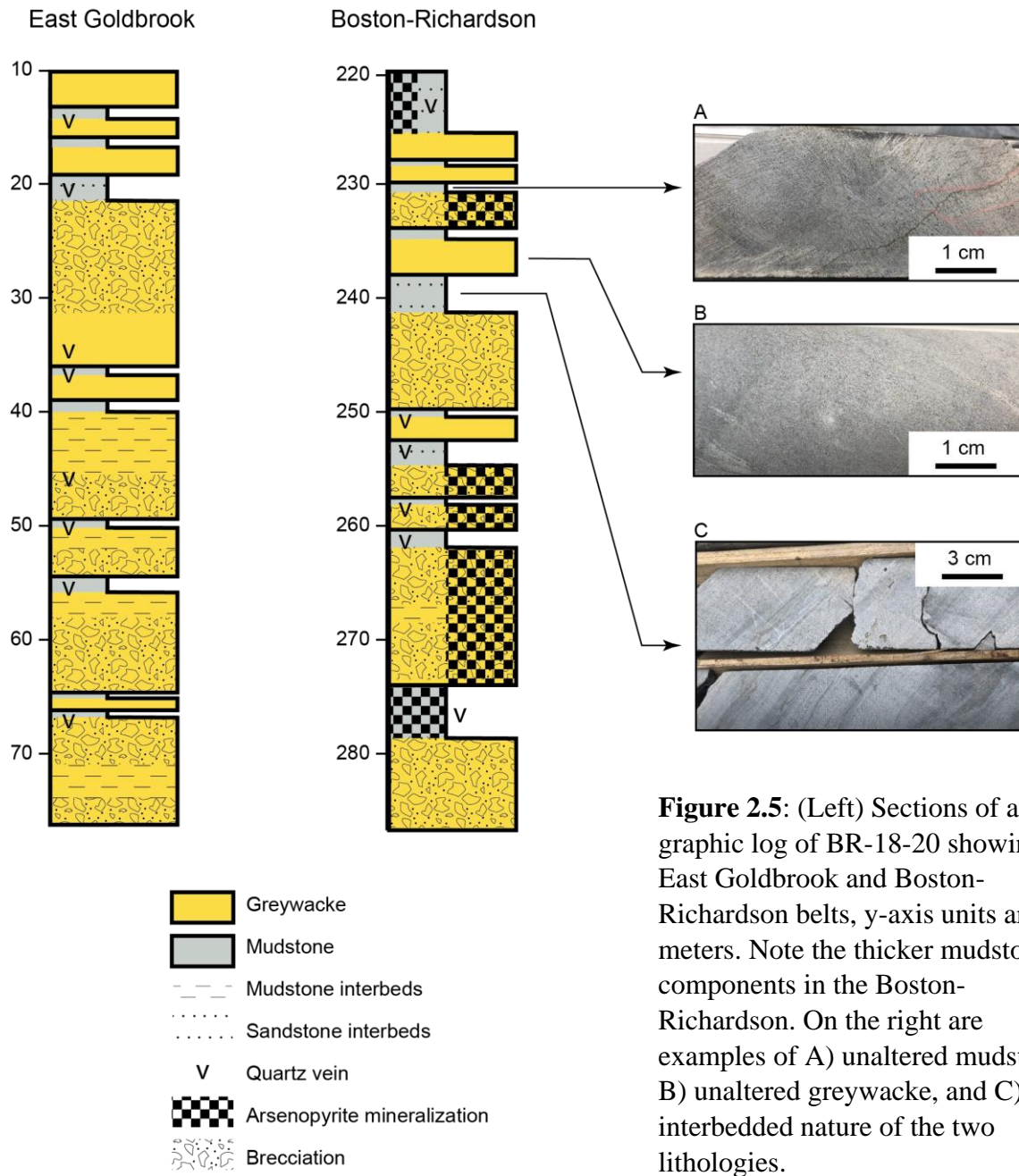


Figure 2.5: (Left) Sections of a graphic log of BR-18-20 showing the East Goldbrook and Boston-Richardson belts, y-axis units are in meters. Note the thicker mudstone components in the Boston-Richardson. On the right are examples of A) unaltered mudstone, B) unaltered greywacke, and C) the interbedded nature of the two lithologies.

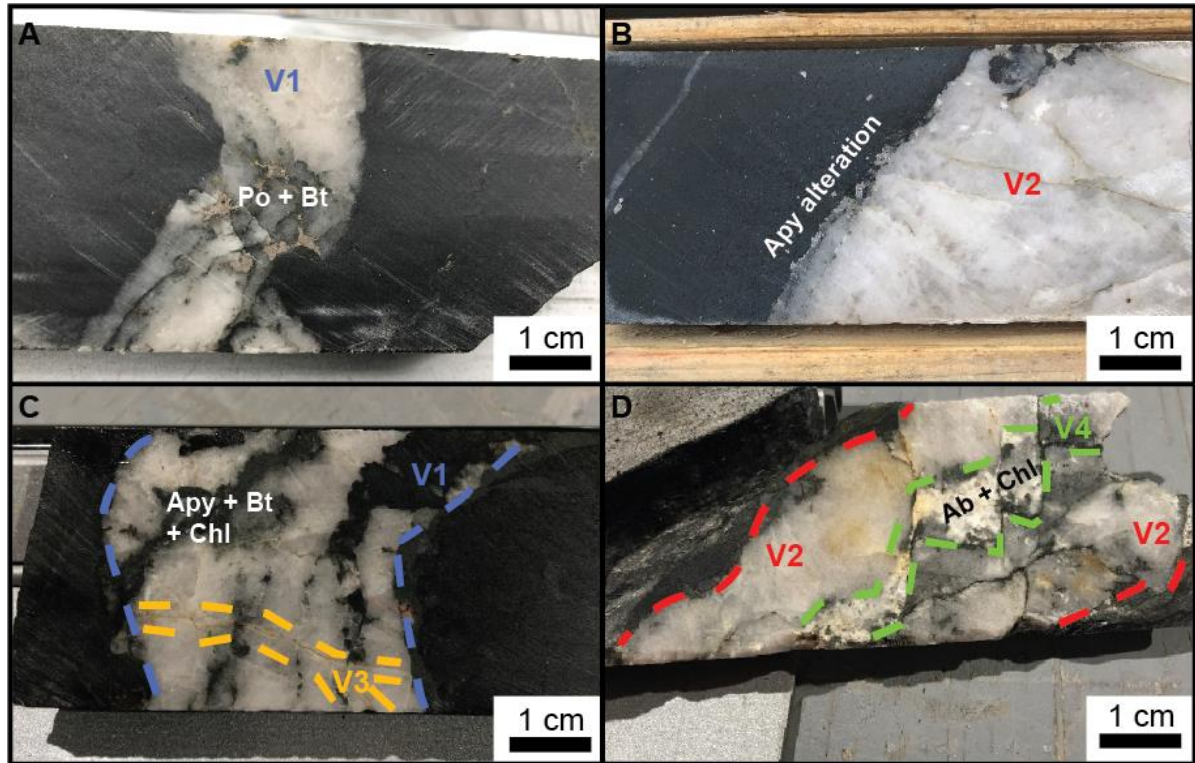


Figure 2.6: The four generations of vein development at Goldboro: a) Foliated V1 vein containing pyrrhotite and biotite, b) V2 vein exhibiting arsenopyrite alteration, c) V3 veinlet (orange) cross-cutting a V1 vein (blue), d) V4 vein (green) cross-cutting a V2 vein (red). Po = pyrrhotite, Bt = biotite, Apy = arsenopyrite, Chl = chlorite, Ab = albite.

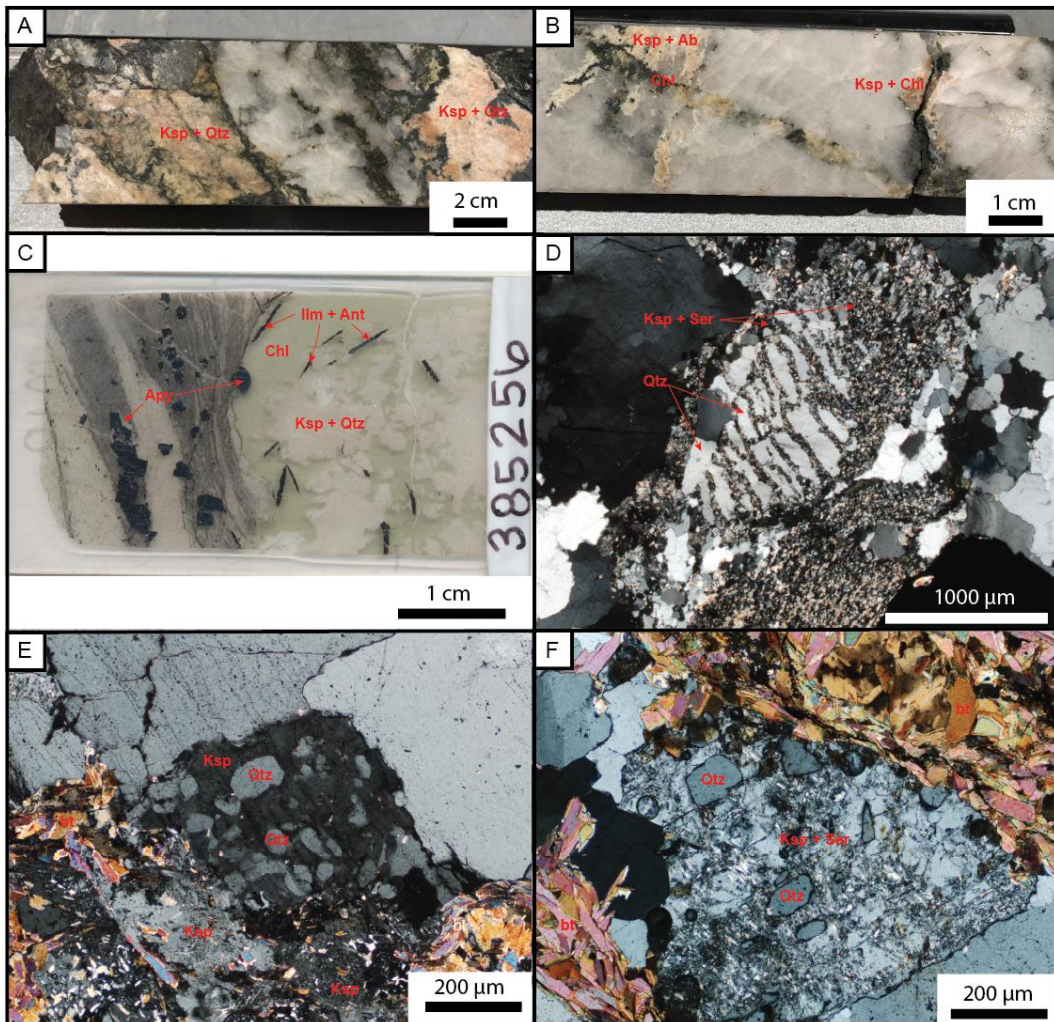


Figure 2.7: V4 veins at varying scales. a,b) V4 vein at hand-sample scale. Note that in b), the V4 vein cross-cuts a pre-existing quartz vein. c) Thin section scan of a V4 vein margin, containing chlorite and euhedral ilmenite that has been partially altered to anatase. d-f) Cross-polarized light photomicrographs of K-feldspar and quartz granophytic intergrowths. Note that K-feldspar is not commonly preserved, and is rather partially or completely altered to sericite. In particular, d) is a relict texture where K-feldspar is entirely replaced by sericite. Qtz = quartz, Ksp = K-feldspar, Chl = chlorite, IIm = ilmenite, Ant = anatase, Ser = sericite.

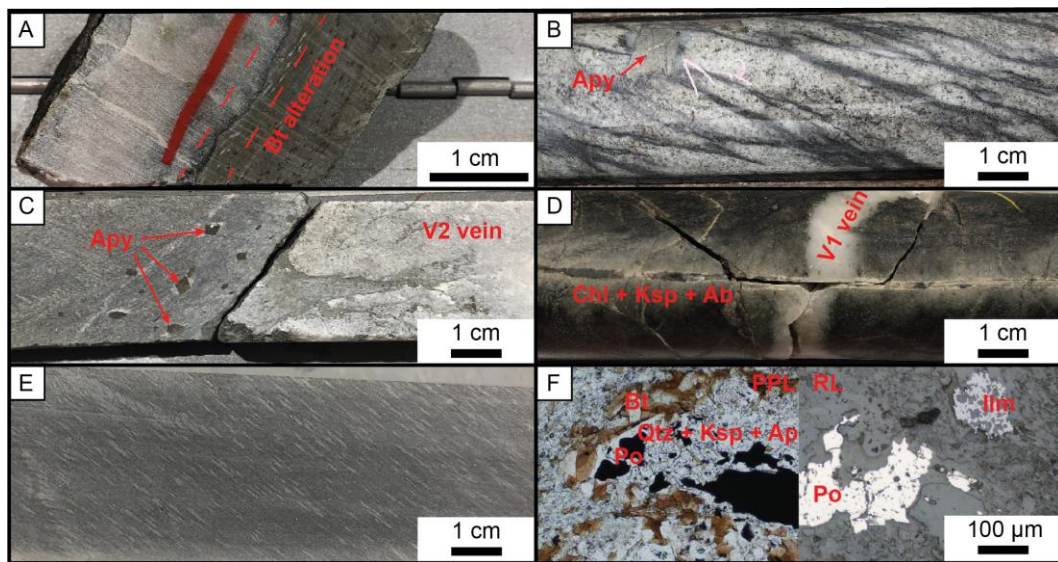


Figure 2.7: Alteration types of the Goldboro deposit. a) Biotite alteration of the margins of a V1 vein. b) Bleaching (sericite+albite) alteration of greywacke. c) Arsenopyrite mineralization associated with a V2 vein. d) bleaching of greywacke extending outwards from a V4 vein cross-cutting a V1 vein. e) Quartzo-feldspathic blebs that are typical of Meguma-type deposits. f) Photomicrograph of a bleb, exhibiting a quartz+K-feldspar+apatite+pyrrhotite+biotite composition. Ab = albite, Apy = arsenopyrite, Bt = biotite, Chl = chlorite, IIm = ilmenite, Ksp = K-feldspar, Po = pyrrhotite.

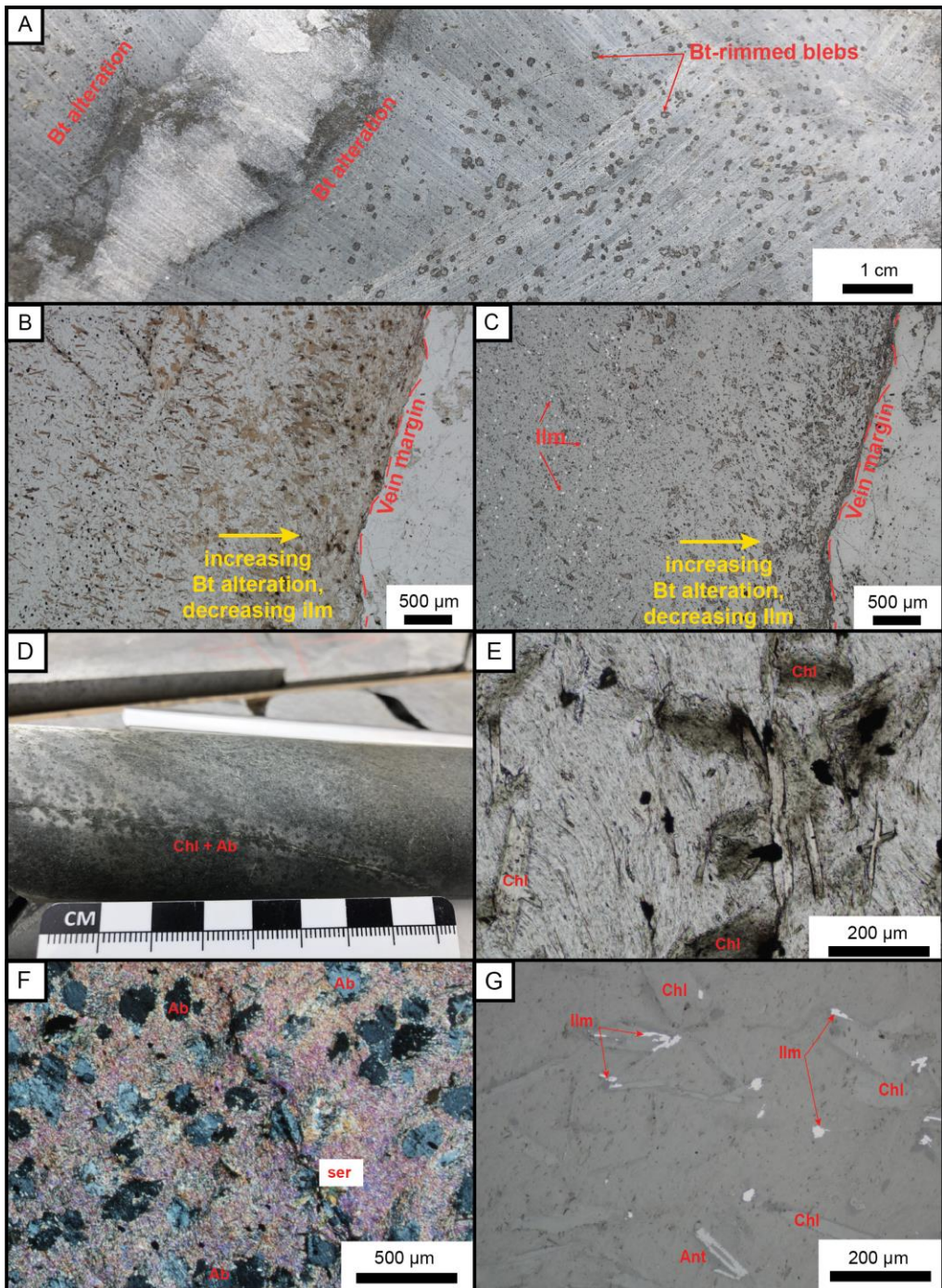


Figure 2.8: Alteration at various scales. a) Hand sample-scale biotite wall-rock alteration at the margin of a V1 vein. b) Photomicrograph in plane-polarized light of increasing biotite intensity proximal to the vein. c) Reflected light photomicrograph of the same location in b), highlighting the decrease in ilmenite proximal to the vein margin. d) albite and chlorite alteration visible at hand-sample scale. e) Photomicrograph in plane-polarized light of chlorite alteration of wall-rock proximal to a V4 vein. f) Cross-polarized light photomicrograph of albite and sericite alteration proximal to a V4 vein. g) Reflected light photomicrograph highlighting the association of ilmenite and anatase with chlorite alteration. Bt = biotite, IIm = ilmenite, Chl = chlorite, Ab = albite, Ser = sericite, Ant = anatase.

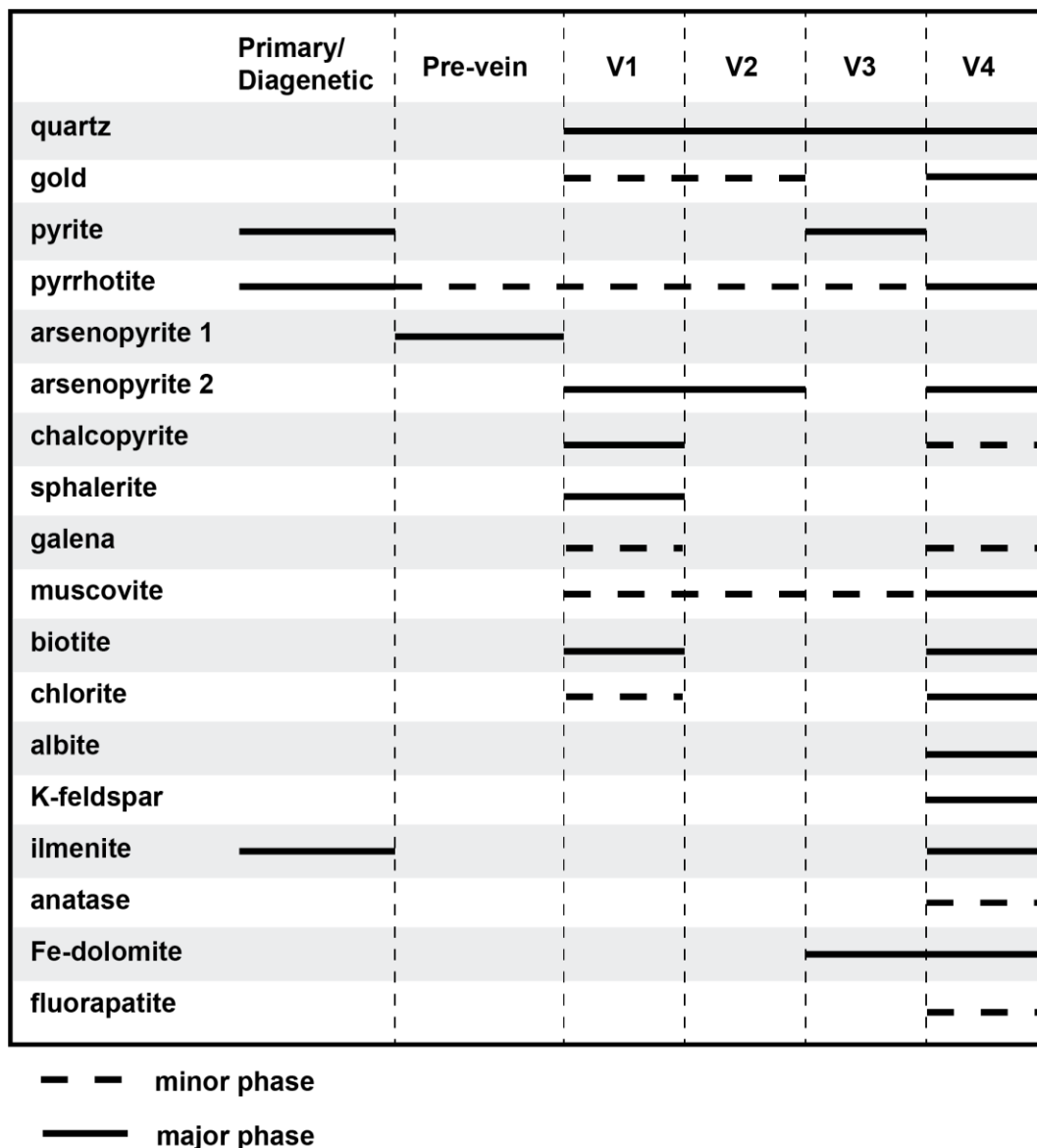


Figure 2.10: Mineral paragenesis of the Goldboro deposit.

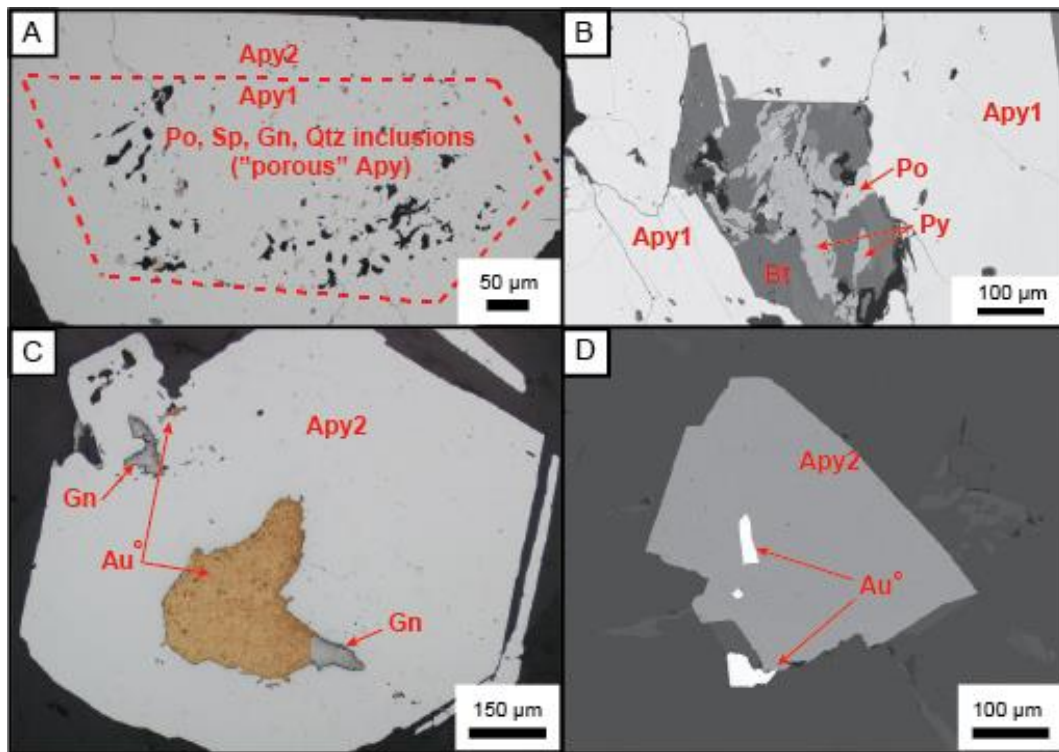


Figure 2.11: Arsenopyrite generations and gold morphology at the Goldboro deposit. a) Reflected light photomicrograph of zoned arsenopyrite, consisting of a porous arsenopyrite 1 core and arsenopyrite 2 overgrowth. b) SEM image of arsenopyrite containing a pyrite core, c) photomicrograph of gold cores inside of arsenopyrite 2, hosted in a V1/V4 compound vein, d) SEM image of gold within and proximal to arsenopyrite 2, hosted in a V4 vein. Apy = arsenopyrite, Au° = gold, Gn = galena, Po = pyrrhotite, Sp = sphalerite, Qtz = quartz.

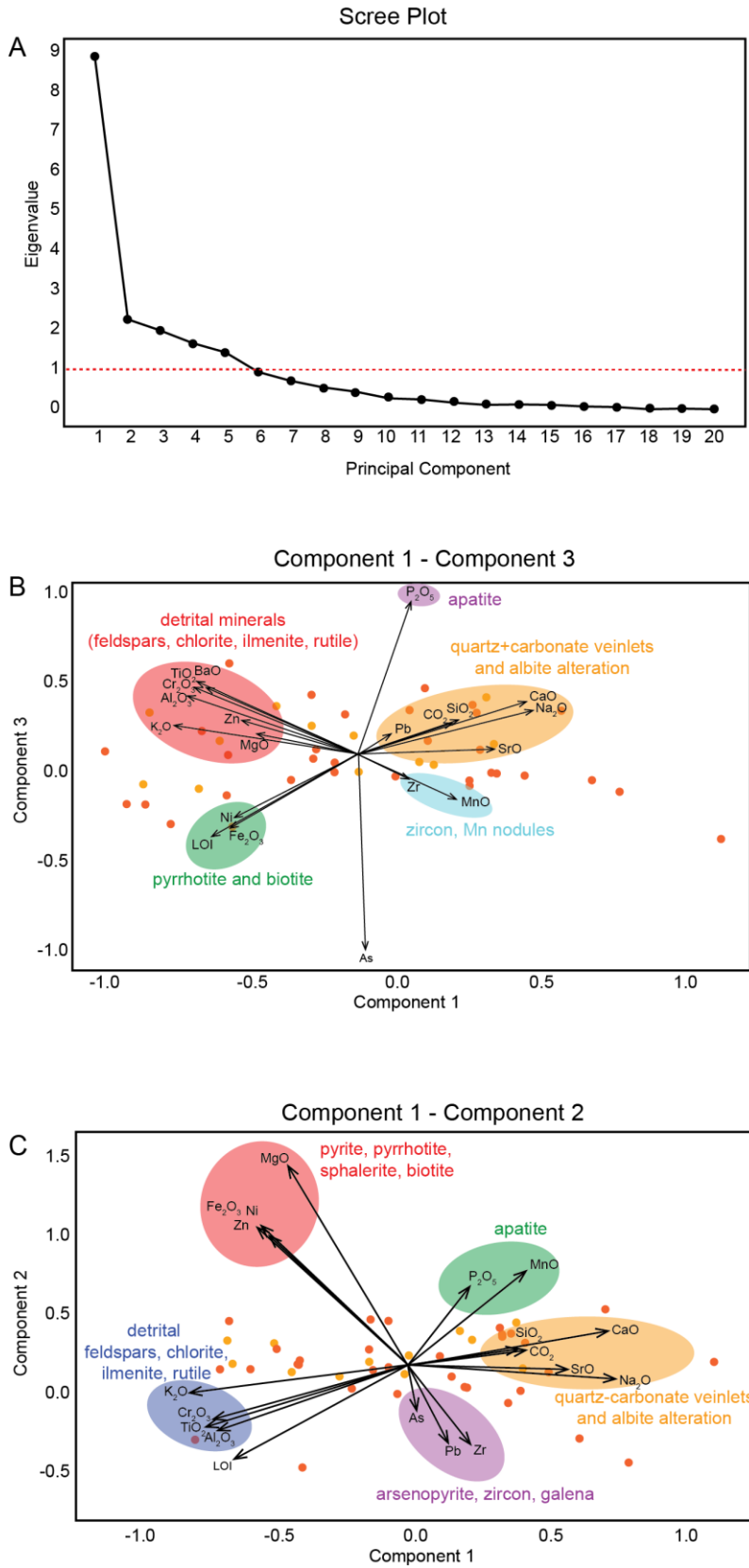


Figure 2.12: Results of principal component analysis (PCA) on lithogeochemical data. The data were corrected using a log-centered ratio transformation prior to PCA. a) Scree plot showing that there are five principal components (eigenvalue > 1). c) Biplot of component 1 vs. component 3, shaded regions are interpretations of the clustered elements based on field and petrographic observations. b) Biplot of component 1 vs. component 2. The inverse directions of the K_2O - Al_2O_3 and Na_2O + CaO - CO_3 - SrO vectors broadly correlates to sericite alteration.

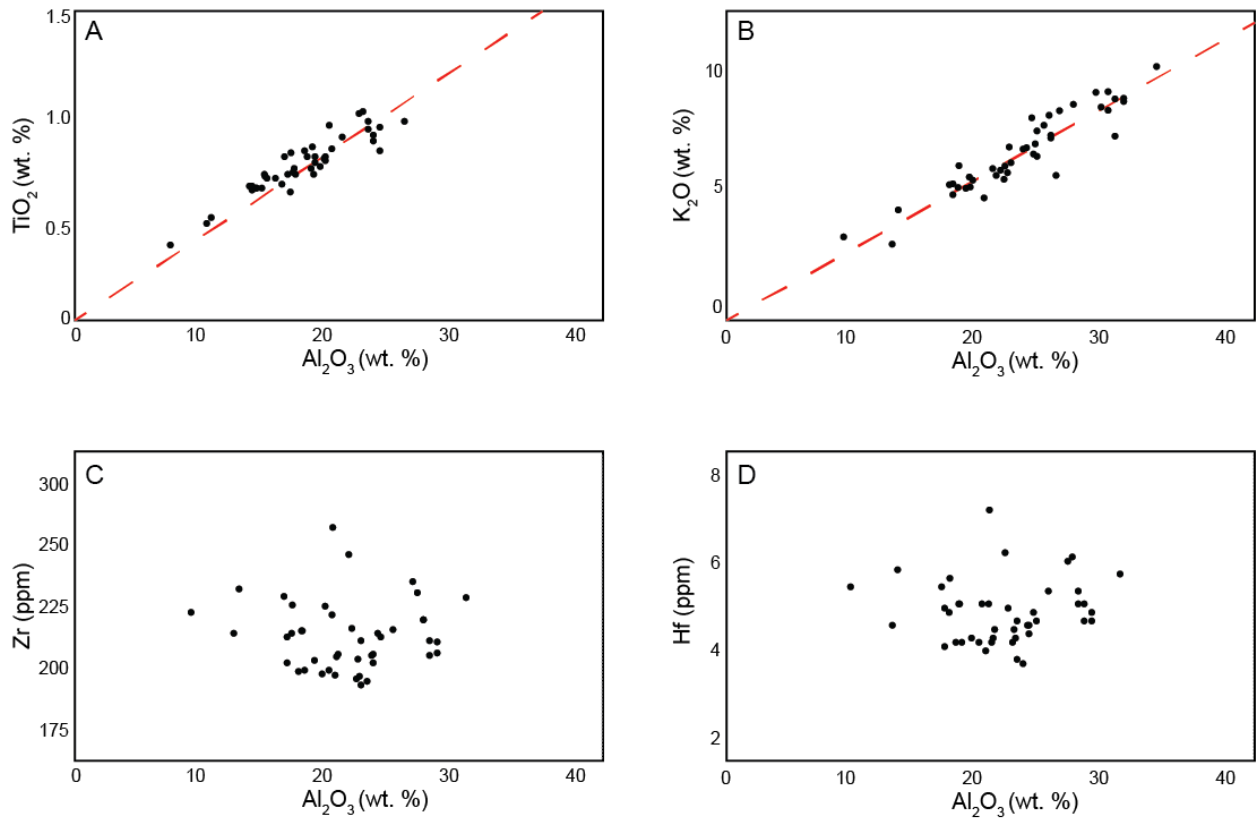


Figure 2.13: Immobile element pair diagrams for the Goldboro mudstones. According to the procedures of Kranidiotis and MacLean (1989), an immobile element pair will form a linear trend when plotted against one another. a,b) TiO_2 vs. Al_2O_3 and K_2O vs. Al_2O_3 form a linear trend along a line that passes through the origin. c,d) Zr and Hf have a “shotgun” pattern that does not form a trend, attributed to the variable sandstone component in the mudstones, which enriches the sample in detrital zircon.

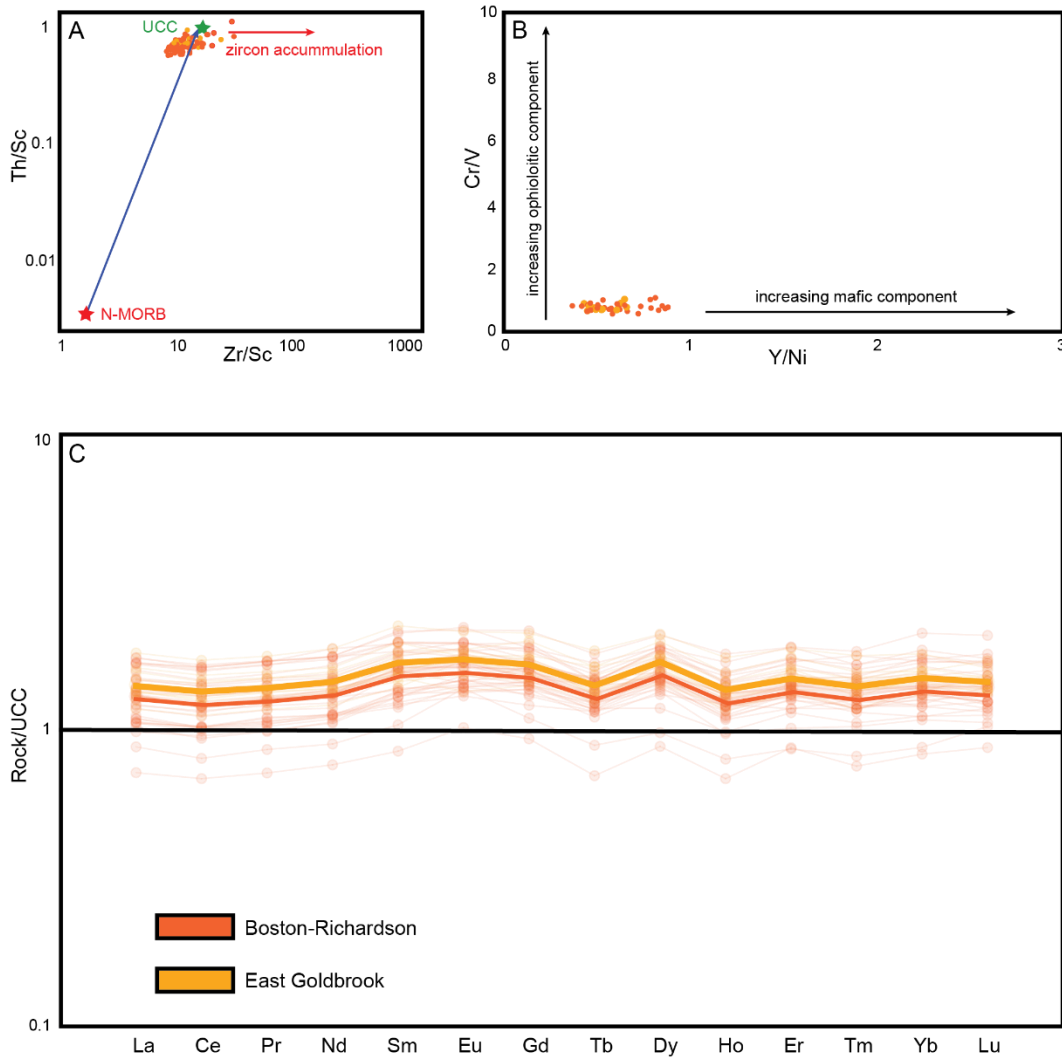


Figure 2.14: Immobile element diagrams of the Goldboro mudstones. a) Th/Sc vs. Zr/Sc. Both Th/Sc and Zr/Sc increase with igneous differentiation; Th/Sc and Zr/Sc of active margin metaturbidite sequences mirror that of the upper continental crust. When subjected to sediment recycling (i.e. zircon addition), the Zr/Sc of sediments increases independently from Th/Sc due to the addition of zircon (after McLennan et al., 2003). UCC = upper continental crust, N-MORB = normal mid-ocean ridge basalt. b) Cr/V vs. Y/Ni; Plotting Y/Ni vs. Cr/V (Fig. 2.13b) provides insight into the ophiolitic and mafic sedimentary components; Y/Ni increases with mafic input, and Cr/V increases with ophiolitic input (McLennan, 2003). c) Rare-earth element diagram normalized to the upper continental crust. transparent lines are each individual sample, whereas the solid lines are the average values for each stratigraphic zone, which are not geochemically unique.

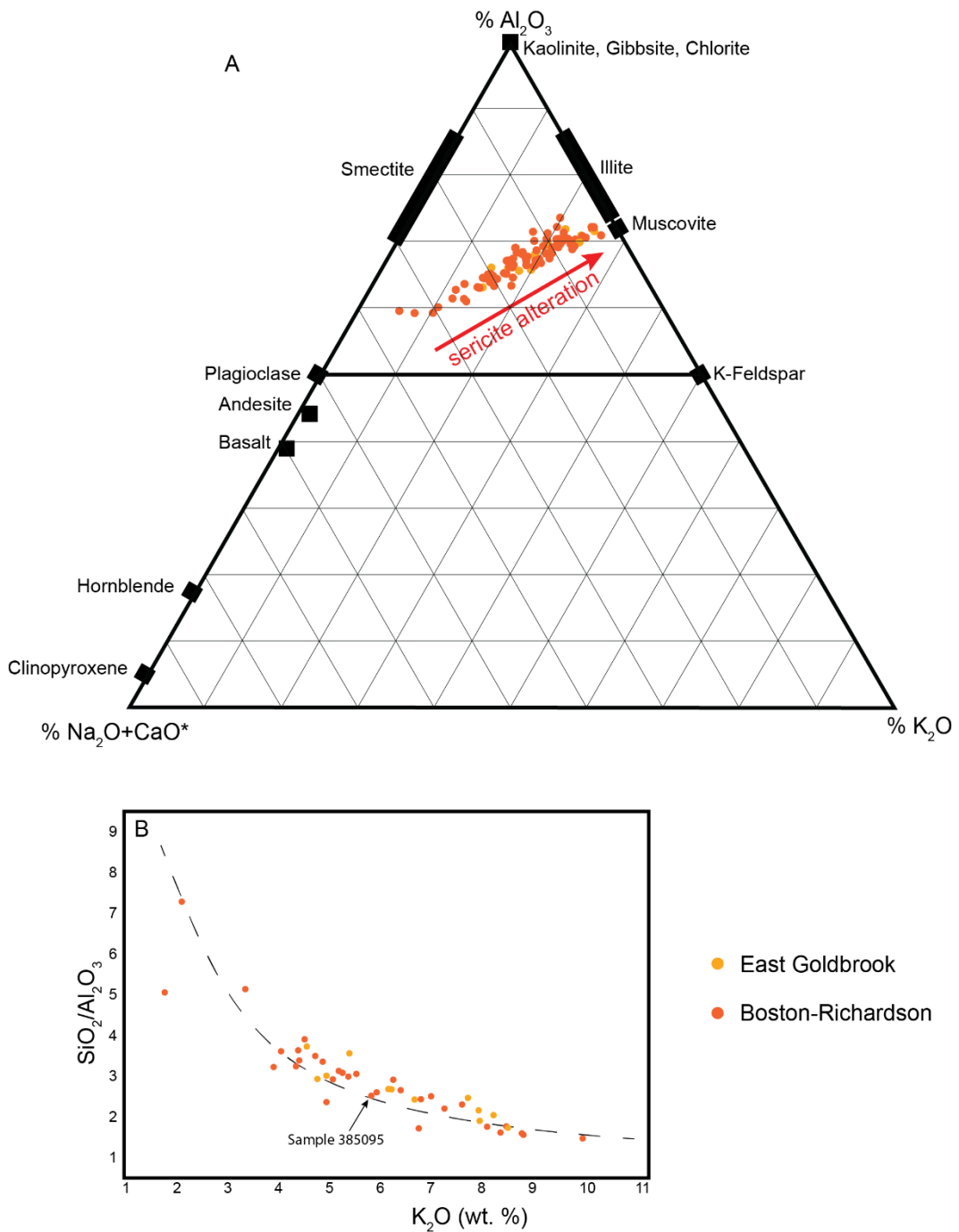


Figure 2.15: a) CIA (chemical index of alteration) plot of the Goldboro mudstones. Note the general trend towards being more Na₂O+CaO* and K₂O-poor parallel to the arrow labeled ‘sericite alteration’, akin to what is expected for weathering processes as feldspars alter to sericite and clays (after Nesbitt and Young, 1996). b) SiO₂/Al₂O₃ vs. K₂O sorting curve. As outlined by Lickley et al. (1987), the least altered samples lie along a hyperbolic curve between two end-member samples; sample 385095 was chosen as the least-altered sample as it had both a low CIA and lies along the hyperbolic curve in b).

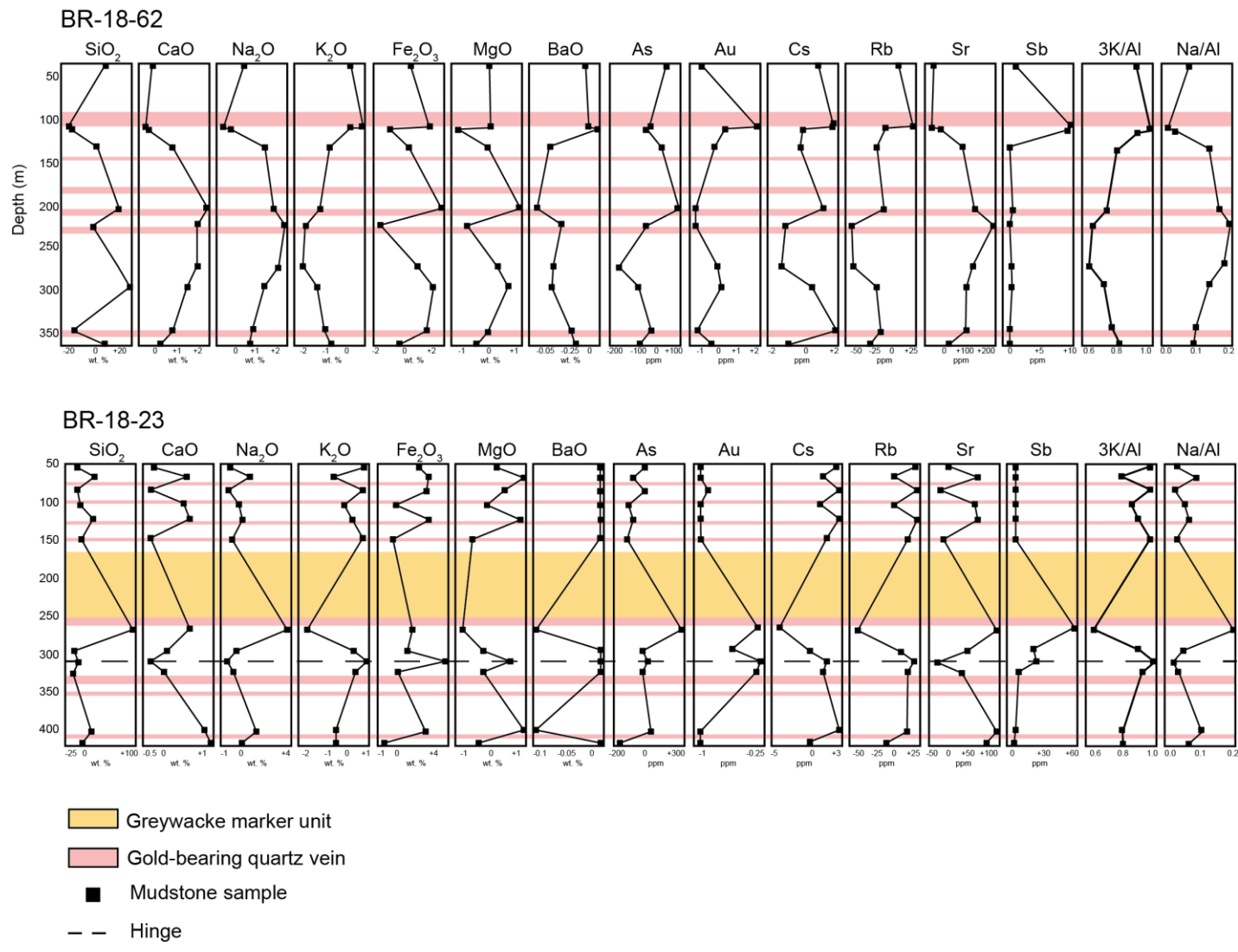


Figure 2.16: Downhole profile of the mass change in mudstones for drillholes BR-18-62 and BR-18-23. Red lines indicate gold-bearing quartz saddles. Note that BR-18-62 consists only of the Boston-Richardson belt, whereas BR-18-23 contains both the Boston-Richardson and East Goldbrook belts, which respectively overlie and underlie the greywacke marker unit (yellow). BR-18-62 is drilled along the hinge line, whereas BR-18-23 goes through the south limb of the anticline and is shown in Figure 2.4

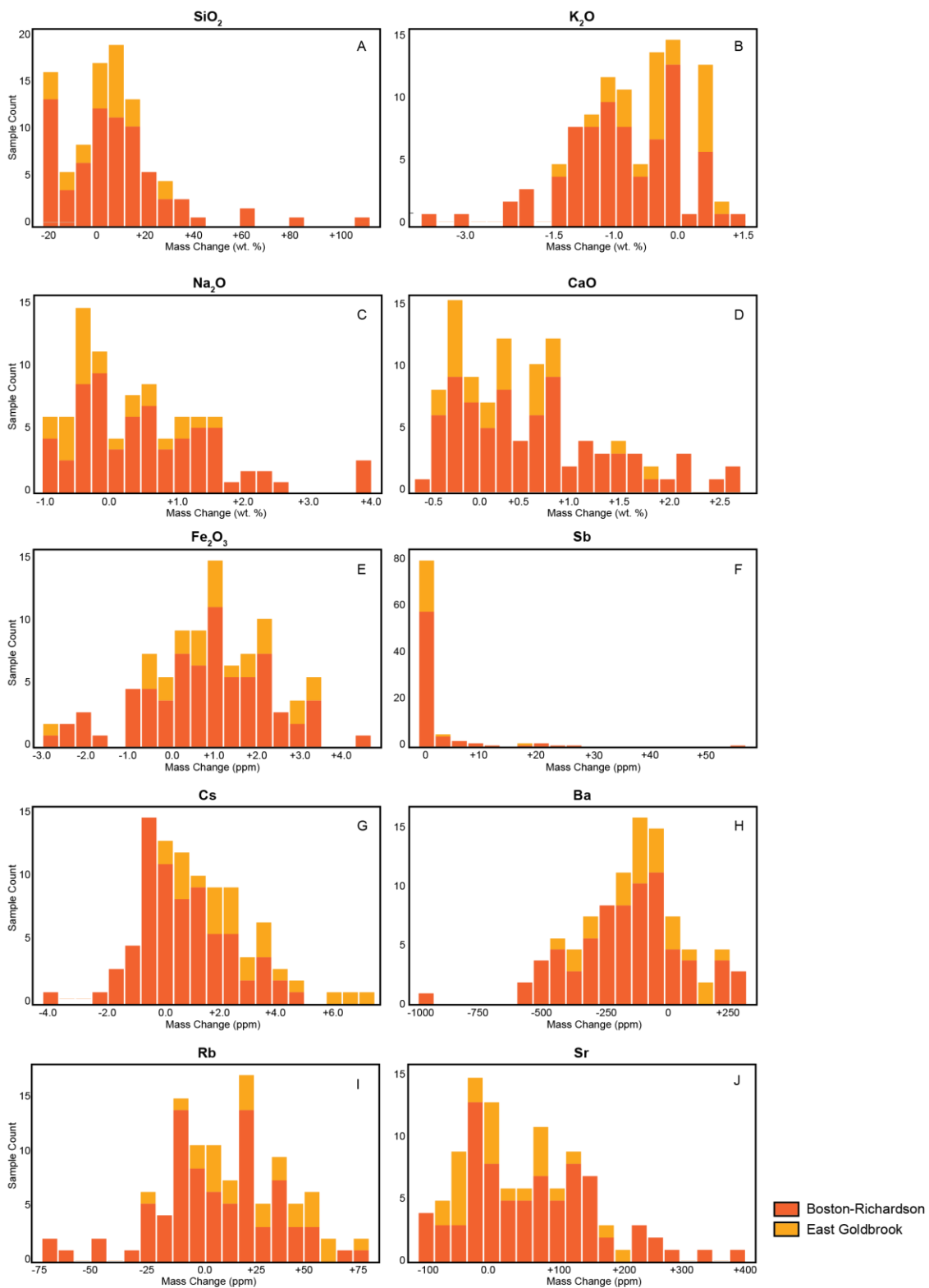


Figure 2.17: Mass change plots for major elements exhibiting mass changes. a) SiO₂ exhibits a general mass increase, mostly attributed to quartz veins and veinlets, b) K₂O exhibits both a mass increase and a mass loss. Mass loss is attributed to the removal of K during the alteration of feldspar to sericite; mass gain is attributed to K addition during V4-stage hydrothermal alteration. c-d) both Na₂O and CaO exhibit a general mass gain, attributed to V4-stage albite alteration of the wall-rock. e) Fe₂O₃ shows both a gain and a loss, likely reflecting the mobilization and refocusing of Fe during alteration. f) Sb exhibits very little mass change across the property, but exhibits local mass gains proximal to certain quartz veins, as is shown in Fig. 2.16. g) Cs exhibits a general mass gain. h) Ba exhibits a general mass loss. i) Rb exhibits a general mass gain. The mass changes of LILE, except Sr, is related to mass changes in K₂O, as is shown in Fig. 2.16. j) Sr exhibits an overall mass gain as a results of carbonate mineralization in V3 veins.

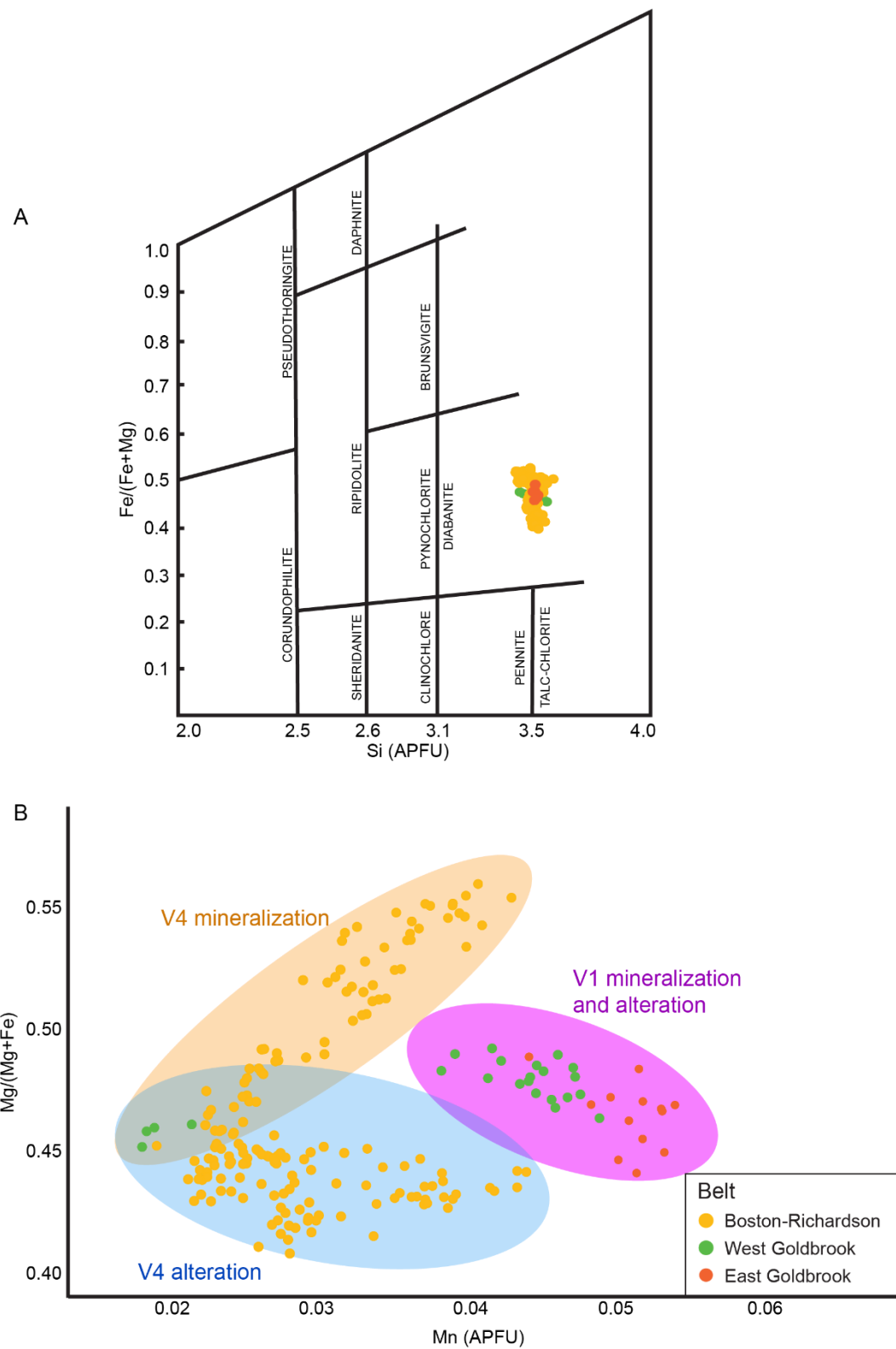


Figure 2.18: Electron probe micro-analysis data for chlorite. a) chlorite composition diagram of $\text{Fe}/(\text{Fe}+\text{Mg})$ vs. Si atoms per formula unit. All chlorite plots within the diabanite field (after Hey, 1954). b) $\text{Mg}/(\text{Mg}+\text{Fe})$ vs. Mn atoms per formula unit. Note that V1-stage chlorite is more Mn-rich than V4 chlorite. Additionally, in-vein V4 chlorite contains has higher $\text{Mg}/(\text{Mg}+\text{Fe})$ than V4 chlorite that exists as a wall-rock alteration product. Note that samples were very limited and may not be representative of mica alteration between mineralized areas.

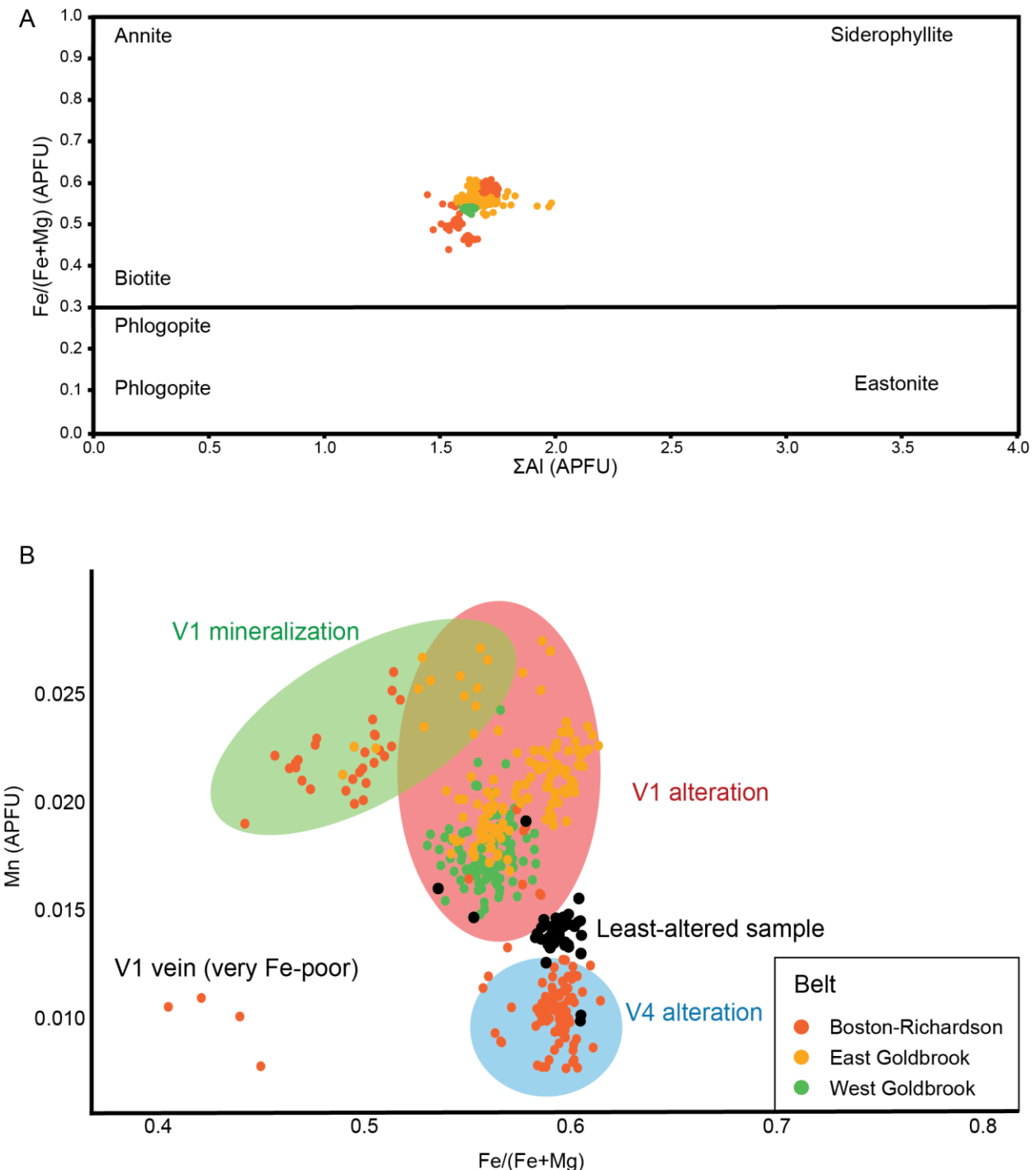


Figure 2.19: Electron probe micro-analysis results for Goldboro biotite. a) Compositional diagram for biotite (after Deer et al., 1992). b) Mn atoms per formula unit vs. $\text{Fe}/(\text{Fe}+\text{Mg})$ for the Goldboro biotites. Note that, like the chlorites in Figure 2.14b, V1 biotite is relatively enriched in Mn relative to V4 biotite. Compared to the least-altered sample, V1 stage introduced Mn, whereas the V4 biotite is depleted in Mn, possibly due to some degree of acid leaching. Note that samples were very limited and may not be representative of mica alteration between mineralized zones.

Chapter 3: Summary and Future Research

3.1 Summary

The Goldboro deposit is a Meguma-type orogenic gold deposit located on the eastern shore of Nova Scotia. This study utilized fieldwork, petrography, lithogeochemistry, mineral imaging, and electron probe micro-analysis (EPMA) to provide key insights into the controls of gold mineralization and its associated alteration. The study also provides geological, mineral, and chemical vectors towards gold mineralization in Goldboro and other Meguma-type orogenic gold deposits. The major conclusions of this thesis are:

The Goldboro deposit is a product of at least four stages of vein development. Gold mineralization of economic interest is closely associated with V4-stage veins rather than V1 and V2 veins, as previously proposed. Gold-hosting V4 veins are pegmatitic in nature, as evidenced by their mineral assemblages, granophytic intergrowths of K-feldspar and quartz, and a high (370-400 °C) temperature of formation of V4 chlorite. Thus, these veins provide a potential direct link between granitic intrusions in the Meguma Terrane and gold metallogeny.

Hydrothermal alteration at Goldboro is distinct for each vein generation. Biotite wall-rock alteration is localized to V1 veins, with a later biotite and chlorite alteration event associated with gold-bearing V4 veins. Albite+sericite wall-rock alteration is local to V4 veins. The broader hydrothermal footprint of

Goldboro consists of sericite alteration that spans >150 m from the hinge line of the Upper Seal Harbour anticline.

Hydrothermal alteration zoning can be recognized using mass balance calculations, mineral assemblages, and mineral chemistry. Mass changes in major element oxides SiO₂, Fe₂O₃, MgO, Na₂O, and CaO can be used to identify each alteration assemblage. Trace elements Rb, Cs, and Ba can be used as proxies for K₂O, and Sr can be used as a proxy for CaO in carbonates. EPMA data reveal that biotite and chlorite have different Mn content between vein generations; V1 micas are Mn-enriched relative to a least-altered sample, whereas V4 micas are Mn-depleted.

The quartzo-feldspathic blebs that are common features in Meguma-type gold deposits likely represent relict features of early sulfides that were broken down and replaced during the V1 and V4 stages.

3.2 Future Research

This study provides a valuable framework for additional research to constrain alteration further and answer fundamental questions regarding the genesis of the Goldboro deposit. Potential areas of research are as follows:

Vein generations are typically not well understood in orogenic gold deposits. As a result, achieving well-constrained results for bulk analyses has been a challenge, especially in the Meguma Terrane. As presented in this study, there are multiple vein generations with possibly multiple fluid sources. The well-established vein paragenesis from this study sets the framework for targeted in-

situ analyses that examine these separate vein types. The combined use of fluid inclusion, cathodoluminescence (CL), and stable isotope (viz. ^{18}O and ^{34}S) analyses could provide valuable insight into potential sources of fluids and metals in Meguma gold deposits. The Goldboro deposit would also benefit from further lithgeochemistry of the mudstones and greywacke host rocks on a finer scale to determine how mass gains and losses change with respect to distance from veins, as well as geochronology on vein-stage minerals (e.g., arsenopyrite 1 and 2, biotite) to constrain timing of mineralization. Our study does not provide a large enough dataset to create a 3D alteration model of Goldboro. With additional alteration data, it would be possible to create shell models for alteration and reconstruct fluid pathways. Goldboro would also benefit from short-wave infrared (SWIR) spectroscopy of rock core; SWIR absorption spectra may be a cost and time-efficient way to differentiate V1 biotite from V4 biotite, and this is a potential core-logging and exploration tool.

Detailed EPMA and LA-ICP-MS analysis of minor, major, and trace element zonation in arsenopyrite would be helpful to compare elemental trends throughout the paragenesis to those of pre-existing studies of arsenopyrite in the greater Meguma Terrane. In addition, understanding the chemical zonation of arsenopyrite at Goldboro would provide insight into the behaviour of elements at different paragenetic stages, as well as into the origin of gold and the zone refining process.

The characterization of V4 veins at Goldboro in this study raises the question of whether these vein types are present in other Meguma-type gold

deposits but not recognized as a discrete vein generation. The presence of these veins at Goldboro provide a direct link between plutonism and gold metallogeny; if V4 veins are identified at other deposits in Meguma, it would provide evidence that Meguma-type gold deposits as a whole may not exclusively adhere to the metamorphic model of sediment-hosted orogenic gold deposit formation.

Appendix A: Graphic Logs

Legend

Lithology

-  Mudstone
-  Greywacke
-  Greywacke Marker Unit

Abbreviations

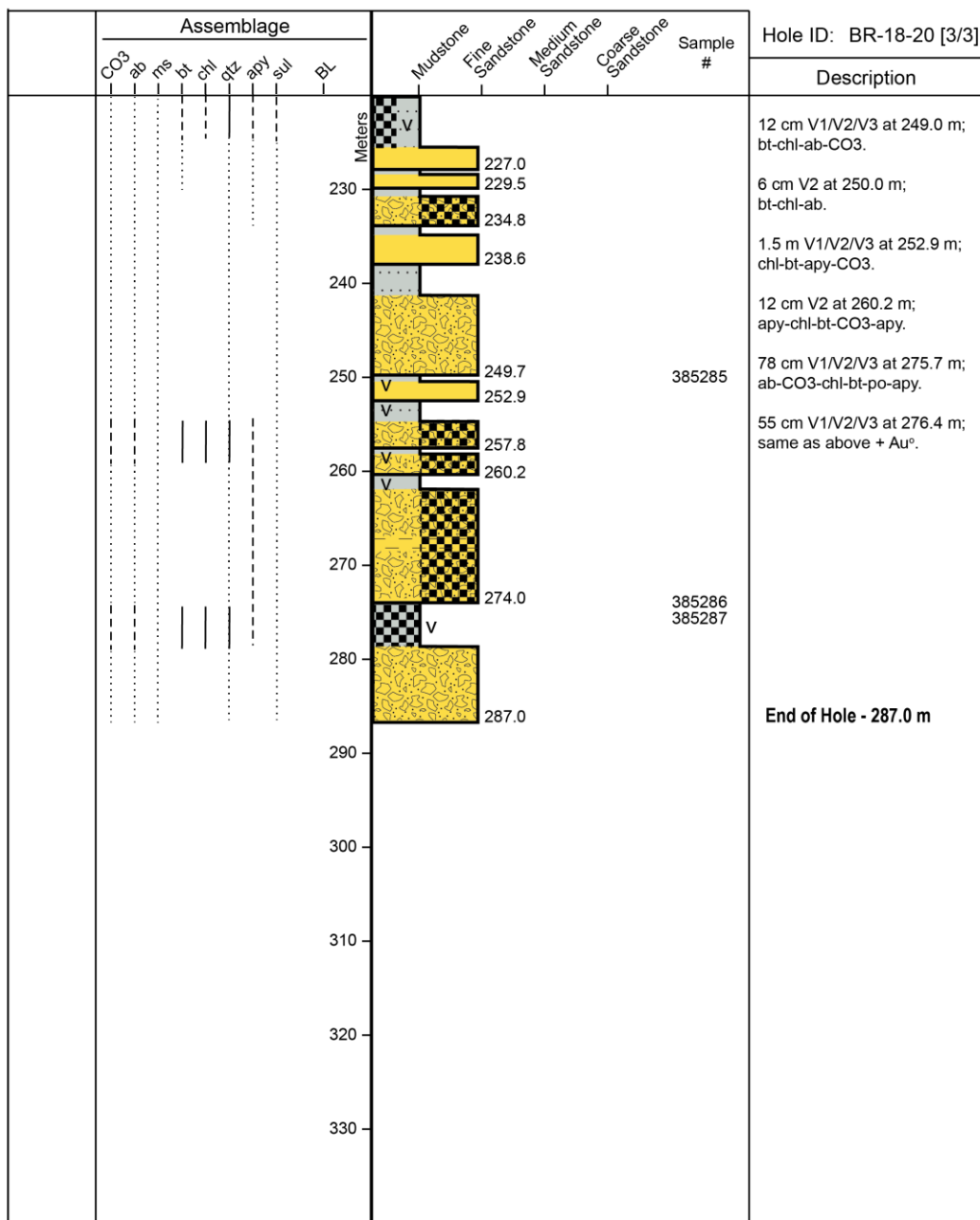
- ab: Albite
- asp: Arsenopyrite
- bt: Biotite
- cpy: Chalcopyrite
- chl: Chlorite
- CO₃: Carbonate
- ms: Muscovite
- po: Pyrrhotite
- py: Pyrite
- sp: Sphalerite
- sul: Sulfides
- qtz: Quartz
- BL: Bleaching

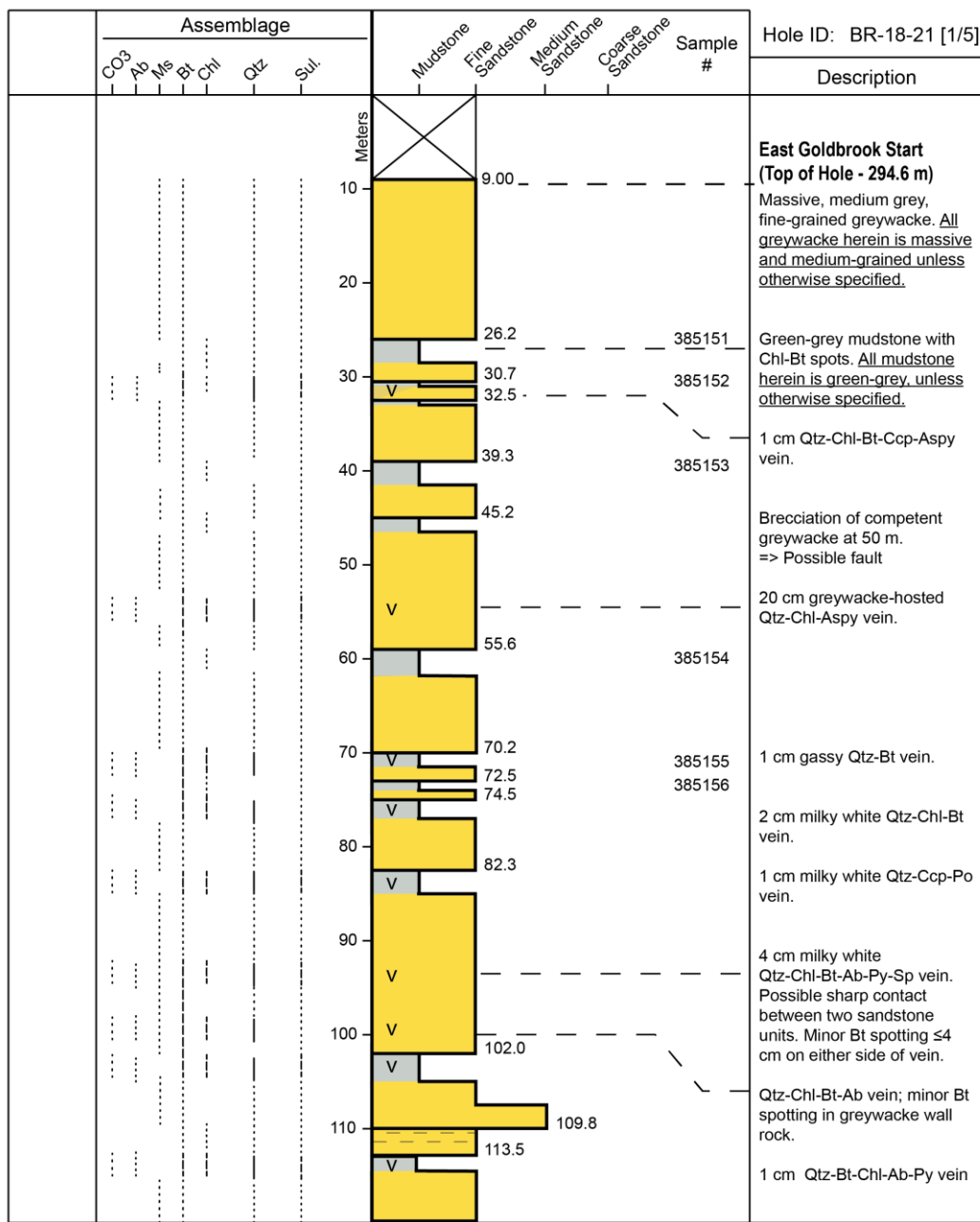
Textures

-  Argillite Interbeds
-  Sandstone Interbeds
-  Vein
-  Disseminated Arsenopyrite
-  Brecciation

	Assemblage	Meters	Sample #	Hole ID: BR-18-20 [1/3]
				Description
				East Goldbrook Start (Top of Hole - 219.9 m) 4 cm V1 at 12.6 m; ab-chl-CO ₃ .
		10.2		1 cm V1 at 25.4 m; ab-chl-bt.
		12.6		7 cm V2 at 31.4 m; CO ₃ -ab-chl-bt.
		16.3		1 cm V1 at 35.6 m; ab-chl-CO ₃ .
		19.7		4 cm V2 at 36.6 m; bt-chl-ab-po-cpy.
				5 cm V2/V3 at 45.7 m; CO ₃ -ab-chl-po-cpy-py.
		36.6		1 cm V1/V3 at 51.3 m; chl-bt-ab-py-po.
		38.6		6 cm V2/V3 at 54.0 m; bt-chl-ab-CO ₃ .
				20 cm V1/V3 at 54.5 m; bt-chl-ab-CO ₃ .
		49.4		30 cm V2 at 55.2 m; chl-ab-bt-po-cpy.
		54.0		3 cm V1 at 56.0 m; bt-chl-ab.
		64.5		12 cm V1 at 66.0 m; chl-ab-bt-po.
		66.0		Possible fault at 73.0 m.
				20 cm V1/V4 at 76.5 m; ab-chl-ksp-CO ₃ .
		76.5		4 cm V1 at 77.6 m; chl-bt-ab-CO ₃ -po.
		77.6		14 cm 96.0 m; chl-ab-CO ₃ -bt-po.
				8 cm V2/V3 at 112.7 m; ab-chl-CO ₃ .
		96.0		22 cm V2 at 113.3 m; chl-ab-CO ₃ .
		98.4		
		101.0		
		104.1		
		107.0		
		109.8		
		112.7		

	Assemblage	Meters	Sample #	Hole ID: BR-18-20 [2/3]									
				<th>CO₃</th> <th>ab</th> <th>ms</th> <th>bt</th> <th>chl</th> <th>dz</th> <th>apy</th> <th>sul</th> <th>BL</th> <th>Mudstone</th> <th>Fine Sandstone</th> <th>Medium Sandstone</th> <th>Coarse Sandstone</th>	CO ₃	ab	ms	bt	chl	dz	apy	sul	BL
		112.7	385280	2 cm V2 at 120.2 m; ab-chl-bt-CO ₃ -apy.									
	V	120		Framboidal py at 127.4 m.									
		126.0		3 cm V1 at 128.0 m; bt-chl, intense bt-chl wallrock alteration.									
	V	127.9	385281	2 cm V1 at 129.0 m; same as above.									
	V	129.0	385282	1-5 cm V1 between 138.5 m-152.2 m; bt-chl-ab-CO ₃ -apy.									
	V	131.4		9 cm V2 at 166.7 m; ab-chl-bt-po-CO ₃ .									
		140		4 cm V1 at 172.3 m; bt-chl-ab.									
	V	145.6	385283	4 cm V1 at 192.0 m; bt-chl-ab-CO ₃ .									
	V	166.7		3 cm V1/V2 at 200.6 m; apy-bt-chl-CO ₃ .									
	V	169.3		8 cm V2 at 212.2 m; ab-bt-CO ₃ -chl.									
	V	170		5 cm V1 at 218.5 m; bt-chl-CO ₃ -ab.									
	V	180	385284	6 cm V2 at 215.0 m; ab-CO ₃ -chl-bt.									
	V	190		13 cm V1/V2 at 219.9; po-cpy-apy-ab-chl-bt-CO ₃ .									
	V	200		2 cm V1 at 229.0 m; same as above.									
	V	210		5 cm V2 at 225.6; same as above.									
	V	219.9		Boston-Richardson Start (219.9 m - End of Hole)									
		220											
	V	227.0											
		229.9											





	Assemblage								Sample #	Hole ID: BR-18-21 [2/5]
		CO ₃	Ab	Ms	Bt ¹	Chl	Qtz	Sul.		
										Meters
										113.5
									V	118.7
									V	129.0
									V	134.5
									V	146.7
									V	156.5
									V	170.0
									V	181.1
									V	186.5
									V	199.5
									V	203.0
									V	206.1
									V	209.0
									V	211.8
									V	216.7
									V	221.1

Description

3 cm Qtz-Bt-Chl-Po-Ccp vein

1 cm (glassy) and 3 cm (milky white) Qtz-Chl-Bt-Po-CO₃-Ccp-Py veins.

12 cm Qtz-Chl-Bt-Ab-Ccp-Po-CO₃ vein.

10 cm Qtz-Chl-Bt-Ab-CO₃+Au(?) vein.

12 cm Qtz-Chl-Bt-Ab-Po-Ccp vein. Disseminated Py and Aspy in mudstone wall rock. Abundant Py along S1 cleavage.

50 cm Qtz-Bt-Chl-Aspy-Ab vein.

30 cm Qtz-Chl-Bt-Aspy-Au vein. Aspy is coarse (<4 cm) Sequence of several coarsening-upwards sequences, punctuated by Qtz-Chl-Bt-Ab-CO₃-Po-Aspy veins.

15 cm Qtz-Chl-Bl-Aspy-Ab-Au vein with trace CO₃.

10 cm Qtz-Bt-Chl-Po-Ab-CO₃ vein.

3 cm Qtz-Bt-Chl-Po-Py-Ccp-CO₃ vein.

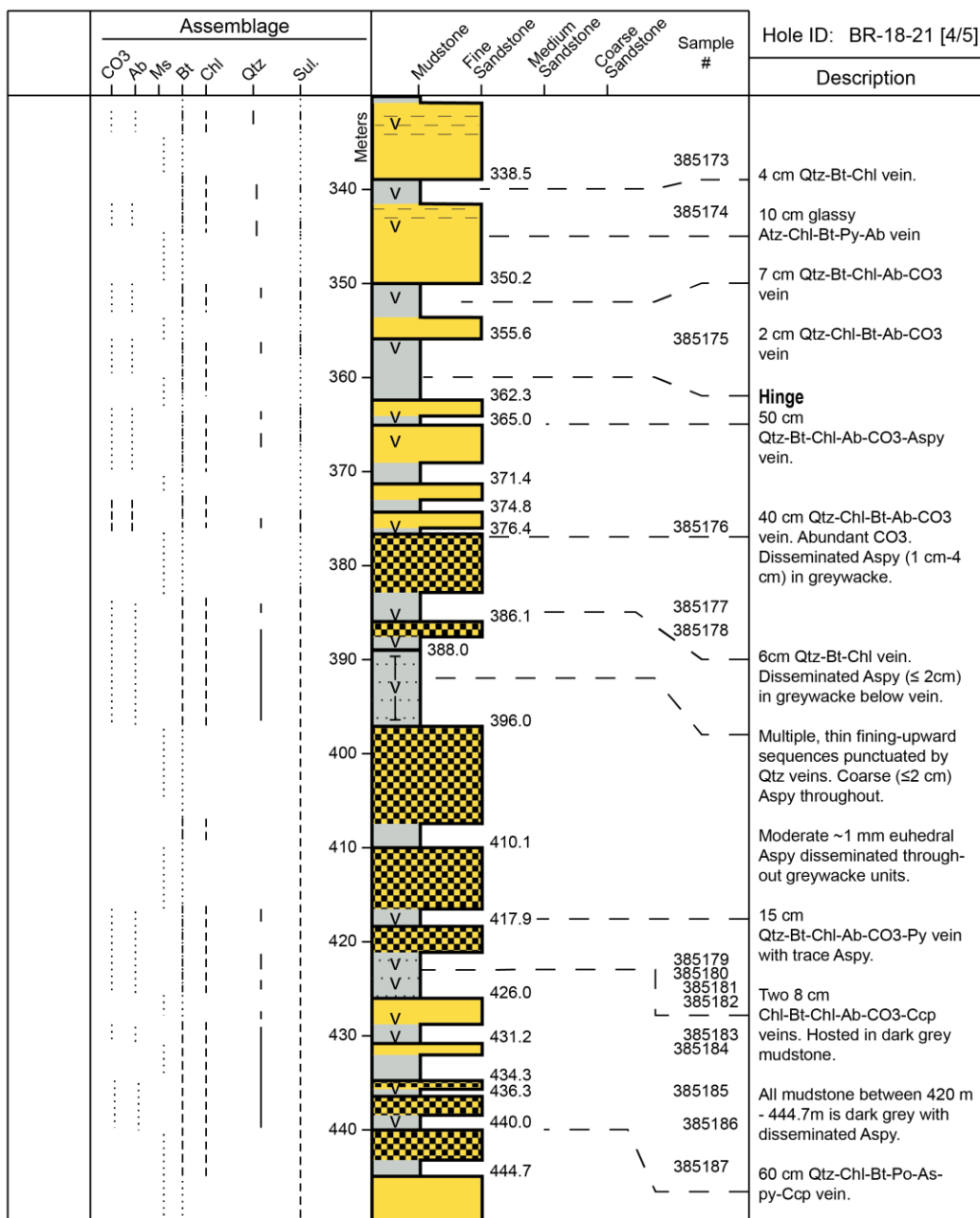
Multiple fining-upwards sequences with very thin (~1 cm) mudstone beds, punctuated by glassy, base metal-bearing quartz veins.

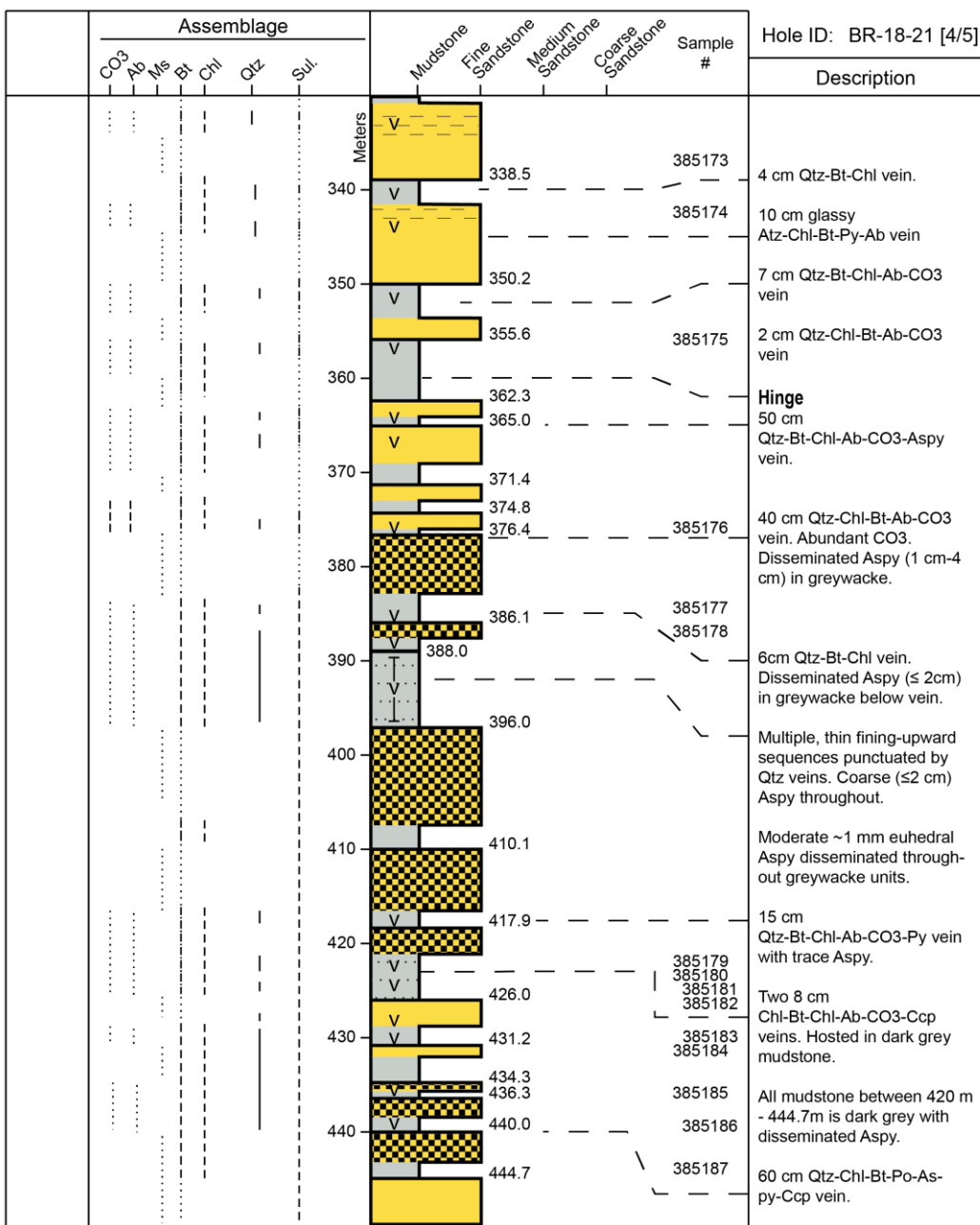
4 cm glassy Qtz-Chl-Bt-Po vein.

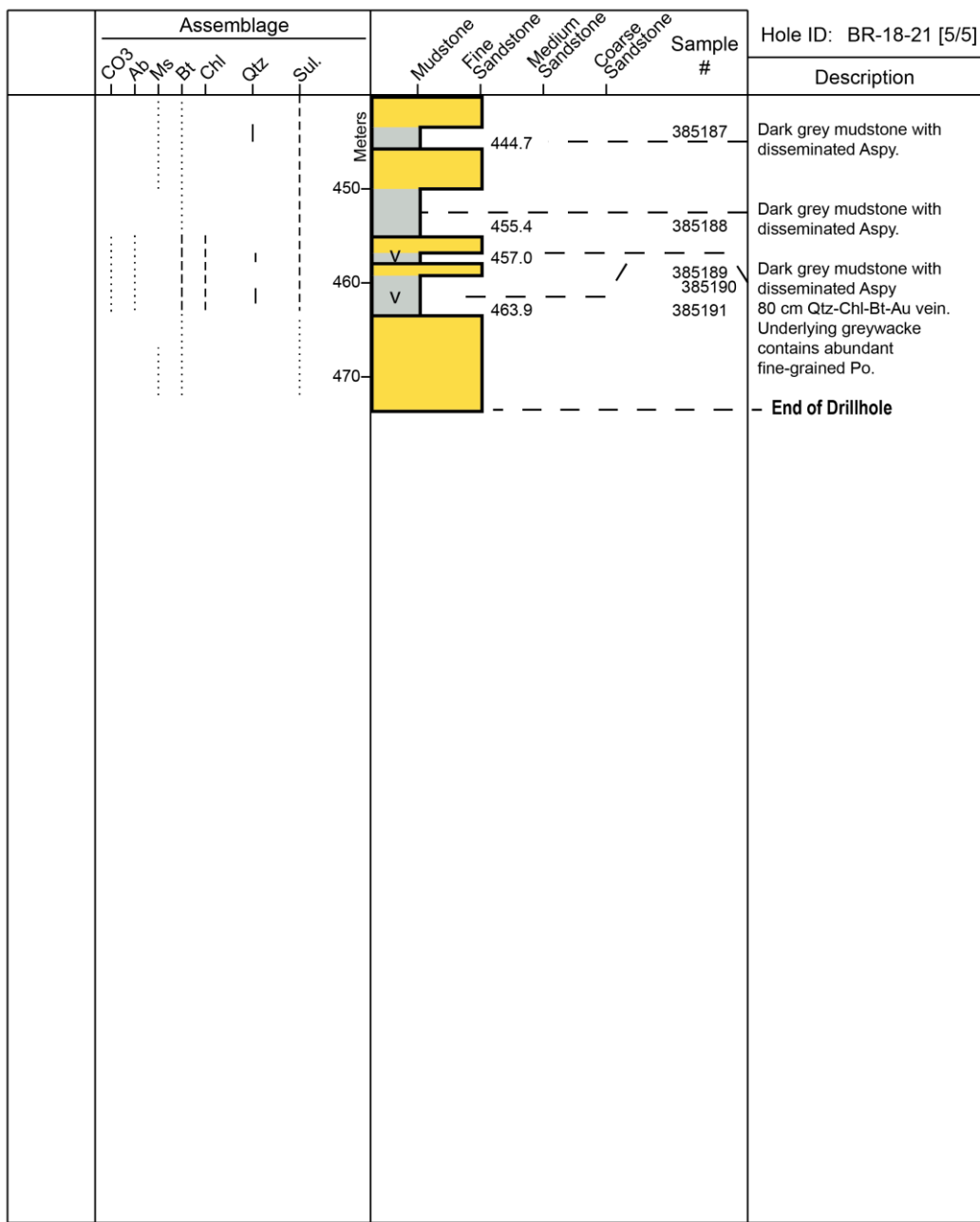
8 cm Qtz-Bt-Chl-Po-Ab-CO₃ vein.

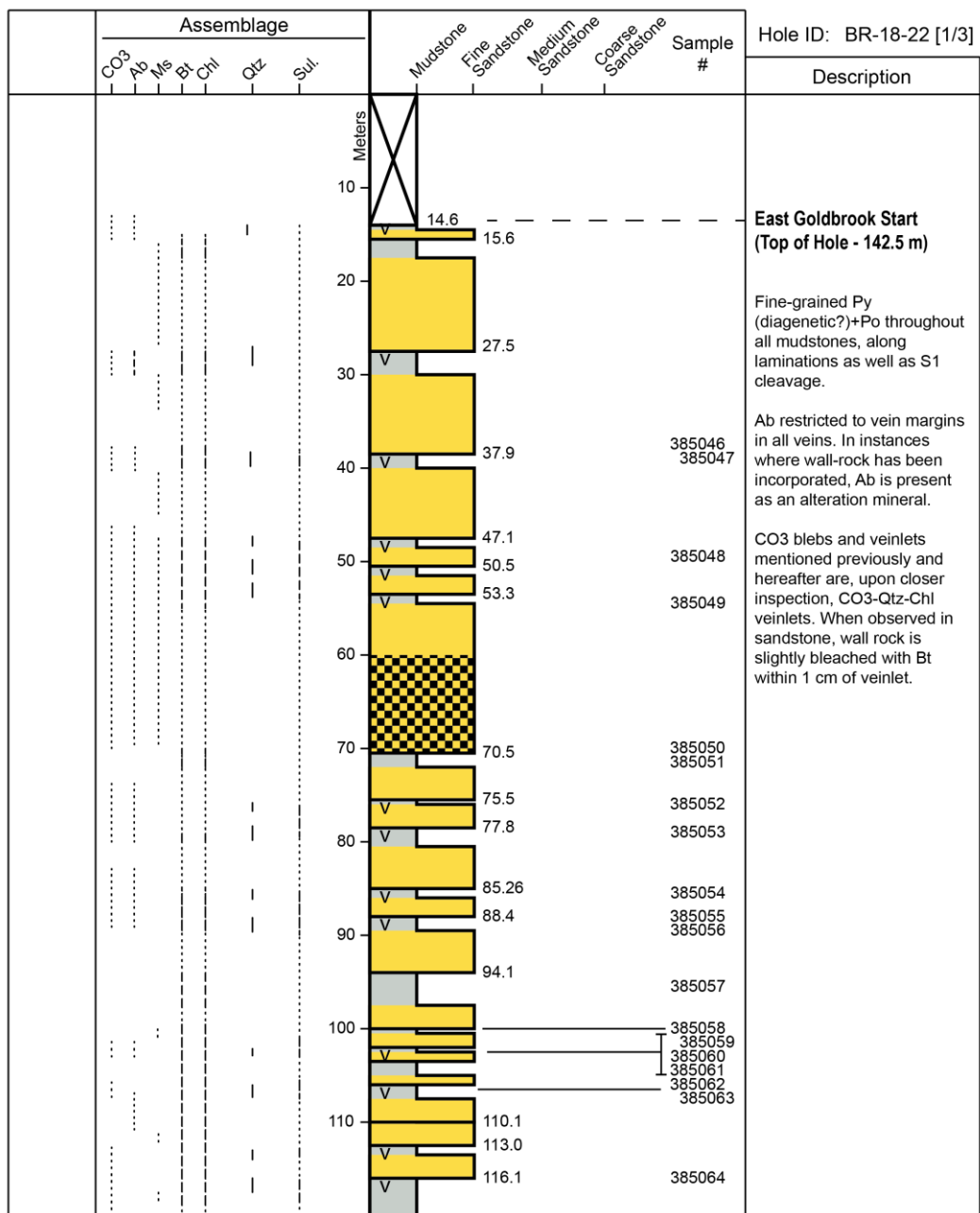
10 cm Qtz-Aspy-Bt-Chl-Ab vein. Po disseminated in mudstone wall rock.

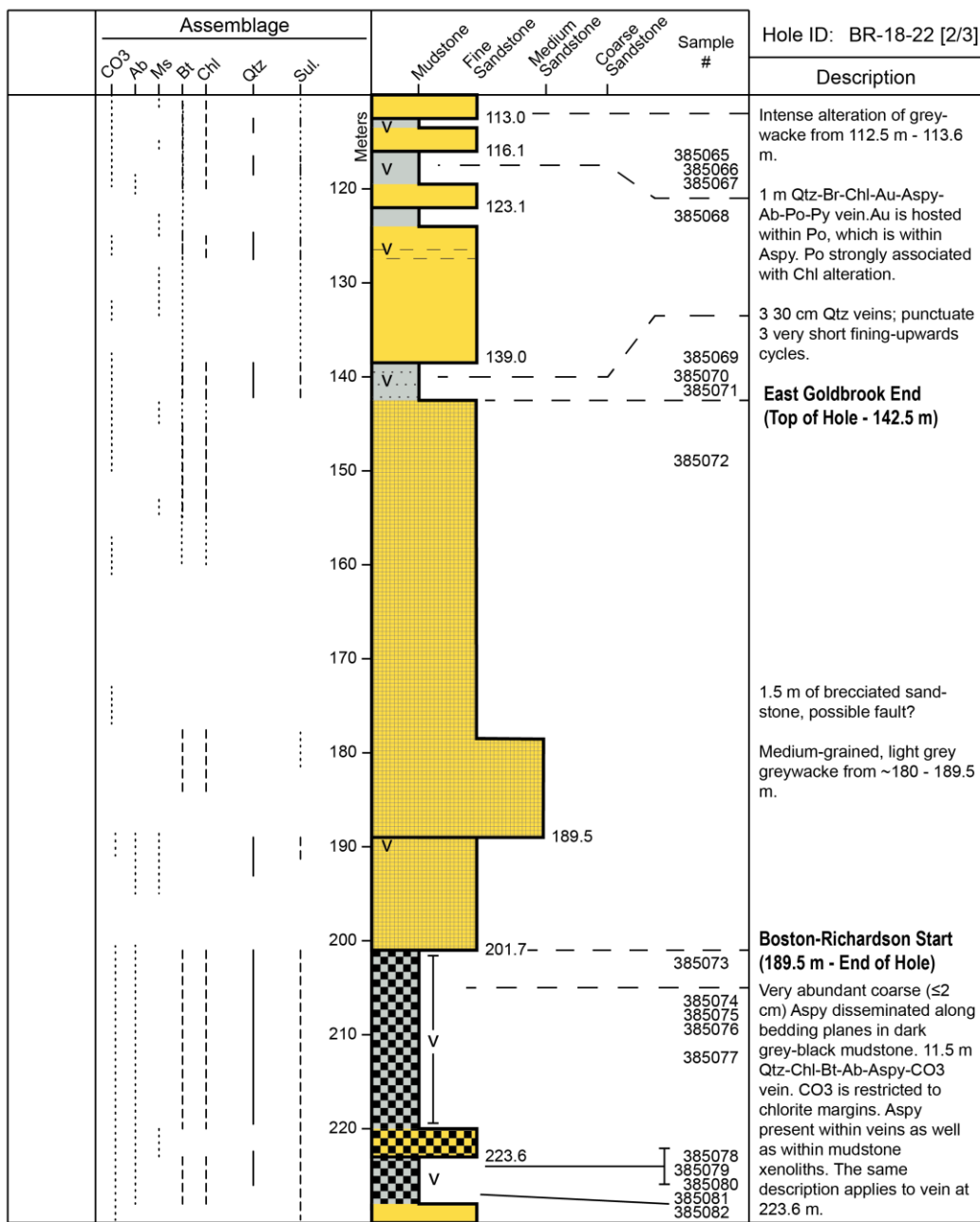
60 cm Qtz-Ab-Chl-CO₃ vein; Po proximal to wall rock.

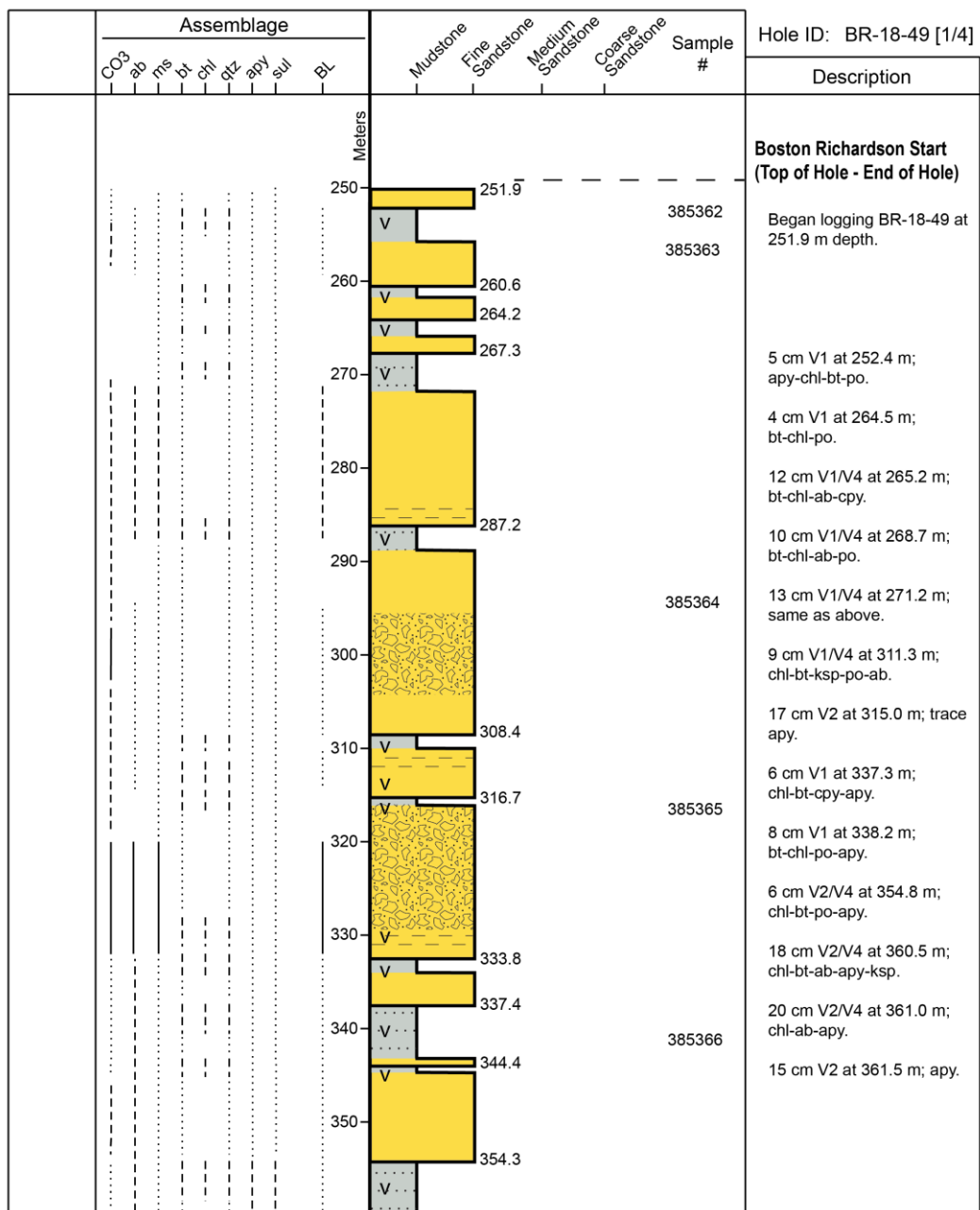




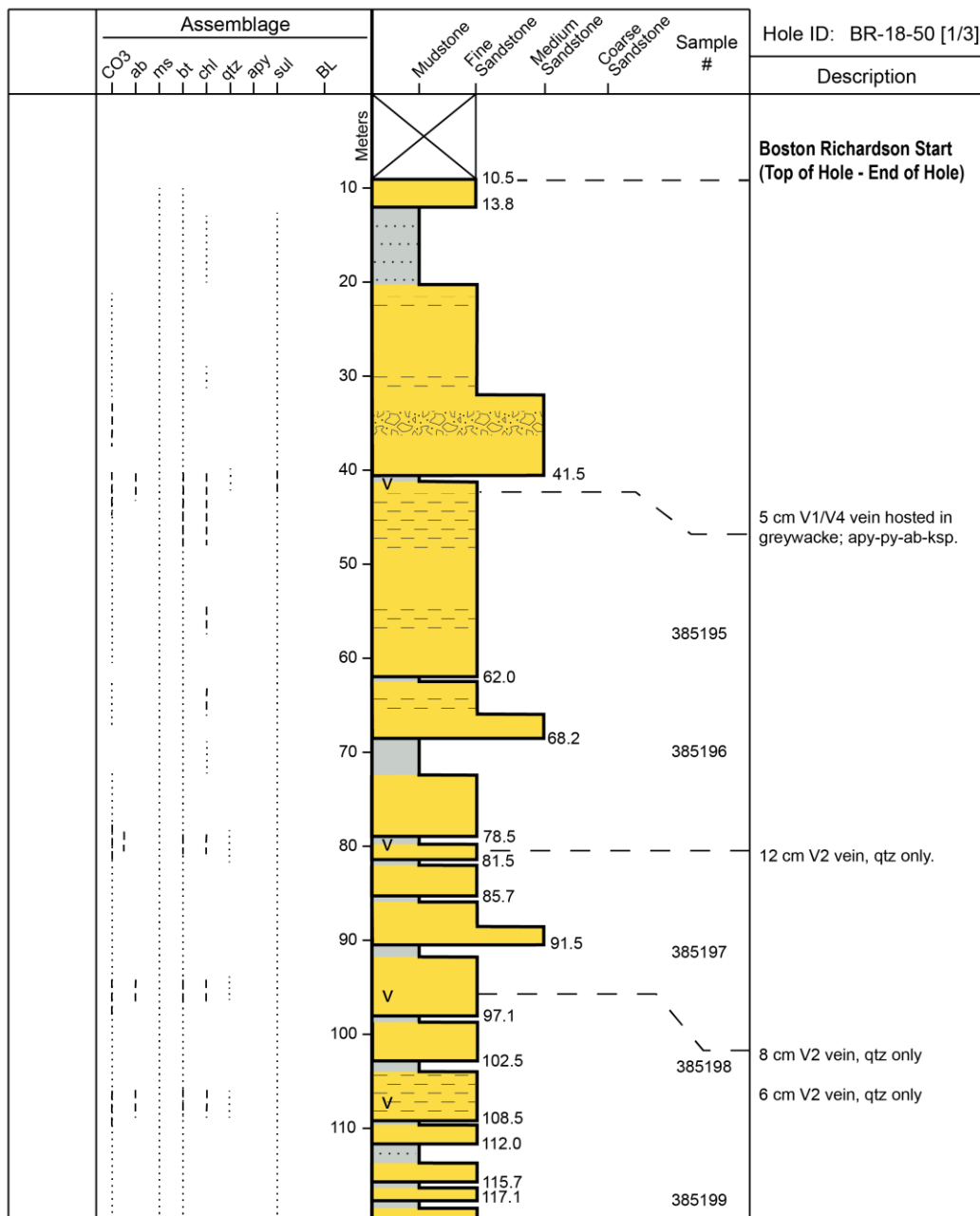


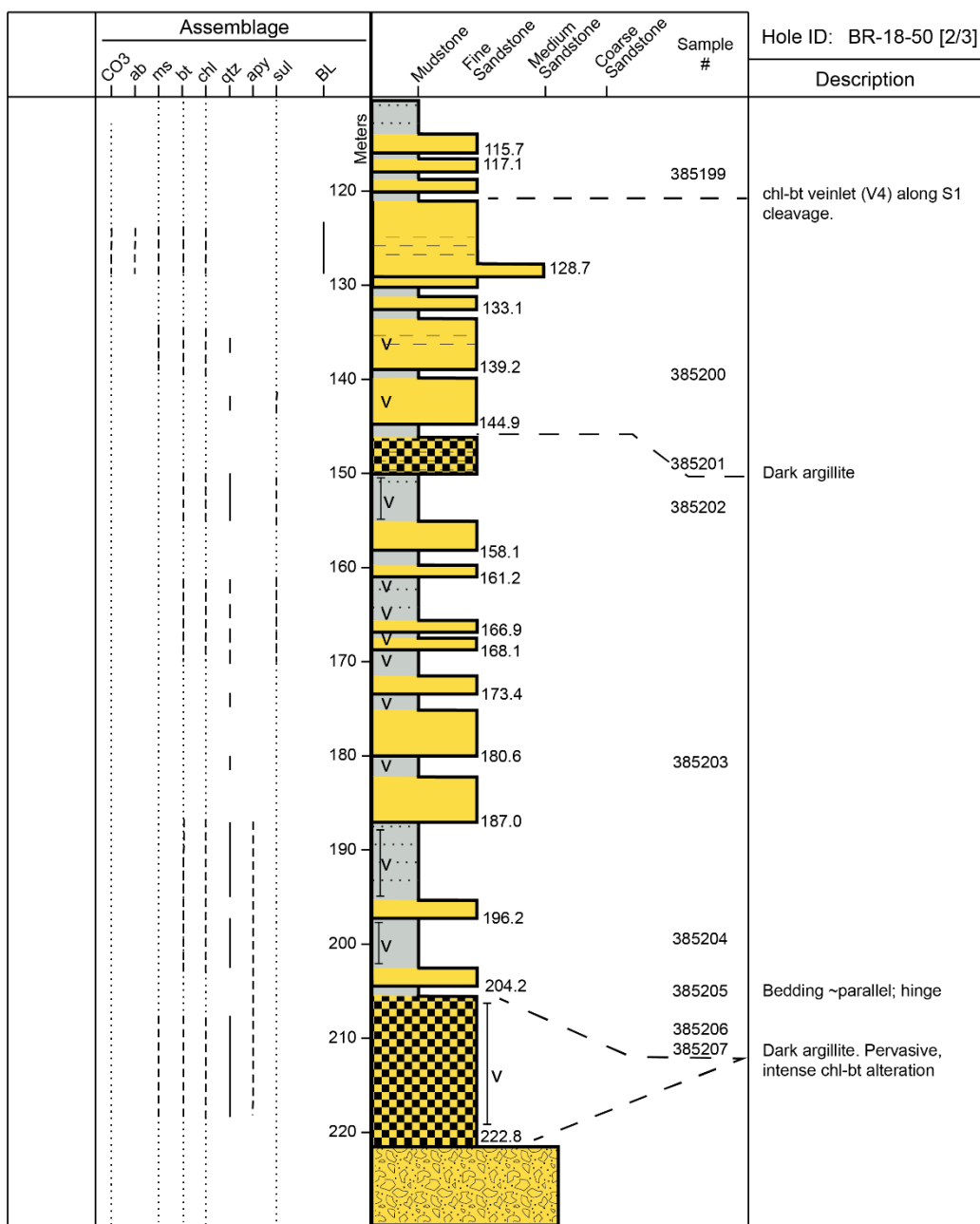


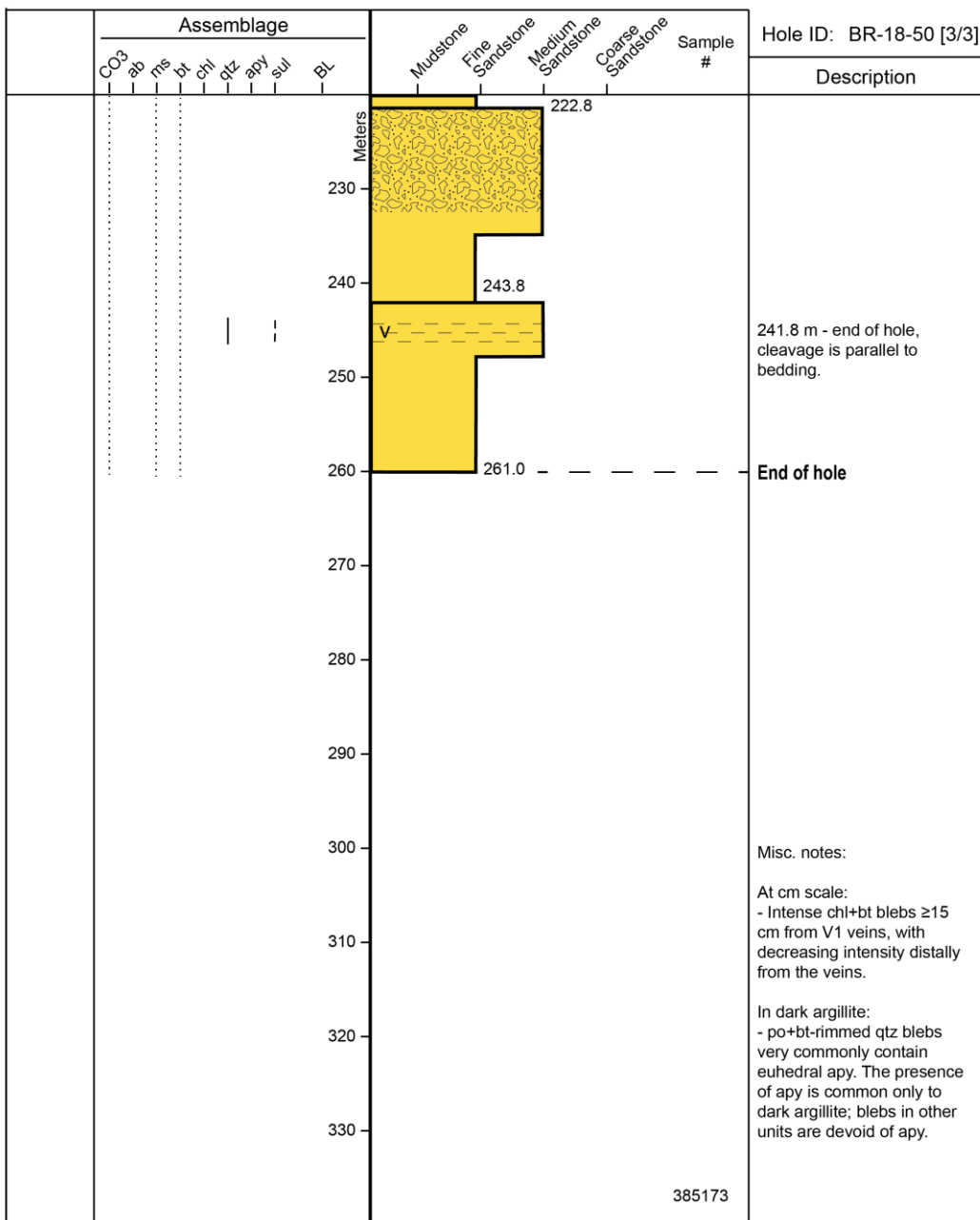


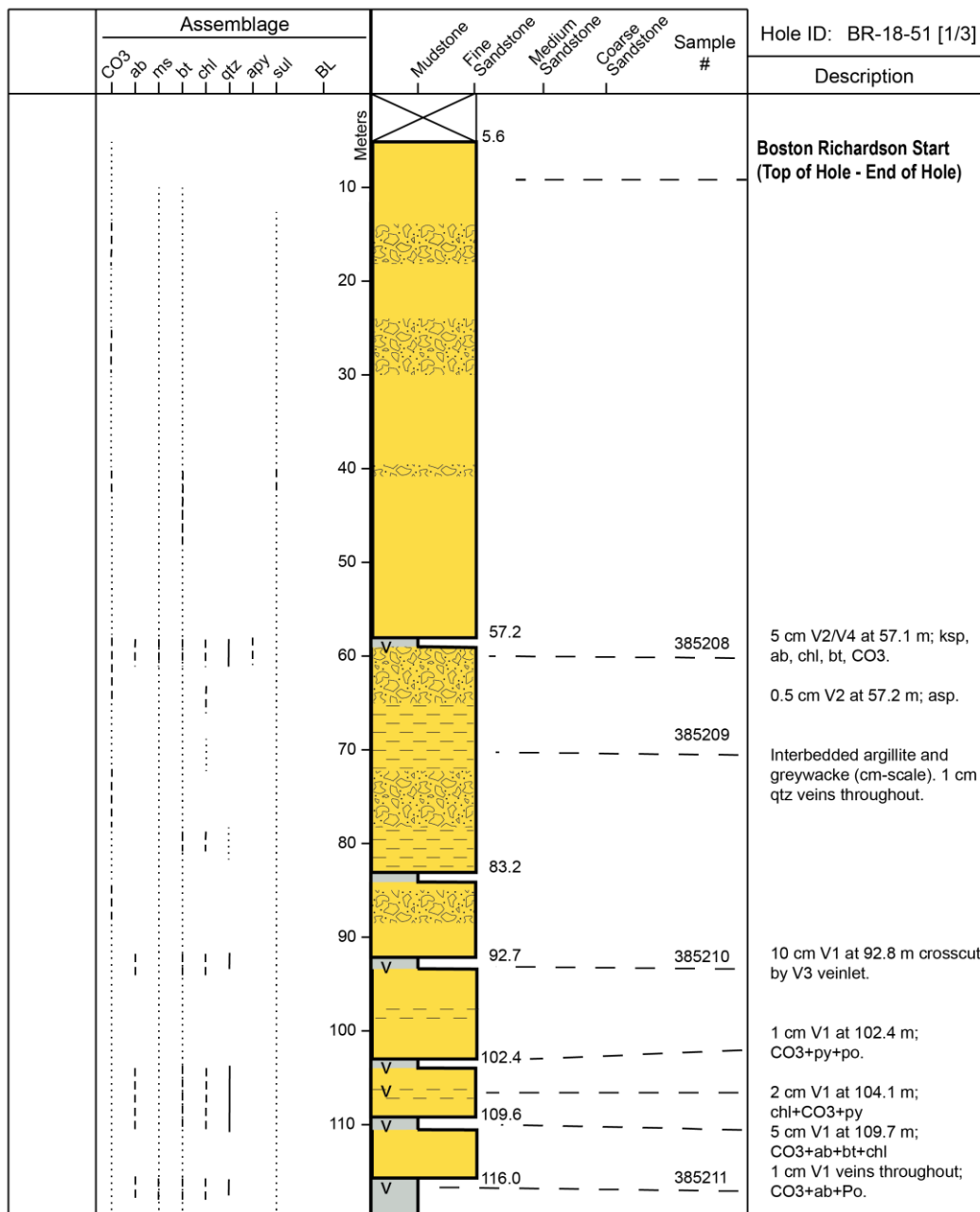


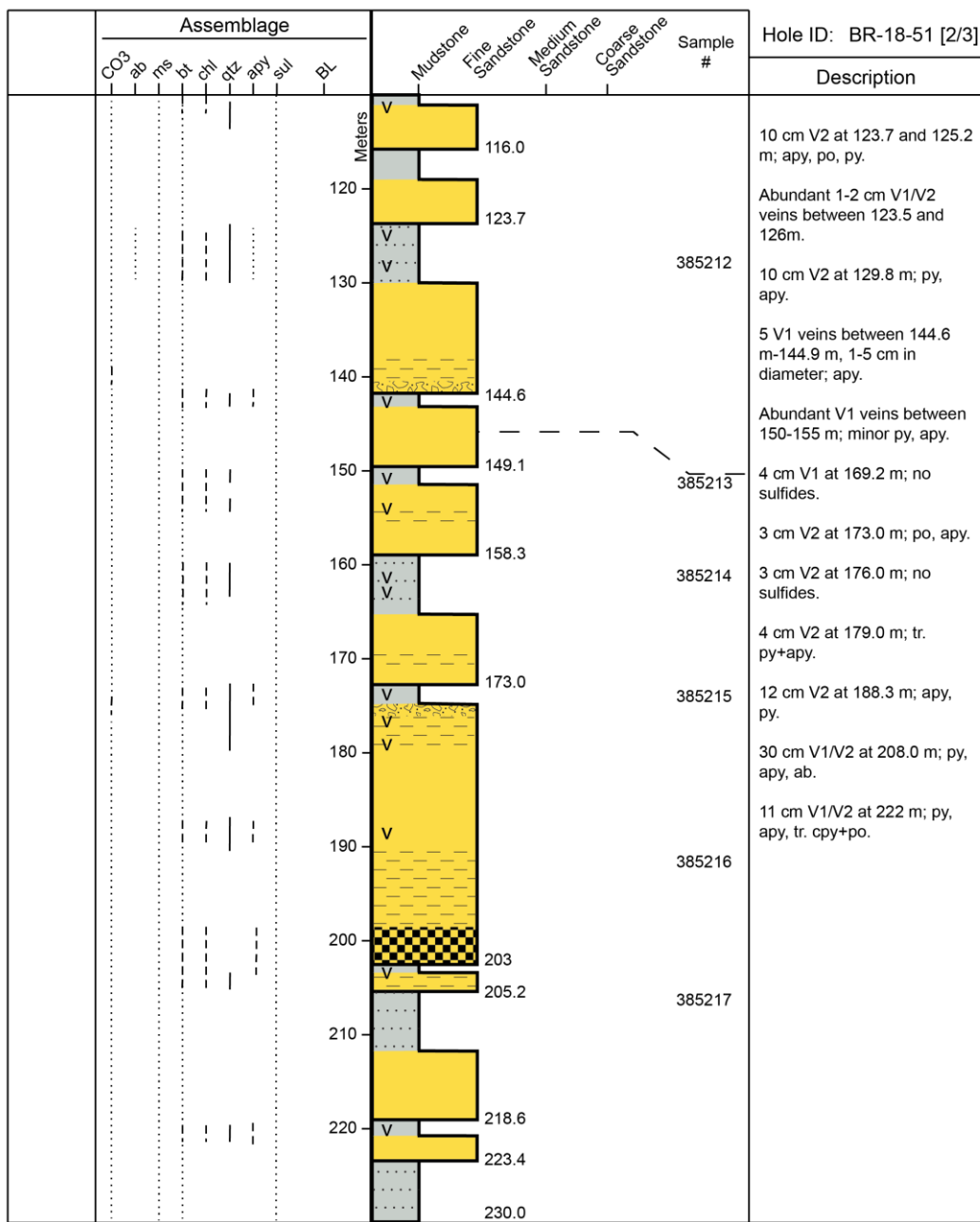
	Assemblage	Meters	Sample #	Hole ID: BR-18-49 [2/4]									
				CO ₃ ab ms bt chl qz apy sul BL	Mudstone	Fine Sandstone	Medium Sandstone	Coarse Sandstone					
		354.3	385369										
	V	360											
		370	385370	8 cm V1/V4 at 373.8 m; bt-chl-po-ab.									
	V	373.4	385371	33 cm V2/V4 at 381.4 m; bt-chl-apo-ab-ksp.									
	V	378.0		9 cm V1/V4 at 388.7 m; chl-bt-ab-apo-po.									
	V	380.7		Fault from 392.5 m-392.7 m.									
		383.5	385372	10 cm V1/V4 at 400.6 m; chl-bt-ab-po-apo.									
	V	388.5		4 cm V1/V4 at 404.3 m; chl-bt-ab-po-apo.									
	V	390.7		8 cm V1 at 404.8 m; bt-chl-ab-cpy-po-apo.									
	V	400.8		10 cm V1 at 407.6 m; bt-chl-ab-cpy-po-apo.									
	V	402.4		9 cm V1/V4 at 415.3 m; chl-ab-bt-po-apo.									
	V	407.4		8 cm V1/V2 at 416.3 m; chl-bt-apo.									
	V	418.6	385373	10 cm V1 at 422.8 m; bt-chl-po-apo.									
	V	422.8		6 cm V1 at 427.3 m; bt-chl-po-apo.									
	V	427.1		6 cm V1 at 428.0 m; same as above.									
	V	437.0		5 cm V1 at 428.9 m; same as above.									
	V	440		43 cm V1/V2/V4 at 428.4 m; bt-chl-po-apo.									
		451.7		20 cm V1/V4 at 434.2 m; chl-bt-po-apo-ab.									
	V	452.6		104 cm V1/V2/V4 at 436.0 m; bt-chl-po-apo-ab. Dark argillite ≤ 6 cm.									
	V	457.8		14 cm V2/V4 at 442.7 m; bt-chl.									
		460											

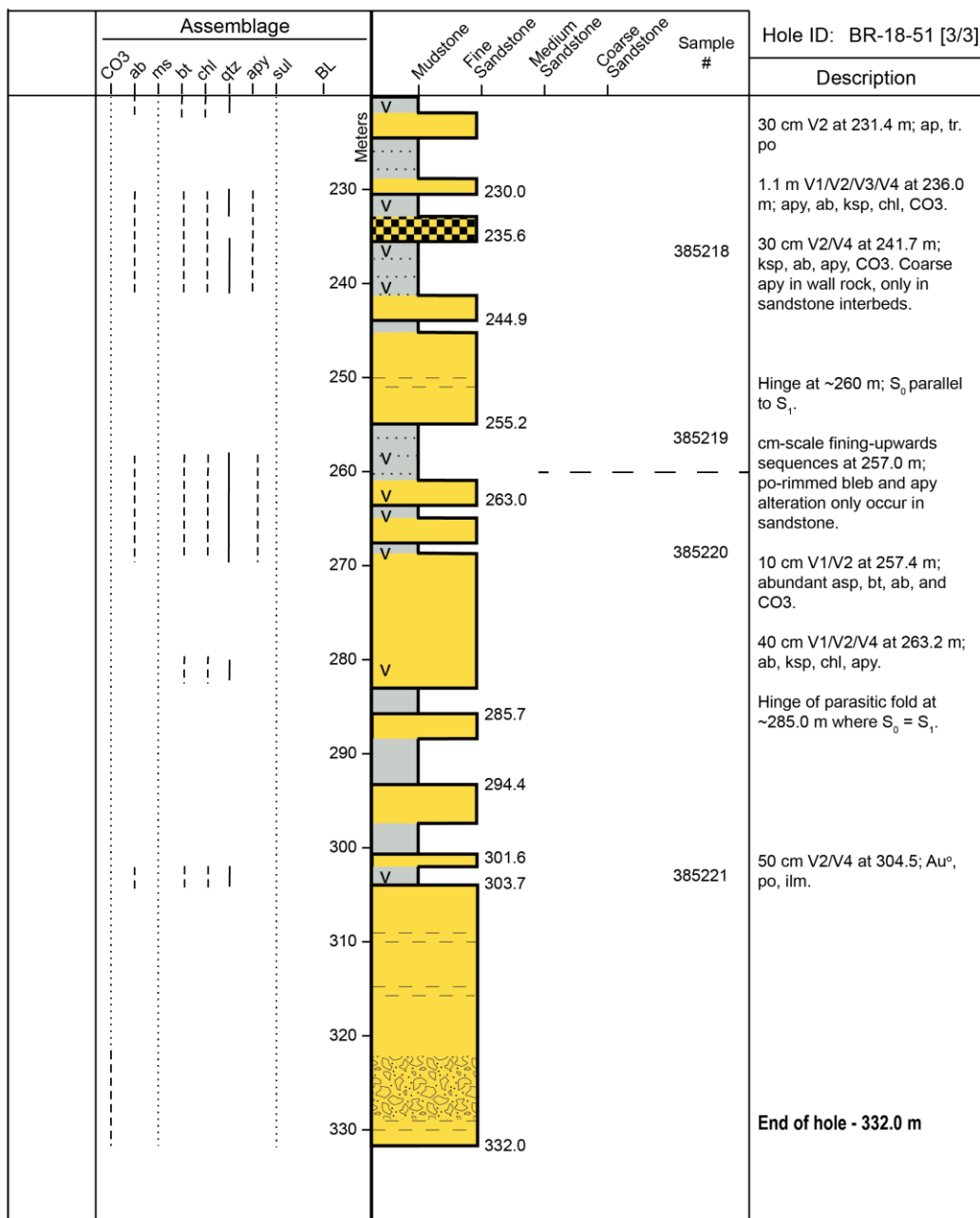


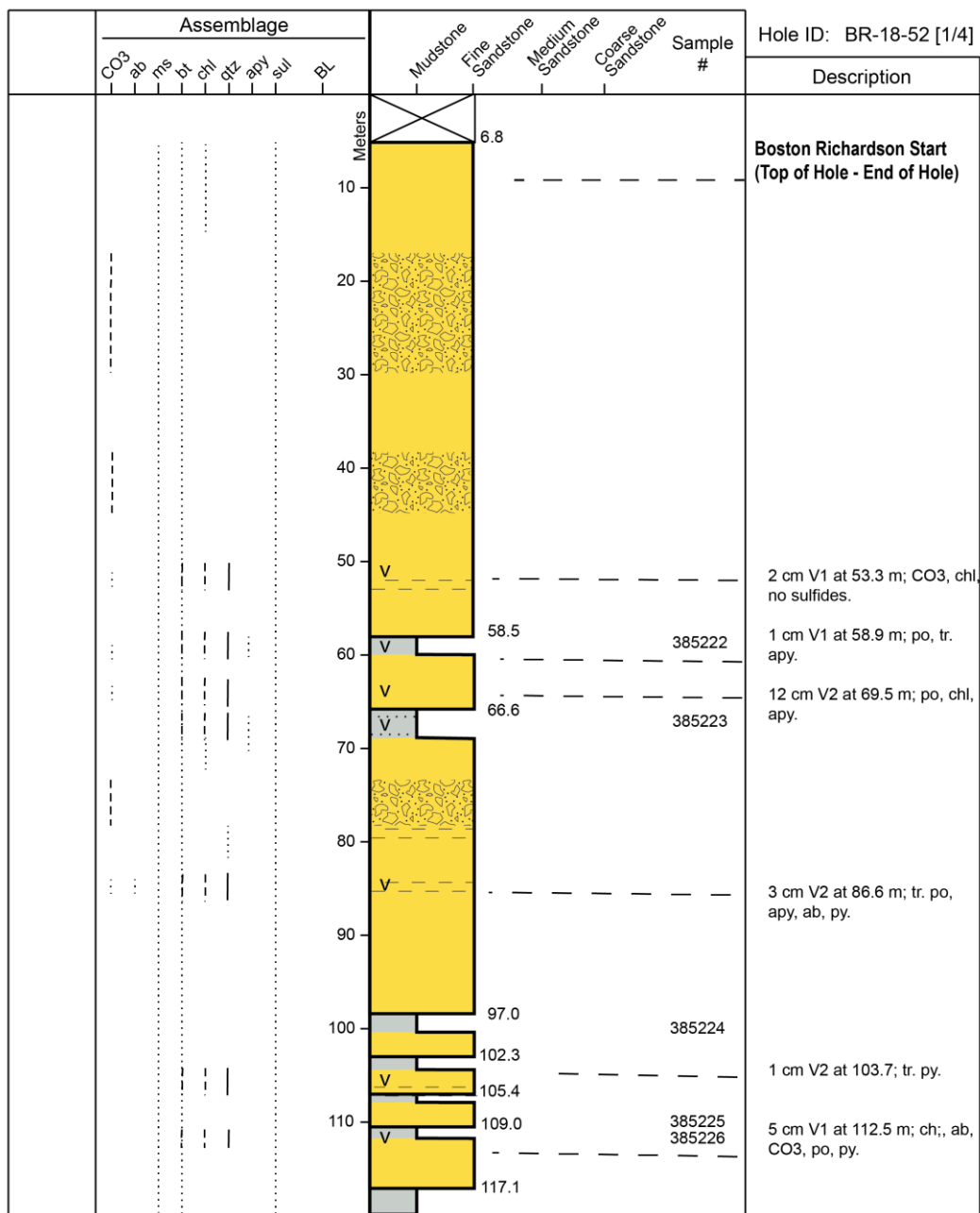


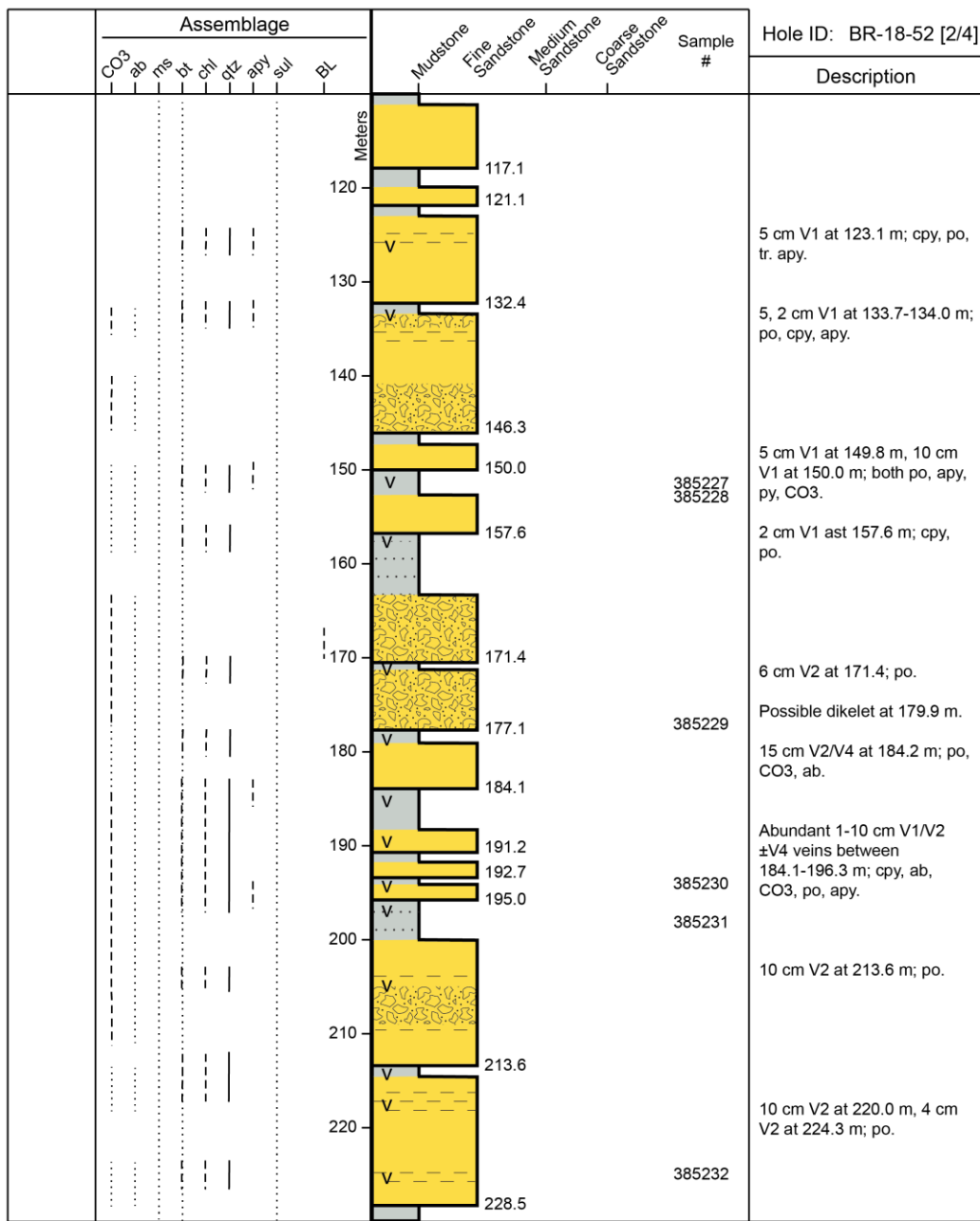




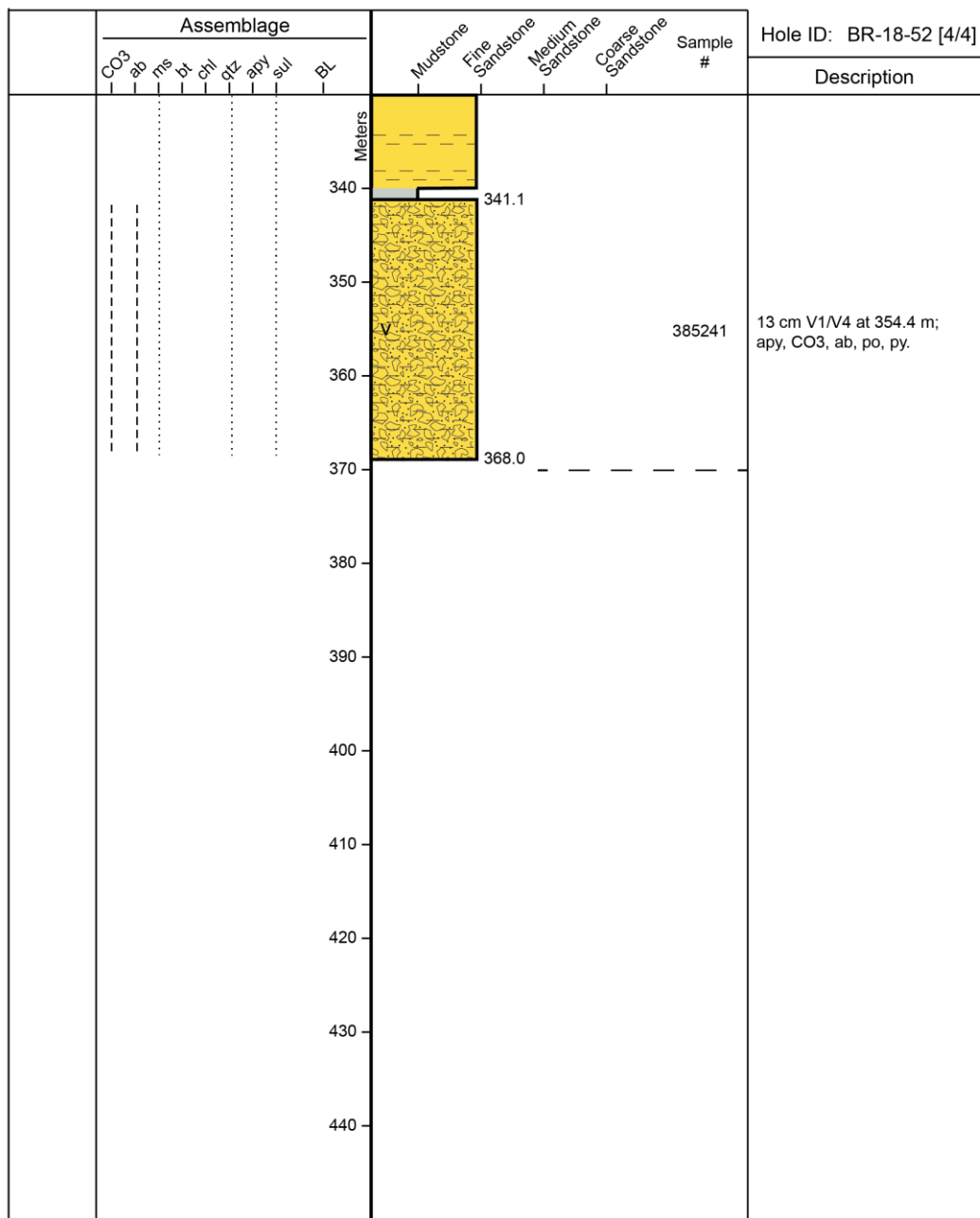


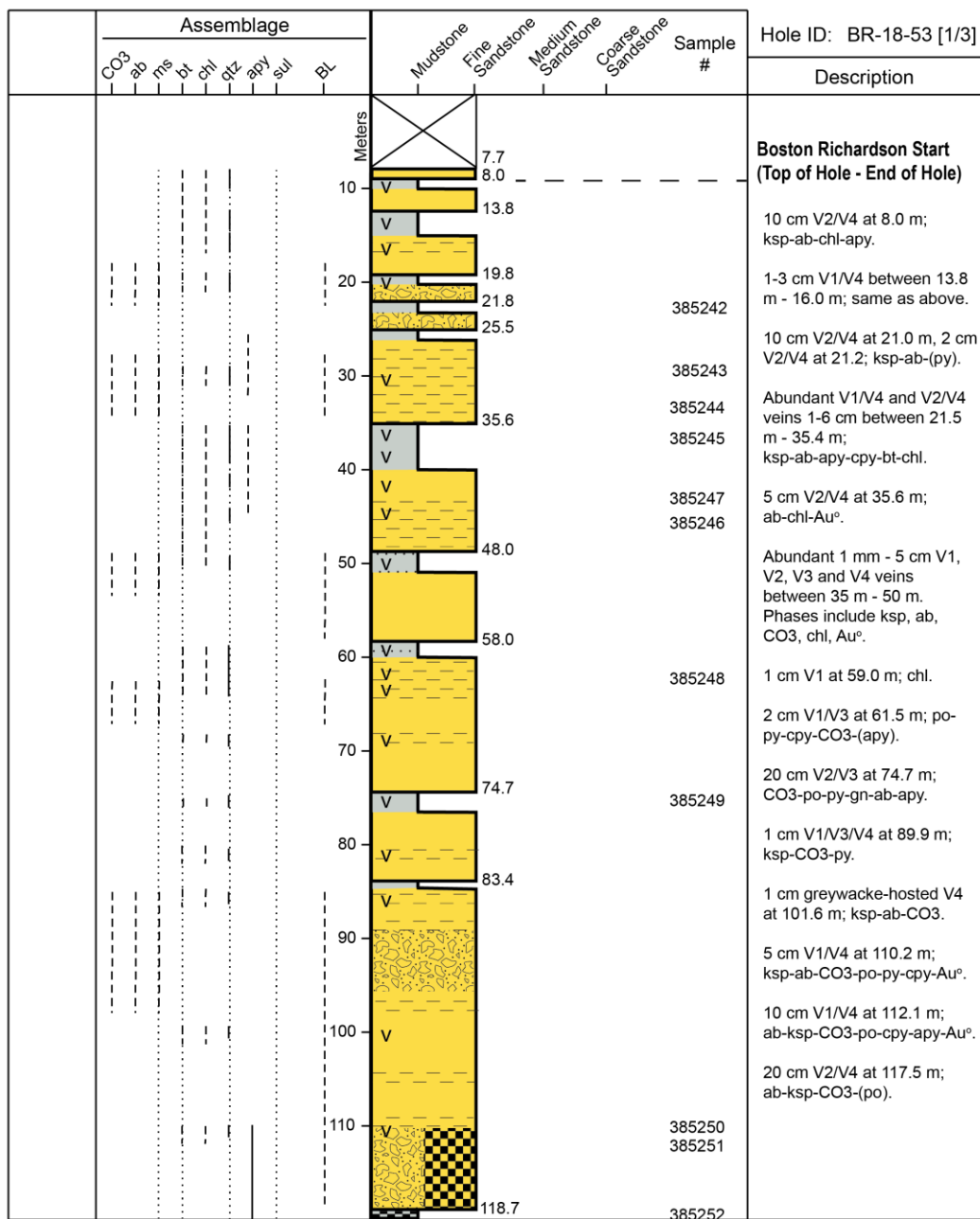


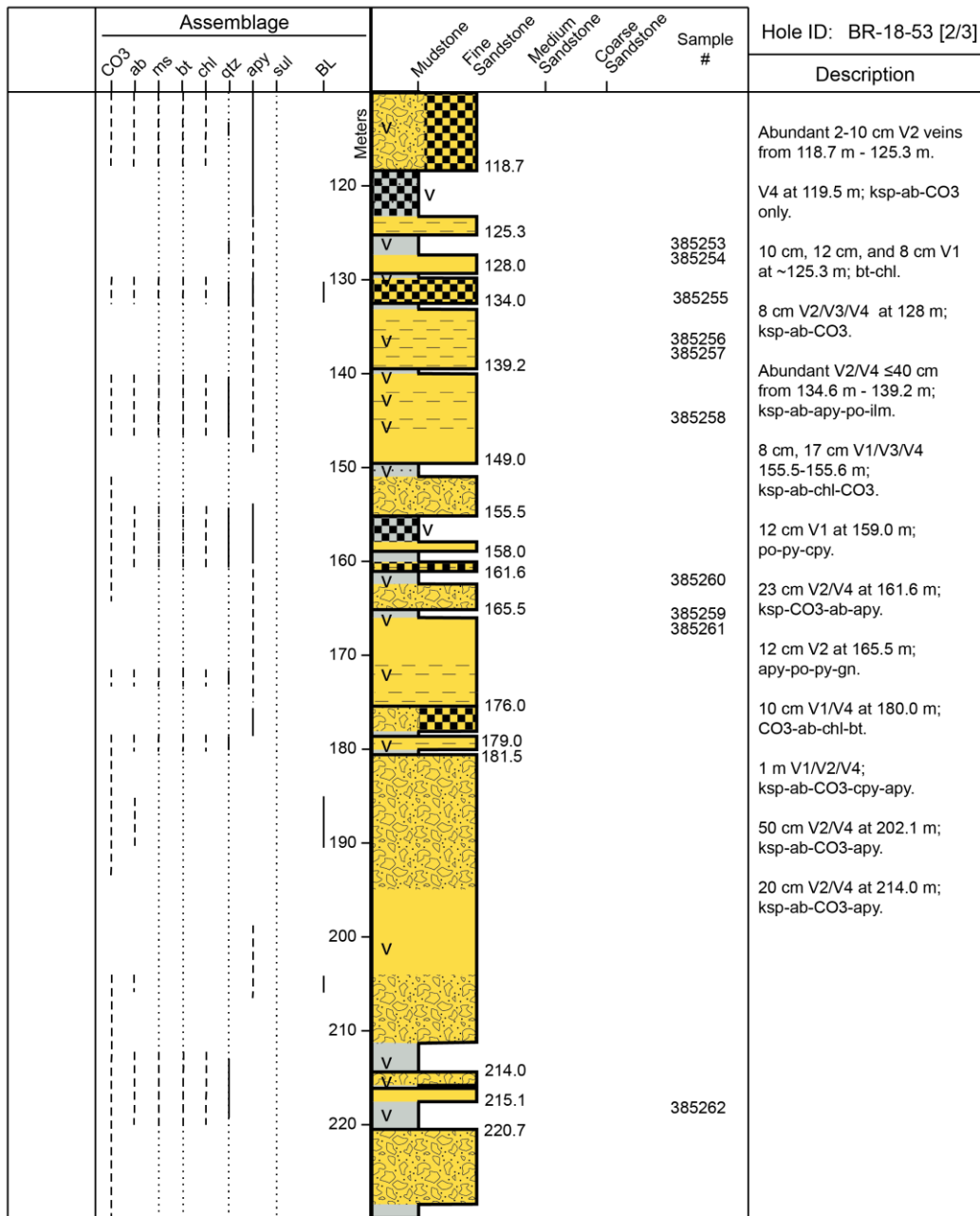


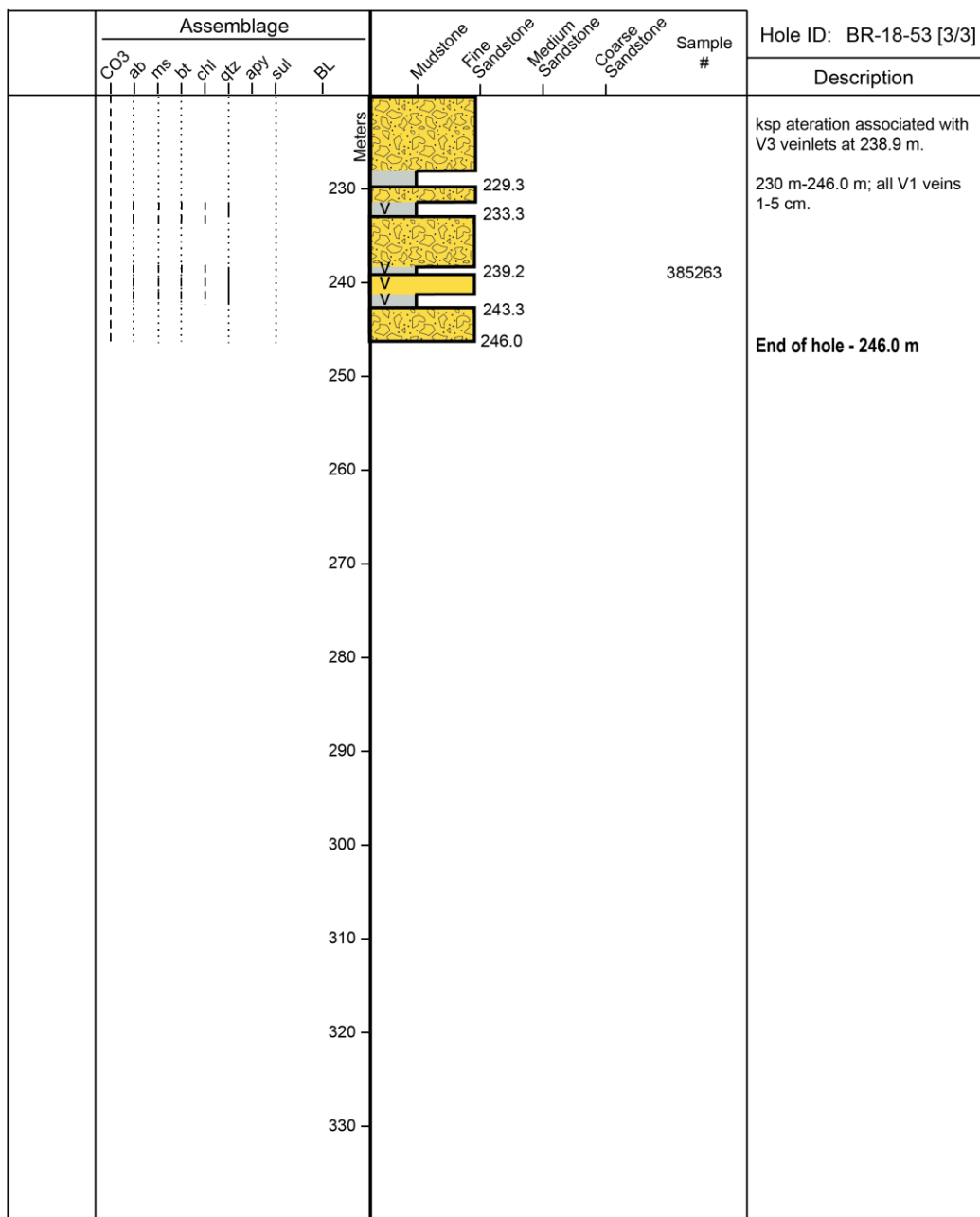


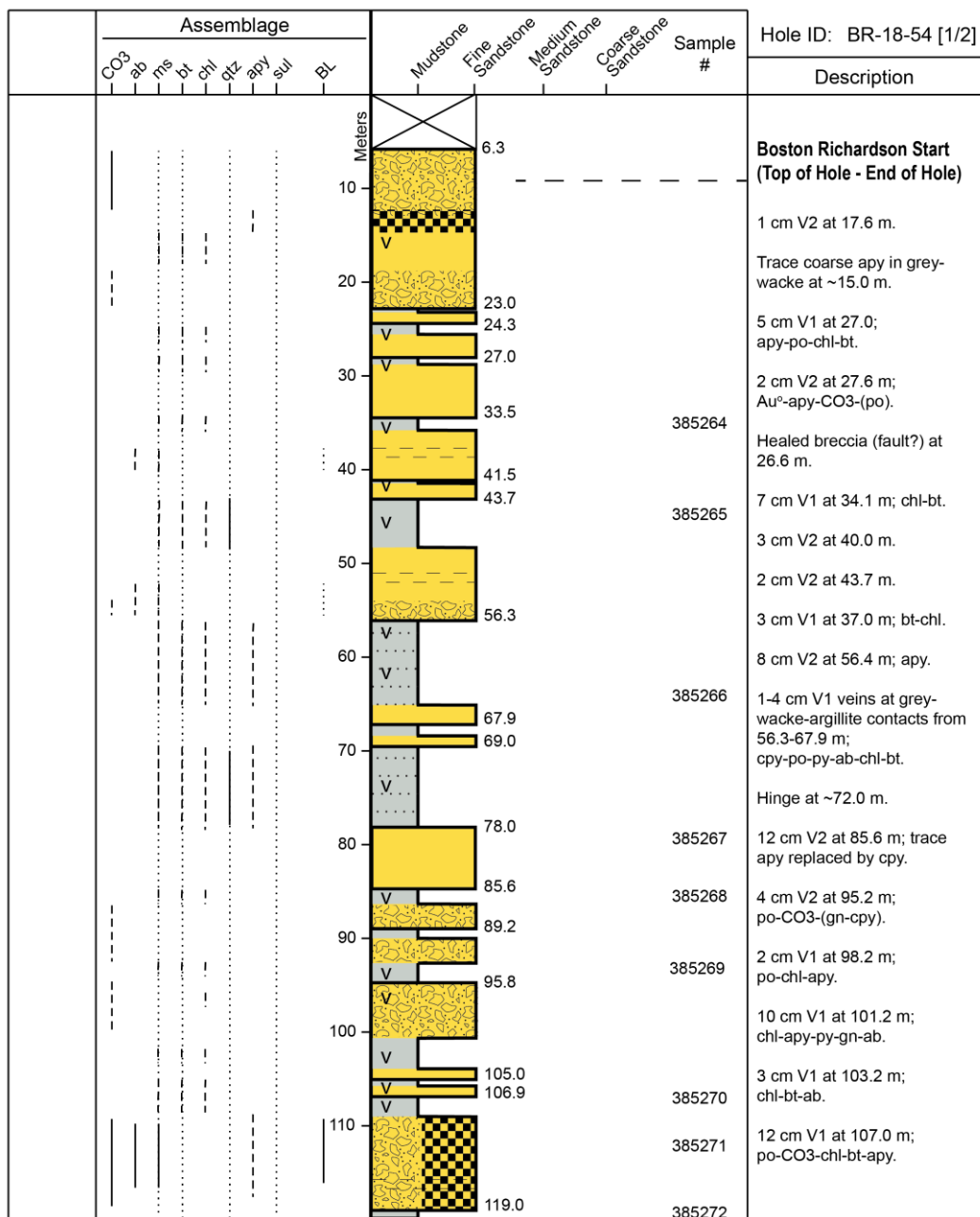
	Assemblage	Sample #									Hole ID: BR-18-52 [3/4]
		CO ₃	ab	ms	br	chl	dz	apy	sul	BL	
		Meters									
		V									228.5
		230	V								385233
		240									12 cm V2/V4 at 247.0 m; apy, ilm.
		V									243.2
		246.0	V								385234
		250	V								10 cm V2 at 248.4 m; abundant apy, ilm.
		260	V								261.7
		264.8	V								385236
		268.0	V								385237
		270	V								271.2
		275.0	V								385238
		280	V								Hinge ~270.0 m - 302.0 m.
		285.5	V								385239
		287.8	V								
		290	V								292.1
		300									302.0
		310									
		316.7									
		320									318.9
		V									2, 5 cm V1 veins; po.
		V									328.7
		330									

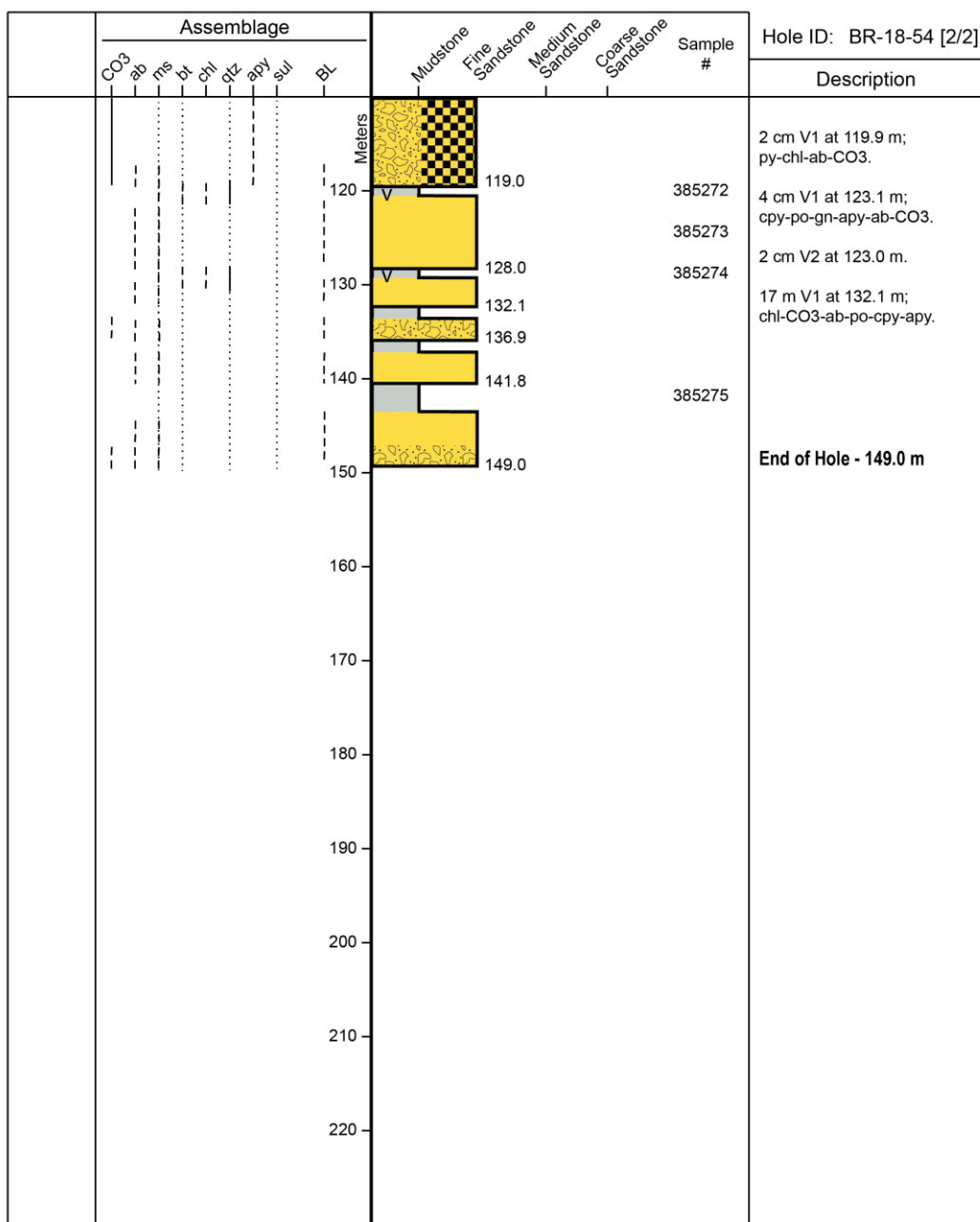


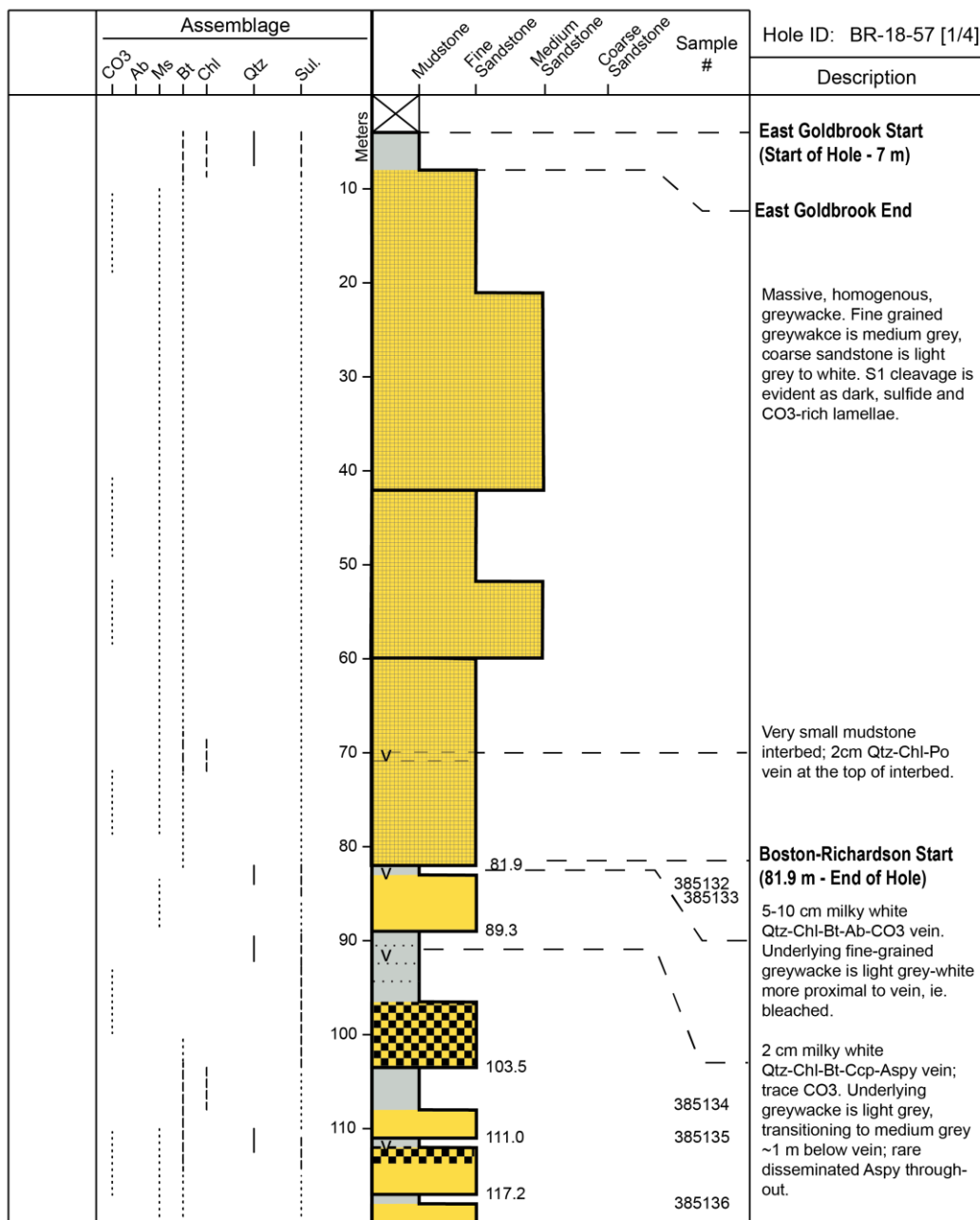


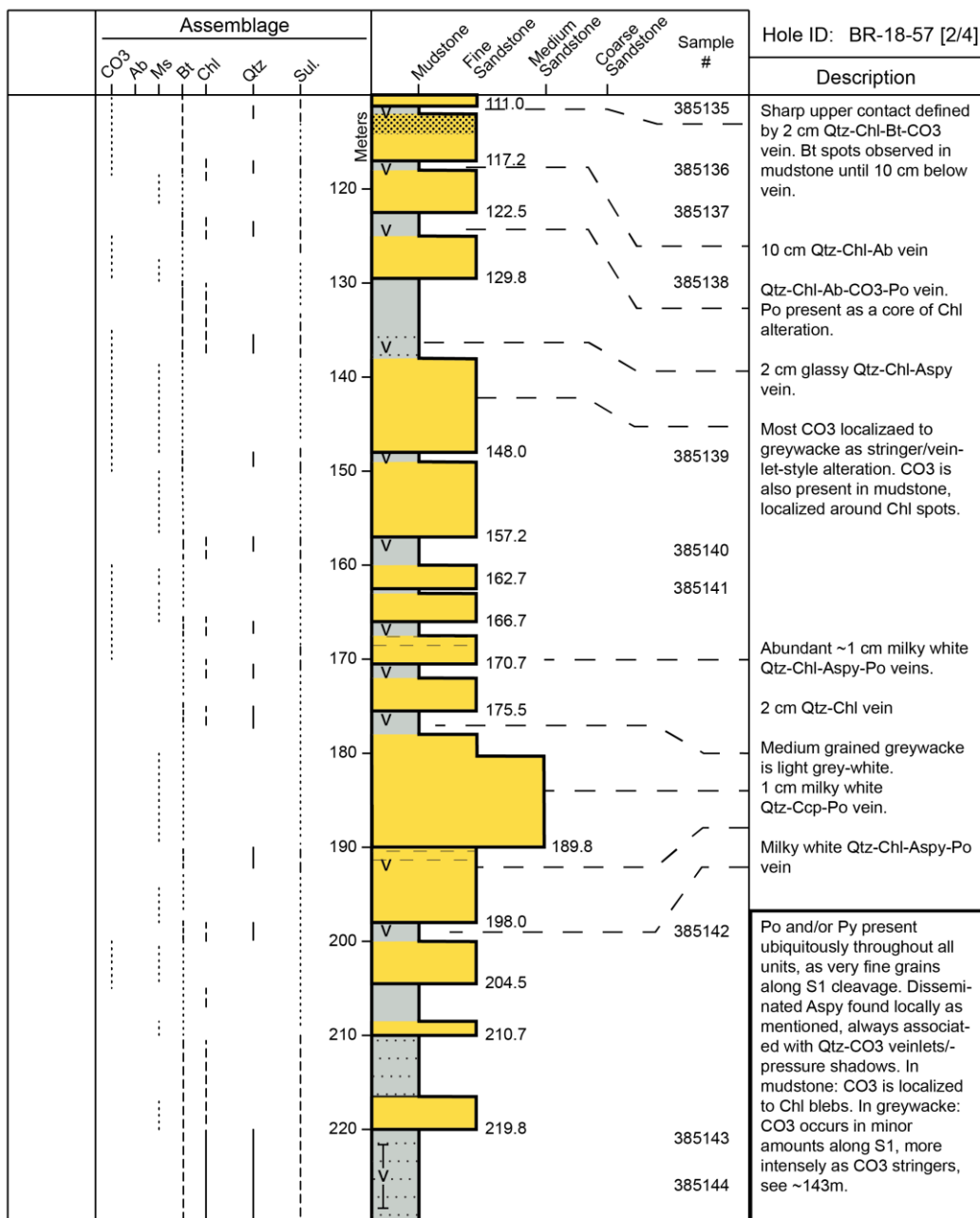


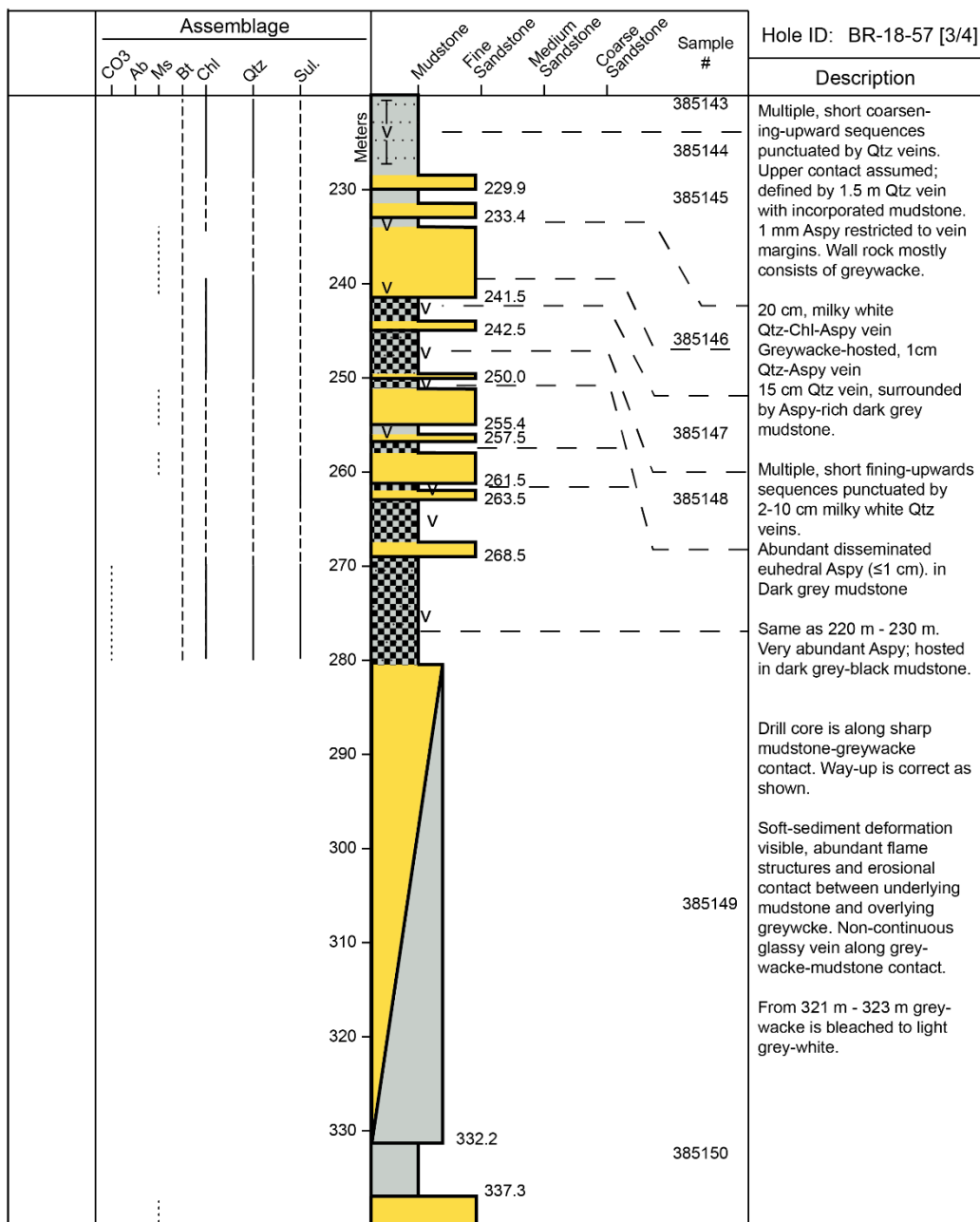


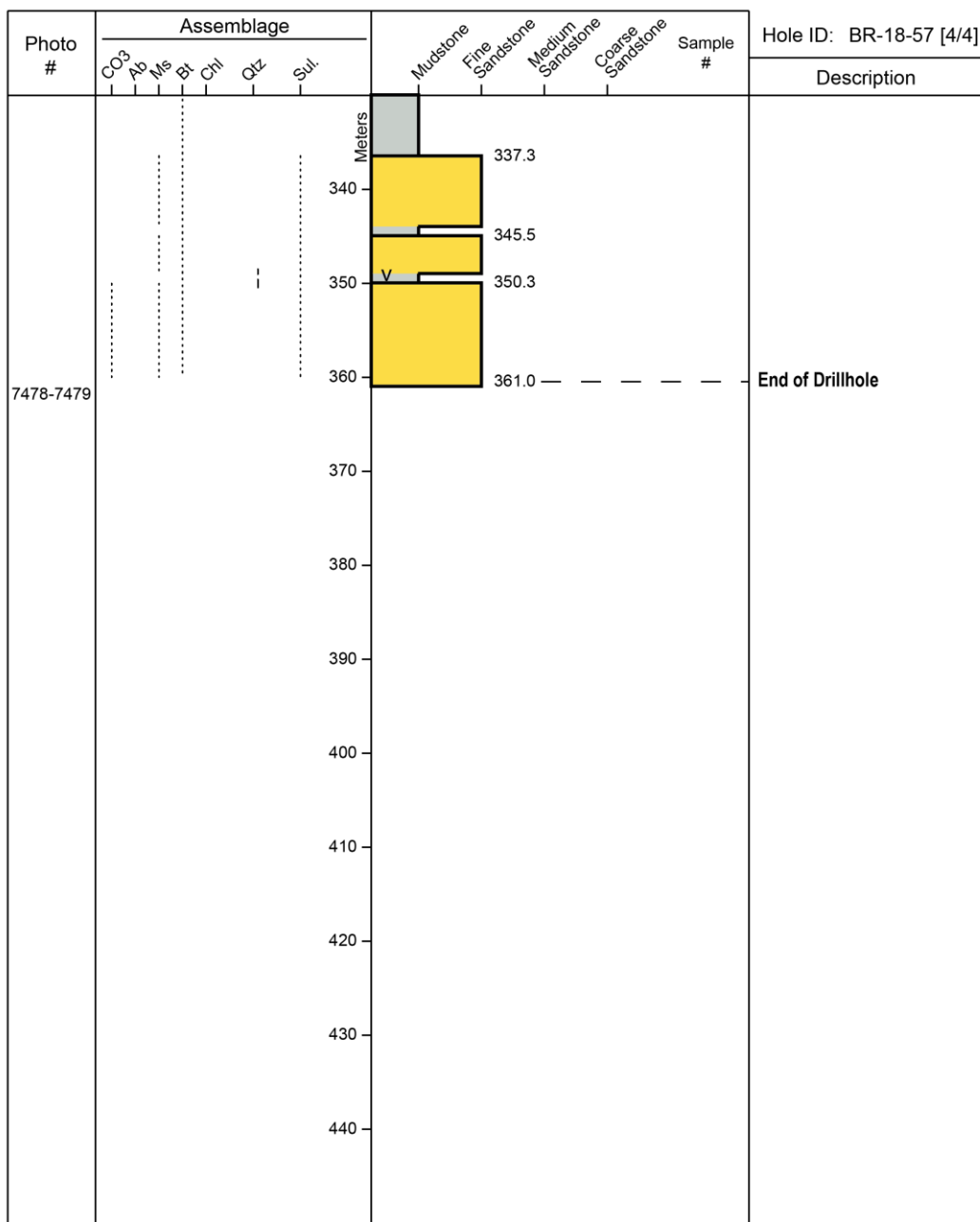


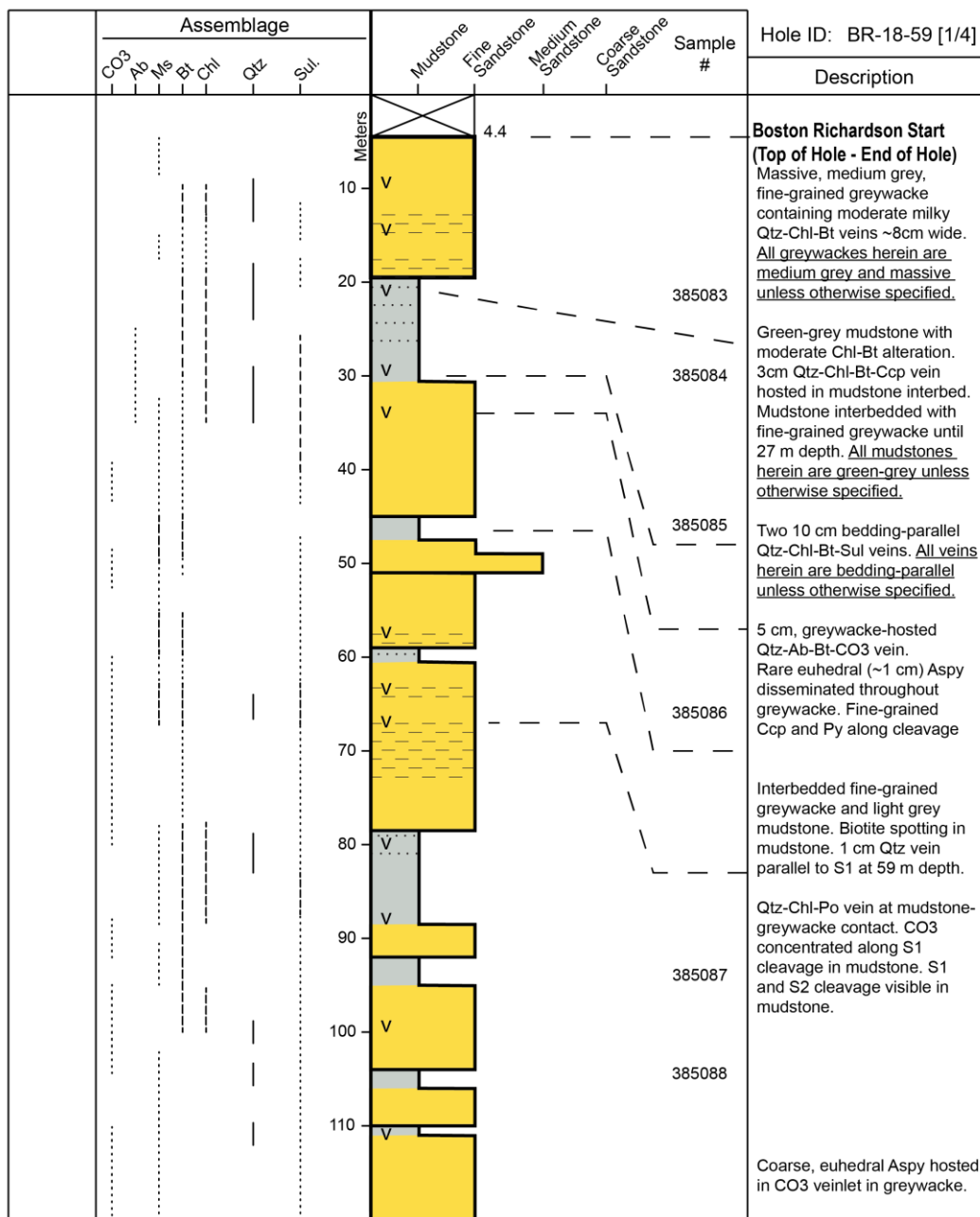


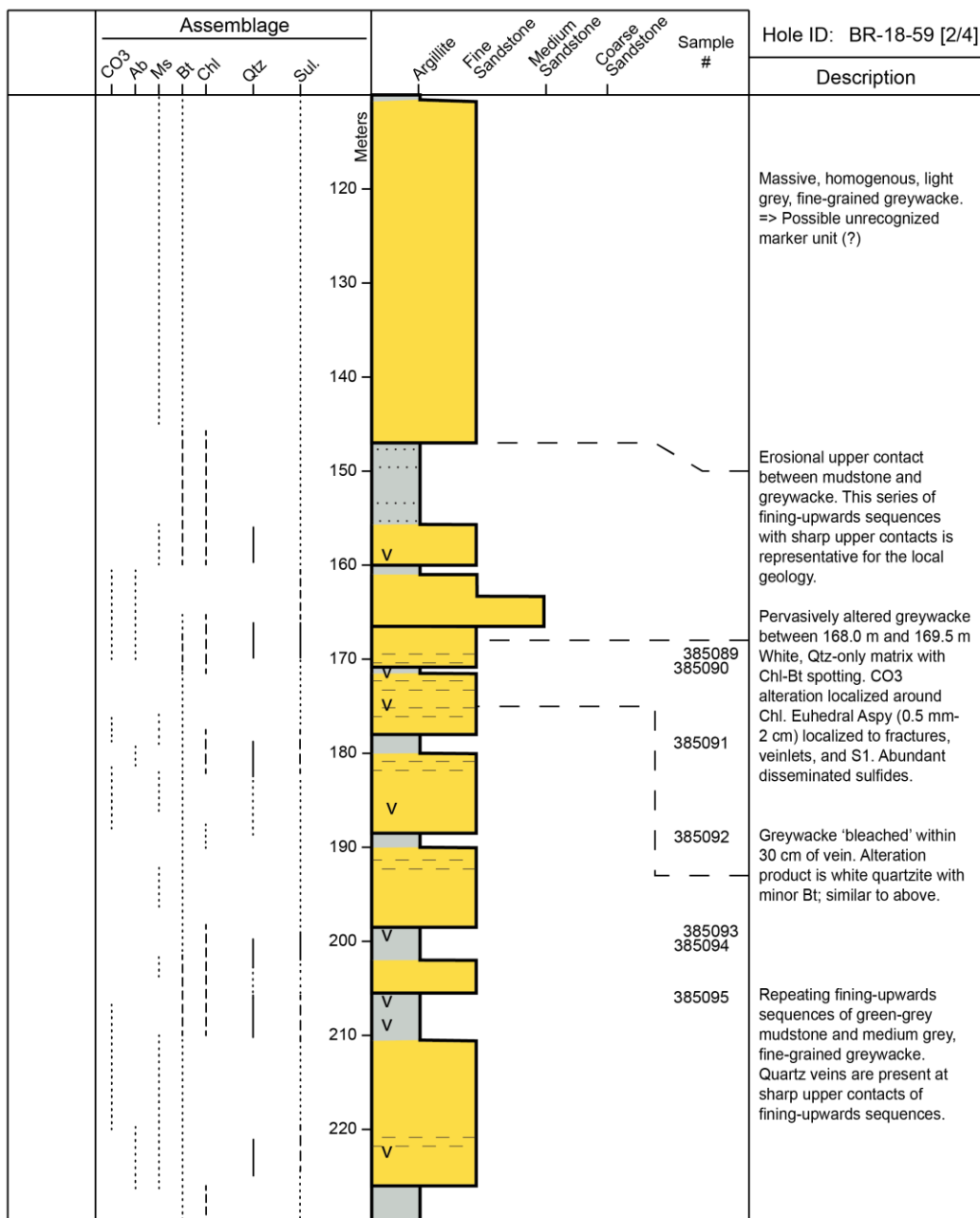


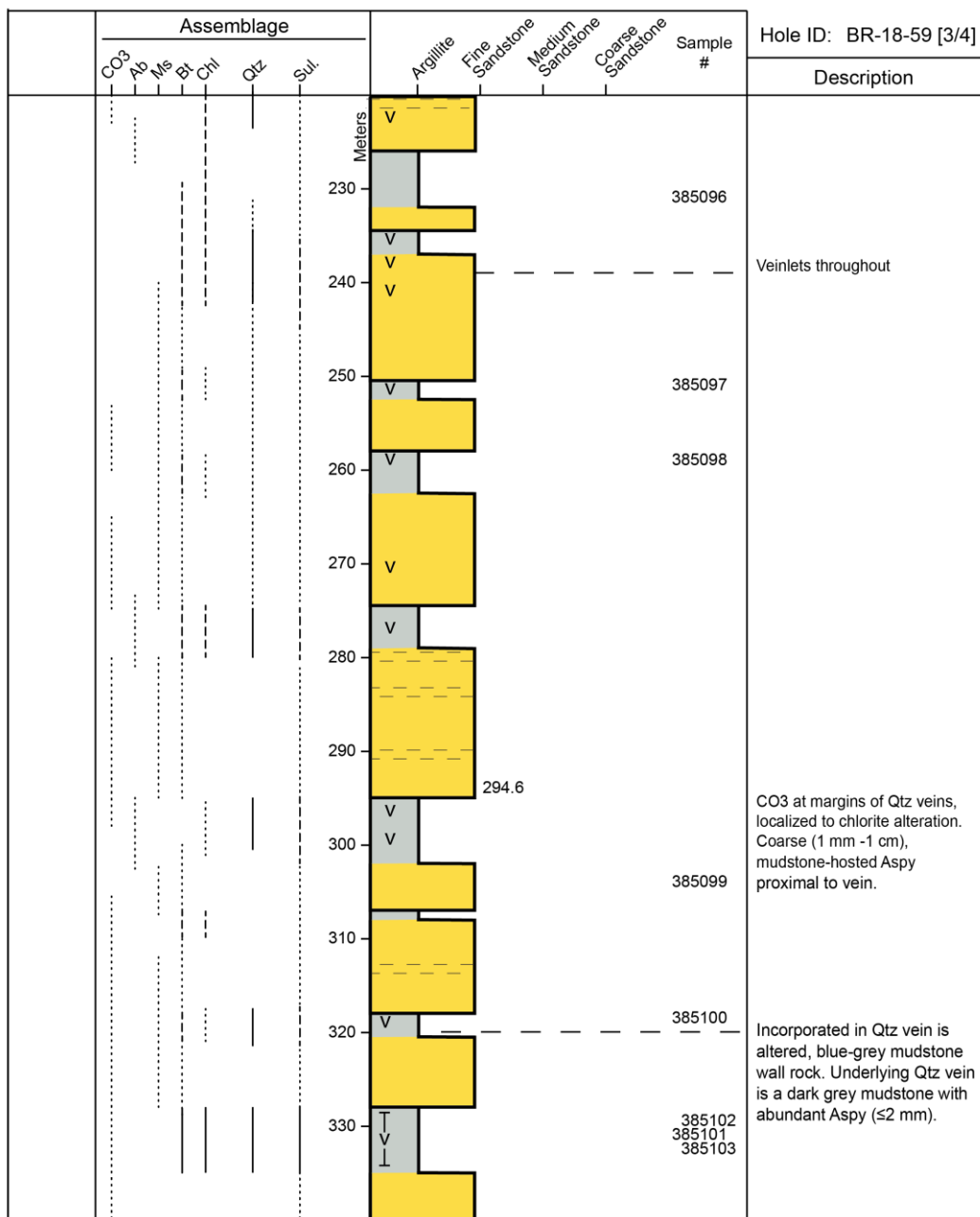


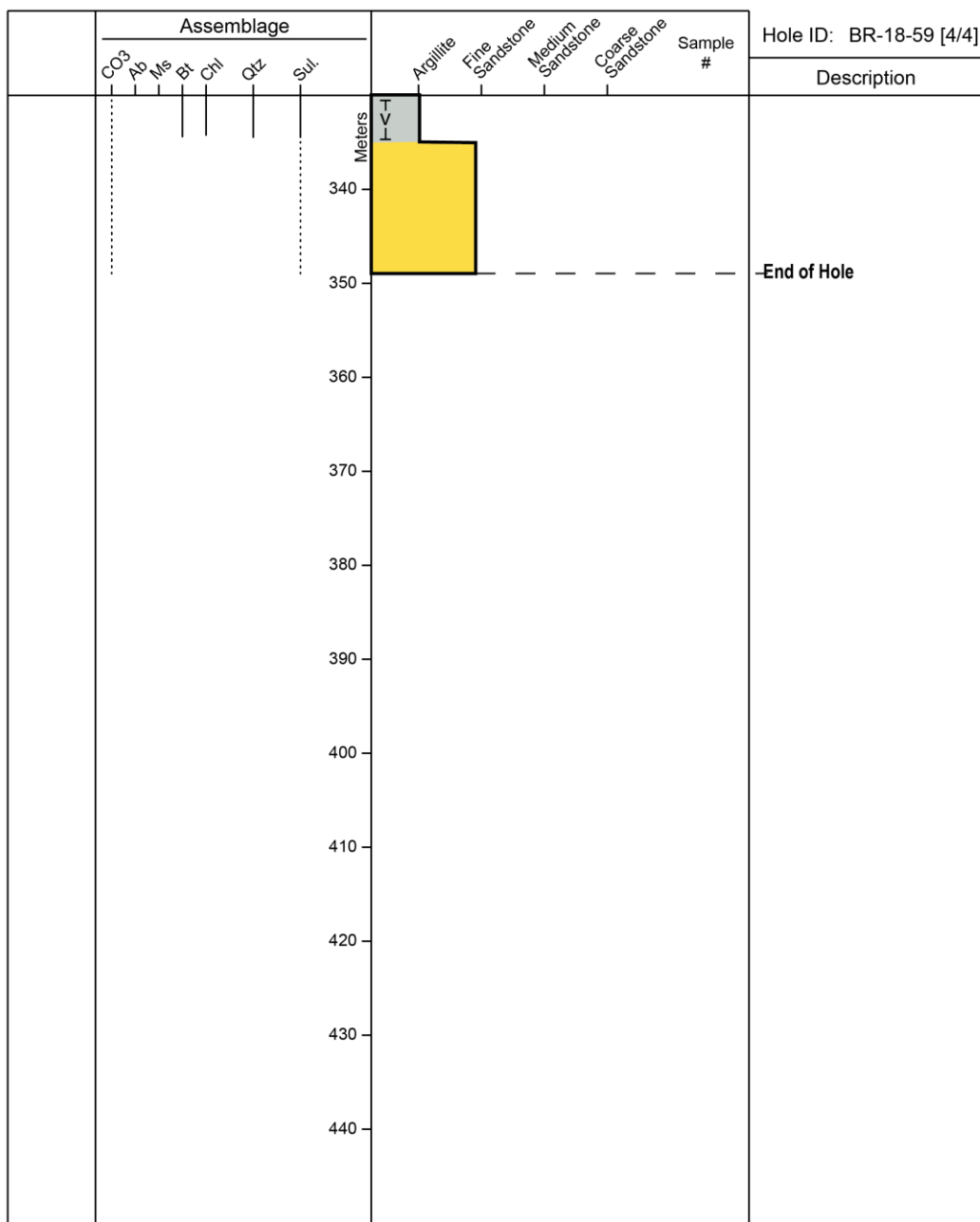


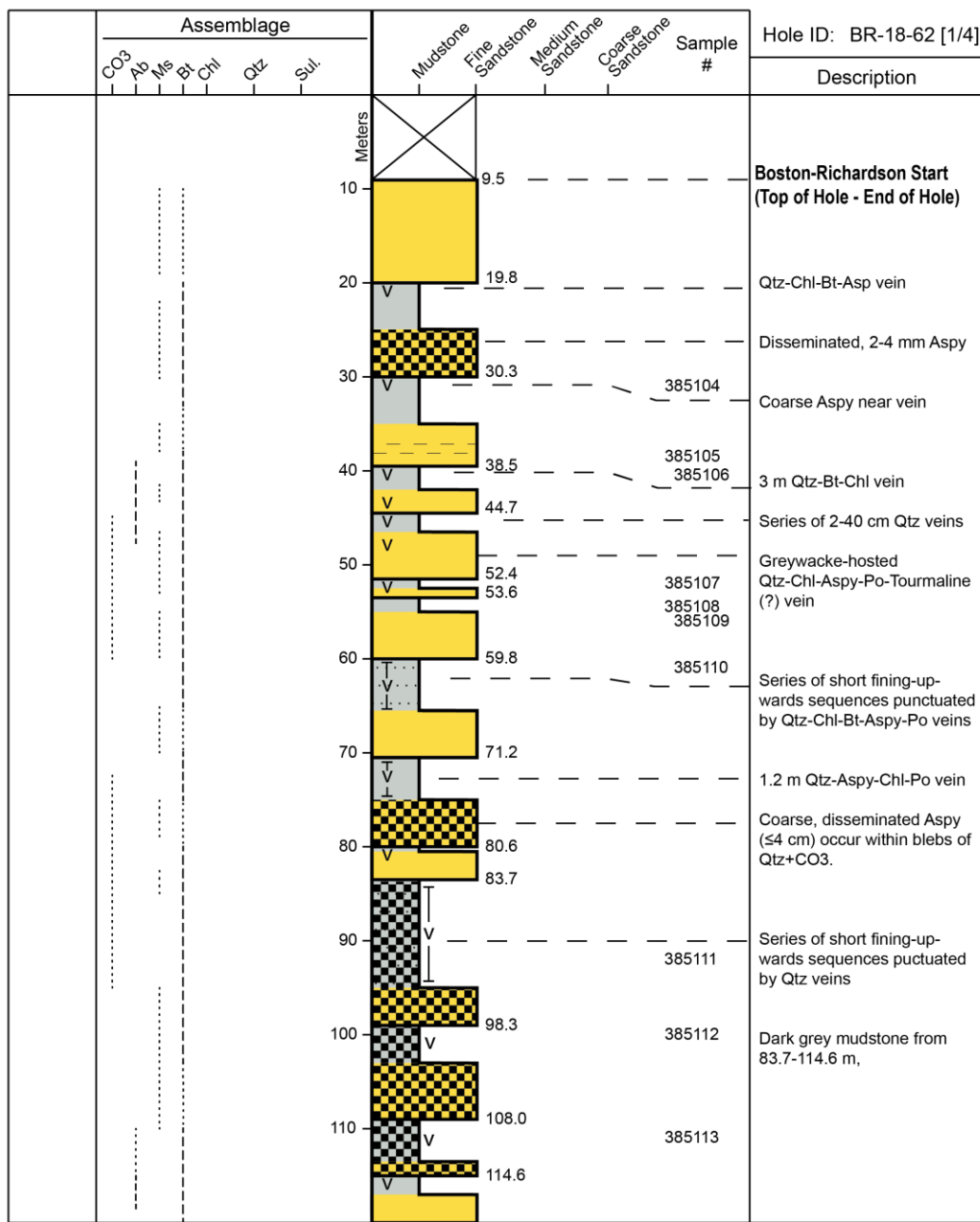


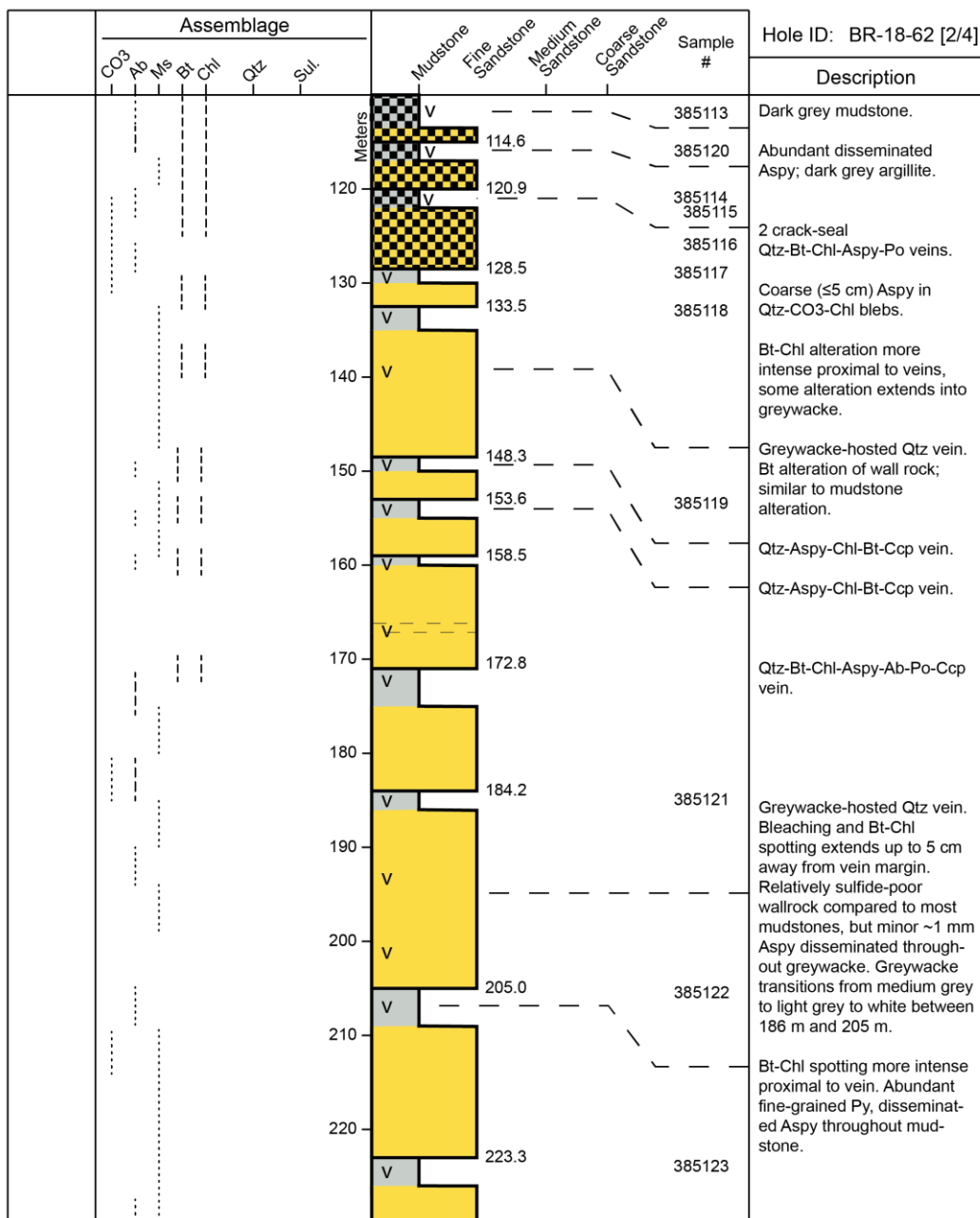


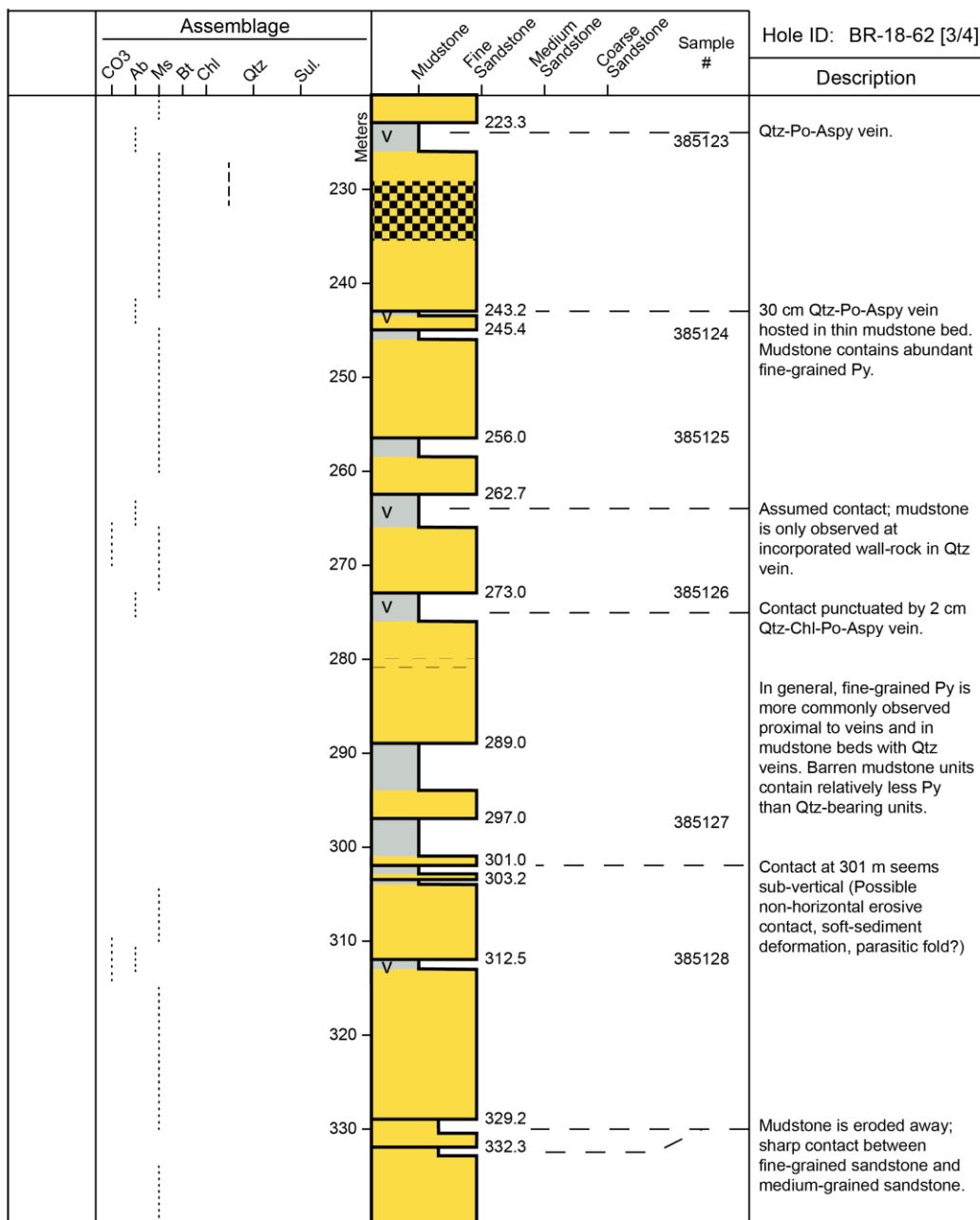


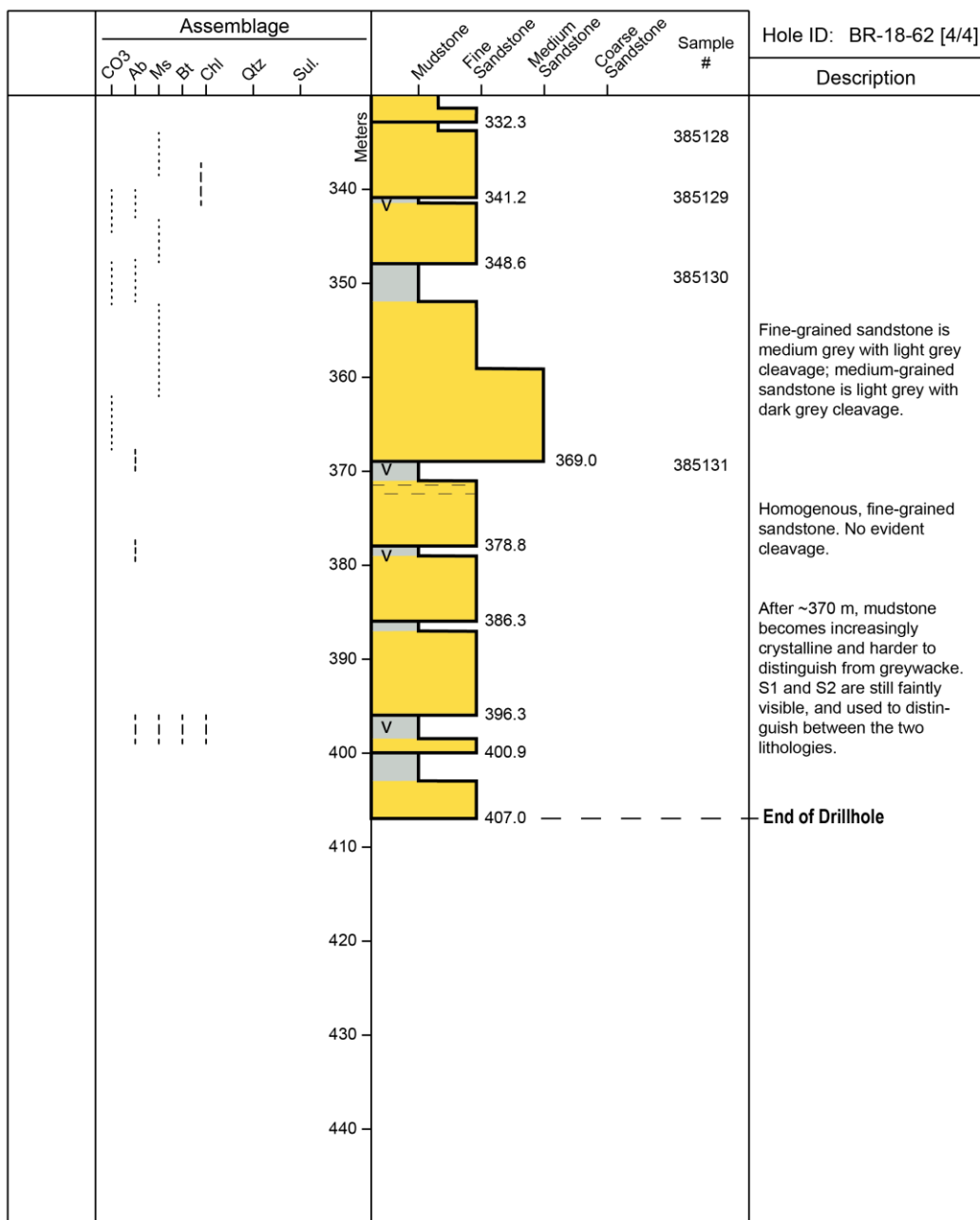


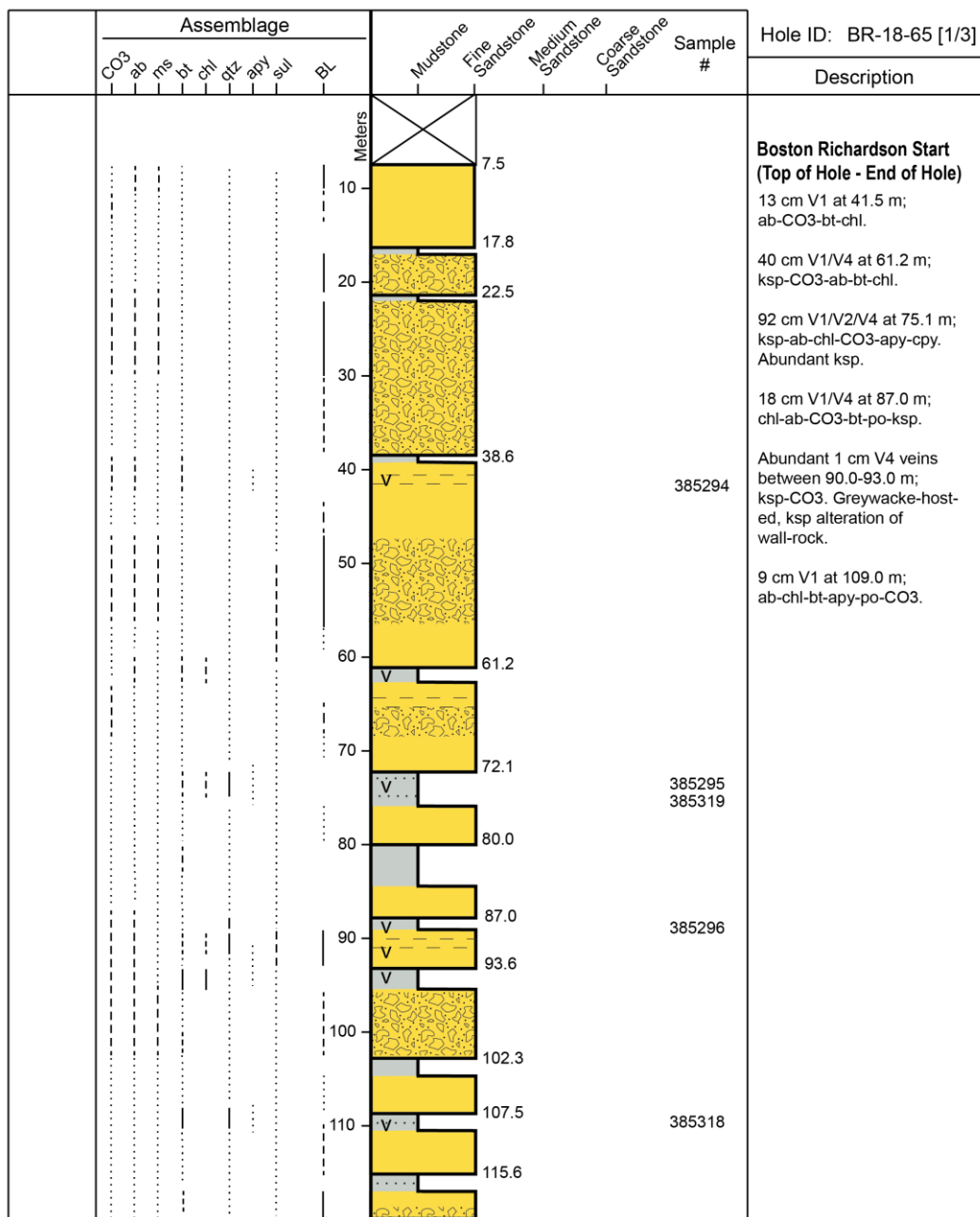


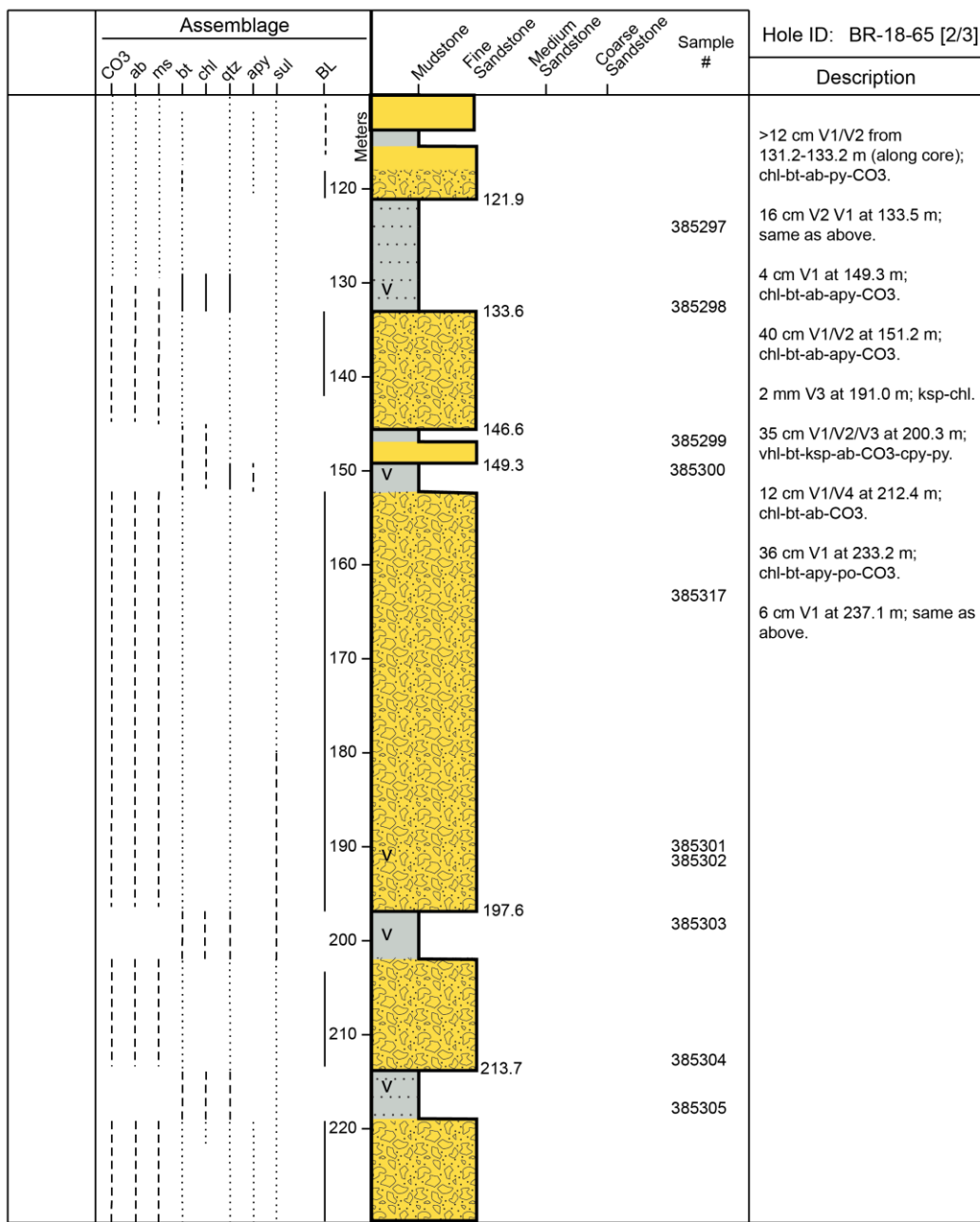




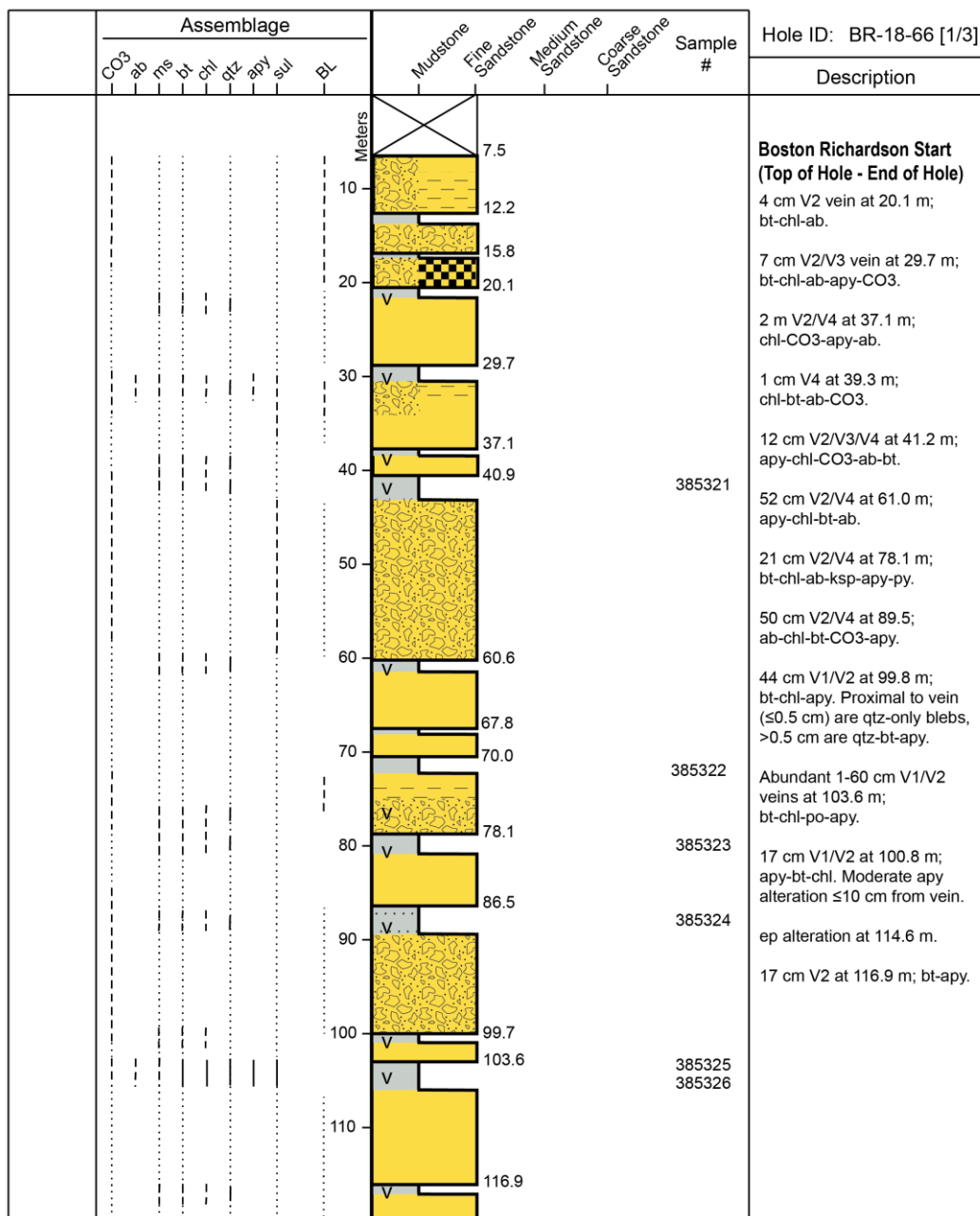




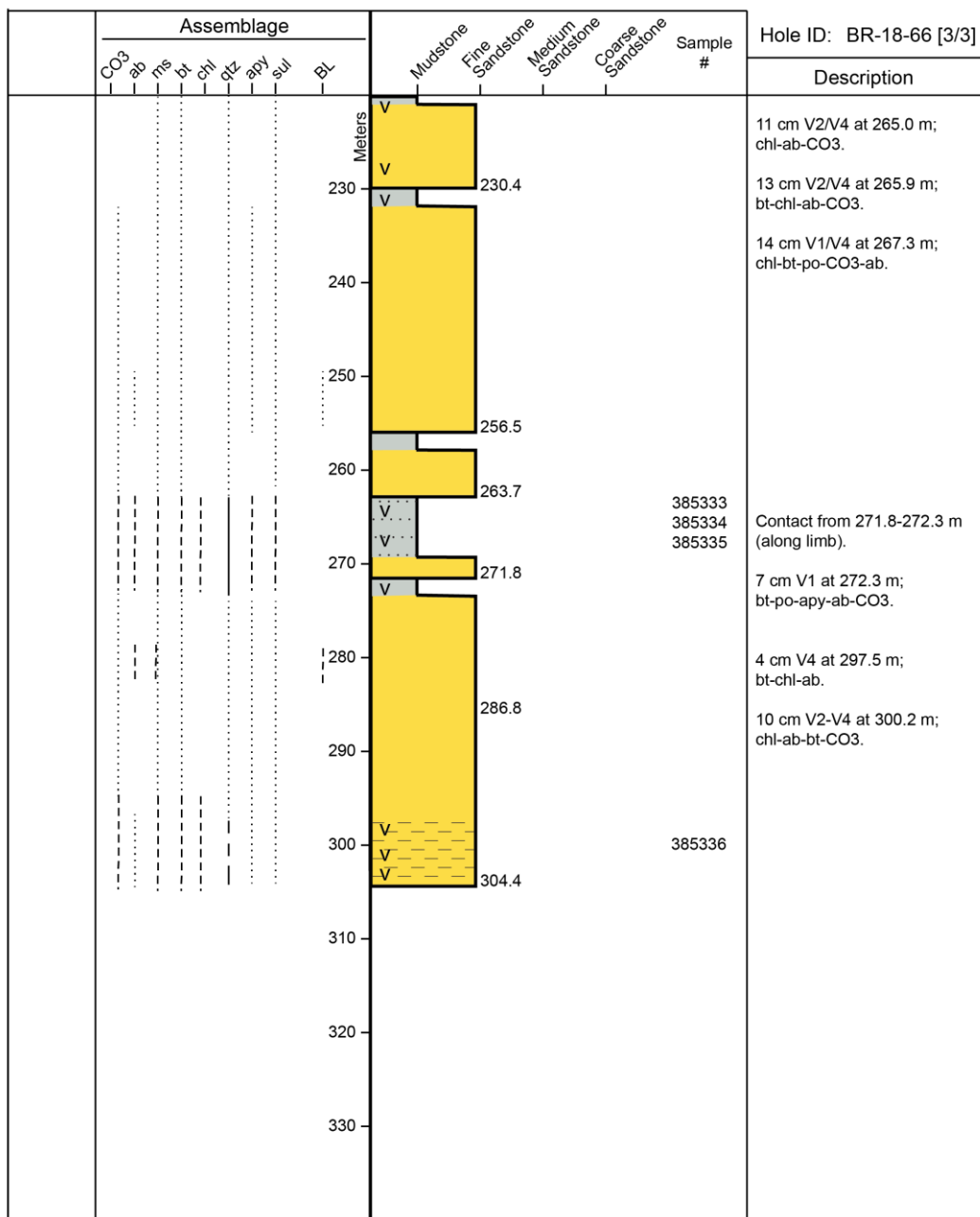


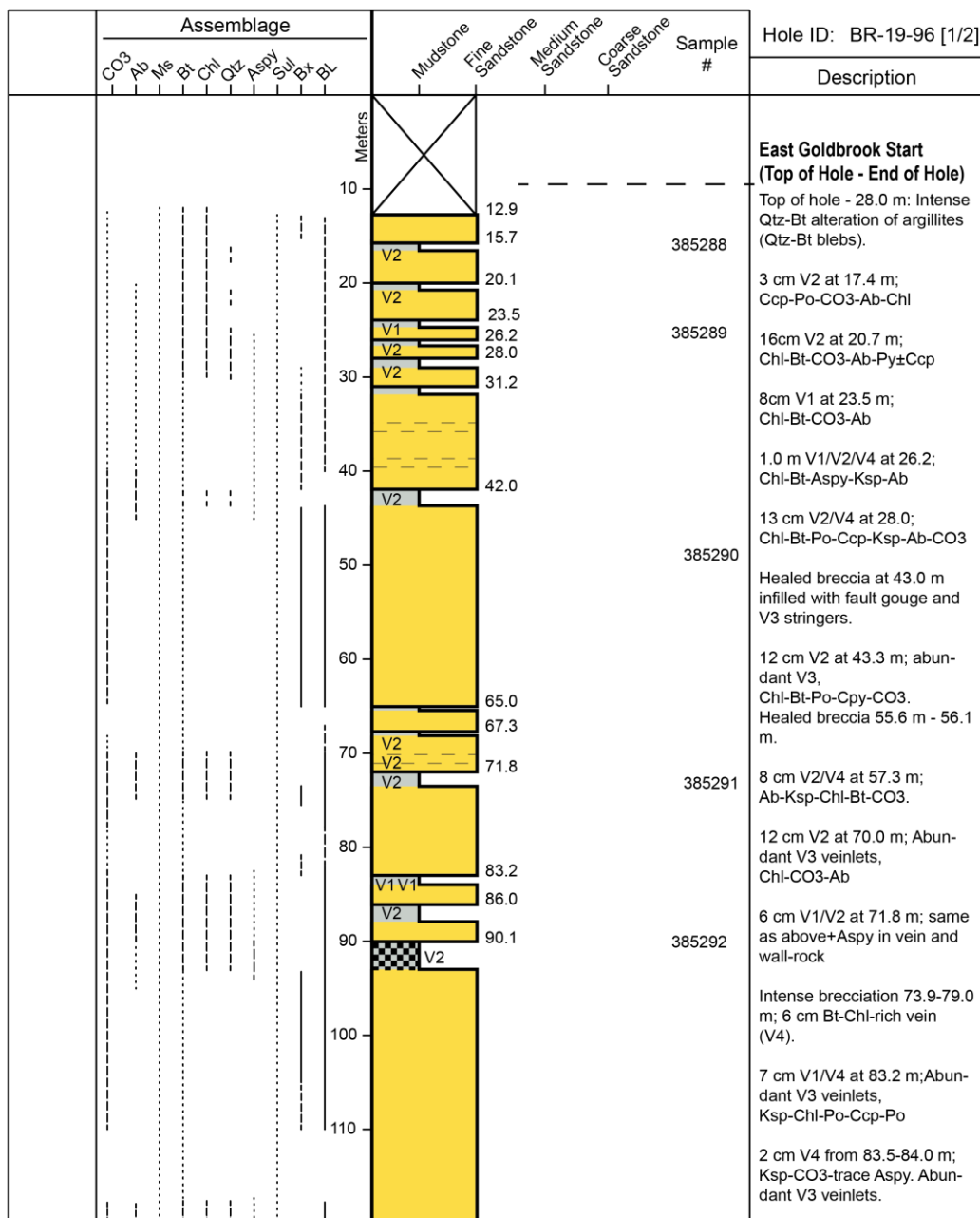


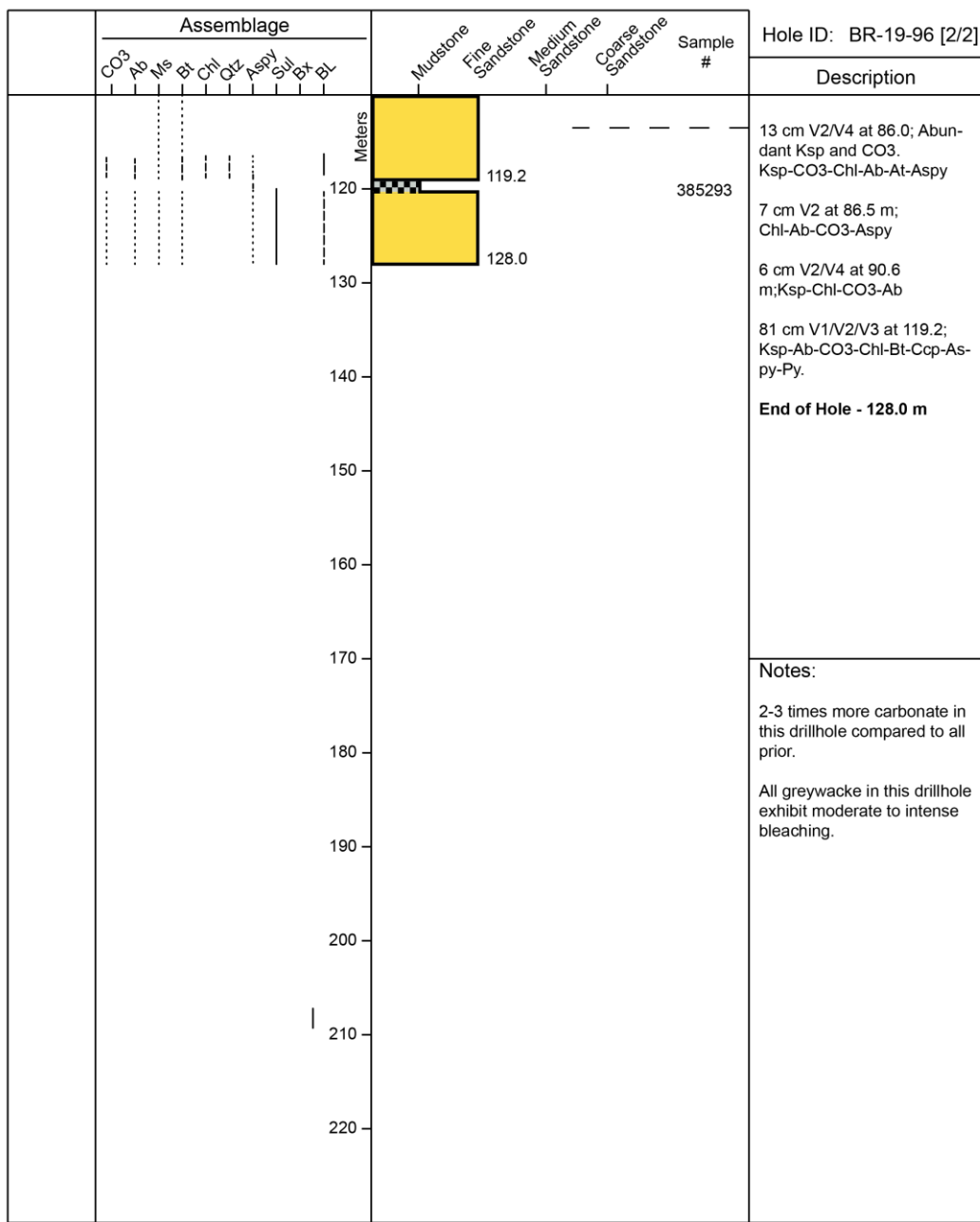
	Assemblage	Meters	Sample #	Hole ID: BR-18-65 [3/3]									
				CO ₃	ab	ms	bt	chl	dz	apy	sul	BL	Description
		230	385306 385307	Mudstone								231.3	28 cm V1/V2/V4 at 238.3 m; bt-chl-ab. Ksp alteration of greywacke.
		235.6	385308	Fine Sandstone									Wallrock-altering (ksp/ab-sericite) V4 veinlets (?) from 227.0-229.0 m; 100% chl.
		240	385309	Medium Sandstone								241.0	6 cm V1 at 241.0 m; bt-chl-ab-apy-cpy.
		244.7	385310	Coarse Sandstone								V	7 cm V1 at 244.7 m; bt-chl-ab-CO3-apy.
		247.5	385311									V	42 cm V2/V4 at 247.5 m; bt-chl-ab-ksp-CO3.
		249.1	385312									V	6 cm V1 at 249.1 m; chl-apy-CO3.
		257.9	385313									V	20 cm V2 at 249.3; same as above.
		269.0	385314									V	6 cm V4 at 257.9 m; ksp-ab-chl-po-cpy-CO3.
		290	385315									V	95 cm V1/V2 at 269.0 m; chl-bt-ab-apy-CO3.
		290.8-291.4	385316										Contact extending from 290.8-291.4 m.
		303.7										V	20 cm V1/V2 at 303.7 m; vhl-ab-CO3.
		307.5										V	32 cm V1/V2/V4 at 307.5 m; chl-ab-ksp-ilm-CO3.
		310	385313									V	6 cm V2 at 318.3 m; CO3.
		318.3	385314									V	5 cm V1 at 319.7 m; bt-chl-ab-CO3.
		319.7	385315									V	34 cm V1/V2 at 335.6 m; chl-bt-ab-apy-CO3.
		335.6	385316									V	
		338.0											



	Assemblage	Meters	Sample #	Hole ID: BR-18-66 [2/3]
				Description
		116.9	385327	25 cm V1/V2 at 125.6 m; bt-chl. Abundant healed breccia 126.0-132.0 m; ksp-ab.
		120		Possible fault at 130.1 m; 10 cm V1 at 130.2; CO ₃ -chl-ab.
		130		159.0-160.5 m along grey-wacke-argillite contact.
		140		15 cm V2/V4 at 180.3 m; bt-chl-ab-ksp-apy.
		150		20 cm V4 at 182.0 m; chl-ab-ksp-bt.
		160		10 cm V4 at 182.4 m; Same as above.
		170		12 cm V1 at 184.2 m; apy-bt-chl-po-ab.
		180	385328 385329 385330	11 cm V2/V4 at 193.8 m; chl-ab. 13 cm V1 at 216.4 m; chl. 23 cm V2 at 228.7 m; barren.
		180.1		1.8 m V1/V2/V4 at 230.4 m; chl-bt-ab-CO ₃ -apy.
		190		
		193.8		
		200		
		205.2	385331	
		210		
		214.9		
		220	385332	
		221.8		
		V		
		V		







Appendix B: Whole-rock Geochemical Analysis

Results

Table B1: Whole-rock geochemistry results

	L.O.D.	385004	385006	385008	385010	385012	385015	385022	385024	385025	385032	385043	385045	
SiO₂	wt. %	0.01	49.1	63.4	50.2	55.1	61.8	55.8	77.5	45.1	49.8	46.8	60.3	56.5
Al₂O₃	wt. %	0.01	23.8	16.85	23	22.5	17.2	22.4	10.55	25.4	21.4	26.2	17.8	21.5
Fe₂O₃	wt. %	0.01	9.61	7.33	9.82	6.99	7.62	6.54	3.97	8.88	10.85	8.2	7.59	5.64
CaO	wt. %	0.01	0.68	1.17	0.51	1.52	1.28	0.53	0.81	1.2	0.5	1.03	1.65	2.15
MgO	wt. %	0.01	3.3	2.89	3.36	2.85	2.93	2.47	1.01	3.05	3.33	3.19	3.09	2.49
Na₂O	wt. %	0.01	0.81	1.76	0.62	1.46	1.34	0.83	2.5	1.46	0.49	1.18	2.22	1.69
K₂O	wt. %	0.01	7.89	4.39	7.61	6.41	5.19	7.41	2.05	7.77	7.3	8.13	4.69	5.7
Cr₂O₃	wt. %	0.002	0.018	0.014	0.017	0.017	0.013	0.018	0.01	0.02	0.016	0.019	0.015	0.015
TiO₂	wt. %	0.01	0.98	0.71	0.92	0.88	0.72	0.87	0.43	1.11	0.82	0.99	0.79	0.93
MnO	wt. %	0.01	0.12	0.13	0.1	0.12	0.12	0.07	0.06	0.15	0.1	0.1	0.14	0.14
P₂O₅	wt. %	0.01	0.13	0.16	0.14	0.19	0.16	0.16	0.12	0.19	0.15	0.2	0.13	0.17
SrO	wt. %	0.01	0.02	0.02	0.01	0.03	0.02	0.01	0.01	0.03	0.01	0.02	0.03	0.03
BaO	wt. %	0.01	0.14	0.08	0.13	0.14	0.09	0.15	0.04	0.16	0.11	0.17	0.08	0.15
LOI	wt. %	0.01	3.02	1.88	3.09	2.74	1.95	2.71	2	5.39	4.8	3.67	1.85	2.3
Total	wt. %	0.01	99.62	100.78	99.53	100.95	100.43	99.97	101.06	99.91	99.68	99.9	100.38	99.41
C	wt. %	0.01	0.03	0.06	0.03	0.15	0.08	0.04	0.09	0.38	0.1	0.24	0.1	0.13
S	wt. %	0.01	0.28	0.03	0.17	0.05	0.06	0.03	0.72	1.19	1.45	0.48	0.08	0.01
Ba	ppm	0.5	1260	752	1215	1255	797	1350	361	1435	1045	1555	700	1355
Ce	ppm	0.1	87.4	78.4	93.9	85.4	71.9	81.8	44	91.8	83.6	102.5	61.3	73.7
Cr	ppm	10	120	100	120	110	90	110	60	130	110	130	100	100
Cs	ppm	0.01	11.75	7.04	11.95	9.18	8.94	9.89	1.96	9.38	9.8	11.4	9.27	7.64
Dy	ppm	0.05	5.95	6.01	5.64	5.42	5.62	5.03	3.09	6.63	5.52	6.56	5.08	5
Er	ppm	0.03	3.42	3.34	3.26	3.1	3.16	3.04	2.01	3.92	3.3	3.68	2.93	2.91
Eu	ppm	0.02	1.5	1.59	1.63	1.5	1.52	1.19	0.9	1.75	1.44	1.72	1.35	1.48
Ga	ppm	0.1	36.3	23.9	35.7	34	24.8	34.7	12.3	38.7	31.6	38.5	25	32.3
Gd	ppm	0.05	5.97	6.41	6.59	6.09	5.74	5.39	3.56	6.63	6.1	7.5	5.45	5.45
Ge	ppm	5	<5	<5	<5	<5	<5	<5	<5	<5	<5	<5	<5	<5
Hf	ppm	0.1	5.4	5	4.7	4.4	5.7	4.6	5.5	6.2	4.2	5.1	5.1	4.5
Ho	ppm	0.01	1.07	1.12	1.02	0.93	1.06	0.96	0.55	1.17	1.06	1.16	0.88	0.89
La	ppm	0.1	41.8	39.1	47.2	41.6	35.4	40.5	21.6	45.1	40.7	50.7	29.7	36.7
Lu	ppm	0.01	0.49	0.46	0.47	0.44	0.44	0.43	0.28	0.54	0.45	0.55	0.38	0.45
Nb	ppm	0.1	16	12.3	15.2	14.9	13.2	14.4	8.1	16.1	12.4	16.6	13.5	16.3
Nd	ppm	0.1	37.2	35	39.7	37.8	31.7	36	19.9	40.4	37.8	45.2	27.5	33.5
Pr	ppm	0.02	9.68	9	10.7	9.77	8.35	9.53	5.1	10.6	9.66	11.85	7.1	8.77
Rb	ppm	0.2	258	154	252	207	188.5	230	68.7	252	234	270	179	185
Sm	ppm	0.03	7.28	7.03	8.09	7.84	6.28	6.82	3.83	8.27	7.37	8.95	5.84	7
Sn	ppm	1	3	2	3	3	2	3	1	4	3	4	2	3
Sr	ppm	0.1	129.5	171.5	95.6	223	175.5	105	145	224	76	210	237	251
Ta	ppm	0.1	1	0.8	1	1	0.8	1	0.6	1.2	0.8	1.2	0.9	1.1
Tb	ppm	0.01	0.79	0.86	0.84	0.87	0.81	0.83	0.45	0.93	0.79	0.94	0.75	0.79
Th	ppm	0.05	13.05	9.16	12	11.55	9.33	11.2	5.29	12.85	11.4	13.1	8.91	10.35
Tm	ppm	0.01	0.5	0.47	0.46	0.39	0.45	0.42	0.25	0.59	0.45	0.51	0.38	0.4
U	ppm	0.05	2.57	1.93	2.25	2.45	2.12	2.34	1.33	2.86	2.07	2.65	1.92	2.14
V	ppm	5	126	92	165	132	94	134	53	158	126	157	94	123
W	ppm	1	15	12	12	10	7	17	7	12	10	12	6	10
Y	ppm	0.1	29.8	30.8	28.3	25.5	28.5	26.2	16.4	33.9	27.7	33.9	25.9	25.5
Yb	ppm	0.03	3.32	3.24	3.04	3.05	3.2	2.9	1.83	3.77	3.09	3.73	2.45	2.7
Zr	ppm	2	183	177	177	156	203	162	197	213	143	174	182	159
As	ppm	0.1	>250	111.5	>250	117	118.5	99.9	>250	>250	>250	>250	230	48
Bi	ppm	0.01	0.13	0.11	0.08	0.07	0.29	0.05	0.86	0.58	0.52	0.35	0.03	0.03
Hg	ppm	0.005	<0.005	<0.005	<0.005	<0.005	<0.005	<0.005	<0.005	<0.005	<0.005	<0.005	<0.005	<0.005
In	ppm	0.005	0.023	0.026	0.017	0.02	0.018	0.029	0.012	0.018	0.021	0.019	0.025	0.016
Re	ppm	0.001	<0.001	<0.001	<0.001	<0.001	<0.001	<0.001	<0.001	<0.001	<0.001	<0.001	<0.001	<0.001
Sb	ppm	0.05	0.89	0.36	0.22	0.43	0.14	0.45	27	21	19.85	3.7	0.22	0.17
Se	ppm	0.2	<0.2	<0.2	<0.2	<0.2	<0.2	<0.2	0.5	0.3	0.3	<0.2	<0.2	<0.2
Te	ppm	0.01	<0.01	0.02	<0.01	<0.01	<0.01	<0.01	0.62	0.14	0.1	0.02	<0.01	<0.01
Tl	ppm	0.02	0.7	0.55	0.75	0.53	0.67	0.58	0.09	0.54	0.64	0.71	0.68	0.51
Ag	ppm	0.5	<0.5	<0.5	<0.5	<0.5	<0.5	<0.5	<0.5	<0.5	<0.5	<0.5	0.6	<0.5
Cd	ppm	0.5	1.5	<0.5	<0.5	<0.5	<0.5	0.7	<0.5	<0.5	<0.5	<0.5	<0.5	<0.5
Co	ppm	1	25	19	26	24	18	24	9	27	26	28	21	17
Cu	ppm	1	66	35	40	46	31	60	7	14	123	35	15	2
Li	ppm	10	90	70	90	70	80	70	30	80	90	80	90	70
Mo	ppm	1	1	1	<1	<1	<1	<1	1	1	1	1	1	<1
Ni	ppm	1	68	47	62	53	45	53	20	62	65	65	48	32
Pb	ppm	2	22	26	16	32	23	17	49	27	26	25	17	19
Sc	ppm	1	17	15	19	18	14	18	7	19	19	22	16	19
Zn	ppm	2	154	89	100	75	79	238	32	101	150	172	97	79
C	wt. %	0.05	<0.05	<0.05	<0.05	<0.05	<0.05	<0.05	<0.05	<0.05	<0.05	<0.05	0.06	0.06
CO₂	wt. %	2	<0.2	<0.2	<0.2	<0.2	0.2	<0.2	<0.2	<0.2	<0.2	<0.2	0.2	0.2
Au	ppm	0.001	0.016	0.008	0.045	0.006	0.005	0.006	0.314	0.429	0.787	0.763	0.009	0.004

	L.O.D.	385083	385085	385087	385095	385096	385098	385100	385101	385104	385112	385113	385118	
SiO₂	wt. %	0.01	61.9	63.5	59.6	55.3	59	59.9	40.5	42.5	59.1	40.7	43.6	55.2
Al₂O₃	wt. %	0.01	19.6	18	19.15	22.5	20	19.85	25.1	28.6	20.1	25.8	26.7	21.7
Fe₂O₃	wt. %	0.01	5.57	7.32	7.41	6.91	7.16	5.68	11.2	6.01	6.46	9.97	7.04	6.99
CaO	wt. %	0.01	1.45	0.87	0.94	1.02	1.07	1.29	0.67	0.38	0.83	0.76	0.87	1.79
MgO	wt. %	0.01	2.34	2.57	2.95	2.93	2.69	2.58	3.56	2.54	2.67	3.46	2.14	2.83
Na₂O	wt. %	0.01	1.82	1.68	1.24	1.26	1.75	2.07	0.85	0.45	1.57	0.82	1.25	2.6
K₂O	wt. %	0.01	4.99	4.55	5.06	6.53	4.88	5.17	8.42	9.56	6.01	8.45	8.02	5.6
Cr₂O₃	wt. %	0.002	0.015	0.013	0.014	0.016	0.016	0.015	0.019	0.019	0.015	0.02	0.016	0.016
TiO₂	wt. %	0.01	0.79	0.77	0.74	0.86	0.8	0.9	1.1	1.06	0.82	1.02	0.91	0.88
MnO	wt. %	0.01	0.11	0.1	0.1	0.11	0.08	0.14	0.13	0.1	0.11	0.12	0.08	0.09
P₂O₅	wt. %	0.01	0.17	0.14	0.16	0.2	0.18	0.2	0.1	0.16	0.17	0.1	0.04	0.19
SrO	wt. %	0.01	0.03	0.02	0.02	0.02	0.02	0.03	0.02	0.01	0.01	0.01	0.03	0.03
BaO	wt. %	0.01	0.11	0.1	0.1	0.15	0.1	0.12	0.16	0.22	0.13	0.17	0.19	0.1
LOI	wt. %	0.01	2	2.21	2.51	2.8	2.27	2.33	6.87	6.62	2.63	6.8	7.71	1.9
Total	wt. %	0.01	100.9	101.84	99.99	100.61	100.02	100.28	98.7	98.23	100.63	98.2	98.6	99.92
C	wt. %	0.01	0.09	0.03	0.06	0.06	0.04	0.09	0.51	1.45	0.21	0.94	1.26	0.19
S	wt. %	0.01	0.01	0.2	0.08	0.53	0.01	0.07	1.68	0.88	0.04	1.5	1.68	0.06
Ba	ppm	0.5	1045	929	924	1350	960	1085	1485	2050	1175	1530	1785	902
Ce	ppm	0.1	65.3	65.9	63.9	94.7	77.1	84.8	105	104	64.7	101.5	104.5	90.6
Cr	ppm	10	100	90	100	110	110	110	130	130	100	130	110	110
Cs	ppm	0.01	6.52	6.4	7.8	8.49	6.12	6.92	11.45	10.25	8.36	12.6	10.4	7.81
Dy	ppm	0.05	4.91	5.16	5.54	6.49	5.84	5.47	6.75	5.9	4.63	6.69	6.56	6.24
Er	ppm	0.03	2.73	3	2.97	3.59	3.19	3.24	4.01	3.45	2.72	4.4	4.03	3.85
Eu	ppm	0.02	1.31	1.24	1.3	1.63	1.5	1.6	1.74	1.56	1.15	1.96	1.74	1.65
Ga	ppm	0.1	27.6	27.1	27.3	33.6	30.6	29.9	42.6	48.9	30.2	43.5	45.5	32.3
Gd	ppm	0.05	4.97	5.38	5.35	7.26	5.67	6.09	7.13	6.19	4.62	7.22	7	6.48
Ge	ppm	5	<5	<5	<5	<5	<5	<5	<5	<5	<5	<5	<5	<5
Hf	ppm	0.1	4	4.2	4.2	4.6	4.2	7.3	6.1	5.8	4.3	5.4	4.7	4.7
Ho	ppm	0.01	0.87	0.96	0.97	1.15	1.07	1.06	1.24	1.13	0.98	1.36	1.26	1.22
La	ppm	0.1	32.1	32.8	31.8	47.9	38.5	42.1	50.5	50.9	32.9	50.2	52.9	44.3
Lu	ppm	0.01	0.38	0.45	0.44	0.46	0.49	0.51	0.56	0.53	0.4	0.67	0.58	0.49
Nb	ppm	0.1	14.1	13.7	12.5	16.4	13.7	15.7	18.9	16.4	14.5	18.4	16	14.9
Nd	ppm	0.1	28.9	29.4	28.4	43.1	34.6	38.9	46	46.1	29.3	46.4	49.1	39.2
Pr	ppm	0.02	7.5	7.86	7.33	11	9.07	10.05	12.15	12.15	7.43	11.8	12.1	10.45
Rb	ppm	0.2	157	146.5	167	206	164	173	280	282	196.5	286	254	185.5
Sm	ppm	0.03	5.84	5.85	6.13	8.95	7.3	7.36	8.94	8.33	5.51	9.58	8.84	8.22
Sn	ppm	1	3	3	3	3	3	4	5	3	3	4	3	
Sr	ppm	0.1	214	129.5	137	147	156.5	223	134	46.6	111	137.5	194	256
Ta	ppm	0.1	0.9	0.9	0.8	1	0.9	1.1	1.2	1.1	3.5	3.3	3.6	1
Tb	ppm	0.01	0.74	0.77	0.75	0.94	0.81	0.85	1.02	0.88	0.74	1.08	0.99	0.95
Th	ppm	0.05	9.61	8.48	9.52	11.65	10.45	12.5	14.95	13.45	10.35	14.4	13.2	11.7
Tm	ppm	0.01	0.39	0.43	0.42	0.47	0.42	0.48	0.55	0.5	0.42	0.61	0.53	0.49
U	ppm	0.05	2.14	1.62	2.05	2.31	2.3	2.5	3	3.02	2.33	2.98	2.51	2.55
V	ppm	5	158	102	110	127	117	131	156	182	133	162	172	138
W	ppm	1	14	14	13	13	14	15	12	16	14	13	14	15
Y	ppm	0.1	24.8	26.3	28.9	31.9	28.9	29.3	35.1	28.8	25.3	36.8	35.7	32.3
Yb	ppm	0.03	2.81	3.08	2.84	3.2	2.98	3.35	4.11	3.87	2.93	4.69	3.81	3.62
Zr	ppm	2	150	150	147	163	146	266	222	209	161	191	164	174
As	ppm	0.1	64.5	136.5	111.5	>250	38	68.5	>250	>250	>250	>250	>250	>250
Bi	ppm	0.01	0.09	0.09	0.29	0.35	0.04	0.13	1.37	0.97	0.07	1.07	1.43	0.2
Hg	ppm	0.005	<0.005	<0.005	<0.005	<0.005	<0.005	<0.005	<0.005	<0.005	<0.005	<0.005	<0.005	<0.005
In	ppm	0.005	0.016	0.028	0.02	0.016	0.017	0.019	0.03	0.016	0.021	0.035	0.027	0.018
Re	ppm	0.001	<0.001	<0.001	<0.001	<0.001	<0.001	<0.001	<0.001	<0.001	<0.001	<0.001	<0.001	<0.001
Sb	ppm	0.05	0.22	0.4	0.26	1.28	0.22	0.21	13.6	6.27	0.22	12.7	13.05	0.29
Se	ppm	0.2	0.2	0.2	<0.2	<0.2	<0.2	<0.2	0.6	0.2	<0.2	0.6	0.4	<0.2
Te	ppm	0.01	<0.01	0.01	0.01	0.02	<0.01	0.01	0.59	0.36	0.01	0.81	0.79	0.04
Tl	ppm	0.02	0.44	0.44	0.56	0.57	0.53	0.44	0.68	0.31	0.49	0.67	0.24	0.64
Ag	ppm	0.5	<0.5	<0.5	<0.5	<0.5	<0.5	0.5	<0.5	<0.5	<0.5	<0.5	<0.5	<0.5
Cd	ppm	0.5	<0.5	<0.5	<0.5	<0.5	<0.5	<0.5	1.2	0.9	0.5	0.7	<0.5	<0.5
Co	ppm	1	15	19	26	16	17	16	39	27	21	28	20	19
Cu	ppm	1	18	157	51	60	6	19	6	15	54	4	4	10
Li	ppm	10	60	70	80	80	70	80	100	70	70	100	70	70
Mo	ppm	1	1	<1	<1	<1	<1	<1	1	1	1	1	1	<1
Ni	ppm	1	42	70	63	43	47	33	74	43	53	63	49	37
Pb	ppm	2	27	11	16	22	26	33	47	26	17	27	43	44
Sc	ppm	1	17	16	16	19	18	19	24	23	17	23	20	19
Zn	ppm	2	81	128	125	120	103	74	159	98	82	151	66	107
C	wt. %	0.05	<0.05	<0.05	<0.05	<0.05	<0.05	<0.05	<0.05	<0.05	0.05	<0.05	<0.05	<0.05
CO₂	wt. %	2	<0.2	<0.2	<0.2	<0.2	<0.2	<0.2	0.2	<0.2	0.2	<0.2	<0.2	<0.2
Au	ppm	0.001	0.004	0.008	0.043	0.973	0.03	0.006	0.384	0.355	0.009	4.16	1.13	0.035

	L.O.D.	385122	385123	385126	385127	385130	385131	385157	385158	385159	385160	385162	385167	
SiO₂	wt. %	0.01	57.6	54.4	60.7	61.4	45.5	62.3	57	46.8	58.8	56.6	49.6	58.6
Al₂O₃	wt. %	0.01	17.6	22.8	18.65	16.85	26.2	20.2	21.1	26.7	19.35	20.9	25.8	19.8
Fe₂O₃	wt. %	0.01	7.5	5.33	6.51	6.75	9.94	5.57	6.99	7.81	7.12	7.91	8.46	7.53
CaO	wt. %	0.01	2.68	2.98	2.44	1.86	2.17	1.05	0.93	1.12	2.32	1.45	1.17	2
MgO	wt. %	0.01	3.27	2.16	2.72	2.77	3.44	2.2	2.75	3.08	2.7	2.86	3.28	3.2
Na₂O	wt. %	0.01	2.48	3.78	2.83	2.01	2.41	1.75	1.54	1.1	2.4	1.98	1.41	2.08
K₂O	wt. %	0.01	4.19	4.76	3.77	3.91	6.49	5.32	5.98	8.16	4.76	5.92	7.63	4.59
Cr₂O₃	wt. %	0.002	0.014	0.017	0.013	0.013	0.018	0.015	0.015	0.019	0.015	0.016	0.019	0.014
TiO₂	wt. %	0.01	0.72	1.04	0.77	0.73	0.96	0.79	0.88	1.03	0.88	0.91	1.06	0.7
MnO	wt. %	0.01	0.19	0.12	0.14	0.14	0.11	0.08	0.1	0.1	0.13	0.1	0.11	0.1
P₂O₅	wt. %	0.01	0.19	0.21	0.18	0.18	0.16	0.19	0.16	0.19	0.19	0.17	0.21	0.38
SrO	wt. %	0.01	0.03	0.04	0.02	0.02	0.04	0.01	0.02	0.02	0.04	0.02	0.02	0.03
BaO	wt. %	0.01	0.07	0.12	0.09	0.08	0.15	0.12	0.13	0.18	0.1	0.1	0.17	0.09
LOI	wt. %	0.01	1.55	1.88	1.3	1.47	2.99	2	2.26	3.09	1.44	2.16	3.05	2.15
Total	wt. %	0.01	98.08	99.64	100.13	98.18	100.58	101.6	99.86	99.4	100.25	101.1	101.99	101.26
C	wt. %	0.01	0.26	0.23	0.07	0.08	0.23	0.08	0.11	0.15	0.09	0.07	0.09	0.07
S	wt. %	0.01	0.18	0.06	0.01	0.09	0.36	0.05	0.02	0.14	0.04	0.2	0.35	0.01
Ba	ppm	0.5	615	1030	744	733	1295	1065	1170	1570	844	878	1475	790
Ce	ppm	0.1	71.3	90.3	78.3	65.4	106.5	77	83.3	110.5	80.5	76.9	98.3	92.4
Cr	ppm	10	90	120	90	80	120	100	100	130	100	100	120	90
Cs	ppm	0.01	7.58	7.11	5.55	6.67	12.55	5.55	10.7	13.2	8.63	14.6	12.1	7.88
Dy	ppm	0.05	6.19	5.5	5.21	5.28	7.34	5.24	6.24	7.4	5.76	6.11	6.3	6.99
Er	ppm	0.03	3.34	3.25	3.15	3.13	4.39	3.05	3.63	4.35	3.71	3.3	3.75	4.07
Eu	ppm	0.02	1.49	1.67	1.27	1.26	1.92	1.3	1.39	1.9	1.51	1.35	1.56	1.65
Ga	ppm	0.1	26.1	34.4	26.5	23.8	39.5	28.9	31.1	40.7	27.6	29.2	38.5	29
Gd	ppm	0.05	5.74	6.36	6.26	5.52	8.25	5.75	5.77	8.1	6.66	5.57	6.81	7.63
Ge	ppm	5	<5	<5	<5	<5	<5	<5	<5	<5	<5	<5	<5	<5
Hf	ppm	0.1	4.2	4.9	4.3	4.1	4.7	4.5	5	4.9	5.1	6.3	5.1	5.1
Ho	ppm	0.01	1.09	0.97	0.97	0.96	1.45	0.9	1.08	1.41	1.05	1.12	1.17	1.25
La	ppm	0.1	35.6	44.6	39.4	33.6	52.6	38.1	40.2	54.8	40.7	38	48.8	44.6
Lu	ppm	0.01	0.42	0.47	0.4	0.37	0.54	0.39	0.46	0.52	0.43	0.44	0.48	0.55
Nb	ppm	0.1	12.6	18	13.4	13.6	14.7	13.9	14.8	17	15.4	17	17.9	12.7
Nd	ppm	0.1	30.9	38.3	35.8	29.3	46.2	33.6	36	49.1	35.4	34.6	42.4	41.1
Pr	ppm	0.02	8.32	10.05	9.1	7.81	12.2	8.98	9.58	12.65	9.24	8.8	11.2	10.65
Rb	ppm	0.2	156.5	162	133	142.5	231	161	196	258	169	211	243	157
Sm	ppm	0.03	7.05	8	7.17	6.07	9.74	6.16	7	10.15	7.22	6.59	8.91	8.37
Sn	ppm	1	3	3	3	3	3	3	4	3	3	4	3	
Sr	ppm	0.1	250	420	257	211	326	157	151	172.5	309	222	181.5	294
Ta	ppm	0.1	0.9	1.1	0.9	0.8	1	0.9	1.1	1.1	1	1.2	1.2	0.8
Tb	ppm	0.01	0.91	0.96	0.95	0.86	1.16	0.83	0.98	1.19	0.9	0.87	1.05	1.05
Th	ppm	0.05	9.27	12.25	8.89	8.49	13.25	9.99	11.5	14	10.9	11	13.9	11.3
Tm	ppm	0.01	0.46	0.45	0.39	0.43	0.55	0.39	0.43	0.59	0.45	0.48	0.49	0.52
U	ppm	0.05	2.07	2.57	1.92	1.85	2.69	2.31	2.52	2.75	2.51	2.49	2.84	2.38
V	ppm	5	109	161	116	107	152	130	129	169	119	114	158	119
W	ppm	1	7	11	8	15	10	13	9	16	9	9	13	7
Y	ppm	0.1	29.9	26.8	25.2	26.1	38.7	25.2	31.1	37.6	29.3	28.9	31.9	33.1
Yb	ppm	0.03	3.11	3.12	2.91	2.65	3.95	3.01	3.33	3.99	3.17	3.48	3.58	3.48
Zr	ppm	2	149	180	158	156	162	163	184	173	202	244	191	195
As	ppm	0.1	>250	199.5	58.6	117	>250	131	63.9	164	153	>250	53.6	42.3
Bi	ppm	0.01	0.07	0.07	0.04	0.21	0.53	0.12	0.63	0.19	0.08	0.04	0.1	0.09
Hg	ppm	0.005	<0.005	<0.005	<0.005	<0.005	<0.005	<0.005	0.006	0.005	<0.005	0.009	0.005	<0.005
In	ppm	0.005	0.045	0.018	0.039	0.03	0.019	0.015	0.028	0.021	0.027	0.017	0.02	0.027
Re	ppm	0.001	<0.001	<0.001	<0.001	<0.001	<0.001	<0.001	<0.001	<0.001	<0.001	<0.001	<0.001	<0.001
Sb	ppm	0.05	0.3	0.21	0.2	0.22	0.5	0.16	0.39	0.98	0.44	0.59	0.31	0.38
Se	ppm	0.2	<0.2	<0.2	<0.2	<0.2	<0.2	<0.2	<0.2	<0.2	<0.2	<0.2	<0.2	<0.2
Te	ppm	0.01	0.01	0.01	0.01	0.01	0.08	<0.01	0.08	0.02	0.01	<0.01	0.04	0.01
Tl	ppm	0.02	0.71	0.52	0.57	0.56	0.82	0.5	0.67	0.75	0.73	0.85	0.74	0.59
Ag	ppm	0.5	<0.5	<0.5	<0.5	<0.5	<0.5	<0.5	<0.5	<0.5	<0.5	<0.5	<0.5	<0.5
Cd	ppm	0.5	<0.5	<0.5	<0.5	<0.5	0.7	<0.5	<0.5	<0.5	<0.5	0.5	<0.5	<0.5
Co	ppm	1	21	14	20	21	35	23	32	29	25	26	24	22
Cu	ppm	1	35	18	4	23	74	19	101	58	14	74	57	32
Li	ppm	10	70	50	70	70	90	60	70	80	70	80	90	80
Mo	ppm	1	<1	<1	1	1	<1	<1	1	<1	<1	1	1	<1
Ni	ppm	1	48	32	44	44	73	40	58	75	44	62	60	54
Pb	ppm	2	30	53	18	42	46	39	36	24	43	21	193	62
Sc	ppm	1	16	20	16	16	22	17	18	22	17	18	22	17
Zn	ppm	2	119	78	80	88	144	107	106	99	91	161	171	148
C	wt. %	0.05	0.13	0.09	<0.05	<0.05	0.08	<0.05	<0.05	<0.05	<0.05	<0.05	<0.05	<0.05
CO ₂	wt. %	2	0.5	0.3	<0.2	<0.2	0.3	<0.2	<0.2	<0.2	<0.2	<0.2	<0.2	0.2
Au	ppm	0.001	0.002	0.003	0.005	0.068	0.084	0.042	0.084	0.05	0.003	0.003	0.011	<0.001

	L.O.D.	385174	385175	385177	385180	385188	385189	385211	385212	385213	385215	385218	385219	
SiO₂	wt. %	0.01	54.9	65.6	68.1	62.9	49.2	61	59.4	52.9	59.2	46.1	50.5	48.4
Al₂O₃	wt. %	0.01	21.7	16.65	13.35	17.15	22.1	17.85	19.6	21.7	19.15	27.3	23.8	22.9
Fe₂O₃	wt. %	0.01	7.63	5.55	5.31	7.05	9.79	6.31	7.72	7.92	6.89	9.08	8.55	7.99
CaO	wt. %	0.01	0.69	1.27	2.15	1.92	0.66	1.82	1.24	2.02	0.75	0.77	0.63	2.78
MgO	wt. %	0.01	2.81	2.14	1.93	2.91	2.91	2.65	3.15	3.23	2.5	3.15	3.42	3.27
Na₂O	wt. %	0.01	0.97	1.83	3.05	1.8	0.85	2.1	1.62	1.92	1.44	1.13	0.99	2.92
K₂O	wt. %	0.01	6.72	4.35	1.73	4.23	6.97	4.25	4.77	5.65	5.39	8.44	7.78	5.52
Cr₂O₃	wt. %	0.002	0.015	0.012	0.009	0.013	0.016	0.013	0.014	0.015	0.013	0.018	0.016	0.016
TiO₂	wt. %	0.01	0.85	0.73	0.54	0.72	0.83	0.78	0.81	0.91	0.76	1.1	0.89	1.05
MnO	wt. %	0.01	0.08	0.11	0.13	0.14	0.1	0.14	0.12	0.14	0.06	0.09	0.08	0.15
P₂O₅	wt. %	0.01	0.16	0.16	0.11	0.14	0.18	0.2	0.19	0.19	0.2	0.16	0.16	0.19
SrO	wt. %	0.01	0.01	0.02	0.04	0.02	0.01	0.03	0.02	0.03	0.01	0.01	0.01	0.04
BaO	wt. %	0.01	0.13	0.08	0.02	0.07	0.13	0.08	0.1	0.13	0.11	0.17	0.15	0.12
LOI	wt. %	0.01	2.63	1.57	1.86	1.5	5.98	1.7	2.51	2.2	2.22	3.32	3.96	4.3
Total	wt. %	0.01	99.3	100.07	98.33	100.56	99.73	98.92	101.26	98.96	98.69	100.84	100.94	99.65
C	wt. %	0.01	0.12	0.04	0.06	0.07	0.32	0.1	0.04	0.04	0.04	0.01	0.6	0.58
S	wt. %	0.01	0.1	0.11	0.58	0.29	1.75	0.23	0.01	0.07	0.06	0.48	0.69	0.93
Ba	ppm	0.5	1110	729	207	615	1155	714	925	1210	868	1585	1415	1170
Ce	ppm	0.1	77.5	65.7	51.5	66	74.6	76.2	69.1	73.3	61.1	103	92.1	93.5
Cr	ppm	10	100	80	60	80	100	90	100	120	80	130	120	120
Cs	ppm	0.01	10.05	8.57	4.81	7.6	10.2	7.51	8.36	12.85	6.61	12.1	10.45	8.41
Dy	ppm	0.05	5.15	4.83	3.44	4.16	5.22	5.12	6.04	5.88	4.8	6.54	6.39	7.29
Er	ppm	0.03	3.2	3.04	1.99	2.64	3.29	3.15	3.36	3.43	2.65	3.89	3.82	3.96
Eu	ppm	0.02	1.44	1.2	1.22	1.23	1.23	1.54	1.38	1.62	1.18	1.66	1.56	1.96
Ga	ppm	0.1	31.7	21.5	16.3	23.6	33.5	24	26.9	32.7	24.2	43.8	36.8	34.7
Gd	ppm	0.05	6.11	5.22	4.18	5.04	5.57	6.48	5.91	5.61	4.72	6.61	6.58	6.77
Ge	ppm	5	<5	<5	<5	<5	<5	<5	<5	<5	<5	<5	<5	<5
Hf	ppm	0.1	3.8	5.5	4.6	4.9	3.7	5.1	4.9	4.9	3.8	6.2	4.7	7.8
Ho	ppm	0.01	1.02	0.93	0.64	0.79	1	0.94	1.15	1.12	0.98	1.3	1.28	1.35
La	ppm	0.1	39.2	32	26.4	31.7	36.4	39.6	34.8	36.6	30.2	50.2	46.7	45.8
Lu	ppm	0.01	0.4	0.4	0.33	0.36	0.4	0.42	0.43	0.48	0.39	0.59	0.55	0.61
Nb	ppm	0.1	14.4	13	10.8	12.7	13.6	14.2	14.3	16.2	11.4	18.1	16.4	19.3
Nd	ppm	0.1	34.1	29.6	23.4	29.1	32.2	34.5	32.1	34.6	28.7	43.9	40.3	43.8
Pr	ppm	0.02	8.95	7.58	6.12	7.64	8.61	8.87	8.34	8.69	7.29	11.6	11.05	11.4
Rb	ppm	0.2	217	160	78.8	157.5	236	153	174.5	229	162.5	288	272	207
Sm	ppm	0.03	7.29	5.6	4.7	5.39	6.26	7.67	6.57	6.81	5.54	8.14	8.08	8.85
Sn	ppm	1	3	2	1	2	3	2	3	3	2	5	4	3
Sr	ppm	0.1	109	185.5	321	216	96.5	234	184.5	282	117.5	141	125.5	395
Ta	ppm	0.1	0.9	0.8	0.6	0.8	0.9	0.9	1	1.3	1	1.3	1.2	1.4
Tb	ppm	0.01	0.81	0.79	0.57	0.76	0.79	0.91	0.85	0.9	0.72	1.04	0.99	1.05
Th	ppm	0.05	10.95	10.2	6.3	9.38	11.25	8.68	10.75	10.8	8.83	14.8	12.85	13.25
Tm	ppm	0.01	0.4	0.39	0.27	0.35	0.44	0.41	0.49	0.47	0.4	0.59	0.56	0.56
U	ppm	0.05	2.74	2.35	1.48	1.92	2.27	1.89	2.22	2.55	1.8	2.73	2.72	3.02
V	ppm	5	133	89	62	98	141	99	114	142	103	166	157	149
W	ppm	1	16	12	3	6	11	18	11	11	14	18	13	8
Y	ppm	0.1	26	25.6	18.4	21.4	27.3	26.6	30.2	32.1	24.5	33.1	34.9	36.9
Yb	ppm	0.03	2.65	2.91	1.93	2.46	3.06	2.78	3.23	3.56	2.6	3.97	3.62	4.22
Zr	ppm	2	138	210	180	180	141	182	170	177	124	214	164	267
As	ppm	0.1	97.1	>250	>250	212	>250	>250	51.5	77.1	74.1	>250	>250	>250
Bi	ppm	0.01	0.14	0.12	0.56	0.06	1.5	0.13	0.25	0.13	0.21	0.11	0.62	0.36
Hg	ppm	0.005	<0.005	0.007	<0.005	<0.005	<0.005	<0.005	<0.005	<0.005	<0.005	<0.005	<0.005	<0.005
In	ppm	0.005	0.017	0.015	0.025	0.021	0.021	0.027	0.026	0.035	0.02	0.019	0.019	0.028
Re	ppm	0.001	0.001	<0.001	<0.001	<0.001	0.001	<0.001	0.001	0.001	0.001	<0.001	0.001	0.001
Sb	ppm	0.05	0.37	2.04	12.05	0.22	28.7	0.42	0.14	0.31	0.25	0.21	1.34	8.65
Se	ppm	0.2	<0.2	<0.2	<0.2	0.2	<0.2	<0.2	<0.2	<0.2	<0.2	<0.2	<0.2	<0.2
Te	ppm	0.01	0.01	0.01	0.08	<0.01	0.3	0.01	0.02	0.01	0.01	0.02	0.2	0.33
Tl	ppm	0.02	0.66	0.65	0.44	0.68	0.68	0.59	0.57	0.86	0.68	0.7	0.82	0.7
Ag	ppm	0.5	<0.5	<0.5	<0.5	<0.5	1.3	<0.5	<0.5	<0.5	<0.5	<0.5	<0.5	<0.5
Cd	ppm	0.5	<0.5	<0.5	<0.5	<0.5	<0.5	<0.5	<0.5	<0.5	<0.5	1	<0.5	<0.5
Co	ppm	1	27	15	17	19	25	22	24	24	23	28	25	19
Cu	ppm	1	48	14	14	43	43	53	36	18	37	100	44	3
Li	ppm	10	80	60	60	70	70	70	80	90	70	80	80	70
Mo	ppm	1	<1	1	1	1	1	<1	<1	<1	<1	<1	1	<1
Ni	ppm	1	55	39	39	42	60	52	53	59	54	63	52	47
Pb	ppm	2	23	30	96	22	85	26	19	41	18	10	43	50
Sc	ppm	1	19	13	10	15	20	16	17	18	17	23	20	20
Zn	ppm	2	109	58	67	80	129	112	98	101	89	127	135	110
C	wt. %	0.05	<0.05	<0.05	<0.05	<0.05	<0.05	<0.05	<0.05	<0.05	<0.05	<0.05	<0.05	<0.05
CO ₂	wt. %	2	<0.2	<0.2	<0.2	<0.2	<0.2	<0.2	<0.2	<0.2	<0.2	<0.2	<0.2	<0.2
Au	ppm	0.001	0.019	0.015	0.126	0.097	5.81	0.078	0.004	0.018	0.042	0.026	0.228	0.201

	L.O.D.	385221	385225	385227	385229	385232	385233	385235	385236	385238	385241	385243	385245	
SiO₂	wt. %	0.01	53.8	65.9	43.6	48.8	59.7	60	53.4	53	42.7	53.6	56.7	63.5
Al₂O₃	wt. %	0.01	23	16.85	27	25.9	19.3	18.45	21.5	21.2	25.7	19.75	19.9	16.05
Fe₂O₃	wt. %	0.01	6.09	6.28	8.94	7.1	6.23	6.34	7.31	7.94	8.35	7.98	8.96	6.39
CaO	wt. %	0.01	1.63	1.62	1.07	0.74	1.54	1.37	1.12	0.88	0.46	2.57	0.88	2.63
MgO	wt. %	0.01	2.87	2.59	3.65	2.78	2.6	2.58	3	2.85	3.09	3.39	3.33	2.56
Na₂O	wt. %	0.01	1.74	2.12	1.36	1.35	2.46	1.62	1.3	1.68	0.73	2.68	1.23	2.81
K₂O	wt. %	0.01	6.33	3.96	7.42	7.81	4.58	4.71	6.77	6.53	8.57	4.13	4.97	3.14
Cr₂O₃	wt. %	0.002	0.015	0.012	0.019	0.016	0.014	0.012	0.015	0.015	0.017	0.014	0.013	0.011
TiO₂	wt. %	0.01	1.01	0.74	1.17	1.03	0.83	0.77	0.86	0.88	0.96	0.85	0.81	0.75
MnO	wt. %	0.01	0.13	0.12	0.16	0.07	0.08	0.11	0.11	0.07	0.09	0.15	0.1	0.15
P₂O₅	wt. %	0.01	0.18	0.15	0.17	0.15	0.17	0.17	0.17	0.15	0.09	0.21	0.15	0.23
SrO	wt. %	0.01	0.03	0.02	0.02	0.01	0.02	0.02	0.02	0.02	<0.01	0.04	0.01	0.04
BaO	wt. %	0.01	0.15	0.09	0.22	0.17	0.1	0.1	0.14	0.12	0.21	0.08	0.1	0.07
LOI	wt. %	0.01	2.84	1.51	3.96	3.17	1.92	1.97	2.66	2.25	7.36	2.57	2.78	1.11
Total	wt. %	0.01	99.82	101.96	98.76	99.1	99.54	98.22	98.38	97.59	98.33	98.01	99.93	99.44
C	wt. %	0.01	0.13	0.05	0.11	0.03	0.05	0.06	0.23	0.07	1.46	0.14	0.02	0.06
S	wt. %	0.01	0.31	0.01	0.03	0.07	0.01	0.15	0.21	0.35	1.43	0.49	0.02	0.01
Ba	ppm	0.5	1365	820	1855	1595	909	950	1265	980	1935	715	981	638
Ce	ppm	0.1	80.1	76	92.4	84.1	83.4	71.5	91.7	76.3	78.1	83.4	66.7	77.1
Cr	ppm	10	110	90	130	120	100	100	110	100	120	100	100	90
Cs	ppm	0.01	9.12	7	10.25	10.75	6.72	6.66	9.71	8.13	11.25	8.02	7.94	6.37
Dy	ppm	0.05	5.01	4.68	5.93	6.67	5.37	4.45	7.28	5.64	5.71	5.92	5.57	5.47
Er	ppm	0.03	3.04	2.6	3.21	3.61	3.42	2.86	3.74	3.07	3.18	3.38	3.23	2.93
Eu	ppm	0.02	1.64	1.24	1.76	1.69	1.71	1.42	1.77	1.24	1.38	1.82	1.09	1.66
Ga	ppm	0.1	33.1	23.6	37.8	41.9	28.1	27.1	31.8	28.7	44	26.7	27.5	21
Gd	ppm	0.05	5.72	5.5	6.41	5.95	6	5.22	7.04	5.3	5.23	6.1	5.51	5.64
Ge	ppm	5	<5	<5	<5	<5	<5	<5	<5	<5	<5	<5	<5	<5
Hf	ppm	0.1	5.4	5	5.1	5.8	5.3	4.4	4.9	4.4	5	5.7	4.4	5.5
Ho	ppm	0.01	0.88	0.86	1.1	1.26	1	0.94	1.31	1.04	0.97	1.11	1.04	1.08
La	ppm	0.1	39.6	39.3	47.2	39.6	42	35.4	46.2	36.6	38.6	41.7	31.5	39.1
Lu	ppm	0.01	0.47	0.38	0.53	0.58	0.42	0.44	0.54	0.46	0.43	0.51	0.48	0.39
Nb	ppm	0.1	16.9	14	19.7	18.3	15.1	13.7	15.8	12.3	17.7	17.8	14.5	14.1
Nd	ppm	0.1	37	35.4	42.1	36.8	38	33.3	43.1	32.7	35	39.2	28.8	37.2
Pr	ppm	0.02	9.75	9.05	10.8	9.62	9.91	8.51	11.05	8.88	9.29	10.1	7.9	9.48
Rb	ppm	0.2	232	146	243	260	167	168	247	203	291	174.5	180	124.5
Sm	ppm	0.03	6.66	7.2	8.67	7.4	7.44	6.21	8.09	6.24	6.54	7.28	5.98	7.82
Sn	ppm	1	4	3	4	5	3	3	3	3	4	2	3	2
Sr	ppm	0.1	225	237	166.5	136.5	209	193	166.5	134	84.6	359	133.5	335
Ta	ppm	0.1	1.2	1.1	1.4	1.2	1.2	1.1	1.2	0.9	1.2	1.1	1.1	1.1
Tb	ppm	0.01	0.75	0.69	0.84	0.93	0.88	0.75	1.12	0.85	0.82	0.91	0.8	0.81
Th	ppm	0.05	11.9	8.67	14.05	13.8	10.35	9.89	11.75	11.25	13.5	10.9	11.05	9.43
Tm	ppm	0.01	0.46	0.38	0.55	0.53	0.46	0.4	0.52	0.4	0.47	0.49	0.42	0.41
U	ppm	0.05	2.73	1.94	2.99	2.74	2.25	2.18	2.57	1.97	2.88	2.45	2.01	2.19
V	ppm	5	153	106	161	169	120	123	138	114	169	121	114	98
W	ppm	1	13	8	12	18	11	11	10	9	13	13	11	7
Y	ppm	0.1	25.9	23.4	28.2	33.5	28.6	25.5	35.4	27.3	26.7	30.4	28	27.8
Yb	ppm	0.03	3.23	2.32	3.43	3.64	3.25	2.64	3.59	3.21	3.26	3.19	3.21	3
Zr	ppm	2	184	174	174	204	187	155	169	159	173	211	154	198
As	ppm	0.1	>250	75.9	168.5	97.7	57.2	51.8	>250	>250	>250	>250	63.4	57.8
Bi	ppm	0.01	0.16	0.15	0.24	0.05	0.02	0.1	0.12	0.06	1.76	0.12	0.06	0.05
Hg	ppm	0.005	<0.005	<0.005	<0.005	<0.005	0.005	<0.005	<0.005	<0.005	0.007	0.006	0.007	<0.005
In	ppm	0.005	0.016	0.029	0.027	0.017	0.023	0.024	0.014	0.016	0.024	0.027	0.024	0.036
Re	ppm	0.001	<0.001	0.001	0.001	<0.001	<0.001	<0.001	<0.001	0.001	<0.001	0.001	0.001	0.001
Sb	ppm	0.05	4.67	0.17	0.17	0.15	0.21	0.15	0.17	0.21	7.84	6.32	0.33	0.24
Se	ppm	0.2	<0.2	<0.2	<0.2	<0.2	<0.2	<0.2	0.2	0.2	0.4	<0.2	<0.2	<0.2
Te	ppm	0.01	0.04	0.01	0.01	0.01	<0.01	0.01	0.04	0.02	0.67	0.07	0.02	0.01
Tl	ppm	0.02	0.63	0.55	0.56	0.62	0.6	0.59	0.7	0.68	0.55	0.71	0.57	0.48
Ag	ppm	0.5	<0.5	<0.5	<0.5	<0.5	<0.5	<0.5	<0.5	<0.5	<0.5	<0.5	<0.5	<0.5
Cd	ppm	0.5	<0.5	<0.5	<0.5	<0.5	<0.5	<0.5	<0.5	<0.5	1.2	<0.5	<0.5	<0.5
Co	ppm	1	15	17	29	22	19	18	23	20	27	22	22	17
Cu	ppm	1	1	19	14	12	6	30	42	38	41	2	19	11
Li	ppm	10	70	70	100	70	50	50	70	70	80	90	80	60
Mo	ppm	1	<1	<1	<1	<1	<1	<1	1	<1	1	<1	<1	<1
Ni	ppm	1	38	42	65	44	44	45	48	48	62	49	55	43
Pb	ppm	2	13	17	28	25	11	19	26	15	27	21	22	14
Sc	ppm	1	19	14	23	21	17	17	20	19	21	16	17	12
Zn	ppm	2	94	92	198	107	80	93	114	107	129	102	125	73
C	wt. %	0.05	<0.05	<0.05	<0.05	<0.05	<0.05	<0.05	<0.05	<0.05	<0.05	0.05	<0.05	0.05
CO ₂	wt. %	2	<0.2	<0.2	<0.2	<0.2	<0.2	<0.2	<0.2	<0.2	<0.2	0.2	<0.2	0.2
Au	ppm	0.001	0.18	0.004	0.136	0.011	0.003	0.037	0.005	0.023	0.455	0.067	0.005	0.002

	L.O.D.	385249	385252	385254	385259	385262	385288	385289	385292	385294	385295	385296	385297	
SiO₂	wt. %	0.01	53.9	54.4	45.8	43.9	59.2	57.1	47.6	57.5	54.5	45.8	56.9	56.5
Al₂O₃	wt. %	0.01	20.1	21.6	29.8	27.5	19.35	21	21.9	19.8	21.9	27.4	21.6	21.3
Fe₂O₃	wt. %	0.01	7.16	6.94	5.9	8.77	6.41	6	9.92	7	8.87	7.89	6.92	6.49
CaO	wt. %	0.01	1.31	2.23	0.24	0.36	1.38	0.55	0.45	0.62	0.99	1.07	0.78	1.37
MgO	wt. %	0.01	2.73	3.04	2.46	3.64	2.68	2.55	3.2	2.72	2.89	3.18	2.63	2.53
Na₂O	wt. %	0.01	1.52	2.58	0.57	0.31	1.84	0.77	0.25	0.56	1.88	1.26	0.82	2.44
K₂O	wt. %	0.01	5.55	5.41	10.05	9.95	4.87	6.23	7.55	6.7	6.6	8.14	7.29	5.67
Cr₂O₃	wt. %	0.002	0.012	0.015	0.017	0.018	0.013	0.014	0.015	0.013	0.015	0.02	0.017	0.015
TiO₂	wt. %	0.01	0.77	0.82	1.03	1.11	0.79	0.85	0.86	0.81	1.09	1.23	0.94	0.87
MnO	wt. %	0.01	0.1	0.13	0.09	0.09	0.1	0.06	0.07	0.08	0.12	0.11	0.09	0.09
P₂O₅	wt. %	0.01	0.19	0.17	0.01	0.18	0.17	0.16	0.21	0.16	0.22	0.12	0.2	0.17
SrO	wt. %	0.01	0.02	0.04	<0.01	<0.01	0.02	0.01	<0.01	0.01	0.02	0.02	0.01	0.02
BaO	wt. %	0.01	0.12	0.11	0.24	0.21	0.11	0.13	0.15	0.12	0.13	0.21	0.16	0.13
LOI	wt. %	0.01	2.47	2.82	4.39	4.58	1.98	3.29	5.94	2.88	2.32	4.02	2.79	2.37
Total	wt. %	0.01	95.95	100.31	100.6	100.62	98.91	98.71	98.12	98.97	101.55	100.47	101.15	99.97
C	wt. %	0.01	0.07	0.47	0.23	0.54	0.09	0.03	0.27	0.22	0.05	0.05	0.07	0.09
S	wt. %	0.01	0.33	0.25	0.38	0.57	0.02	0.03	1.45	0.07	0.01	0.01	0.01	0.01
Ba	ppm	0.5	1050	1015	2230	1955	1035	1250	1325	1090	1205	1920	1385	1165
Ce	ppm	0.1	65	74.1	92.4	102	81.3	72.4	84.7	83.6	86	108	83.5	77.5
Cr	ppm	10	90	110	130	140	100	110	110	90	120	150	120	110
Cs	ppm	0.01	8.59	8.03	11.8	12.95	6.95	7.97	11.8	11.2	11.4	11.6	10.6	9.65
Dy	ppm	0.05	4.71	5.12	3.97	7.55	5.46	5.74	5.59	5.56	5.82	7.65	5.79	5.35
Er	ppm	0.03	2.42	3.14	2.4	4.27	3.11	3.51	3.28	3.01	3.46	3.98	3.17	3.1
Eu	ppm	0.02	1.18	1.5	1.34	1.7	1.5	1.32	1.48	1.37	1.8	1.9	1.48	1.55
Ga	ppm	0.1	26.4	28.9	51.4	49.3	31.4	34.9	35	29.9	32.7	41.6	33.1	30.3
Gd	ppm	0.05	4.85	5.7	5.31	7.26	5.42	5.61	5.9	5.67	6.4	7.52	5.88	5.7
Ge	ppm	5	<5	<5	<5	<5	<5	<5	<5	<5	<5	<5	<5	<5
Hf	ppm	0.1	4	5.4	5.4	5.9	4.6	4.3	4.3	4.1	7.6	7.2	4.9	4.5
Ho	ppm	0.01	0.89	0.91	0.72	1.5	1.06	1.14	1.1	1.04	1.19	1.41	1.11	1
La	ppm	0.1	31.9	35.8	45.4	51	40.6	35.5	42.4	41.1	43.1	54.6	40.5	38
Lu	ppm	0.01	0.38	0.48	0.39	0.61	0.43	0.5	0.47	0.44	0.53	0.74	0.53	0.48
Nb	ppm	0.1	12.7	16	15.5	20.8	15	15.1	15.1	17	19.8	21	16.2	15.2
Nd	ppm	0.1	30.6	33.9	41.5	45.8	36.6	32.2	38.4	37.3	39.9	48.5	37.6	35.1
Pr	ppm	0.02	7.65	8.38	10.55	12	9.52	8.58	9.73	9.72	10.4	12.65	9.76	9.29
Rb	ppm	0.2	188.5	191	308	354	181	223	266	232	251	260	240	208
Sm	ppm	0.03	5.69	6.65	7.43	8.99	6.97	6.28	7.21	7.12	8.07	8.75	7.23	6.66
Sn	ppm	1	3	3	5	5	3	3	3	3	3	5	4	3
Sr	ppm	0.1	194	360	67.4	46.9	196.5	90	62.3	86.5	201	231	110.5	215
Ta	ppm	0.1	1	1.1	1.1	1.3	1	1.1	1	0.9	1.5	1.6	1.2	1.1
Tb	ppm	0.01	0.77	0.77	0.63	1.19	0.91	0.89	0.88	0.9	0.96	1.13	0.95	0.88
Th	ppm	0.05	8.94	11.1	13.75	16.05	11.5	12.2	12.05	11.3	11.75	16.55	12.7	11.6
Tm	ppm	0.01	0.33	0.46	0.35	0.57	0.48	0.5	0.49	0.46	0.55	0.7	0.49	0.43
U	ppm	0.05	1.95	2.59	2.88	3.29	2.39	2.44	2.5	2.3	2.78	3.48	2.77	2.27
V	ppm	5	108	124	186	181	125	143	146	118	139	181	156	132
W	ppm	1	9	8	19	17	19	11	13	11	10	18	16	9
Y	ppm	0.1	23.7	26.2	19	37.5	28	30.5	28.2	28.2	31.6	38.5	29.4	28
Yb	ppm	0.03	2.63	3.02	2.69	4.25	3.47	3.33	3.29	3.06	3.78	4.71	3.86	2.97
Zr	ppm	2	131	188	181	220	173	170	150	148	271	258	163	150
As	ppm	0.1	>250	>250	>250	>250	164.5	168	>250	163	93.2	181.5	84.5	97.1
Bi	ppm	0.01	0.61	0.2	0.27	0.41	0.12	0.07	1.22	0.14	0.03	0.08	0.63	0.06
Hg	ppm	0.005	<0.005	0.007	<0.005	<0.005	<0.005	0.007	<0.005	<0.005	0.006	0.006	<0.005	<0.005
In	ppm	0.005	0.023	0.02	0.014	0.018	0.021	0.01	0.02	0.015	0.017	0.018	0.014	0.019
Re	ppm	0.001	0.001	0.001	0.001	<0.001	0.001	0.001	0.001	0.001	<0.001	<0.001	<0.001	<0.001
Sb	ppm	0.05	0.5	1.03	1.12	1.57	0.26	0.44	18.4	0.24	0.29	0.43	0.36	0.19
Se	ppm	0.2	<0.2	<0.2	<0.2	<0.2	<0.2	<0.2	0.2	<0.2	<0.2	<0.2	<0.2	<0.2
Te	ppm	0.01	0.02	0.18	0.08	0.15	<0.01	0.01	0.66	0.01	0.01	0.02	0.02	0.01
Tl	ppm	0.02	0.74	0.62	0.37	0.74	0.58	0.27	0.67	0.66	0.75	0.42	0.65	0.74
Ag	ppm	0.5	<0.5	<0.5	<0.5	<0.5	<0.5	<0.5	<0.5	<0.5	<0.5	<0.5	<0.5	<0.5
Cd	ppm	0.5	<0.5	<0.5	<0.5	<0.5	<0.5	0.7	0.7	<0.5	<0.5	<0.5	<0.5	<0.5
Co	ppm	1	16	19	20	24	20	20	28	19	24	23	20	17
Cu	ppm	1	51	2	25	35	11	12	64	41	23	47	40	36
Li	ppm	10	70	80	70	80	60	70	70	70	70	100	60	60
Mo	ppm	1	5	1	1	<1	<1	<1	2	<1	<1	<1	<1	<1
Ni	ppm	1	44	46	50	55	44	54	59	50	58	67	49	48
Pb	ppm	2	24	36	11	9	28	21	45	20	11	20	44	26
Sc	ppm	1	17	18	23	22	17	17	19	17	18	23	19	19
Zn	ppm	2	115	111	76	123	85	116	281	95	56	97	73	84
C	wt. %	0.05	<0.05	0.05	<0.05	<0.2	<0.2	<0.2	<0.2	<0.2	<0.2	<0.2	<0.2	0.2
CO ₂	wt. %	2	<0.2	0.2	<0.2	<0.05	<0.05	<0.05	<0.05	<0.05	<0.05	<0.05	<0.05	<0.05
Au	ppm	0.001	0.01	0.006	0.121	0.099	0.003	0.029	3.51	0.015	0.004	0.012	0.003	0.009

	L.O.D.	385299	385303	385305	385310	385315	385316	385318	385320	385321	385323	385324	385325	
SiO₂	wt. %	0.01	56.9	48	57.4	66.7	55.5	49.8	61.1	55.2	56.4	59	55.5	47.9
Al₂O₃	wt. %	0.01	21.1	25.4	21	15.55	23	22.2	19.7	20.1	20.1	19.95	20.3	27.3
Fe₂O₃	wt. %	0.01	7.4	8.43	6.36	6.2	4.95	8.34	4.3	6.96	7.02	6.65	8.24	5.09
CaO	wt. %	0.01	0.56	1.76	1.83	1.86	0.71	1.75	1.28	0.93	1.33	0.55	0.34	1.66
MgO	wt. %	0.01	2.7	3.35	2.78	2.5	2.09	3.18	1.79	2.6	3.02	2.45	3.21	2.5
Na₂O	wt. %	0.01	0.82	1.9	2.51	2.47	1.05	2.08	1.66	1.62	0.7	0.8	0.24	1.2
K₂O	wt. %	0.01	7.1	7.64	5.04	3.58	7.03	5.92	5.65	5.93	6.27	5.96	6.87	7.67
Cr₂O₃	wt. %	0.002	0.015	0.017	0.015	0.01	0.015	0.015	0.013	0.014	0.014	0.013	0.013	0.022
TiO₂	wt. %	0.01	0.86	1.1	0.85	0.68	0.93	0.93	0.83	0.82	0.92	0.79	0.81	1.36
MnO	wt. %	0.01	0.07	0.14	0.11	0.11	0.07	0.14	0.07	0.09	0.13	0.06	0.09	0.19
P₂O₅	wt. %	0.01	0.17	0.18	0.19	0.15	0.16	0.21	0.17	0.19	0.17	0.18	0.14	0.03
SrO	wt. %	0.01	0.01	0.03	0.03	0.03	0.01	0.03	0.02	0.01	0.01	0.01	<0.01	0.03
BaO	wt. %	0.01	0.15	0.17	0.12	0.07	0.18	0.13	0.13	0.12	0.13	0.12	0.12	0.19
LOI	wt. %	0.01	2.67	2.74	2.52	1.37	2.89	2.57	2.1	2.76	3.44	3.28	3.62	4.65
Total	wt. %	0.01	100.53	100.86	100.76	101.28	98.59	97.3	98.81	97.34	99.65	99.81	99.49	99.79
C	wt. %	0.01	0.04	0.11	0.11	0.19	0.05	0.23	0.03	0.07	0.22	0.1	0.03	0.61
S	wt. %	0.01	0.02	0.05	0.01	0.17	0.07	0.43	<0.01	0.01	0.15	0.28	0.75	0.41
Ba	ppm	0.5	1370	1470	1120	639	1365	1085	1225	1045	1245	1150	1100	1850
Ce	ppm	0.1	84.1	102.5	78.1	58.3	63	91.6	72.4	72.9	91.3	92.7	69.7	125.5
Cr	ppm	10	110	130	110	80	100	110	100	100	110	100	100	170
Cs	ppm	0.01	13.8	13.55	7.15	8.44	7.57	10.7	7.13	9.89	11.6	8.39	12.8	10.4
Dy	ppm	0.05	4.74	6.74	5.86	4.18	3.79	6.51	4.45	4.87	6.31	5.65	4.27	5.21
Er	ppm	0.03	3.08	3.54	3.45	2.38	2.17	3.62	2.65	2.76	3.29	2.85	2.37	2.89
Eu	ppm	0.02	1.46	2.04	1.56	1.18	1.06	1.62	1.35	1.45	1.67	1.68	1.28	1.98
Ga	ppm	0.1	31	38.6	30.2	20	30.7	30.4	28.6	29.9	29.9	30.4	30	42.5
Gd	ppm	0.05	5.35	7.14	5.56	4.73	3.68	6.51	4.97	5.64	6.8	6.54	4.7	6.86
Ge	ppm	5	<5	<5	<5	<5	<5	<5	<5	<5	<5	<5	<5	<5
Hf	ppm	0.1	4.7	7.1	4.4	4.9	4.2	5.7	4.5	4.5	4.8	3.9	4.7	6.5
Ho	ppm	0.01	0.91	1.19	1.1	0.76	0.66	1.18	0.87	0.95	1.09	1.02	0.77	1.03
La	ppm	0.1	42	51.5	38.7	29.5	30.8	46.4	36.3	36.2	46.7	47.3	34.2	64.2
Lu	ppm	0.01	0.45	0.59	0.54	0.35	0.42	0.52	0.43	0.49	0.48	0.42	0.42	0.57
Nb	ppm	0.1	14.3	18.8	14.6	13.5	14.2	16.6	14.7	14.2	15.9	14.1	13.6	25.1
Nd	ppm	0.1	37.2	46.9	35.3	27.8	27.4	41.3	31.9	32.7	42.9	42.1	30.1	53.9
Pr	ppm	0.02	10.1	12.3	9.21	7.14	7.22	11.1	8.49	8.71	11.05	10.85	8.02	14.55
Rb	ppm	0.2	240	280	168	153.5	192.5	224	181	207	230	207	259	276
Sm	ppm	0.03	6.71	8.8	6.32	5.23	4.9	7.65	6.23	6.86	8.49	8.03	5.86	9.84
Sn	ppm	1	3	4	3	2	3	3	3	3	3	3	3	4
Sr	ppm	0.1	95.8	259	283	287	119	298	199	135.5	144.5	88.8	69.2	339
Ta	ppm	0.1	1.1	1.5	1.1	0.9	1.1	1.1	1.1	1	1.2	1.1	1.1	1.9
Tb	ppm	0.01	0.77	1.06	0.88	0.65	0.64	1.02	0.75	0.78	0.95	0.94	0.74	0.95
Th	ppm	0.05	11.5	14.2	11.95	7.36	11.05	12.1	9.55	10.55	11.95	11.35	11.5	18.9
Tm	ppm	0.01	0.41	0.54	0.49	0.34	0.34	0.51	0.38	0.43	0.44	0.41	0.42	0.5
U	ppm	0.05	2.21	3.16	2.53	1.65	2.2	2.73	2.31	2.37	2.46	2.34	1.86	3.8
V	ppm	5	134	163	142	82	129	136	133	132	131	133	116	192
W	ppm	1	11	11	10	5	13	8	10	11	10	580	13	13
Y	ppm	0.1	25.8	34.4	31.5	21.9	18.6	32.4	23	27.4	31.7	27.6	21.6	25.9
Yb	ppm	0.03	3.08	3.68	3.5	2.61	2.49	3.38	2.73	3.04	3.22	2.57	2.68	3.49
Zr	ppm	2	156	239	156	176	148	193	158	162	171	142	163	238
As	ppm	0.1	216	154.5	43.1	61.6	55.2	>250	58	87.8	>250	>250	>250	>250
Bi	ppm	0.01	0.05	0.04	0.19	0.09	0.06	0.33	0.04	0.25	0.16	0.94	0.13	0.44
Hg	ppm	0.005	<0.005	<0.005	<0.005	<0.005	<0.005	<0.005	<0.005	<0.005	<0.005	<0.005	<0.005	<0.005
In	ppm	0.005	0.013	0.024	0.02	0.023	0.01	0.022	0.01	0.018	0.022	0.079	0.015	0.016
Re	ppm	0.001	0.001	0.001	<0.001	0.001	<0.001	0.001	0.001	<0.001	0.001	0.003	<0.001	<0.001
Sb	ppm	0.05	0.28	0.27	0.15	0.08	0.07	0.46	0.42	0.28	0.9	0.81	1.62	5.61
Se	ppm	0.2	<0.2	<0.2	<0.2	<0.2	<0.2	<0.2	<0.2	<0.2	<0.2	<0.2	<0.2	<0.2
Te	ppm	0.01	0.01	0.01	0.02	0.03	0.01	0.11	<0.01	0.01	0.08	0.02	0.06	0.19
Tl	ppm	0.02	0.75	0.92	0.44	0.73	0.44	0.86	0.39	0.69	0.66	0.59	0.7	0.18
Ag	ppm	0.5	<0.5	<0.5	<0.5	<0.5	<0.5	<0.5	<0.5	<0.5	<0.5	<0.5	<0.5	<0.5
Cd	ppm	0.5	<0.5	<0.5	<0.5	<0.5	<0.5	<0.5	<0.5	<0.5	<0.5	1.7	<0.5	<0.5
Co	ppm	1	20	27	17	15	11	24	19	20	19	22	17	41
Cu	ppm	1	36	19	15	23	32	52	2	15	24	68	102	1
Li	ppm	10	70	90	70	60	60	80	50	70	70	60	80	70
Mo	ppm	1	<1	<1	<1	1	<1	<1	<1	1	<1	<1	<1	1
Ni	ppm	1	59	62	44	38	37	56	41	53	50	55	53	73
Pb	ppm	2	10	53	28	18	14	30	12	45	49	188	19	47
Sc	ppm	1	18	21	17	12	19	20	17	18	19	18	19	22
Zn	ppm	2	107	83	116	64	82	111	38	146	103	1145	124	105
C	wt. %	0.05	<0.2	<0.2	0.2	<0.2	<0.2	<0.2	<0.2	<0.2	0.4	<0.2	<0.2	<0.05
CO ₂	wt. %	2	<0.05	<0.05	0.05	<0.05	<0.05	<0.05	<0.05	<0.05	0.11	<0.05	<0.05	<0.2
Au	ppm	0.001	0.007	0.003	0.026	0.002	0.004	0.004	0.002	0.003	0.462	0.195	3.25	0.09

	L.O.D.	385330	385331	385335	385339	385351	385353	385355	385357	385359	385362	385364	385368	
SiO₂	wt. %	0.01	46.1	57.2	57.7	56.7	43.9	53.7	44.2	53.4	56.3	59.2	54.5	63.5
Al₂O₃	wt. %	0.01	26.2	19.35	21.5	20.6	25.7	21.4	28.6	22	20.1	21	22.4	17.85
Fe₂O₃	wt. %	0.01	7.22	8.72	6.03	8.31	7.57	6.6	5.98	7.02	7.36	5.72	7.75	6.14
CaO	wt. %	0.01	1.6	0.36	0.65	0.61	1.34	1.41	0.45	1.13	0.76	0.64	1.15	1.53
MgO	wt. %	0.01	3.17	3.23	2.43	3.18	2.44	2.77	2.93	2.92	3.12	2.24	3.39	2.44
Na₂O	wt. %	0.01	1.28	1.99	1.08	0.87	1.13	2.35	0.35	1.94	1.15	0.94	1.3	2.21
K₂O	wt. %	0.01	8.15	5.06	6.61	6.37	7.89	6.06	9.65	6.17	6.07	6.49	6.41	4.21
Cr₂O₃	wt. %	0.002	0.018	0.013	0.014	0.015	0.021	0.014	0.019	0.016	0.013	0.014	0.015	0.011
TiO₂	wt. %	0.01	1.14	0.81	0.84	0.86	1.46	0.87	1.15	0.98	0.8	0.84	0.91	0.73
MnO	wt. %	0.01	0.13	0.11	0.09	0.1	0.09	0.1	0.1	0.12	0.09	0.06	0.13	0.1
P₂O₅	wt. %	0.01	0.15	0.14	0.14	0.17	0.06	0.2	0.17	0.14	0.17	0.19	0.18	0.17
SrO	wt. %	0.01	0.03	0.01	0.01	0.01	0.02	0.03	<0.01	0.02	0.01	0.01	0.01	0.02
BaO	wt. %	0.01	0.18	0.11	0.16	0.13	0.17	0.13	0.22	0.13	0.11	0.13	0.13	0.1
LOI	wt. %	0.01	3.51	2.6	2.69	2.53	8.11	3.28	4.35	2.5	2.71	2.6	2.84	1.57
Total	wt. %	0.01	98.88	99.7	99.94	100.46	99.9	98.91	98.17	98.49	98.76	100.07	101.12	100.58
C	wt. %	0.01	0.26	0.03	0.1	0.06	0.58	0.75	0.31	0.07	0.22	0.07	0.12	0.06
S	wt. %	0.01	0.23	0.11	0.08	0.04	1.94	0.57	0.31	0.46	0.11	0.03	0.16	0.01
Ba	ppm	0.5	1635	1010	1505	1320	1560	1200	2060	1255	1105	1145	1305	926
Ce	ppm	0.1	109	74.9	78.4	91.9	142	73.1	92.4	105.5	86.7	79.7	95.4	79.7
Cr	ppm	10	130	100	100	110	160	110	140	120	110	100	120	90
Cs	ppm	0.01	13.9	9.28	10.15	11.25	9.11	8.17	10.7	8.11	11.25	8.09	11.55	7.4
Dy	ppm	0.05	6.45	5.01	4.64	5.94	8.28	5.72	5.11	6.36	5.82	4.93	6.15	5.21
Er	ppm	0.03	3.57	2.86	2.75	3.34	4.97	4.02	3.47	3.81	3.4	2.84	3.4	3.11
Eu	ppm	0.02	1.9	1.34	1.24	1.55	2.4	1.5	1.56	1.79	1.58	1.38	1.8	1.45
Ga	ppm	0.1	40.7	30.4	33.3	33.5	44.4	33.3	47.9	35.9	33.1	31.2	35.6	26.6
Gd	ppm	0.05	6.8	5.3	5.24	6.08	8.77	5.25	5.58	6.49	6.24	4.6	6.6	5.95
Ge	ppm	5	<5	<5	<5	<5	<5	<5	<5	<5	<5	<5	<5	<5
Hf	ppm	0.1	6.3	4.2	3.9	4.1	10.8	5.1	5.5	6.3	4.4	3.8	4.7	3.8
Ho	ppm	0.01	1.33	0.96	0.94	1.1	1.63	1.23	1.13	1.24	1.13	0.94	1.21	1.03
La	ppm	0.1	54.4	37.7	37.7	46.7	72.2	36	46	50.2	43.2	38.5	50	39.8
Lu	ppm	0.01	0.57	0.42	0.4	0.46	0.72	0.59	0.62	0.54	0.46	0.4	0.54	0.39
Nb	ppm	0.1	20.4	14.1	14.6	16.2	32	15.8	19.9	17.9	14.6	13.7	16.2	13.4
Nd	ppm	0.1	48.1	33	34.1	41.3	63.1	32.1	40	44.5	38.8	34.7	41.5	35.7
Pr	ppm	0.02	12.9	8.46	8.95	10.65	16.45	8.38	10.75	12.15	10.3	9.35	10.85	9.08
Rb	ppm	0.2	287	197	217	249	272	220	310	214	229	197.5	246	178.5
Sm	ppm	0.03	9.05	6.04	6.82	7.88	11.95	5.86	7.56	8.71	7.67	6.38	8.45	6.8
Sn	ppm	1	4	3	4	4	4	3	5	4	3	3	4	3
Sr	ppm	0.1	238	96.3	129	114	236	266	66.8	191	125	102	178	222
Ta	ppm	0.1	1.3	1	1	1.1	1.9	1.1	1.3	1.2	1	0.9	1.2	0.9
Tb	ppm	0.01	1.12	0.86	0.7	0.94	1.29	0.93	0.9	0.96	0.89	0.77	0.97	0.91
Th	ppm	0.05	14.85	11.35	11.6	12.75	17.85	11.95	15.9	14.7	11.5	10.85	12.9	10.5
Tm	ppm	0.01	0.58	0.44	0.37	0.5	0.76	0.61	0.47	0.55	0.48	0.45	0.51	0.39
U	ppm	0.05	3.13	2.14	2.32	2.56	3.96	2.73	3.25	2.82	2.44	2.36	2.93	2.16
V	ppm	5	166	111	136	137	179	135	195	142	131	128	153	119
W	ppm	1	14	12	12	12	17	10	20	11	13	19	13	12
Y	ppm	0.1	33.3	26.1	23.8	30.9	45.9	34.2	27.4	34.5	31.4	25.8	32.4	25.3
Yb	ppm	0.03	3.63	2.74	2.59	3.43	4.76	3.82	3.49	3.84	3.05	2.57	3.32	2.91
Zr	ppm	2	240	156	143	153	410	195	199	245	154	141	175	144
As	ppm	0.1	>250	50.1	145.5	66.7	>250	>250	>250	>250	198.5	76.5	>250	69.7
Bi	ppm	0.01	0.1	0.05	0.23	0.15	0.57	0.39	0.19	0.07	0.06	0.26	0.19	0.15
Hg	ppm	0.005	<0.005	0.005	<0.005	<0.005	<0.005	<0.005	0.005	<0.005	<0.005	<0.005	<0.005	0.006
In	ppm	0.005	0.014	0.245	0.015	0.02	0.017	0.014	0.011	0.017	0.022	0.011	0.029	0.028
Re	ppm	0.001	0.001	<0.001	0.001	<0.001	<0.001	<0.001	<0.001	<0.001	<0.001	0.001	<0.001	0.001
Sb	ppm	0.05	0.47	0.56	0.16	0.24	30.9	1.5	2.72	0.26	0.22	0.3	1.82	0.14
Se	ppm	0.2	<0.2	<0.2	<0.2	<0.2	0.2	<0.2	<0.2	<0.2	<0.2	<0.2	<0.2	<0.2
Te	ppm	0.01	0.05	<0.01	0.06	0.02	0.33	0.22	0.05	0.03	0.01	0.01	0.01	0.02
Tl	ppm	0.02	0.69	0.61	0.53	0.8	0.21	0.53	0.39	0.49	0.7	0.54	0.72	0.69
Ag	ppm	0.5	<0.5	0.5	<0.5	<0.5	<0.5	1	<0.5	<0.5	<0.5	<0.5	<0.5	<0.5
Cd	ppm	0.5	<0.5	3.6	<0.5	<0.5	<0.5	<0.5	0.6	<0.5	<0.5	<0.5	<0.5	<0.5
Co	ppm	1	21	19	24	24	33	21	22	22	20	19	21	17
Cu	ppm	1	33	44	22	25	<1	41	16	56	33	11	65	30
Li	ppm	10	90	80	60	80	80	70	100	70	80	70	90	70
Mo	ppm	1	<1	<1	<1	<1	1	<1	<1	<1	<1	<1	<1	<1
Ni	ppm	1	60	50	49	54	59	53	44	44	47	41	53	42
Pb	ppm	2	23	197	20	12	54	98	172	27	26	47	26	41
Sc	ppm	1	20	17	18	18	22	18	23	19	18	18	20	15
Zn	ppm	2	125	1750	89	118	50	120	542	130	106	110	107	74
C	wt. %	0.05	<0.05	<0.05	<0.05	<0.05	<0.05	<0.05	<0.05	<0.05	<0.05	<0.05	<0.05	<0.05
CO ₂	wt. %	2	<0.2	<0.2	<0.2	<0.2	<0.2	<0.2	<0.2	<0.2	<0.2	<0.2	<0.2	<0.2
Au	ppm	0.001	0.059	0.004	0.002	0.006	0.218	1.685	0.428	0.047	0.042	0.059	0.032	0.057

	L.O.D.	385370	385373	385375	385376
SiO₂ wt. %	0.01	57.5	56.2	51.8	47.6
Al₂O₃ wt. %	0.01	19.7	20	22.4	26.6
Fe₂O₃ wt. %	0.01	8.14	8.24	7.43	4.7
CaO wt. %	0.01	0.37	0.5	1.59	1.18
MgO wt. %	0.01	3.03	2.98	3.2	2.82
Na₂O wt. %	0.01	0.76	0.89	2.61	1.73
K₂O wt. %	0.01	5.37	5.61	6.57	8
Cr₂O₃ wt. %	0.002	0.013	0.013	0.014	0.02
TiO₂ wt. %	0.01	0.77	0.75	0.97	1.17
MnO wt. %	0.01	0.07	0.06	0.17	0.11
P₂O₅ wt. %	0.01	0.14	0.16	0.18	0.02
SrO wt. %	0.01	<0.01	0.01	0.03	0.03
BaO wt. %	0.01	0.11	0.12	0.12	0.16
LOI wt. %	0.01	2.87	2.81	3.66	4.02
Total wt. %	0.01	98.84	98.34	100.74	98.16
C wt. %	0.01	0.02	0.08	0.36	0.85
S wt. %	0.01	0.12	0.18	0.69	0.19
Ba ppm	0.5	1080	1075	1140	1530
Ce ppm	0.1	65.3	84.5	117.5	127
Cr ppm	10	100	100	110	160
Cs ppm	0.01	6.61	7.59	10.65	10.3
Dy ppm	0.05	4.21	5.06	7.16	6.22
Er ppm	0.03	2.58	2.92	3.86	3.88
Eu ppm	0.02	1.14	1.36	2.03	2.38
Ga ppm	0.1	31.3	32.1	36	45.5
Gd ppm	0.05	4.99	5.51	8.54	6.51
Ge ppm	5	<5	<5	<5	<5
Hf ppm	0.1	3.7	3.8	6.3	5.9
Ho ppm	0.01	0.86	0.98	1.27	1.21
La ppm	0.1	32.1	42.2	60.3	63.7
Lu ppm	0.01	0.42	0.43	0.54	0.65
Nb ppm	0.1	14.4	13.5	17.8	25.6
Nd ppm	0.1	28	36.7	53.3	52.4
Pr ppm	0.02	7.55	9.83	13.65	14.5
Rb ppm	0.2	186	198	258	296
Sm ppm	0.03	5.13	7.22	10.15	9.91
Sn ppm	1	3	3	3	5
Sr ppm	0.1	65.4	87.1	277	281
Ta ppm	0.1	0.9	0.9	1.2	1.8
Tb ppm	0.01	0.7	0.81	1.25	1.02
Th ppm	0.05	11.05	11.35	12.45	17.4
Tm ppm	0.01	0.43	0.42	0.57	0.65
U ppm	0.05	1.99	2.24	2.91	3.75
V ppm	5	120	126	141	184
W ppm	1	18	9	10	14
Y ppm	0.1	22.7	25.5	37.3	32.9
Yb ppm	0.03	2.58	2.87	3.8	4.35
Zr ppm	2	134	140	239	227
As ppm	0.1	53	33.3	>250	>250
Bi ppm	0.01	0.19	0.16	0.36	0.27
Hg ppm	0.005	<0.005	<0.005	0.006	<0.005
In ppm	0.005	0.019	0.018	0.026	0.013
Re ppm	0.001	0.001	0.001	0.001	0.001
Sb ppm	0.05	0.16	0.23	5.26	2.32
Se ppm	0.2	<0.2	<0.2	<0.2	<0.2
Te ppm	0.01	0.01	0.01	0.27	0.13
Tl ppm	0.02	0.52	0.54	0.58	0.36
Ag ppm	0.5	<0.5	<0.5	<0.5	<0.5
Cd ppm	0.5	<0.5	<0.5	<0.5	<0.5
Co ppm	1	19	24	24	33
Cu ppm	1	34	58	15	<1
Li ppm	10	80	70	90	90
Mo ppm	1	<1	<1	<1	<1
Ni ppm	1	50	50	59	37
Pb ppm	2	27	26	27	18
Sc ppm	1	18	17	17	22
Zn ppm	2	140	135	86	101
C wt. %	0.05	<0.05	<0.05	0.07	<0.05
CO ₂ wt. %	2	<0.2	<0.2	0.3	<0.2
Au ppm	0.001	0.078	0.039	0.476	0.068

Appendix C: Mass Change Results

Table C1: Mass balance calculation results

Drillhole Depth Belt	Units m	385004	385006	385008	385010	385012
		BR-18-23	BR-18-23	BR-18-23	BR-18-23	BR-18-23
		57.42	70.26	87.3	105.87	125.26
		East Goldbrook				
SiO ₂	%	-9.1	30.2	-6.4	-0.2	26.3
Al ₂ O ₃	%	0	0	0	0	0
Fe ₂ O ₃	%	2.2	3	2.8	0.1	3.1
CaO	%	-0.4	0.6	-0.5	0.5	0.7
MgO	%	0.2	1	0.4	-0.1	0.9
Na ₂ O	%	-0.5	1.1	-0.7	0.2	0.5
K ₂ O	%	1	-0.7	0.9	-0.1	0.3
Cr ₂ O ₃	%	0	0	0	0	0
TiO ₂	%	0.1	0.1	0	0	0.1
MnO	%	0	0.1	0	0	0
P ₂ O ₅	%	-0.1	0	-0.1	0	0
SrO	%	0	0	0	0	0
BaO	%	0	0	0	0	0
LOI	%	0.1	-0.3	0.2	-0.1	-0.3
Total	%	-6.6	34.9	-3.3	0.3	31.6
C	%	0	0	0	0.1	0
S	%	-0.3	-0.5	-0.4	-0.5	-0.5
Ba	ppm	-161.4	-336.8	-164.8	-94.3	-298.7
Ce	ppm	-12.3	10.9	-3.1	-9.3	0.1
Cr	ppm	3.2	24.7	7.1	0.1	8.7
Cs	ppm	2.6	1	3.2	0.7	3.3
Dy	ppm	-0.9	1.6	-1	-1.1	0.9
Er	ppm	-0.4	0.9	-0.4	-0.5	0.6
Eu	ppm	-0.2	0.5	0	-0.1	0.4
Ga	ppm	0.6	-1.4	1.2	0.4	-0.9
Gd	ppm	-1.6	1.4	-0.8	-1.2	0.3
Ge	ppm	-0.3	1.7	-0.1	0	1.6
Hf	ppm	0.5	2.1	0	-0.2	2.9
Ho	ppm	-0.1	0.4	-0.2	-0.2	0.2
La	ppm	-8.5	4.8	-1.9	-6.3	-1.2
Lu	ppm	0	0.2	0	0	0.1
Nb	ppm	-1.3	0.2	-1.6	-1.5	1
Nd	ppm	-8	4.1	-4.4	-5.3	-1.3
Pr	ppm	-1.9	1.1	-0.6	-1.2	0
Rb	ppm	37.4	1.5	39.8	1.1	42.6
Sm	ppm	-2.1	0.5	-1.1	-1.1	-0.7
Sn	ppm	-0.2	-0.3	-0.1	0	-0.4
Sr	ppm	-24.8	84.1	-53.7	76.1	84.5
Ta	ppm	-0.1	0.1	0	0	0.1
Tb	ppm	-0.2	0.2	-0.1	-0.1	0.1
Th	ppm	0.7	0.7	0.1	-0.1	0.7
Tm	ppm	0	0.2	0	-0.1	0.1
U	ppm	0.1	0.3	-0.1	0.1	0.5
V	ppm	-8.1	-3	34	5.1	-3
W	ppm	1.2	3.2	-1.3	-3	-3.8
Y	ppm	-3.8	9.6	-4.3	-6.4	5.7
Yb	ppm	-0.1	1.2	-0.2	-0.1	1
Zr	ppm	9.6	75.5	9.7	-6.9	104.8
As	ppm	-14.2	-99.8	-6.1	-132.9	-93.7
Bi	ppm	-0.2	-0.2	-0.3	-0.3	0
Hg	ppm	0	0	0	0	0
In	ppm	0	0	0	0	0
Re	ppm	0	0	0	0	0
Sb	ppm	-0.4	-0.8	-1.1	-0.8	-1.1
Se	ppm	0	0.1	0	0	0.1
Te	ppm	0	0	0	0	0
Tl	ppm	0.1	0.2	0.2	0	0.3
Ag	ppm	0	0.2	0	0	0.2
Cd	ppm	0.9	0.2	0	0	0.2
Co	ppm	7.6	9.6	9.4	8	7.7
Cu	ppm	2.3	-12.8	-21	-14	-19.1
Li	ppm	4.9	14.3	7.8	-10	25.5
Mo	ppm	-0.1	0.3	0	0	0.3
Ni	ppm	21.1	20.3	17.5	10	16.4
Pb	ppm	-1.2	13	-6.4	10	8.3
Sc	ppm	-3	1.2	-0.5	-1	-0.5
Zn	ppm	25.3	-0.1	-22.4	-45	-15.8
C	%	0	0	0	0	0
CO ₂	%	0	0.1	0	0	0.1
Au	ppm	-1	-1	-0.9	-1	-1

Table C1: Mass balance calculation results

Drillhole Depth Belt	Units	385015	385022	385024	385025
		BR-18-23	BR-18-23	BR-18-23	BR-18-23
		m	151.39	269.45	311.33
East Goldbrook	Boston Richardson	Boston Richardson	Boston Richardson	Boston Richardson	
SiO ₂	%	0.8	113.1	-15.8	-3
Al ₂ O ₃	%	0	0	0	0
Fe ₂ O ₃	%	-0.4	1.6	1	4.6
CaO	%	-0.5	0.7	0	-0.5
MgO	%	-0.5	-0.8	-0.2	0.6
Na ₂ O	%	-0.4	4.2	0	-0.8
K ₂ O	%	0.9	-2.2	0.4	1.2
Cr ₂ O ₃	%	0	0	0	0
TiO ₂	%	0	0.1	0.1	0
MnO	%	0	0	0	0
P ₂ O ₅	%	0	0.1	0	0
SrO	%	0	0	0	0
BaO	%	0	-0.1	0	0
LOI	%	-0.1	1.5	2	2.3
Total	%	-0.2	118.1	-12.4	4.3
C	%	0	0.1	0.3	0
S	%	-0.5	1	0.5	1
Ba	ppm	7.2	-574.1	-110.1	-272.3
Ce	ppm	-12.5	-0.1	-15.4	-8.5
Cr	ppm	0.6	19	2.3	3.4
Cs	ppm	1.5	-4.3	-0.4	1.6
Dy	ppm	-1.4	0.2	-0.8	-0.8
Er	ppm	-0.5	0.7	-0.2	-0.2
Eu	ppm	-0.4	0.3	-0.1	-0.1
Ga	ppm	1.3	-7.2	-0.2	-1
Gd	ppm	-1.8	0.4	-1.5	-1
Ge	ppm	0	5.7	-0.7	0.2
Hf	ppm	0	7.2	0.8	-0.3
Ho	ppm	-0.2	0	-0.1	-0.1
La	ppm	-7.2	-1.5	-8.9	-5.9
Lu	ppm	0	0.1	0	0
Nb	ppm	-1.9	1	-2.5	-3.6
Nd	ppm	-6.9	-0.3	-8.2	-4.1
Pr	ppm	-1.4	0	-1.8	-1
Rb	ppm	25.2	-58.3	11.7	35.3
Sm	ppm	-2.1	-0.7	-1.8	-1.3
Sn	ppm	0	-0.9	0.5	0.1
Sr	ppm	-41.4	164.7	46.5	-68.6
Ta	ppm	0	0.3	0	-0.2
Tb	ppm	-0.1	0	-0.1	-0.1
Th	ppm	-0.4	-0.3	-0.5	0.1
Tm	ppm	0	0.1	0	0
U	ppm	0	0.5	0.2	-0.2
V	ppm	7.7	-13.1	9.5	2.9
W	ppm	4.1	2	-2.6	-2.7
Y	ppm	-5.6	3.4	-2.6	-3.3
Yb	ppm	-0.3	0.7	0.1	0
Zr	ppm	-0.1	260.4	21	-15.5
As	ppm	-149.6	287.4	-34	7.8
Bi	ppm	-0.3	1.5	0.2	0.2
Hg	ppm	0	0	0	0
In	ppm	0	0	0	0
Re	ppm	0	0	0	0
Sb	ppm	-0.8	56.8	16.9	19.2
Se	ppm	0	0.9	0.1	0.1
Te	ppm	0	1.3	0.1	0.1
Tl	ppm	0	-0.4	-0.1	0.1
Ag	ppm	0	0.6	-0.1	0
Cd	ppm	0.2	0.6	-0.1	0
Co	ppm	8.1	3.3	7.3	10.8
Cu	ppm	0.3	-45	-47.9	66.9
Li	ppm	-9.6	-15.5	-10.9	12.8
Mo	ppm	0	1.1	-0.1	0
Ni	ppm	10.3	0	10.6	24
Pb	ppm	-4.9	83.3	1.3	4.8
Sc	ppm	-0.9	-4	-2.6	0.6
Zn	ppm	119.3	-51.2	-32.7	34.7
C	%	0	0.1	0	0
CO ₂	%	0	0.2	0	0
Au	ppm	-1	-0.3	-0.6	-0.2

Table C1: Mass balance calculation results

Drillhole Depth Belt	Units m	385032	385043	385045	385083
		BR-18-23 325.67	BR-18-23 402.75	BR-18-23 418	BR-18-59 20.5
SiO ₂	%	-15.5	21.5	3.9	16.2
Al ₂ O ₃	%	0	0	0	0
Fe ₂ O ₃	%	0.1	2.8	-1	-0.5
CaO	%	-0.1	1.1	1.3	0.7
MgO	%	-0.2	1	-0.3	-0.3
Na ₂ O	%	-0.3	1.6	0.5	0.9
K ₂ O	%	0.5	-0.6	-0.6	-0.8
Cr ₂ O ₃	%	0	0	0	0
TiO ₂	%	0	0.1	0.1	0
MnO	%	0	0.1	0	0
P ₂ O ₅	%	0	0	0	0
SrO	%	0	0	0	0
BaO	%	0	-0.1	0	0
LOI	%	0.4	-0.5	-0.4	-0.5
Total	%	-15.2	27	3.5	15.6
C	%	0.1	0.1	0.1	0
S	%	-0.1	-0.4	-0.5	-0.5
Ba	ppm	-25.8	-456.9	75	-141
Ce	ppm	-7.4	-16.5	-17.2	-19.2
Cr	ppm	0.7	17.6	-4.8	5.7
Cs	ppm	1.2	3.3	-0.5	-0.9
Dy	ppm	-0.9	0	-1.2	-0.8
Er	ppm	-0.5	0.1	-0.5	-0.4
Eu	ppm	-0.2	0.1	-0.1	-0.1
Ga	ppm	-0.8	-1.7	0.4	-1.7
Gd	ppm	-0.9	-0.3	-1.5	-1.5
Ge	ppm	-0.7	1.4	0.3	0.8
Hf	ppm	-0.3	1.9	0.1	0
Ho	ppm	-0.2	0	-0.2	-0.1
La	ppm	-4.7	-10	-9.3	-10.8
Lu	ppm	0	0	0	0
Nb	ppm	-2.3	0.8	0.7	-0.1
Nd	ppm	-4.6	-8	-7.9	-9.7
Pr	ppm	-0.9	-1.9	-1.8	-2.3
Rb	ppm	23.9	22.4	-11.4	-24.4
Sm	ppm	-1.3	-1.5	-1.6	-2.2
Sn	ppm	0.4	-0.4	0.2	0.5
Sr	ppm	31.8	155.4	117	100.6
Ta	ppm	0	0.1	0.2	0
Tb	ppm	-0.1	0	-0.1	-0.1
Th	ppm	-0.5	-0.3	-0.8	-0.5
Tm	ppm	0	0	0	0
U	ppm	-0.1	0.1	-0.1	0.2
V	ppm	6.7	-7.1	2.4	55.8
W	ppm	-2.8	-5.3	-2.5	3.2
Y	ppm	-3	1.1	-5.1	-3.2
Yb	ppm	0	-0.1	-0.4	0.1
Zr	ppm	-14.8	69.2	4.2	10.5
As	ppm	-37.1	43.4	-199.5	-175.4
Bi	ppm	-0.1	-0.3	-0.3	-0.2
Hg	ppm	0	0	0	0
In	ppm	0	0	0	0
Re	ppm	0	0	0	0
Sb	ppm	1.9	-1	-1.1	-1
Se	ppm	0	0.1	0	0
Te	ppm	0	0	0	0
Tl	ppm	0	0.3	0	-0.1
Ag	ppm	-0.1	0.3	0	0.1
Cd	ppm	-0.1	0.1	0	0.1
Co	ppm	7.8	10.8	1.9	1.4
Cu	ppm	-30.2	-40.9	-57.9	-39.2
Li	ppm	-11.9	34.8	-6.4	-10.6
Mo	ppm	-0.1	0.3	0.1	0.2
Ni	ppm	12.4	18.2	-9.3	5.6
Pb	ppm	-0.7	-0.3	-2	9.2
Sc	ppm	-0.3	1.4	1	0.7
Zn	ppm	26.5	3.8	-36.9	-26.3
C	%	0	0	0	0
CO ₂	%	0	0.1	0	0
Au	ppm	-0.3	-1	-1	-1

Table C1: Mass balance calculation results

Drillhole Depth Belt	Units	385085	385087	385092	385094
		BR-18-59	BR-18-59	BR-18-59	BR-18-59
		45.83	94.3	188.05	200.95
Boston	Boston	Boston	Boston	Boston	Boston
Richardson	Richardson	Richardson	Richardson	Richardson	Richardson
SiO ₂	%	24.7	15.1	5.2	63
Al ₂ O ₃	%	0	0	0	0
Fe ₂ O ₃	%	2.3	1.8	0.7	1
CaO	%	0.1	0.1	-0.2	0.6
MgO	%	0.3	0.6	0.1	0.3
Na ₂ O	%	0.9	0.2	0	2.3
K ₂ O	%	-0.9	-0.6	-0.1	-1.2
Cr ₂ O ₃	%	0	0	0	0
TiO ₂	%	0.1	0	0	0.1
MnO	%	0	0	0	0.1
P ₂ O ₅	%	0	0	0	0
SrO	%	0	0	0	0
BaO	%	0	0	0	-0.1
LOI	%	0	0.2	-0.3	-0.6
Total	%	27.4	17.3	5.3	65.6
C	%	0	0	0	0
S	%	-0.3	-0.4	-0.5	-0.1
Ba	ppm	-182	-261.3	-205.1	-475.6
Ce	ppm	-11.8	-19.4	-7.4	5.6
Cr	ppm	3.1	7.8	5	6.6
Cs	ppm	-0.4	0.7	-0.6	-0.3
Dy	ppm	0	0	-0.3	1.4
Er	ppm	0.2	-0.1	-0.2	0.3
Eu	ppm	-0.1	-0.1	0	0.3
Ga	ppm	0.5	-1.4	1.4	-5.3
Gd	ppm	-0.5	-1	-1	1.5
Ge	ppm	1.3	0.9	0.2	3.3
Hf	ppm	0.7	0.3	-0.1	5.2
Ho	ppm	0.1	0	-0.1	0.1
La	ppm	-6.7	-10.4	-4.6	3.6
Lu	ppm	0.1	0.1	0	0.1
Nb	ppm	0.8	-1.7	-2.5	1.1
Nd	ppm	-6.1	-9.6	-4.6	3.2
Pr	ppm	-1.1	-2.4	-0.9	0.7
Rb	ppm	-21.8	-9.2	-1.6	-10.3
Sm	ppm	-1.6	-1.7	-1.1	1.1
Sn	ppm	0.8	0.5	0.1	0.3
Sr	ppm	15.8	14.4	-10.6	127.8
Ta	ppm	0.1	-0.1	-0.1	0.2
Tb	ppm	0	-0.1	0	0.2
Th	ppm	-1	-0.4	-0.2	0.2
Tm	ppm	0.1	0	0	0.1
U	ppm	-0.3	0.1	0.2	0.2
V	ppm	1.2	2.6	3.7	-18.7
W	ppm	4.6	2.3	0.6	3.7
Y	ppm	1.2	2.2	-0.5	5.1
Yb	ppm	0.7	0.1	0.4	0.8
Zr	ppm	25.6	10.2	-11.4	196.7
As	ppm	-78.4	-118.6	-229.9	166.4
Bi	ppm	-0.2	0	0	-0.2
Hg	ppm	0	0	0	0
In	ppm	0	0	0	0
Re	ppm	0	0	0	0
Sb	ppm	-0.8	-1	-1	2.7
Se	ppm	0.1	0	0	0.1
Te	ppm	0	0	0	0
Tl	ppm	0	0.1	0	0.3
Ag	ppm	0.1	0.1	0	0.3
Cd	ppm	0.1	0.1	0	0.3
Co	ppm	7.9	14.6	-1.4	5.7
Cu	ppm	137.4	0.1	-54.8	-15
Li	ppm	8	14.3	-6.8	3.3
Mo	ppm	0.3	0.2	0	0.7
Ni	ppm	45	31.2	-6.4	3.6
Pb	ppm	-8.2	-3.1	50.1	-8.7
Sc	ppm	1.1	-0.1	-0.2	-2.3
Zn	ppm	40.9	27.3	18	-1.7
C	%	0	0	0	0
CO ₂	%	0.1	0	0	0.1
Au	ppm	-1	-0.9	-1	-0.8

Table C1: Mass balance calculation results

Drillhole Depth Belt	Units m	385095	385096	385098	385100
		BR-18-59 205.6	BR-18-59 232.7	BR-18-59 259.4	BR-18-59 318.65
		Boston Richardson	Boston Richardson	Boston Richardson	Boston Richardson
SiO ₂	%	0	11.4	12.9	-19.5
Al ₂ O ₃	%	0	0	0	0
Fe ₂ O ₃	%	0	1.2	-0.5	3.2
CaO	%	0	0.2	0.5	-0.4
MgO	%	0	0.1	0	0.3
Na ₂ O	%	0	0.7	1.1	-0.5
K ₂ O	%	0	-1.1	-0.7	1
Cr ₂ O ₃	%	0	0	0	0
TiO ₂	%	0	0	0.2	0.1
MnO	%	0	0	0.1	0
P ₂ O ₅	%	0	0	0	-0.1
SrO	%	0	0	0	0
BaO	%	0	0	0	0
LOI	%	0	-0.3	-0.2	3.5
Total	%	0	12.2	13.4	-12.5
C	%	0	0	0	0.4
S	%	0	-0.5	-0.5	0.9
Ba	ppm	0	-264.4	-114.5	-69.5
Ce	ppm	0	-7.5	1.9	-4.2
Cr	ppm	0	14.4	15.3	2.1
Cs	ppm	0	-1.6	-0.6	1.4
Dy	ppm	0	0.1	-0.3	-0.7
Er	ppm	0	0	0.1	-0.1
Eu	ppm	0	0.1	0.2	-0.1
Ga	ppm	0	1	0.4	3.1
Gd	ppm	0	-0.8	-0.3	-1.1
Ge	ppm	0	0.7	0.7	-0.7
Hf	ppm	0	0.1	3.7	0.7
Ho	ppm	0	0.1	0.1	-0.1
La	ppm	0	-4.4	0	-4.4
Lu	ppm	0	0.1	0.1	0
Nb	ppm	0	-0.9	1.5	-0.1
Nd	ppm	0	-4	1.2	-3.4
Pr	ppm	0	-0.7	0.4	-0.5
Rb	ppm	0	-20.5	-9	35.4
Sm	ppm	0	-0.7	-0.6	-1.2
Sn	ppm	0	0.4	0.4	0.4
Sr	ppm	0	30	106.9	-31.5
Ta	ppm	0	0	0.3	0
Tb	ppm	0	0	0	-0.1
Th	ppm	0	0.2	2.6	1.2
Tm	ppm	0	0	0.1	0
U	ppm	0	0.3	0.5	0.3
V	ppm	0	5.3	22.2	7.5
W	ppm	0	2.8	4.1	-2.7
Y	ppm	0	0.8	1.5	-1.6
Yb	ppm	0	0.2	0.6	0.3
Zr	ppm	0	2.1	139.9	28.4
As	ppm	0	-207	-172	-34.4
Bi	ppm	0	-0.3	-0.2	0.8
Hg	ppm	0	0	0	0
In	ppm	0	0	0	0
Re	ppm	0	0	0	0
Sb	ppm	0	-1	-1	10.4
Se	ppm	0	0	0	0.3
Te	ppm	0	0	0	0.5
Tl	ppm	0	0	-0.1	0
Ag	ppm	0	0.1	0.1	-0.1
Cd	ppm	0	0.1	0.1	0.5
Co	ppm	0	3.2	2.2	17.6
Cu	ppm	0	-53.2	-38.4	-54.8
Li	ppm	0	-0.8	11.1	6.2
Mo	ppm	0	0.1	0.1	-0.1
Ni	ppm	0	10.1	-5.4	20.8
Pb	ppm	0	7.4	15.6	18.5
Sc	ppm	0	1.4	2.6	1.7
Zn	ppm	0	-3.5	-35.7	17.1
C	%	0	0	0	0
CO ₂	%	0	0	0	0
Au	ppm	0	-0.9	-1	-0.6

Table C1: Mass balance calculation results

Drillhole Depth Belt	Units	385101	385104	385112	385113
		BR-18-59	BR-18-62	BR-18-62	BR-18-62
		m	331.8	30.8	109.3
Boston	Richardson	Boston	Richardson	Boston	Richardson
SiO ₂	%	-22.5	11.2	-20.4	-19.1
Al ₂ O ₃	%	0	0	0	0
Fe ₂ O ₃	%	-2.2	0.3	1.8	-1
CaO	%	-0.7	-0.1	-0.4	-0.3
MgO	%	-1	0.1	0.1	-1.2
Na ₂ O	%	-0.9	0.5	-0.6	-0.2
K ₂ O	%	1	0.2	0.9	0.2
Cr ₂ O ₃	%	0	0	0	0
TiO ₂	%	0	0.1	0	-0.1
MnO	%	0	0	0	0
P ₂ O ₅	%	-0.1	0	-0.1	-0.2
SrO	%	0	0	0	0
BaO	%	0	0	0	0
LOI	%	2.5	0.1	3.2	3.8
Total	%	-24	12.4	-15.4	-18
C	%	1	0.2	0.7	1
S	%	0.1	-0.5	0.7	0.8
Ba	ppm	205	-32.5	-65.7	85.6
Ce	ppm	-15.8	-22.2	-9.5	-10.7
Cr	ppm	-11.4	2.1	-0.9	-21.5
Cs	ppm	-0.7	0.9	2.1	-0.1
Dy	ppm	-2	-1.3	-0.9	-1.2
Er	ppm	-1	-0.5	0.1	-0.3
Eu	ppm	-0.4	-0.3	0	-0.2
Ga	ppm	3.5	0.3	2.9	3
Gd	ppm	-2.6	-2.1	-1.2	-1.6
Ge	ppm	-1.2	0.6	-0.8	-1
Hf	ppm	-0.2	0.2	-0.1	-0.8
Ho	ppm	-0.3	-0.1	0	-0.1
La	ppm	-9.3	-11	-5.8	-5.4
Lu	ppm	-0.1	0	0.1	0
Nb	ppm	-4	-0.1	-1	-3.5
Nd	ppm	-8.1	-10.2	-4.2	-3.6
Pr	ppm	-1.8	-2.7	-1.1	-1.3
Rb	ppm	7.9	14.3	34.1	-1.7
Sm	ppm	-2.6	-2.8	-0.9	-1.8
Sn	ppm	0.8	0.4	-0.5	0.2
Sr	ppm	-111.7	-22.5	-31.6	9
Ta	ppm	-0.2	2.9	1.8	1.9
Tb	ppm	-0.3	-0.1	0	-0.1
Th	ppm	-1.4	0	0.4	-1
Tm	ppm	-0.1	0	0	0
U	ppm	0	0.3	0.2	-0.3
V	ppm	11.1	22.1	9	11.3
W	ppm	-0.9	2.7	-2.1	-1.7
Y	ppm	-10.1	-3.5	-1	-3.2
Yb	ppm	-0.3	0.1	0.7	-0.1
Zr	ppm	-4.5	17.5	-2.7	-31.1
As	ppm	-60.4	30.3	-40.1	-48.9
Bi	ppm	0.4	-0.3	0.5	0.8
Hg	ppm	0	0	0	0
In	ppm	0	0	0	0
Re	ppm	0	0	0	0
Sb	ppm	3.5	-1	9.4	9.2
Se	ppm	0	0	0.3	0.1
Te	ppm	0.3	0	0.7	0.6
Tl	ppm	-0.3	0	0	-0.4
Ag	ppm	-0.1	0.1	-0.1	-0.1
Cd	ppm	0.2	0.1	0.1	-0.1
Co	ppm	4.5	7.5	7.5	0.1
Cu	ppm	-48.6	0.5	-56.6	-56.8
Li	ppm	-26.9	-1.5	3.9	-23.7
Mo	ppm	-0.2	0.1	-0.2	-0.2
Ni	ppm	-10.4	16.4	9.9	-3.6
Pb	ppm	-2.3	-2.9	0.7	12.6
Sc	ppm	-1.6	0.1	0.3	-2.9
Zn	ppm	-45.7	-28.1	6.8	-66.9
C	%	0	0	0	0
CO ₂	%	0	0	0	0
Au	ppm	-0.7	-1	2.5	-0.1

Table C1: Mass balance calculation results

Drillhole Depth Belt	Units m	385118	385122	385123	385126
		BR-18-62	BR-18-62	BR-18-62	BR-18-62
		133.37	205.45	225	273.5
Boston	Boston	Boston	Boston	Boston	Boston
Richardson	Richardson	Richardson	Richardson	Richardson	Richardson
SiO ₂	%	2	18.8	-1.7	18.4
Al ₂ O ₃	%	0	0	0	0
Fe ₂ O ₃	%	0.3	2.8	-1.7	1
CaO	%	0.9	2.5	2	2
MgO	%	0	1.3	-0.8	0.4
Na ₂ O	%	1.5	2	2.5	2.2
K ₂ O	%	-0.7	-1.2	-1.9	-2
Cr ₂ O ₃	%	0	0	0	0
TiO ₂	%	0.1	0.1	0.2	0.1
MnO	%	0	0.1	0	0.1
P ₂ O ₅	%	0	0	0	0
SrO	%	0	0	0	0
BaO	%	0	-0.1	0	0
LOI	%	-0.9	-0.8	-1	-1.3
Total	%	3.1	25.5	-2.3	20.8
C	%	0.1	0.3	0.2	0
S	%	-0.5	-0.3	-0.5	-0.5
Ba	ppm	-406.5	-554.1	-324.4	-439.1
Ce	ppm	0.1	-2.4	-4.8	1.2
Cr	ppm	5.1	6.5	9.5	0.2
Cs	ppm	-0.3	1.3	-1.4	-1.7
Dy	ppm	0	1.5	-1	-0.1
Er	ppm	0.4	0.7	-0.4	0.3
Eu	ppm	0.1	0.3	0	-0.1
Ga	ppm	0.2	0.2	0.7	-1.2
Gd	ppm	-0.5	0.2	-0.9	0.4
Ge	ppm	0.2	1.5	0	1.1
Hf	ppm	0.3	0.8	0.3	0.7
Ho	ppm	0.1	0.3	-0.2	0
La	ppm	-1.6	-1.8	-3.5	0.3
Lu	ppm	0.1	0.1	0	0
Nb	ppm	-0.8	-0.1	1.5	0
Nd	ppm	-2.1	-3.1	-5	0.7
Pr	ppm	-0.1	-0.2	-1	0.1
Rb	ppm	-12	-3.5	-44.7	-43.2
Sm	ppm	-0.4	0.2	-1	-0.2
Sn	ppm	0.1	0.9	0	0.7
Sr	ppm	120.8	176.5	271.2	167.6
Ta	ppm	0	0.2	0.1	0.1
Tb	ppm	0.1	0.2	0	0.2
Th	ppm	0.6	0.3	0.5	-0.8
Tm	ppm	0	0.1	0	0
U	ppm	0.4	0.4	0.2	0
V	ppm	17.4	14.1	33.3	15
W	ppm	2.7	-3.9	-2	-3.2
Y	ppm	1.9	6.8	-5.2	-1
Yb	ppm	0.6	0.8	-0.1	0.4
Zr	ppm	19	29.8	16.2	30.4
As	ppm	11.5	73.5	-51.3	-178.3
Bi	ppm	-0.1	-0.3	-0.3	-0.3
Hg	ppm	0	0	0	0
In	ppm	0	0	0	0
Re	ppm	0	0	0	0
Sb	ppm	-1	-0.9	-1.1	-1
Se	ppm	0	0.1	0	0
Te	ppm	0	0	0	0
Tl	ppm	0.1	0.3	-0.1	0.1
Ag	ppm	0	0.1	0	0.1
Cd	ppm	0	0.1	0	0.1
Co	ppm	3.9	11.2	-2.1	8.5
Cu	ppm	-49.5	-14.7	-42.1	-55.1
Li	ppm	-6.8	10.6	-30.2	5.7
Mo	ppm	0	0.3	0	0.2
Ni	ppm	-4.3	19.1	-11.1	10.9
Pb	ppm	24	16.8	30.8	0
Sc	ppm	0.9	1.7	0.9	0.6
Zn	ppm	-8.1	34	-42.3	-22.1
C	%	0	0.1	0	0
CO ₂	%	0	0.4	0.1	0
Au	ppm	-0.9	-1	-1	-1

Table C1: Mass balance calculation results

Drillhole Depth Belt	Units m	385127	385130	385131	385157
		BR-18-62	BR-18-62	BR-18-62	BR-18-21
		297.83	349.48	369.38	119.2
Boston Richardson	Boston Richardson	Boston Richardson	Boston Richardson	East Goldbrook	
SiO ₂	%	27.4	-16.7	14.5	5.6
Al ₂ O ₃	%	0	0	0	0
Fe ₂ O ₃	%	2.2	1.7	-0.7	0.6
CaO	%	1.5	0.9	0.2	0
MgO	%	0.8	0	-0.5	0
Na ₂ O	%	1.5	0.8	0.7	0.4
K ₂ O	%	-1.3	-1	-0.6	-0.2
Cr ₂ O ₃	%	0	0	0	0
TiO ₂	%	0.1	0	0	0.1
MnO	%	0.1	0	0	0
P ₂ O ₅	%	0	-0.1	0	0
SrO	%	0	0	0	0
BaO	%	0	0	0	0
LOI	%	-0.9	-0.2	-0.6	-0.4
Total	%	31.3	-14.6	12.9	6
C	%	0	0.1	0	0.1
S	%	-0.4	-0.2	-0.5	-0.5
Ba	ppm	-358.4	-239.9	-154.4	-95.8
Ce	ppm	-6.2	-3.4	-8.3	-5.4
Cr	ppm	-1.8	-7.1	2.3	-2.8
Cs	ppm	0.5	2.3	-2.3	3
Dy	ppm	0.7	-0.2	-0.6	0.2
Er	ppm	0.6	0.2	-0.2	0.3
Eu	ppm	0.1	0	-0.2	-0.1
Ga	ppm	-1.4	0.3	-1.2	-0.3
Gd	ppm	0.2	-0.2	-0.8	-1.1
Ge	ppm	1.8	-0.7	0.6	0.4
Hf	ppm	0.9	-0.6	0.5	0.8
Ho	ppm	0.1	0.1	-0.1	0
La	ppm	-2.4	-2.8	-5.1	-4.8
Lu	ppm	0	0	0	0
Nb	ppm	2	-3.8	-0.8	-0.5
Nd	ppm	-3.5	-3.5	-5.4	-4.5
Pr	ppm	-0.4	-0.5	-0.9	-0.7
Rb	ppm	-13.2	-8	-25.3	4.1
Sm	ppm	-0.7	-0.6	-2	-1.4
Sn	ppm	1.1	-0.4	0.4	0.2
Sr	ppm	138.4	132.4	29.2	14.9
Ta	ppm	0.1	-0.1	0	0.2
Tb	ppm	0.2	0.1	0	0.1
Th	ppm	-0.2	-0.3	-0.4	0.7
Tm	ppm	0.1	0	0	0
U	ppm	0.2	0	0.3	0.4
V	ppm	17.8	3.3	18.9	11.3
W	ppm	7.3	-4.4	1.6	-3.4
Y	ppm	3.4	1.3	-3.6	1.4
Yb	ppm	0.4	0.2	0.2	0.4
Zr	ppm	48	-24.1	20	34.2
As	ppm	-91.7	-35.7	-102.9	-181.5
Bi	ppm	-0.1	0.1	-0.2	0.3
Hg	ppm	0	0	0	0
In	ppm	0	0	0	0
Re	ppm	0	0	0	0
Sb	ppm	-1	-0.9	-1.1	-0.9
Se	ppm	0.1	0	0	0
Te	ppm	0	0	0	0.1
Tl	ppm	0.2	0.1	0	0.1
Ag	ppm	0.2	-0.1	0.1	0
Cd	ppm	0.2	0.1	0.1	0
Co	ppm	12.4	14	9.8	18.3
Cu	ppm	-28.9	3.4	-38.7	48.3
Li	ppm	14.7	-2.9	-12.6	-5
Mo	ppm	0.4	-0.1	0.1	0.1
Ni	ppm	16.5	19.6	1.9	19.2
Pb	ppm	34.8	17.4	21.8	16.6
Sc	ppm	2.6	-0.1	0.1	0.3
Zn	ppm	-1	3.4	0.1	-6.4
C	%	0	0	0	0
CO ₂	%	0.1	0.1	0	0
Au	ppm	-0.9	-0.9	-0.9	-0.9

Table C1: Mass balance calculation results

Drillhole Depth Belt	Units m	385158	385159	385160	385162	385167
		BR-18-21 134.96	BR-18-21 146.64	BR-18-21 160.5	BR-18-21 187.51	BR-18-21 249.15
		East Goldbrook	East Goldbrook	East Goldbrook	East Goldbrook	East Goldbrook
SiO ₂	%	-16.3	13.4	5.8	-12.4	11.6
Al ₂ O ₃	%	0	0	0	0	0
Fe ₂ O ₃	%	-0.3	1.4	1.7	0.5	1.7
CaO	%	-0.1	1.7	0.6	0	1.3
MgO	%	-0.3	0.2	0.2	-0.1	0.7
Na ₂ O	%	-0.3	1.6	0.9	0	1.1
K ₂ O	%	0.4	-1	-0.2	0.1	-1.4
Cr ₂ O ₃	%	0	0	0	0	0
TiO ₂	%	0	0.2	0.1	0.1	-0.1
MnO	%	0	0	0	0	0
P ₂ O ₅	%	0	0	0	0	0.2
SrO	%	0	0	0	0	0
BaO	%	0	0	0	0	0
LOI	%	-0.2	-1.2	-0.5	-0.1	-0.4
Total	%	-17.3	16.4	8.5	-12	14.9
C	%	0.1	0	0	0	0
S	%	-0.4	-0.5	-0.3	-0.2	-0.5
Ba	ppm	-30.7	-355.4	-398.9	-66.8	-446.6
Ce	ppm	-1.8	0.2	-11.4	-9.2	11
Cr	ppm	-0.8	7.8	-1.7	-5.6	-7.1
Cs	ppm	2.6	1.7	7.3	2	0.5
Dy	ppm	-0.3	0.3	0.1	-1	1.5
Er	ppm	0.1	0.8	0	-0.3	1.1
Eu	ppm	0	0.1	-0.2	-0.3	0.3
Ga	ppm	0.6	-1.1	-2	-0.1	-0.4
Gd	ppm	-0.5	0.6	-1.2	-1.3	1.5
Ge	ppm	-0.8	0.9	0.4	-0.7	0.7
Hf	ppm	-0.5	1.4	2.2	-0.2	1.2
Ho	ppm	0	0.1	0.1	-0.1	0.3
La	ppm	-1.9	0.1	-6.7	-5.4	3.1
Lu	ppm	0	0	0	0	0.2
Nb	ppm	-2.1	1.7	2	-0.8	-1.9
Nd	ppm	-1.8	-1.4	-5.6	-6.2	3.9
Pr	ppm	-0.4	-0.1	-1.5	-1.3	1.2
Rb	ppm	10.8	-6.9	22.6	5.4	-26.5
Sm	ppm	-0.4	-0.4	-1.8	-1.2	0.6
Sn	ppm	0.4	0.5	0.2	0.5	0.4
Sr	ppm	-2	217.1	93.5	10.9	189.2
Ta	ppm	-0.1	0.2	0.3	0	-0.1
Tb	ppm	0.1	0.1	0	0	0.3
Th	ppm	0.1	1.2	0.3	0.4	1.3
Tm	ppm	0	0.1	0	0	0.1
U	ppm	0	0.6	0.4	0.2	0.4
V	ppm	15	13.2	-3.5	10.5	9.1
W	ppm	0.4	-2.4	-3.3	-1.7	-5
Y	ppm	-0.3	2.6	-0.6	-4.1	6
Yb	ppm	0.2	0.5	0.6	-0.1	0.8
Zr	ppm	-17.6	75	101.3	3.2	60
As	ppm	-112.2	-69.7	20.8	-203.4	-201.6
Bi	ppm	-0.2	-0.3	-0.3	-0.3	-0.2
Hg	ppm	0	0	0	0	0
In	ppm	0	0	0	0	0
Re	ppm	0	0	0	0	0
Sb	ppm	-0.5	-0.8	-0.6	-1	-0.8
Se	ppm	0	0	0	0	0
Te	ppm	0	0	0	0	0
Tl	ppm	0.1	0.3	0.4	0.1	0.1
Ag	ppm	-0.1	0.1	0	-0.1	0.1
Cd	ppm	-0.1	0.1	0	-0.1	0.1
Co	ppm	8.4	13.5	12.2	4.9	9.2
Cu	ppm	-11.3	-43.5	20.2	-10.4	-23.4
Li	ppm	-12.8	2.5	6.7	-1.7	11.5
Mo	ppm	-0.2	0.2	0.1	-0.1	0.1
Ni	ppm	20	8.8	24.2	9.2	18.8
Pb	ppm	-1.8	28.7	0.7	145.9	48.9
Sc	ppm	-0.5	1	0.5	0.1	0.4
Zn	ppm	-36.8	-12.8	54.4	28.8	49.3
C	%	0	0	0	0	0
CO ₂	%	0	0	0	0	0
Au	ppm	-0.9	-1	-1	-1	-1

Table C1: Mass balance calculation results

Drillhole Depth Belt	Units	385174	385175	385177	385180
		BR-18-21	BR-18-21	BR-18-21	BR-18-21
		m	343.8	356.2	385.83
Boston	Richardson	Boston	Richardson	Boston	Richardson
SiO ₂	%	1.7	34.3	61.1	28
Al ₂ O ₃	%	0	0	0	0
Fe ₂ O ₃	%	1	0.6	2.1	2.4
CaO	%	-0.3	0.7	2.7	1.5
MgO	%	0	0	0.3	0.9
Na ₂ O	%	-0.3	1.2	4	1.1
K ₂ O	%	0.4	-0.7	-3.7	-1
Cr ₂ O ₃	%	0	0	0	0
TiO ₂	%	0	0.1	0.1	0.1
MnO	%	0	0	0.1	0.1
P ₂ O ₅	%	0	0	0	0
SrO	%	0	0	0	0
BaO	%	0	0	-0.1	-0.1
LOI	%	-0.1	-0.7	0.3	-0.9
Total	%	2.4	35.6	66.9	32.2
C	%	0.1	0	0	0
S	%	-0.4	-0.4	0.5	-0.1
Ba	ppm	-197.2	-352.9	-997.9	-532.8
Ce	ppm	-14.2	-4.8	-7.1	-7
Cr	ppm	-6.1	-0.6	-7.9	-3.7
Cs	ppm	1.9	3.2	-0.3	1.6
Dy	ppm	-1.1	0.1	-0.6	-1
Er	ppm	-0.3	0.6	-0.2	-0.1
Eu	ppm	-0.1	0	0.4	0
Ga	ppm	-0.7	-4.2	-5.9	-2.2
Gd	ppm	-0.9	-0.1	-0.2	-0.6
Ge	ppm	0.2	1.8	3.5	1.6
Hf	ppm	-0.7	2.9	3.2	1.9
Ho	ppm	-0.1	0.1	-0.1	-0.1
La	ppm	-7.2	-4.1	-3	-5.8
Lu	ppm	0	0.1	0.1	0
Nb	ppm	-1.4	1.4	2	0.5
Nd	ppm	-7.7	-2.6	-3.3	-4.4
Pr	ppm	-1.7	-0.6	-0.6	-0.8
Rb	ppm	19.4	12.8	-72	3.3
Sm	ppm	-1.4	-1.3	-1	-1.8
Sn	ppm	0.1	-0.3	-1.3	-0.3
Sr	ppm	-33.8	106.7	399	140
Ta	ppm	-0.1	0.1	0	0.1
Tb	ppm	-0.1	0.1	0	0.1
Th	ppm	-0.3	2.3	-0.9	0.8
Tm	ppm	-0.1	0.1	0	0
U	ppm	0.5	0.9	0.2	0.2
V	ppm	11.1	-5.3	-21.5	3.2
W	ppm	3.6	3.4	-7.9	-5
Y	ppm	-4.9	3.1	-0.6	-3.5
Yb	ppm	-0.4	0.8	0.1	0.1
Zr	ppm	-19.7	124.2	143.2	76.2
As	ppm	-149.2	91.9	175.2	31.7
Bi	ppm	-0.2	-0.2	0.6	-0.3
Hg	ppm	0	0	0	0
In	ppm	0	0	0	0
Re	ppm	0	0	0	0
Sb	ppm	-0.9	1.5	19.2	-1
Se	ppm	0	0.1	0.1	0.1
Te	ppm	0	0	0.1	0
Tl	ppm	0.1	0.3	0.2	0.3
Ag	ppm	0	0.2	0.4	0.2
Cd	ppm	0	0.2	0.4	0.2
Co	ppm	12	4.5	12.9	9.2
Cu	ppm	-10.1	-40.9	-36.2	-2.9
Li	ppm	3.1	2.1	22.1	13
Mo	ppm	0	0.4	0.7	0.3
Ni	ppm	14.1	10.3	23.3	12.8
Pb	ppm	1.9	19	141.3	7.2
Sc	ppm	0.7	-1.2	-2	0.9
Zn	ppm	-6.8	-40.7	-6	-13.7
C	%	0	0	0	0
CO ₂	%	0	0.1	0.1	0.1
Au	ppm	-1	-1	-0.8	-0.8

Table C1: Mass balance calculation results

Drillhole Depth Belt	Units m	385188	385189	385211	385212
		BR-18-21	BR-18-21	BR-18-51	BR-18-51
		454.73	459.37	116.17	127
Boston	Boston	Boston	Boston	Boston	Boston
Richardson	Richardson	Richardson	Richardson	Richardson	Richardson
SiO ₂	%	-5.4	22.2	13.2	-0.5
Al ₂ O ₃	%	0	0	0	0
Fe ₂ O ₃	%	3.1	1.1	2	1.3
CaO	%	-0.4	1.3	0.4	1.1
MgO	%	0	0.4	0.7	0.4
Na ₂ O	%	-0.4	1.4	0.6	0.8
K ₂ O	%	0.6	-1.2	-1.1	-0.7
Cr ₂ O ₃	%	0	0	0	0
TiO ₂	%	0	0.1	0.1	0.1
MnO	%	0	0.1	0	0
P ₂ O ₅	%	0	0.1	0	0
SrO	%	0	0	0	0
BaO	%	0	-0.1	0	0
LOI	%	3.4	-0.7	0.1	-0.5
Total	%	1	24.8	16.1	2.1
C	%	0.3	0.1	0	0
S	%	1.2	-0.2	-0.5	-0.5
Ba	ppm	-209.4	-440.3	-285.1	-88
Ce	ppm	-21	2.4	-15.2	-18.3
Cr	ppm	-11.2	4.7	5.1	15.2
Cs	ppm	1.6	1.1	1.1	4.9
Dy	ppm	-1.3	0	0.5	-0.4
Er	ppm	-0.3	0.4	0.3	0
Eu	ppm	-0.4	0.3	0	0.1
Ga	ppm	-0.5	-3	-2.6	0.5
Gd	ppm	-1.8	1	-0.5	-1.4
Ge	ppm	-0.1	1.4	0.8	0.2
Hf	ppm	-0.9	1.9	1	0.5
Ho	ppm	-0.2	0	0.2	0
La	ppm	-12	2.6	-7.8	-9.7
Lu	ppm	-0.1	0.1	0	0
Nb	ppm	-3	1.7	0.1	0.5
Nd	ppm	-11.3	0.9	-6.1	-7
Pr	ppm	-2.5	0.3	-1.4	-1.9
Rb	ppm	27.1	-11.1	-5.1	32.8
Sm	ppm	-2.8	0.8	-1.4	-1.8
Sn	ppm	0	-0.5	0.5	0.1
Sr	ppm	-51.7	151.1	65.4	147.1
Ta	ppm	-0.1	0.1	0.2	0.4
Tb	ppm	-0.2	0.2	0	0
Th	ppm	-0.5	-0.6	0.7	-0.4
Tm	ppm	0	0.1	0.1	0
U	ppm	-0.1	0.1	0.2	0.3
V	ppm	12.2	-0.9	4.2	21.1
W	ppm	-2.1	9.9	-0.3	-1.5
Y	ppm	-4.9	2	2.9	1.6
Yb	ppm	-0.2	0.3	0.5	0.5
Zr	ppm	-23.8	68.9	32.7	21.6
As	ppm	-3.1	68.5	-190.7	-169.6
Bi	ppm	1.1	-0.2	-0.1	-0.2
Hg	ppm	0	0	0	0
In	ppm	0	0	0	0
Re	ppm	0	0	0	0
Sb	ppm	27.1	-0.7	-1.1	-1
Se	ppm	0	0.1	0	0
Te	ppm	0.3	0	0	0
Tl	ppm	0.1	0.2	0.1	0.3
Ag	ppm	0.8	0.1	0.1	0
Cd	ppm	0	0.1	0.1	0
Co	ppm	8.7	12	11.6	9
Cu	ppm	-17.5	7.5	-18.6	-41.2
Li	ppm	-10.9	9.2	12.1	13.9
Mo	ppm	0	0.3	0.2	0
Ni	ppm	16.3	23.3	18	18.5
Pb	ppm	61.9	11.1	-0.1	20.8
Sc	ppm	0.8	1.4	0.6	-0.2
Zn	ppm	7.4	22.7	-7.2	-14.7
C	%	0	0	0	0
CO ₂	%	0	0.1	0	0
Au	ppm	4.8	-0.9	-1	-1

Table C1: Mass balance calculation results

Drillhole Depth Belt	Units	385213	385215	385218	385219
		BR-18-51	BR-18-51	BR-18-51	BR-18-51
		149.42	173	236.57	257
Boston	Boston	Boston	Boston	Boston	Boston
Richardson	Richardson	Richardson	Richardson	Richardson	Richardson
SiO ₂	%	14.7	-17.8	-7.8	-8
Al ₂ O ₃	%	0	0	0	0
Fe ₂ O ₃	%	1.2	0.6	1.2	1
CaO	%	-0.1	-0.4	-0.4	1.8
MgO	%	0	-0.3	0.3	0.3
Na ₂ O	%	0.4	-0.3	-0.3	1.7
K ₂ O	%	-0.2	0.4	0.8	-1.1
Cr ₂ O ₃	%	0	0	0	0
TiO ₂	%	0	0	0	0.2
MnO	%	0	0	0	0
P ₂ O ₅	%	0	-0.1	-0.1	0
SrO	%	0	0	0	0
BaO	%	0	0	0	0
LOI	%	-0.2	-0.1	1	1.5
Total	%	15.8	-18	-5.3	-2.8
C	%	0	-0.1	0.5	0.5
S	%	-0.5	-0.1	0.1	0.4
Ba	ppm	-324.4	-50.3	-27.2	-217
Ce	ppm	-22.5	-10.2	-8.6	-4.2
Cr	ppm	-15.5	-3.4	2.2	6.2
Cs	ppm	-0.7	1.4	1.3	-0.3
Dy	ppm	-0.8	-1.1	-0.5	0.6
Er	ppm	-0.5	-0.4	0	0.2
Eu	ppm	-0.2	-0.3	-0.2	0.3
Ga	ppm	-5	2.3	0.8	0
Gd	ppm	-1.7	-1.8	-1.1	-0.7
Ge	ppm	0.9	-0.9	-0.3	-0.2
Hf	ppm	-0.1	0.5	-0.2	3
Ho	ppm	0	-0.1	0	0.2
La	ppm	-12.2	-6.7	-4.2	-3.5
Lu	ppm	0	0	0.1	0.1
Nb	ppm	-2.9	-1.6	-1.1	2.3
Nd	ppm	-9.2	-7.1	-5.4	-0.7
Pr	ppm	-2.4	-1.5	-0.7	0
Rb	ppm	-14	30.2	48.3	-5.5
Sm	ppm	-2.4	-2.3	-1.4	-0.4
Sn	ppm	-0.6	1.1	0.7	-0.1
Sr	ppm	-8.2	-31.4	-29.7	235.5
Ta	ppm	0.2	0.1	0.1	0.4
Tb	ppm	-0.1	-0.1	0	0.1
Th	ppm	-1.2	0.5	0.4	1.2
Tm	ppm	0	0	0.1	0.1
U	ppm	-0.2	-0.1	0.2	0.6
V	ppm	-5.3	9.1	19.8	17.3
W	ppm	3.5	1.8	-0.8	-5.3
Y	ppm	-3	-4.8	0.7	3.8
Yb	ppm	-0.1	0.1	0.2	0.9
Zr	ppm	-16.5	12.5	-9.7	95.6
As	ppm	-162.4	-45	-16.3	-7.9
Bi	ppm	-0.1	-0.3	0.2	0
Hg	ppm	0	0	0	0
In	ppm	0	0	0	0
Re	ppm	0	0	0	0
Sb	ppm	-1	-1.1	0	7.1
Se	ppm	0	0	0	0
Te	ppm	0	0	0.2	0.3
Tl	ppm	0.2	0	0.2	0.1
Ag	ppm	0.1	-0.1	0	0
Cd	ppm	0.1	-0.1	0.4	0
Co	ppm	11.2	7	7.4	2.4
Cu	ppm	-16.3	22	-18.9	-57.1
Li	ppm	2.7	-14.4	-5.2	-12.2
Mo	ppm	0.2	-0.2	-0.1	0
Ni	ppm	20.8	8.7	5.6	2.5
Pb	ppm	-0.7	-13.8	18.2	26.4
Sc	ppm	1.1	-0.1	-0.3	0.4
Zn	ppm	-14.8	-15.9	6.2	-13.5
C	%	0	0	0	0
CO ₂	%	0	0	0	0
Au	ppm	-0.9	-1	-0.8	-0.8

Table C1: Mass balance calculation results

Drillhole Depth Belt	Units m	385221	385225	385227	385229
		BR-18-51 303	BR-18-52 109.35	BR-18-52 149.4	BR-18-52 176.6
		Boston Richardson	Boston Richardson	Boston Richardson	Boston Richardson
SiO ₂	%	-2.7	33.6	-19.5	-13.3
Al ₂ O ₃	%	0	0	0	0
Fe ₂ O ₃	%	-1	1.5	0.6	-0.8
CaO	%	0.6	1.2	-0.1	-0.4
MgO	%	-0.1	0.5	0.1	-0.5
Na ₂ O	%	0.5	1.6	-0.1	-0.1
K ₂ O	%	-0.3	-1.3	-0.4	0.3
Cr ₂ O ₃	%	0	0	0	0
TiO ₂	%	0.1	0.1	0.1	0
MnO	%	0	0.1	0	-0.1
P ₂ O ₅	%	0	0	-0.1	-0.1
SrO	%	0	0	0	0
BaO	%	0	0	0	0
LOI	%	0	-0.8	0.5	0
Total	%	-3	36.5	-18.8	-14.9
C	%	0.1	0	0	0
S	%	-0.2	-0.5	-0.5	-0.5
Ba	ppm	-15.2	-241.1	178.6	30.6
Ce	ppm	-16.4	8.1	-18.6	-21.9
Cr	ppm	-2.4	11.7	-2.9	-6.1
Cs	ppm	0.4	1	0	0.8
Dy	ppm	-1.6	-0.2	-1.6	-0.7
Er	ppm	-0.6	-0.1	-0.9	-0.5
Eu	ppm	0	0	-0.2	-0.2
Ga	ppm	-1.2	-1.7	-2.5	2.7
Gd	ppm	-1.7	0.2	-2	-2.1
Ge	ppm	-0.1	1.8	-0.9	-0.7
Hf	ppm	0.7	2.2	-0.4	0.4
Ho	ppm	-0.3	0	-0.2	-0.1
La	ppm	-9.2	5.2	-9	-13.6
Lu	ppm	0	0.1	0	0
Nb	ppm	0.1	2.5	-0.2	-0.6
Nd	ppm	-6.9	4.8	-8.4	-11.2
Pr	ppm	-1.5	1.2	-2.1	-2.7
Rb	ppm	20.9	-8.6	-5.8	19.1
Sm	ppm	-2.4	0.8	-1.8	-2.5
Sn	ppm	0.9	1.1	0.3	1.3
Sr	ppm	73	173.5	-9.8	-28.8
Ta	ppm	0.2	0.5	0.2	0
Tb	ppm	-0.2	0	-0.2	-0.1
Th	ppm	0	0.1	-0.1	0.3
Tm	ppm	0	0	0	0
U	ppm	0.4	0.3	0.2	0.1
V	ppm	22.6	16.3	5.7	19.3
W	ppm	-0.3	-2.2	-3.1	2.6
Y	ppm	-6.6	-0.3	-8.7	-2.9
Yb	ppm	0	-0.1	-0.4	0
Zr	ppm	16.9	72.3	-19.6	13.6
As	ppm	-5.5	-147.4	-111.2	-165.4
Bi	ppm	-0.2	-0.1	-0.2	-0.3
Hg	ppm	0	0	0	0
In	ppm	0	0	0	0
Re	ppm	0	0	0	0
Sb	ppm	3.3	-1.1	-1.1	-1.2
Se	ppm	0	0.1	0	0
Te	ppm	0	0	0	0
Tl	ppm	0	0.2	-0.1	0
Ag	ppm	0	0.2	-0.1	-0.1
Cd	ppm	0	0.2	-0.1	-0.1
Co	ppm	-1.3	7	7.9	3
Cu	ppm	-59	-34.3	-48.5	-49.6
Li	ppm	-11.5	14.7	2.4	-19.4
Mo	ppm	0	0.4	-0.2	-0.1
Ni	ppm	-5.8	13.8	10.6	-4.9
Pb	ppm	-9.3	1	1.1	-0.4
Sc	ppm	-0.4	-0.1	0	-0.8
Zn	ppm	-28.1	4.4	43.2	-27.4
C	%	0	0	0	0
CO ₂	%	0	0.1	0	0
Au	ppm	-0.8	-1	-0.9	-1

Table C1: Mass balance calculation results

Drillhole Depth Belt	Units m	385232	385233	385235	385236
		BR-18-52 224.26	BR-18-52 230.14	BR-18-52 248.47	BR-18-52 265.24
		Boston Richardson	Boston Richardson	Boston Richardson	Boston Richardson
SiO ₂	%	14.7	18.4	0.6	1
Al ₂ O ₃	%	0	0	0	0
Fe ₂ O ₃	%	0.4	0.8	0.8	1.6
CaO	%	0.8	0.7	0.2	-0.1
MgO	%	0.1	0.2	0.2	0.1
Na ₂ O	%	1.7	0.7	0.1	0.5
K ₂ O	%	-1.2	-0.8	0.6	0.4
Cr ₂ O ₃	%	0	0	0	0
TiO ₂	%	0.1	0.1	0	0.1
MnO	%	0	0	0	0
P ₂ O ₅	%	0	0	0	0
SrO	%	0	0	0	0
BaO	%	0	0	0	0
LOI	%	-0.6	-0.4	0	-0.4
Total	%	15.9	19.7	2.4	3
C	%	0	0	0.2	0
S	%	-0.5	-0.3	-0.3	-0.2
Ba	ppm	-281.1	-182	-24.4	-304.3
Ce	ppm	3.4	-6.8	1.4	-13.3
Cr	ppm	7.6	12.9	5.3	-3.3
Cs	ppm	-0.6	-0.3	1.7	0.2
Dy	ppm	-0.2	-1	1.1	-0.5
Er	ppm	0.4	-0.1	0.3	-0.3
Eu	ppm	0.4	0.1	0.2	-0.3
Ga	ppm	-0.6	-0.3	-0.3	-3
Gd	ppm	-0.2	-0.8	0.1	-1.6
Ge	ppm	0.9	1.1	0.2	0.3
Hf	ppm	1.6	0.8	0.5	0.1
Ho	ppm	0	0	0.2	0
La	ppm	1.5	-4.4	0.5	-8.8
Lu	ppm	0	0.1	0.1	0
Nb	ppm	1.4	0.4	0.2	-3.3
Nd	ppm	1.6	-2.2	2.1	-8.2
Pr	ppm	0.7	-0.5	0.6	-1.5
Rb	ppm	-9.6	0.5	52.8	10.6
Sm	ppm	-0.2	-1.3	-0.5	-2.3
Sn	ppm	0.5	0.7	0.1	0.2
Sr	ppm	98.8	90.3	27.5	-4
Ta	ppm	0.4	0.4	0.3	0
Tb	ppm	0.1	0	0.2	0
Th	ppm	0.5	0.5	0.7	0.4
Tm	ppm	0.1	0	0.1	0
U	ppm	0.3	0.4	0.4	-0.2
V	ppm	14.1	24.2	17.6	-5.4
W	ppm	-0.1	0.5	-2.5	-3.4
Y	ppm	1.7	-0.5	5.2	-2.8
Yb	ppm	0.6	0	0.6	0.2
Zr	ppm	56.9	27.6	14.1	6.7
As	ppm	-182.7	-186.3	12	16.8
Bi	ppm	-0.3	-0.2	-0.2	-0.3
Hg	ppm	0	0	0	0
In	ppm	0	0	0	0
Re	ppm	0	0	0	0
Sb	ppm	-1	-1.1	-1.1	-1.1
Se	ppm	0	0	0	0
Te	ppm	0	0	0	0
Tl	ppm	0.1	0.2	0.2	0.2
Ag	ppm	0.1	0.1	0	0
Cd	ppm	0.1	0.1	0	0
Co	ppm	6.3	6.1	8.1	5.3
Cu	ppm	-52.9	-23.1	-16	-19.5
Li	ppm	-21.2	-18.5	-6.6	-5.3
Mo	ppm	0.2	0.2	0	0.1
Ni	ppm	8.7	12.3	7.3	8.2
Pb	ppm	-9.1	1.4	5.2	-6
Sc	ppm	1	1.9	2	1.3
Zn	ppm	-25.9	-5.7	-0.5	-5.8
C	%	0	0	0	0
CO ₂	%	0	0	0	0
Au	ppm	-1	-0.9	-1	-0.9

Table C1: Mass balance calculation results

Drillhole Depth Belt	Units m	385238	385241	385243	385245
		BR-18-52 276	BR-18-52 276.47	BR-18-53 30.17	BR-18-53 36.2
		Boston Richardson	Boston Richardson	Boston Richardson	Boston Richardson
SiO ₂	%	-18.4	5.9	9.1	34.7
Al ₂ O ₃	%	0	0	0	0
Fe ₂ O ₃	%	0.4	2.2	3.3	2.1
CaO	%	-0.6	2	0	2.7
MgO	%	-0.2	1	0.9	0.7
Na ₂ O	%	-0.6	1.8	0.1	2.8
K ₂ O	%	1	-1.9	-0.9	-2.2
Cr ₂ O ₃	%	0	0	0	0
TiO ₂	%	0	0.1	0.1	0.2
MnO	%	0	0.1	0	0.1
P ₂ O ₅	%	-0.1	0	0	0.1
SrO	%	0	0	0	0
BaO	%	0	-0.1	0	-0.1
LOI	%	3.7	0.1	0.4	-1.3
Total	%	-14.9	11.4	12.7	39.9
C	%	1.2	0.1	0	0
S	%	0.7	0	-0.5	-0.5
Ba	ppm	272.1	-533.6	-240.6	-440.7
Ce	ppm	-29.2	0.5	-19.3	15.2
Cr	ppm	-9.4	4.2	3.1	18.3
Cs	ppm	0.9	0.7	0.5	0.6
Dy	ppm	-1.7	0.3	-0.2	1.3
Er	ppm	-0.9	0.3	0.1	0.6
Eu	ppm	-0.5	0.4	-0.4	0.7
Ga	ppm	3.3	-3.1	-2.5	-3.7
Gd	ppm	-2.9	-0.3	-1	0.8
Ge	ppm	-0.8	0.7	0.7	2.1
Hf	ppm	-0.4	1.9	0.4	3.2
Ho	ppm	-0.3	0.1	0	0.4
La	ppm	-15.5	-0.3	-12.3	7.8
Lu	ppm	-0.1	0.1	0.1	0.1
Nb	ppm	-1.6	3.9	0	3.7
Nd	ppm	-13.8	1.7	-10.5	9.9
Pr	ppm	-3.2	0.5	-2.1	2.5
Rb	ppm	37.9	-6.8	-2.4	-28.6
Sm	ppm	-3.5	-0.6	-2.2	2.2
Sn	ppm	0.4	-0.7	0.4	-0.1
Sr	ppm	-76.1	262.9	4	330.5
Ta	ppm	0	0.3	0.2	0.6
Tb	ppm	-0.3	0.1	0	0.2
Th	ppm	-0.3	0.8	0.8	1.8
Tm	ppm	-0.1	0.1	0	0.1
U	ppm	0.1	0.5	0	0.8
V	ppm	14.7	11.2	1.9	12.7
W	ppm	-2.1	1.8	-0.6	-3
Y	ppm	-9.5	2.8	-0.2	7.7
Yb	ppm	-0.5	0.4	0.4	1.1
Zr	ppm	-18	77.9	11.2	119.2
As	ppm	-40.4	35.4	-178.3	-167.6
Bi	ppm	1.1	-0.2	-0.3	-0.3
Hg	ppm	0	0	0	0
In	ppm	0	0	0	0
Re	ppm	0	0	0	0
Sb	ppm	5.3	5.9	-0.9	-0.9
Se	ppm	0.1	0	0	0.1
Te	ppm	0.5	0.1	0	0
Tl	ppm	-0.1	0.2	0.1	0.1
Ag	ppm	-0.1	0.1	0.1	0.2
Cd	ppm	0.5	0.1	0.1	0.2
Co	ppm	6.6	9.1	8.9	8.2
Cu	ppm	-25.6	-57.7	-38.5	-44.3
Li	ppm	-12.9	22.8	10.5	5.5
Mo	ppm	-0.2	0.1	0.1	0.4
Ni	ppm	9	12.9	19.2	18.3
Pb	ppm	0.6	2	2.9	-2
Sc	ppm	-1.4	-0.7	0.2	-1.9
Zn	ppm	-11.9	-3.5	21.4	-16
C	%	0	0	0	0
CO ₂	%	0	0	0	0.1
Au	ppm	-0.6	-0.9	-1	-1

Table C1: Mass balance calculation results

Drillhole Depth Belt	Units	385248	385249	385252	385254
		BR-18-53	BR-18-53	BR-18-53	BR-18-53
		61.3	75.17	10.25	125.75
Boston	Boston	Boston	Boston	Boston	Boston
Richardson	Richardson	Richardson	Richardson	Richardson	Richardson
SiO ₂	%	82.3	5.2	1.4	-21.3
Al ₂ O ₃	%	0	0	0	0
Fe ₂ O ₃	%	1	1.1	0.3	-2.5
CaO	%	1.6	0.5	1.3	-0.9
MgO	%	0.2	0.1	0.2	-1.1
Na ₂ O	%	4.2	0.5	1.5	-0.9
K ₂ O	%	.3	-0.3	-0.9	1.1
Cr ₂ O ₃	%	0	0	0	0
TiO ₂	%	0.1	0	0	-0.1
MnO	%	0.1	0	0	0
P ₂ O ₅	%	0.1	0	0	-0.2
SrO	%	0	0	0	0
BaO	%	-0.1	0	0	0
LOI	%	-0.8	0	0.1	0.5
Total	%	85.7	7	4	-25.3
C	%	0	0	0.4	0.1
S	%	-0.5	-0.2	-0.3	-0.2
Ba	ppm	-520.3	-170.8	-292.9	308.1
Ce	ppm	2.2	-21.7	-17.5	-26
Cr	ppm	4.4	-8.9	4.6	-13.3
Cs	ppm	-1.5	1.2	-0.1	0.3
Dy	ppm	0.9	-1.2	-1.2	-3.5
Er	ppm	0.8	-0.9	-0.3	-1.8
Eu	ppm	0.4	-0.3	-0.1	-0.6
Ga	ppm	-5.9	-4	-3.5	4.6
Gd	ppm	0.3	-1.8	-1.3	-3.3
Ge	ppm	4.5	0.6	0.2	-1.3
Hf	ppm	6.3	-0.1	1	-0.6
Ho	ppm	0.3	-0.2	-0.2	-0.6
La	ppm	-0.8	-12.1	-10.6	-14.1
Lu	ppm	0.2	0	0	-0.2
Nb	ppm	4.4	-2.1	0.3	-4.9
Nd	ppm	1.7	-8.7	-7.8	-12.2
Pr	ppm	0.1	-2.4	-2.3	-3.2
Rb	ppm	-67.7	5.7	-7.1	23
Sm	ppm	0.3	-2.6	-2	-3.4
Sn	ppm	0.8	0.4	0.1	0.7
Sr	ppm	234.5	70.9	227.9	-96.9
Ta	ppm	0.5	0.1	0.1	-0.2
Tb	ppm	0.3	-0.1	-0.1	-0.5
Th	ppm	3.9	-1.6	-0.1	-1.4
Tm	ppm	0.1	-0.1	0	-0.2
U	ppm	1	-0.1	0.4	-0.2
V	ppm	-6.8	-5.7	2.1	11.3
W	ppm	-1.6	-2.9	-4.7	1.1
Y	ppm	8.2	-5.3	-4.6	-17.8
Yb	ppm	1	-0.2	-0.1	-1.2
Zr	ppm	249	-15.9	32.8	-28.4
As	ppm	-164.2	30.8	10.4	-64.1
Bi	ppm	-0.3	0.3	-0.1	-0.1
Hg	ppm	0	0	0	0
In	ppm	0	0	0	0
Re	ppm	0	0	0	0
Sb	ppm	-1	-0.7	-0.2	-0.4
Se	ppm	0.2	0	0	-0.1
Te	ppm	0	0	0.2	0
Tl	ppm	0	0.3	0.1	-0.3
Ag	ppm	0.5	0.1	0	-0.1
Cd	ppm	0.5	0.1	0	-0.1
Co	ppm	5	2	3.8	-1.1
Cu	ppm	-42.8	-2.7	-57.9	-41.4
Li	ppm	15.4	-1.4	3.3	-28
Mo	ppm	0.9	4.6	0	-0.3
Ni	ppm	8.5	6.4	4.9	-5.8
Pb	ppm	4.7	5	15.5	-13.8
Sc	ppm	-3.7	0.1	-0.3	-1.9
Zn	ppm	-7.5	9.1	-4.4	-63.5
C	%	0	0	0	0
CO ₂	%	0.2	0	0	-0.1
Au	ppm	-1	-1	-1	-0.9

Table C1: Mass balance calculation results

Drillhole Depth Belt	Units m	385259	385262	385288	385289
		BR-18-53	BR-18-53	BR-18-96	BR-18-96
		165.35	217.25	15.7	27.5
Boston Richardson	Boston Richardson	East Goldbrook	East Goldbrook		
SiO ₂	%	-19.9	13.9	6	-6.6
Al ₂ O ₃	%	0	0	0	0
Fe ₂ O ₃	%	0.3	0.6	-0.5	3.4
CaO	%	-0.7	0.6	-0.4	-0.6
MgO	%	0	0.2	-0.2	0.4
Na ₂ O	%	-1	0.9	-0.4	-1
K ₂ O	%	1.7	-0.9	0.1	1.3
Cr ₂ O ₃	%	0	0	0	0
TiO ₂	%	0	0.1	0.1	0
MnO	%	0	0	0	0
P ₂ O ₅	%	-0.1	0	0	0
SrO	%	0	0	0	0
BaO	%	0	0	0	0
LOI	%	1	-0.5	0.7	3.4
Total	%	-18.8	14.8	5.3	0.2
C	%	0.4	0	0	0.2
S	%	-0.1	-0.5	-0.5	0.9
Ba	ppm	222.3	-136.8	-17.1	-29
Ce	ppm	-12.7	0.6	-17.5	-10.3
Cr	ppm	2.6	7.2	7.3	-0.3
Cs	ppm	1.9	-0.3	0	3.3
Dy	ppm	-0.4	-0.1	-0.4	-0.9
Er	ppm	-0.2	0.1	0.2	-0.3
Eu	ppm	-0.3	0.1	-0.2	-0.2
Ga	ppm	6	3.2	3.6	1.3
Gd	ppm	-1.4	-0.9	-1.3	-1.4
Ge	ppm	-1	0.9	0.3	0
Hf	ppm	0.1	0.8	0	-0.3
Ho	ppm	0.1	0.1	0.1	-0.1
La	ppm	-6.9	-0.3	-10	-5.6
Lu	ppm	0	0	0.1	0
Nb	ppm	0.3	1.2	-0.3	-1.3
Nd	ppm	-6.3	-0.2	-8.8	-4.8
Pr	ppm	-1.3	0.2	-1.9	-1.3
Rb	ppm	78.7	6.2	31.8	59.2
Sm	ppm	-1.7	-0.8	-2.3	-1.8
Sn	ppm	1	0.5	0.2	0
Sr	ppm	-109.3	83.3	-51	-84.9
Ta	ppm	0	0.2	0.2	0
Tb	ppm	0	0.1	0	-0.1
Th	ppm	1.3	1.8	1.4	0.4
Tm	ppm	0	0.1	0.1	0
U	ppm	0.3	0.5	0.3	0.2
V	ppm	18.6	19.5	25.5	18.6
W	ppm	0.7	9.3	-1.3	0
Y	ppm	-1.7	0.9	0.6	-3.8
Yb	ppm	0.2	0.9	0.4	0.1
Zr	ppm	13.9	39.8	18.3	-13.5
As	ppm	-48.9	-57.2	-70.9	-0.8
Bi	ppm	0	-0.2	-0.3	0.9
Hg	ppm	0	0	0	0
In	ppm	0	0	0	0
Re	ppm	0	0	0	0
Sb	ppm	0	-1	-0.8	17.1
Se	ppm	0	0	0	0
Te	ppm	0.1	0	0	0.6
Tl	ppm	0	0.1	-0.3	0.1
Ag	ppm	-0.1	0.1	0	0
Cd	ppm	-0.1	0.1	0	0.2
Co	ppm	3.3	7.4	5.3	11.9
Cu	ppm	-31.9	-47.1	-47.2	3.8
Li	ppm	-15.7	-9.7	-5.4	-10.2
Mo	ppm	-0.2	0.2	0.1	1
Ni	ppm	1.2	8.6	14.6	15.8
Pb	ppm	-14.8	10.8	0.4	22.9
Sc	ppm	-1.3	0.9	-0.9	-0.1
Zn	ppm	-21.1	-20.4	3.7	160.1
C	%	0	0	0	3.4
CO ₂	%	-0.2	-0.1	-0.1	-0.2
Au	ppm	-0.8	-0.7	-0.8	-0.8

Table C1: Mass balance calculation results

Drillhole Depth Belt	Units m	385292	385294	385295	385296	385297
		BR-18-96	BR-18-65	BR-18-65	BR-18-65	BR-18-65
		91.43	41.8	74.66	89.86	123.6
SiO ₂	%	10.3	0.7	-18.2	4.1	4.5
Al ₂ O ₃	%	0	0	0	0	0
Fe ₂ O ₃	%	1.1	2.3	-0.4	0.3	-0.1
CaO	%	-0.3	0	-0.1	-0.2	0.4
MgO	%	0.2	0	-0.3	-0.2	-0.3
Na ₂ O	%	-0.6	0.7	-0.2	-0.4	1.4
K ₂ O	%	1.1	0.3	0.2	1.1	-0.6
Cr ₂ O ₃	%	0	0	0	0	0
TiO ₂	%	0.1	0.3	0.2	0.1	0.1
MnO	%	0	0	0	0	0
P ₂ O ₅	%	0	0	-0.1	0	0
SrO	%	0	0	0	0	0
BaO	%	0	0	0	0	0
LOI	%	0.5	-0.4	0.5	0.1	-0.3
Total	%	12.2	3.8	-18.6	4.9	5.1
C	%	0.2	0	0	0	0
S	%	-0.5	-0.5	-0.5	-0.5	-0.5
Ba	ppm	-112.3	-106.2	208.2	92.8	-114.2
Ce	ppm	0.2	-5.9	-7.1	-7.7	-12.5
Cr	ppm	-7.8	13.9	11.7	15	6.7
Cs	ppm	4.2	3.3	0.9	2.6	1.7
Dy	ppm	-0.2	-0.5	-0.3	-0.5	-0.8
Er	ppm	-0.2	0	-0.4	-0.3	-0.3
Eu	ppm	-0.1	0.2	-0.1	-0.1	0
Ga	ppm	0.4	0.2	0.2	0.9	-1.5
Gd	ppm	-0.8	-0.7	-1.2	-1.1	-1.2
Ge	ppm	0.7	0.2	-0.9	0.2	0.3
Hf	ppm	0.1	3.2	1.2	0.5	0.2
Ho	ppm	0	0.1	0	0	-0.1
La	ppm	-1.2	-3.4	-3.6	-5.7	-7.6
Lu	ppm	0	0.1	0.1	0.1	0
Nb	ppm	2.9	4	0.6	0.5	-0.3
Nd	ppm	-0.7	-1.9	-3.7	-3.9	-5.9
Pr	ppm	0	-0.3	-0.7	-0.8	-1.1
Rb	ppm	57.4	53.1	5	44	14.6
Sm	ppm	-0.9	-0.6	-1.8	-1.4	-1.9
Sn	ppm	0.4	0.1	1.1	1.2	0.2
Sr	ppm	-48.8	60.5	40.5	-31.9	81.1
Ta	ppm	0	0.5	0.3	0.3	0.2
Tb	ppm	0.1	0.1	0	0	0
Th	ppm	1.2	0.5	1.8	1.6	0.7
Tm	ppm	0.1	0.1	0.1	0	0
U	ppm	0.3	0.6	0.5	0.6	0.1
V	ppm	7	16.5	19.9	35.5	13
W	ppm	-0.5	-2.7	1.6	3.7	-3.5
Y	ppm	0.1	0.7	-0.7	-1.3	-2.2
Yb	ppm	0.3	0.7	0.6	0.8	0
Zr	ppm	5.1	116.7	46.4	6.8	-3.9
As	ppm	-64.9	-153.8	-102.7	-162	-147
Bi	ppm	-0.2	-0.3	-0.3	0.3	-0.3
Hg	ppm	0	0	0	0	0
In	ppm	0	0	0	0	0
Re	ppm	0	0	0	0	0
Sb	ppm	-1	-1	-0.9	-0.9	-1.1
Se	ppm	0	0	0	0	0
Te	ppm	0	0	0	0	0
Tl	ppm	0.2	0.2	-0.2	0.1	0.2
Ag	ppm	0.1	0	-0.1	0	0
Cd	ppm	0.1	0	-0.1	0	0
Co	ppm	5.6	8.8	2.7	4.8	2
Cu	ppm	-13.4	-36.3	-21.9	-18.3	-21.8
Li	ppm	-0.5	-7.7	1.2	-17.5	-16.4
Mo	ppm	0.1	0	-0.2	0	0.1
Ni	ppm	13.8	16.9	11.4	8	7.9
Pb	ppm	0.7	-10.6	-5.8	23.8	5.6
Sc	ppm	0.3	-0.4	-0.3	0.8	1.2
Zn	ppm	-12.1	-62.2	-41.3	-44	-30.9
C	%	0	0	0	0	0
CO ₂	%	-0.1	-0.1	-0.2	-0.1	-0.1
Au	ppm	-0.7	-0.8	-0.8	-0.8	-0.8

Table C1: Mass balance calculation results

Drillhole Depth Belt	Units	385299	385303	385305	385310
		BR-18-65	BR-18-65	BR-18-65	BR-18-65
		m	143.63	201.1	221.5
East Goldbrook	Boston Richardson	Boston Richardson	Boston Richardson	Boston Richardson	
SiO ₂	%	5.5	-13.1	6.4	42.4
Al ₂ O ₃	%	0	0	0	0
Fe ₂ O ₃	%	1	0.6	-0.1	2.1
CaO	%	-0.4	0.6	1	1.7
MgO	%	-0.1	0	0	0.7
Na ₂ O	%	-0.4	0.4	1.5	2.4
K ₂ O	%	1.1	0.2	-1.2	-1.4
Cr ₂ O ₃	%	0	0	0	0
TiO ₂	%	0.1	0.1	0.1	0.1
MnO	%	0	0	0	0.1
P ₂ O ₅	%	0	0	0	0
SrO	%	0	0	0	0
BaO	%	0	0	0	-0.1
LOI	%	0	-0.4	-0.1	-0.8
Total	%	6.8	-11.6	7.6	47.2
C	%	0	0	0.1	0.2
S	%	-0.5	-0.5	-0.5	-0.3
Ba	ppm	112.8	-47.1	-146.7	-412.4
Ce	ppm	-4.9	-3.8	-10.8	-9.2
Cr	ppm	7.4	5.2	8.2	7.4
Cs	ppm	6.2	3.5	-0.8	3.9
Dy	ppm	-1.4	-0.5	-0.2	-0.4
Er	ppm	-0.3	-0.5	0.1	-0.1
Eu	ppm	-0.1	0.2	0	0.1
Ga	ppm	-0.5	0.6	-1.2	-4.3
Gd	ppm	-1.5	-0.9	-1.3	-0.3
Ge	ppm	0.3	-0.6	0.4	2.3
Hf	ppm	0.4	1.7	0.1	2.6
Ho	ppm	-0.2	-0.1	0	0
La	ppm	-3.1	-2.3	-6.3	-4.6
Lu	ppm	0	0.1	0.1	0.1
Nb	ppm	-1.1	0.3	-0.7	3.4
Nd	ppm	-3.4	-1.5	-5.2	-2.3
Pr	ppm	-0.2	-0.1	-1.1	-0.5
Rb	ppm	50.2	42.2	-25.5	19.2
Sm	ppm	-1.8	-1.2	-2.2	-1.3
Sn	ppm	0.2	0.5	0.2	-0.1
Sr	ppm	-44.7	82.6	157	274.1
Ta	ppm	0.2	0.3	0.2	0.3
Tb	ppm	-0.1	0	0	0
Th	ppm	0.6	0.9	1.2	-0.9
Tm	ppm	0	0	0.1	0
U	ppm	0	0.5	0.4	0.1
V	ppm	16.1	17.5	25.6	-6.7
W	ppm	-1.3	-3.3	-2.3	-5.7
Y	ppm	-4.4	-1.4	1.9	0.2
Yb	ppm	0.1	0.1	0.6	0.6
Zr	ppm	3.6	48.8	4.6	95.3
As	ppm	-19.4	-113.1	-203.7	-159.6
Bi	ppm	-0.3	-0.3	-0.1	-0.2
Hg	ppm	0	0	0	0
In	ppm	0	0	0	0
Re	ppm	0	0	0	0
Sb	ppm	-1	-1	-1.1	-1.2
Se	ppm	0	0	0	0.1
Te	ppm	0	0	0	0
Tl	ppm	0.2	0.2	-0.1	0.5
Ag	ppm	0	-0.1	0	0.2
Cd	ppm	0	-0.1	0	0.2
Co	ppm	5.4	7.9	2.3	6
Cu	ppm	-21.6	-43.2	-43.9	-26.3
Li	ppm	-5.3	-0.2	-4.8	8
Mo	ppm	0.1	-0.1	0.1	0.5
Ni	ppm	20	12	4.3	12.8
Pb	ppm	-11.3	25	8.1	4.4
Sc	ppm	0.2	-0.4	-0.7	-1.4
Zn	ppm	-5.8	-46.4	4.6	-26.1
C	%	0	0	0	0
CO ₂	%	-0.1	-0.2	-0.1	-0.1
Au	ppm	-0.8	-0.8	-0.8	-0.7

Table C1: Mass balance calculation results

Drillhole Depth Belt	Units	385315	385316	385318	385320
		BR-18-65	BR-18-65	BR-18-65	BR-18-66
		320.5	335.9	107.85	20.28
Boston	Boston	Richardson	Richardson	Richardson	East Goldbrook
SiO ₂	%	-1	-5	14.9	6.7
Al ₂ O ₃	%	0	0	0	0
Fe ₂ O ₃	%	-2.1	1.6	-2.1	0.9
CaO	%	-0.3	0.8	0.5	0
MgO	%	-0.9	0.3	-0.9	0
Na ₂ O	%	-0.2	0.9	0.7	0.6
K ₂ O	%	0.4	-0.5	-0.1	0.1
Cr ₂ O ₃	%	0	0	0	0
TiO ₂	%	0.1	0.1	0.1	0.1
MnO	%	0	0	0	0
P ₂ O ₅	%	0	0	0	0
SrO	%	0	0	0	0
BaO	%	0	0	0	0
LOI	%	0	-0.2	-0.4	0.3
Total	%	-4.3	-2.1	12.6	8.6
C	%	0	0.2	0	0
S	%	-0.5	-0.1	-0.5	-0.5
Ba	ppm	-15.8	-247.9	58.7	-179.8
Ce	ppm	-33.1	-1.7	-11.4	-13.1
Cr	ppm	-12.3	1.7	5	2
Cs	ppm	-1.1	2.4	-0.3	2.6
Dy	ppm	-2.8	0.1	-1.4	-1
Er	ppm	-1.5	0.1	-0.5	-0.5
Eu	ppm	-0.6	0	-0.1	0
Ga	ppm	-3.6	-2.7	-0.7	-0.1
Gd	ppm	-3.7	-0.6	-1.5	-0.9
Ge	ppm	-0.1	0.1	0.7	0.6
Hf	ppm	-0.5	1.2	0.6	0.4
Ho	ppm	-0.5	0	-0.1	-0.1
La	ppm	-17.8	-0.8	-6.2	-7.4
Lu	ppm	0	0.1	0	0.1
Nb	ppm	-2.5	0.5	0.5	-0.5
Nd	ppm	-16.3	-1.1	-6.4	-6.5
Pr	ppm	-3.9	0.3	-1.2	-1.2
Rb	ppm	-17.8	21.5	2.1	25.8
Sm	ppm	-4.2	-1.2	-1.8	-1.3
Sn	ppm	-0.1	0	0.4	0.4
Sr	ppm	-30.7	155.7	81.8	4.7
Ta	ppm	0.1	0.1	0.3	0.1
Tb	ppm	-0.3	0.1	-0.1	-0.1
Th	ppm	-0.8	0.6	-0.7	0.2
Tm	ppm	-0.1	0	0	0
U	ppm	-0.2	0.5	0.3	0.3
V	ppm	-0.9	11.1	25.9	20.8
W	ppm	-0.3	-4.9	-1.5	-0.7
Y	ppm	-13.7	1	-5.5	-1.2
Yb	ppm	-0.8	0.2	-0.1	0.2
Zr	ppm	-18.3	33	18.7	18.4
As	ppm	-196	3.9	-183.3	-151.7
Bi	ppm	-0.3	0	-0.3	-0.1
Hg	ppm	0	0	0	0
In	ppm	0	0	0	0
Re	ppm	0	0	0	0
Sb	ppm	-1.2	-0.8	-0.8	-1
Se	ppm	0	0	0	0
Te	ppm	0	0.1	0	0
Tl	ppm	-0.1	0.3	-0.1	0.2
Ag	ppm	0	0	0.1	0.1
Cd	ppm	0	0	0.1	0.1
Co	ppm	-5.2	8.4	5.8	6.4
Cu	ppm	-28.7	-7.2	-57.7	-43.2
Li	ppm	-21.4	1.3	-22.5	-1.6
Mo	ppm	0	0	0.1	0.1
Ni	ppm	-6.8	13.9	4.1	16.4
Pb	ppm	-8.3	8.5	-8.2	28.4
Sc	ppm	-0.4	1.3	0.5	1.2
Zn	ppm	-39.9	-7.2	-76.3	43.5
C	%	0	0	0	0
CO ₂	%	-0.2	-0.1	-0.1	-0.1
Au	ppm	-0.8	-0.8	-0.7	-0.7

Table C1: Mass balance calculation results

Drillhole Depth Belt	Units m	385321	385323	385324	385325	385330
		BR-18-66 41	BR-18-66 80	BR-18-66 90.67	BR-18-66 105.35	BR-18-66 183
		East Goldbrook	East Goldbrook	East Goldbrook	East Goldbrook	Boston Richardson
SiO ₂	%	8.1	11.6	6.4	-16.3	-16.2
Al ₂ O ₃	%	0	0	0	0	0
Fe ₂ O ₃	%	1	0.6	2.3	-2.8	-0.7
CaO	%	0.5	-0.4	-0.7	0.4	0.4
MgO	%	0.5	-0.2	0.6	-0.9	-0.2
Na ₂ O	%	-0.5	-0.4	-1	-0.3	-0.2
K ₂ O	%	0.5	0.2	1.1	-0.2	0.5
Cr ₂ O ₃	%	0	0	0	0	0
TiO ₂	%	0.2	0	0	0.3	0.1
MnO	%	0	0	0	0	0
P ₂ O ₅	%	0	0	0	-0.2	-0.1
SrO	%	0	0	0	0	0
BaO	%	0	0	0	0	0
LOI	%	1.1	0.9	1.2	1.1	0.2
Total	%	11.2	12.3	9.9	-18.9	-16.1
C	%	0.2	0.1	0	0.4	0.2
S	%	-0.4	-0.2	0.3	-0.2	-0.3
Ba	ppm	35	-59	-140.4	147.8	44.5
Ce	ppm	6.9	9.4	-18.1	6.9	-1.7
Cr	ppm	12.4	2.3	0	27.6	0.9
Cs	ppm	4.4	0.9	5.6	-0.1	3.4
Dy	ppm	0.5	-0.1	-1.8	-2.3	-1
Er	ppm	0.1	-0.4	-1	-1.3	-0.5
Eu	ppm	0.2	0.3	-0.2	0	0
Ga	ppm	-0.3	0.5	-0.6	0.8	1.1
Gd	ppm	0.3	0.1	-2.1	-1.7	-1.5
Ge	ppm	0.6	0.6	0.5	-1	-0.7
Hf	ppm	0.7	-0.2	0.6	0.7	0.8
Ho	ppm	0.1	0	-0.3	-0.3	0
La	ppm	4.1	5.2	-10.3	4.1	-1.5
Lu	ppm	0.1	0	0	0	0
Nb	ppm	1.3	-0.6	-1.4	3.9	1
Nd	ppm	4.6	4.2	-10	0.5	-2.1
Pr	ppm	1.3	1.2	-2.2	0.8	0
Rb	ppm	49.9	26.4	78.8	17.5	38.8
Sm	ppm	0.5	0.1	-2.5	-1	-1.2
Sn	ppm	0.3	0.4	0.3	0.2	0.4
Sr	ppm	13.8	-47.3	-70.9	127.5	56
Ta	ppm	0.3	0.2	0.2	0.5	0.1
Tb	ppm	0.1	0.1	-0.1	-0.2	0
Th	ppm	1.6	1.1	1	3.7	1
Tm	ppm	0	0	0	-0.1	0
U	ppm	0.4	0.3	-0.3	0.8	0.4
V	ppm	18.7	22.3	0.6	28.4	14.6
W	ppm	-1.9	638.1	1.3	-2.5	-1.1
Y	ppm	3.4	-0.9	-8.1	-10.9	-3.5
Yb	ppm	0.4	-0.3	-0.3	-0.4	-0.1
Zr	ppm	27.2	-3.6	16.2	29.7	41.7
As	ppm	28.1	30.6	24.9	-47.6	-36.8
Bi	ppm	-0.2	0.7	-0.2	0	-0.3
Hg	ppm	0	0	0	0	0
In	ppm	0	0.1	0	0	0
Re	ppm	0	0	0	0	0
Sb	ppm	-0.3	-0.4	0.5	3.3	-0.9
Se	ppm	0	0	0	0	0
Te	ppm	0.1	0	0	0.1	0
Tl	ppm	0.2	0.1	0.2	-0.4	0
Ag	ppm	0.1	0.1	0	-0.1	-0.1
Cd	ppm	0.1	1.4	0	-0.1	-0.1
Co	ppm	5.1	8.7	2.7	17.2	1.9
Cu	ppm	-33.3	16.3	52.2	-59.2	-31.9
Li	ppm	-2.1	-12.6	8	-23.3	-3.2
Mo	ppm	0.1	0.1	0.1	-0.2	-0.1
Ni	ppm	12.6	18.7	15.3	16.1	8.2
Pb	ppm	32.5	189	-1.1	16.1	-2.4
Sc	ppm	2.1	1.2	1.9	-1.2	-1.9
Zn	ppm	-5.4	1165.4	16.4	-35	-13.4
C	%	0.5	0.2	3.5	0	0
CO ₂	%	-0.1	-0.1	-0.1	0	0
Au	ppm	-0.5	-0.7	-0.8	-0.9	-0.9

Table C1: Mass balance calculation results

Drillhole Depth Belt	Units m	385331	385335	385339	385351
		BR-18-66 207.7	BR-18-66 267.5	BR-18-45 225.72	BR-18-45 364.06
		Boston Richardson	Boston Richardson	Boston Richardson	Boston Richardson
SiO ₂	%	11.5	5.2	6.8	-17.3
Al ₂ O ₃	%	0	0	0	0
Fe ₂ O ₃	%	3.3	-0.6	2.2	-0.3
CaO	%	-0.6	-0.3	-0.4	0.2
MgO	%	0.8	-0.4	0.6	-0.8
Na ₂ O	%	1.1	-0.1	-0.3	-0.3
K ₂ O	%	-0.7	0.4	0.4	0.4
Cr ₂ O ₃	%	0	0	0	0
TiO ₂	%	0.1	0	0.1	0.4
MnO	%	0	0	0	0
P ₂ O ₅	%	0	-0.1	0	-0.2
SrO	%	0	0	0	0
BaO	%	0	0	0	0
LOI	%	0.2	0	0	4.4
Total	%	15.7	4.1	9.4	-13.5
C	%	0	0	0	0.4
S	%	-0.4	-0.4	-0.5	1.1
Ba	ppm	-173.3	226.7	95.5	-51.3
Ce	ppm	-7.4	-12.6	5.9	23.5
Cr	ppm	6.5	-5.2	10.5	23.2
Cs	ppm	2.3	2.1	3.8	-0.9
Dy	ppm	-0.7	-1.6	0	0.4
Er	ppm	-0.3	-0.7	0.1	0.5
Eu	ppm	-0.1	-0.3	0.1	0.4
Ga	ppm	1.8	1.3	3.1	3.4
Gd	ppm	-1.1	-1.8	-0.6	0
Ge	ppm	0.8	0.2	0.5	-0.8
Hf	ppm	0.3	-0.5	-0.1	4.4
Ho	ppm	0	-0.2	0.1	0.2
La	ppm	-4	-8.4	3.2	12.2
Lu	ppm	0	0	0	0.1
Nb	ppm	0	-1.1	1.3	10.2
Nd	ppm	-4.7	-7.4	2.1	9.4
Pr	ppm	-1.1	-1.6	0.7	2.7
Rb	ppm	23.5	21.3	66.7	20.4
Sm	ppm	-1.9	-1.8	-0.3	1
Sn	ppm	0.5	1.2	1.4	0.3
Sr	ppm	-34.8	-11.9	-22.2	49.5
Ta	ppm	0.2	0	0.2	0.6
Tb	ppm	0.1	-0.2	0.1	0.1
Th	ppm	1.6	0.5	2.3	3.2
Tm	ppm	0	-0.1	0.1	0.2
U	ppm	0.2	0.1	0.5	1
V	ppm	2.3	15.5	23	22
W	ppm	1	-0.4	0.1	1.2
Y	ppm	-1.5	-7	1.9	6.3
Yb	ppm	0	-0.5	0.6	0.8
Zr	ppm	18.7	-13.2	4.6	178.3
As	ppm	-191.6	-97.6	-177	-41.9
Bi	ppm	-0.3	-0.1	-0.2	0.1
Hg	ppm	0	0	0	0
In	ppm	0.3	0	0	0
Re	ppm	0	0	0	0
Sb	ppm	-0.6	-1.1	-1	24.4
Se	ppm	0	0	0	0
Te	ppm	0	0	0	0.3
Tl	ppm	0.1	0	0.3	-0.4
Ag	ppm	0.1	0	0	-0.1
Cd	ppm	3.7	0	0	-0.1
Co	ppm	6.1	9.1	10.3	11.5
Cu	ppm	-8.7	-37	-32.6	-59.2
Li	ppm	13.2	-17.1	7.6	-13.4
Mo	ppm	0.2	0	0.1	-0.2
Ni	ppm	15.3	8.3	16.1	6.1
Pb	ppm	207.5	-1	-8.9	23
Sc	ppm	0.8	-0.1	0.7	-0.7
Zn	ppm	1918.9	-26.8	9.2	-78.4
C	%	0	0	0	0
CO ₂	%	0	0	0	0
Au	ppm	-1	-1	-1	-0.8

Table C1: Mass balance calculation results

Drillhole Depth Belt	Units m	385353	385355	385357	385359
		BR-18-45	BR-18-45	BR-18-45	BR-18-45
		383.27	414.2	477.5	502.3
Boston	Boston	Boston	Boston	Boston	Boston
Richardson	Richardson	Richardson	Richardson	Richardson	Richardson
SiO ₂	%	1.2	-21.1	-0.7	7.9
Al ₂ O ₃	%	0	0	0	0
Fe ₂ O ₃	%	0	-2.3	0.3	1.4
CaO	%	0.5	-0.7	0.1	-0.2
MgO	%	0	-0.6	0.1	0.6
Na ₂ O	%	1.2	-1	0.7	0
K ₂ O	%	-0.2	1.1	-0.2	0.3
Cr ₂ O ₃	%	0	0	0	0
TiO ₂	%	0.1	0	0.1	0
MnO	%	0	0	0	0
P ₂ O ₅	%	0	-0.1	-0.1	0
SrO	%	0	0	0	0
BaO	%	0	0	0	0
LOI	%	0.7	0.6	-0.2	0.2
Total	%	3.5	-24	0.1	10.2
C	%	0.7	0.2	0	0.2
S	%	0.1	-0.3	-0.1	-0.4
Ba	ppm	-94.2	246.6	-62.7	-112
Ce	ppm	-18.2	-23.1	13.5	2.4
Cr	ppm	5.1	-1.5	13.1	13.2
Cs	ppm	0.1	-0.2	-0.2	4.1
Dy	ppm	-0.5	-2.5	0	0
Er	ppm	0.6	-0.9	0.3	0.2
Eu	ppm	-0.1	-0.4	0.2	0.1
Ga	ppm	1.2	3.5	3.2	3.5
Gd	ppm	-1.8	-2.9	-0.6	-0.3
Ge	ppm	0.2	-1.1	0.1	0.6
Hf	ppm	0.7	-0.3	1.9	0.3
Ho	ppm	0.1	-0.3	0.1	0.1
La	ppm	-10.2	-12.2	3.6	0.5
Lu	ppm	0.2	0	0.1	0.1
Nb	ppm	0.1	-1	2	0
Nd	ppm	-9.5	-12.1	2.5	0.4
Pr	ppm	-2.2	-2.7	1.5	0.5
Rb	ppm	24.2	34.3	13.5	50.6
Sm	ppm	-2.8	-3.1	0	-0.4
Sn	ppm	0.1	0.9	1.1	0.4
Sr	ppm	131.4	-95.2	48.9	-7
Ta	ppm	0.2	0	0.2	0.1
Tb	ppm	0	-0.2	0	0.1
Th	ppm	0.9	0.7	3.4	1.2
Tm	ppm	0.2	-0.1	0.1	0.1
U	ppm	0.5	0.2	0.6	0.4
V	ppm	14.3	24.1	18.7	19.8
W	ppm	-2.5	2.5	-1.7	1.6
Y	ppm	3.9	-10.7	3.5	3.3
Yb	ppm	0.8	-0.5	0.7	0.2
Zr	ppm	41.1	-8.8	88.3	9.5
As	ppm	11.6	-56.2	6.4	-27.6
Bi	ppm	0.1	-0.2	-0.3	-0.3
Hg	ppm	0	0	0	0
In	ppm	0	0	0	0
Re	ppm	0	0	0	0
Sb	ppm	0.3	0.8	-1	-1
Se	ppm	0	0	0	0
Te	ppm	0.2	0	0	0
Tl	ppm	0	-0.3	-0.1	0.2
Ag	ppm	0	0.3	0	0.1
Cd	ppm	0	0	0	0.1
Co	ppm	6	1.1	6.6	6.4
Cu	ppm	-17.1	-47.6	-2.6	-23
Li	ppm	-6.7	-2.5	-8.2	9.6
Mo	ppm	0	-0.2	0	0.1
Ni	ppm	12.5	-8.9	2.1	9.7
Pb	ppm	80.6	111.3	5.7	7.1
Sc	ppm	-0.2	-1.2	0.5	1.2
Zn	ppm	5.6	300.1	13.3	-1.2
C	%	0	0	0	0
CO ₂	%	0	0	0	0
Au	ppm	0.8	-0.6	-0.9	-0.9

Table C1: Mass balance calculation results

Drillhole Depth Belt	Units	385362	385364	385368	385370
		BR-18-49	BR-18-49	BR-18-49	BR-18-49
		221.3	338.25	396.4	409.6
Boston	Boston Richardson				
SiO ₂	%	8.4	-0.6	25.4	10.7
Al ₂ O ₃	%	0	0	0	0
Fe ₂ O ₃	%	-0.8	0.9	0.9	2.5
CaO	%	-0.3	0.1	0.9	-0.6
MgO	%	-0.5	0.5	0.1	0.5
Na ₂ O	%	-0.3	0	1.6	-0.4
K ₂ O	%	0.4	-0.1	-1.3	-0.4
Cr ₂ O ₃	%	0	0	0	0
TiO ₂	%	0	0.1	0.1	0
MnO	%	0	0	0	0
P ₂ O ₅	%	0	0	0	0
SrO	%	0	0	0	0
BaO	%	0	0	0	0
LOI	%	0	0.1	-0.8	0.5
Total	%	6.8	1	26.9	12.6
C	%	0	0.1	0	0
S	%	-0.5	-0.4	-0.5	-0.4
Ba	ppm	-120.8	-39.7	-168.6	-117.3
Ce	ppm	-9.1	1.1	7	-20.2
Cr	ppm	-2.6	10.5	4.8	4.1
Cs	ppm	0.2	3.1	1	-0.9
Dy	ppm	-1.2	-0.3	0.2	-1.7
Er	ppm	-0.5	-0.2	0.4	-0.6
Eu	ppm	-0.1	0.2	0.2	-0.3
Ga	ppm	-0.1	2.1	0.3	2.1
Gd	ppm	-2.3	-0.6	0.3	-1.6
Ge	ppm	0.4	0	1.4	0.7
Hf	ppm	-0.5	0.1	0.2	-0.4
Ho	ppm	-0.1	0.1	0.2	-0.2
La	ppm	-6.6	2.3	2.9	-11.3
Lu	ppm	0	0.1	0	0
Nb	ppm	-1.7	-0.1	0.7	0
Nd	ppm	-5.8	-1.4	2.4	-11.1
Pr	ppm	-1	-0.1	0.6	-2.4
Rb	ppm	6	41	21.7	6.3
Sm	ppm	-2.1	-0.5	-0.3	-3.1
Sn	ppm	0.2	1	0.8	0.4
Sr	ppm	-37.5	31.7	136.2	-72.4
Ta	ppm	0	0.2	0.1	0
Tb	ppm	-0.1	0	0.2	-0.1
Th	ppm	0	1.3	1.7	1
Tm	ppm	0	0	0	0
U	ppm	0.2	0.6	0.4	0
V	ppm	10.4	26.6	24.8	10
W	ppm	7.4	0.1	2.3	7.5
Y	ppm	-4.2	0.6	0.4	-6
Yb	ppm	-0.4	0.1	0.5	-0.3
Zr	ppm	-11.6	12.7	20.7	-10.1
As	ppm	-167.9	1	-161.1	-189.5
Bi	ppm	-0.1	-0.2	-0.2	-0.1
Hg	ppm	0	0	0	0
In	ppm	0	0	0	0
Re	ppm	0	0	0	0
Sb	ppm	-1	0.5	-1.1	-1.1
Se	ppm	0	0	0.1	0
Te	ppm	0	0	0	0
Tl	ppm	0	0.2	0.3	0
Ag	ppm	0	0	0.1	0.1
Cd	ppm	0	0	0.1	0.1
Co	ppm	4.4	5.1	5.7	5.7
Cu	ppm	-48.2	5.3	-21.7	-21.2
Li	ppm	-4.9	10.4	9.3	11.3
Mo	ppm	0.1	0	0.3	0.1
Ni	ppm	1	10.2	10.6	14.1
Pb	ppm	28.5	4.1	30.3	8.8
Sc	ppm	0.3	1.1	0.1	1.5
Zn	ppm	-1.9	-12.6	-25.6	39.8
C	%	0	0	0	0
CO ₂	%	0	0	0.1	0
Au	ppm	-0.9	-0.9	-0.9	-0.9

Table C1: Mass balance calculation results

Drillhole Depth Belt	Units	385373	385375	385376
		BR-18-49	BR-18-49	BR-18-49
		429.97	478.07	502.81
Boston Richardson	Boston Richardson	Boston Richardson	Boston Richardson	Boston Richardson
SiO ₂	%	8.1	-3.4	-15.5
Al ₂ O ₃	%	0	0	0
Fe ₂ O ₃	%	2.4	0.6	-3
CaO	%	-0.5	0.6	0
MgO	%	0.4	0.3	-0.6
Na ₂ O	%	-0.3	1.4	0.2
K ₂ O	%	-0.2	0.1	0.2
Cr ₂ O ₃	%	0	0	0
TiO ₂	%	0	0.1	0.1
MnO	%	0	0.1	0
P ₂ O ₅	%	0	0	-0.2
SrO	%	0	0	0
BaO	%	0	0	0
LOI	%	0.4	0.9	0.6
Total	%	10.3	0.6	-18.1
C	%	0	0.3	0.7
S	%	-0.3	0.2	-0.4
Ba	ppm	-140.7	-214.4	-71
Ce	ppm	0.4	22.3	11.5
Cr	ppm	2.5	-0.4	23.8
Cs	ppm	0	2.1	0.1
Dy	ppm	-0.8	0.6	-1.3
Er	ppm	-0.3	0.3	-0.3
Eu	ppm	-0.1	0.4	0.4
Ga	ppm	2.5	2.3	4.4
Gd	ppm	-1.1	1.2	-1.8
Ge	ppm	0.6	0	-0.8
Hf	ppm	-0.3	1.7	0.3
Ho	ppm	0	0.1	-0.1
La	ppm	-0.4	12.2	5.3
Lu	ppm	0	0.1	0.1
Nb	ppm	-1.2	1.3	5
Nd	ppm	-1.8	10	0.7
Pr	ppm	0.1	2.6	1.1
Rb	ppm	16.7	51	41.4
Sm	ppm	-0.8	1.2	-0.7
Sn	ppm	0.4	0	1.2
Sr	ppm	-49	128.9	87.9
Ta	ppm	0	0.2	0.5
Tb	ppm	0	0.3	-0.1
Th	ppm	1.1	0.8	2.9
Tm	ppm	0	0.1	0.1
U	ppm	0.2	0.6	0.8
V	ppm	14.7	13.5	26.8
W	ppm	-2.9	-3	-1.3
Y	ppm	-3.2	5.3	-4.4
Yb	ppm	0	0.6	0.4
Zr	ppm	-5.5	75.1	26.8
As	ppm	-212.5	-1	-41
Bi	ppm	-0.2	0	-0.1
Hg	ppm	0	0	0
In	ppm	0	0	0
Re	ppm	0	0	0
Sb	ppm	-1	4	0.7
Se	ppm	0	0	0
Te	ppm	0	0.2	0.1
Tl	ppm	0	0	-0.3
Ag	ppm	0.1	0	-0.1
Cd	ppm	0.1	0	-0.1
Co	ppm	11	7.9	11.6
Cu	ppm	5.2	-45.1	-59.2
Li	ppm	-1.3	9.7	-4.8
Mo	ppm	0.1	0	-0.2
Ni	ppm	13.2	15.8	-12.1
Pb	ppm	7.2	4.9	-7
Sc	ppm	0.1	-2.1	-0.6
Zn	ppm	31.9	-34.3	-35.6
C	%	0	0	0
CO ₂	%	0	0.1	0
Au	ppm	-0.9	-0.5	-0.9

Appendix D: EPMA Results

Table D1: Statement of electron microprobe conditions for chlorite and biotite

Element	X-ray	Crystal Spectrometer	Accelerating voltage (kV)	Intensity (nA)	Spot size (μm)	Peak position	Background lower (nm)	Background upper (nm)
F	Ka	LDE1	1	15	20	3	85.0	6.0
Fe	Ka	LIFL	2	15	20	3	134.5	3.5
Ti	Ka	LIFL	2	15	20	3	191.0	3.0
Ba	La	LIFL	2	15	20	3	192.9	4.0
Cl	Ka	PETL	3	15	20	3	151.5	2.0
K	Ka	PETL	3	15	20	3	119.8	2.0
Ca	Ka	PETL	3	15	20	3	107.5	7.0
Sr	La	PETL	3	15	20	3	219.8	3.7
Na	Ka	TAP	4	15	20	3	129.4	4.7
Al	Ka	TAP	4	15	20	3	90.6	6.2
Si	Ka	TAP	4	15	20	3	77.4	3.3
Mg	Ka	TAP	4	15	20	3	107.5	3.3
Mn	Ka	LIFH	5	15	20	3	146.3	7.2
Zn	Ka	LIFH	5	15	20	3	99.9	2.0

Table D2: Electron microprobe results: chlorite atomic proportions

Element	385230.3.1	385230.3.2	385230.3.3	385230.3.4	385230.9.1	385230.9.2	385230.9.3
Si (IV)	3.511	3.487	3.516	3.518	2.606	2.698	2.634
Al (IV)	0.489	0.513	0.484	0.482	1.394	1.302	1.366
Al (VI)	1.678	1.687	1.683	1.707	1.423	1.369	1.408
Al (total)	2.167	2.201	2.168	2.189	2.817	2.672	2.774
FeO	1.576	1.586	1.563	1.541	2.368	2.395	2.356
MgO	1.327	1.368	1.364	1.338	2.121	2.110	2.144
MnO	0.018	0.019	0.022	0.019	0.046	0.049	0.047
CaO	0.003	0.002	0.004	0.001	0.002	0.004	0.001
Na₂O	0.025	0.013	0.009	0.015	0.007	0.002	0.007
K₂O	1.156	1.113	1.077	1.123	0.001	0.004	0.000
TiO₂	0.099	0.087	0.102	0.097	0.004	0.008	0.003
Cr₂O₃	0.001	0.000	0.000	0.001	0.002	0.001	0.001
ZnO	0.005	0.004	0.004	0.005	0.007	0.006	0.008
V₂O₃	0.002	0.004	0.004	0.004	0.001	0.002	0.001
BaO	0.004	0.001	0.004	0.003	0.001	0.002	0.001
SrO	0.001	0.000	0.000	0.001	0.003	0.000	0.001
F	0.000	0.000	0.000	0.000	0.000	0.000	0.000
Cl	0.005	0.005	0.005	0.005	0.000	0.010	0.002
Total	12.064	12.089	12.008	12.047	12.801	12.635	12.753
Tet Al	0.489	0.513	0.484	0.482	1.394	1.302	1.366
Oct Al	1.678	1.687	1.683	1.707	1.423	1.369	1.408
Total Al	2.167	2.201	2.168	2.189	2.817	2.672	2.774

Table D2: Electron microprobe results: chlorite atomic proportions

Element	385230.9.4	385230.23.1	385230.23.2	385230.23.3	385230.23.4	385230.26.1	385230.26.2
Si (IV)	2.700	2.780	2.723	2.737	2.815	2.690	2.669
Al (IV)	1.300	1.220	1.277	1.263	1.185	1.310	1.331
Al (VI)	1.363	1.366	1.331	1.352	1.343	1.349	1.348
Al (total)	2.663	2.587	2.608	2.615	2.528	2.658	2.679
FeO	2.363	2.267	2.320	2.277	2.255	2.343	2.310
MgO	2.161	2.152	2.237	2.218	2.217	2.203	2.248
MnO	0.048	0.038	0.042	0.039	0.042	0.047	0.046
CaO	0.001	0.003	0.004	0.002	0.015	0.003	0.002
Na2O	0.002	0.001	0.004	0.004	0.037	0.004	0.000
K2O	0.002	0.083	0.010	0.050	0.007	0.002	0.002
TiO2	0.006	0.025	0.007	0.014	0.008	0.007	0.011
Cr2O3	0.002	0.000	0.000	0.001	0.000	0.000	0.001
ZnO	0.005	0.004	0.006	0.006	0.006	0.003	0.006
V2O3	0.002	0.001	0.002	0.002	0.000	0.004	0.002
BaO	0.002	0.001	0.001	0.001	0.001	0.000	0.001
SrO	0.001	0.000	0.002	0.001	0.001	0.001	0.001
F	0.000	0.000	0.000	0.000	0.000	0.000	0.000
Cl	0.006	0.004	0.006	0.000	0.004	0.010	0.002
Total	12.627	12.531	12.582	12.582	12.464	12.635	12.659
Tet Al	1.300	1.220	1.277	1.263	1.185	1.310	1.331
Oct Al	1.363	1.366	1.331	1.352	1.343	1.349	1.348
Total Al	2.663	2.587	2.608	2.615	2.528	2.658	2.679

Table D2: Electron microprobe results: chlorite atomic proportions

Element	385230.26.3	385230.26.4	385230.32.1	385230.32.2	385230.32.4	385230.33.1	385230.33.2
Si (IV)	2.690	2.692	2.721	2.718	2.683	2.694	2.737
Al (IV)	1.310	1.308	1.279	1.282	1.317	1.306	1.263
Al (VI)	1.347	1.361	1.350	1.359	1.349	1.357	1.354
Al (total)	2.657	2.668	2.630	2.641	2.666	2.663	2.617
FeO	2.327	2.324	2.376	2.336	2.375	2.316	2.315
MgO	2.219	2.204	2.155	2.181	2.176	2.217	2.175
MnO	0.047	0.045	0.046	0.044	0.045	0.045	0.044
CaO	0.001	0.001	0.005	0.004	0.004	0.004	0.007
Na2O	0.005	0.006	0.002	0.000	0.002	0.013	0.008
K2O	0.013	0.009	0.003	0.006	0.002	0.002	0.015
TiO2	0.011	0.009	0.008	0.008	0.010	0.008	0.015
Cr2O3	0.001	0.001	0.000	0.000	0.001	0.000	0.001
ZnO	0.006	0.006	0.006	0.006	0.007	0.006	0.005
V2O3	0.001	0.001	0.001	0.003	0.000	0.002	0.003
BaO	0.001	0.002	0.000	0.001	0.001	0.000	0.001
SrO	0.000	0.001	0.002	0.001	0.000	0.000	0.001
F	0.000	0.000	0.000	0.000	0.000	0.000	0.000
Cl	0.001	0.001	0.006	0.007	0.003	0.005	0.007
Total	12.636	12.639	12.590	12.598	12.641	12.638	12.567
Tet Al	1.310	1.308	1.279	1.282	1.317	1.306	1.263
Oct Al	1.347	1.361	1.350	1.359	1.349	1.357	1.354
Total Al	2.657	2.668	2.630	2.641	2.666	2.663	2.617

Table D2: Electron microprobe results: chlorite atomic proportions

Element	385230.33.3	385230.33.4	385367.2.34.1	385367.2.34.2	385367.2.34.3	385367.2.34.4
Si (IV)	2.701	2.683	2.738	2.727	2.735	2.737
Al (IV)	1.299	1.317	1.262	1.273	1.265	1.263
Al (VI)	1.362	1.361	1.331	1.318	1.330	1.345
Al (total)	2.661	2.679	2.593	2.592	2.595	2.609
FeO	2.329	2.350	2.525	2.517	2.543	2.526
MgO	2.185	2.185	2.049	2.073	2.032	2.020
MnO	0.042	0.044	0.022	0.022	0.022	0.021
CaO	0.003	0.003	0.003	0.002	0.001	0.004
Na2O	0.005	0.001	0.003	0.007	0.005	0.009
K2O	0.024	0.003	0.006	0.005	0.003	0.005
TiO2	0.013	0.011	0.007	0.008	0.009	0.007
Cr2O3	0.000	0.000	0.002	0.003	0.004	0.003
ZnO	0.004	0.005	0.004	0.006	0.007	0.004
V2O3	0.001	0.003	0.003	0.002	0.001	0.001
BaO	0.001	0.001	0.001	0.000	0.000	0.001
SrO	0.000	0.000	0.000	0.001	0.002	0.001
F	0.000	0.000	0.000	0.000	0.000	0.000
Cl	0.001	0.003	0.007	0.014	0.002	0.013
Total	12.631	12.647	12.555	12.569	12.556	12.569
Tet Al	1.299	1.317	1.262	1.273	1.265	1.263
Oct Al	1.362	1.361	1.331	1.318	1.330	1.345
Total Al	2.661	2.679	2.593	2.592	2.595	2.609

Table D2: Electron microprobe results: chlorite atomic proportions

Element	385367.2.35.1	385367.2.35.2	385367.2.35.3	385367.2.35.4	385367.2.36.1	385367.2.36.2
Si (IV)	2.707	2.700	2.691	2.704	2.726	2.717
Al (IV)	1.293	1.300	1.309	1.296	1.274	1.283
Al (VI)	1.347	1.358	1.353	1.336	1.338	1.329
Al (total)	2.640	2.658	2.663	2.632	2.612	2.612
FeO	2.350	2.317	2.383	2.402	2.389	2.429
MgO	2.204	2.235	2.175	2.188	2.160	2.150
MnO	0.025	0.027	0.025	0.025	0.026	0.023
CaO	0.000	0.001	0.002	0.001	0.005	0.003
Na₂O	0.003	0.006	0.004	0.003	0.008	0.015
K₂O	0.007	0.004	0.002	0.004	0.008	0.006
TiO₂	0.013	0.006	0.008	0.006	0.010	0.007
Cr₂O₃	0.002	0.002	0.004	0.003	0.003	0.004
ZnO	0.006	0.010	0.005	0.003	0.005	0.004
V₂O₃	0.001	0.001	0.002	0.001	0.002	0.001
BaO	0.000	0.000	0.001	0.001	0.002	0.001
SrO	0.001	0.000	0.000	0.001	0.001	0.001
F	0.000	0.000	0.000	0.000	0.000	0.000
Cl	0.004	0.002	0.006	0.002	0.011	0.007
Total	12.604	12.628	12.634	12.608	12.579	12.592
Tet Al	1.293	1.300	1.309	1.296	1.274	1.283
Oct Al	1.347	1.358	1.353	1.336	1.338	1.329
Total Al	2.640	2.658	2.663	2.632	2.612	2.612

Table D2: Electron microprobe results: chlorite atomic proportions

Element	385367.2.37.1	385367.2.37.2	385367.2.38.1	385367.2.38.2	385367.2.38.3	385367.2.38.4
Si (IV)	2.741	2.749	2.720	2.714	2.751	2.716
Al (IV)	1.259	1.251	1.280	1.286	1.249	1.284
Al (VI)	1.353	1.366	1.307	1.327	1.324	1.322
Al (total)	2.612	2.617	2.587	2.613	2.573	2.606
FeO	2.481	2.452	2.511	2.593	2.510	2.515
MgO	2.051	2.068	2.113	2.003	2.069	2.086
MnO	0.023	0.019	0.023	0.022	0.023	0.024
CaO	0.002	0.001	0.000	0.001	0.001	0.000
Na₂O	0.006	0.000	0.008	0.004	0.015	0.007
K₂O	0.014	0.016	0.000	0.003	0.002	0.001
TiO₂	0.007	0.006	0.009	0.009	0.007	0.010
Cr₂O₃	0.003	0.002	0.001	0.001	0.001	0.000
ZnO	0.008	0.003	0.004	0.005	0.004	0.004
V₂O₃	0.001	0.002	0.001	0.002	0.002	0.001
BaO	0.001	0.000	0.000	0.000	0.000	0.001
SrO	0.002	0.001	0.000	0.002	0.002	0.002
F	0.000	0.000	0.000	0.000	0.000	0.000
Cl	0.004	0.004	0.005	0.002	0.003	0.002
Total	12.566	12.560	12.570	12.586	12.536	12.581
Tet Al	1.259	1.251	1.280	1.286	1.249	1.284
Oct Al	1.353	1.366	1.307	1.327	1.324	1.322
Total Al	2.612	2.617	2.587	2.613	2.573	2.606

Table D2: Electron microprobe results: chlorite atomic proportions

Element	385367.2.39.1	385367.2.39.2	385367.2.39.3	385367.2.39.4	385367.2.43.1	385367.2.43.2
Si (IV)	2.669	2.676	2.687	2.674	2.728	2.693
Al (IV)	1.331	1.324	1.313	1.326	1.272	1.307
Al (VI)	1.361	1.341	1.347	1.345	1.332	1.350
Al (total)	2.692	2.665	2.659	2.670	2.605	2.657
FeO	2.310	2.335	2.343	2.354	2.308	2.297
MgO	2.253	2.249	2.231	2.230	2.265	2.255
MnO	0.027	0.027	0.026	0.026	0.026	0.027
CaO	0.001	0.000	0.000	0.000	0.002	0.002
Na ₂ O	0.002	0.004	0.000	0.005	0.001	0.011
K ₂ O	0.002	0.003	0.003	0.003	0.007	0.007
TiO ₂	0.008	0.010	0.010	0.009	0.007	0.009
Cr ₂ O ₃	0.001	0.002	0.002	0.000	0.001	0.001
ZnO	0.008	0.004	0.003	0.006	0.007	0.006
V ₂ O ₃	0.001	0.003	0.003	0.003	0.001	0.001
BaO	0.001	0.000	0.001	0.001	0.001	0.001
SrO	0.000	0.002	0.001	0.001	0.000	0.001
F	0.000	0.000	0.000	0.000	0.000	0.000
Cl	0.002	0.003	0.003	0.001	0.012	0.014
Total	12.671	12.648	12.632	12.655	12.574	12.639
Tet Al	1.331	1.324	1.313	1.326	1.272	1.307
Oct Al	1.361	1.341	1.347	1.345	1.332	1.350
Total Al	2.692	2.665	2.659	2.670	2.605	2.657

Table D2: Electron microprobe results: chlorite atomic proportions

Element	385367.2.43.3	385367.2.44.1	385367.2.44.2	385367.2.44.3	385367.2.44.4	385367.2.45.1
Si (IV)	2.703	2.762	2.740	2.734	2.749	2.748
Al (IV)	1.297	1.238	1.260	1.266	1.251	1.252
Al (VI)	1.362	1.334	1.323	1.331	1.326	1.344
Al (total)	2.659	2.572	2.583	2.597	2.577	2.597
FeO	2.330	2.445	2.459	2.457	2.426	2.520
MgO	2.219	2.114	2.117	2.122	2.165	2.038
MnO	0.026	0.024	0.024	0.023	0.023	0.023
CaO	0.001	0.002	0.002	0.001	0.000	0.002
Na₂O	0.006	0.004	0.002	0.004	0.003	0.004
K₂O	0.002	0.004	0.008	0.005	0.005	0.000
TiO₂	0.006	0.005	0.005	0.006	0.004	0.007
Cr₂O₃	0.001	0.001	0.001	0.001	0.001	0.001
ZnO	0.004	0.005	0.004	0.006	0.006	0.005
V₂O₃	0.002	0.003	0.003	0.003	0.002	0.002
BaO	0.001	0.001	0.001	0.000	0.000	0.000
SrO	0.000	0.001	0.000	0.001	0.000	0.001
F	0.000	0.000	0.000	0.000	0.000	0.000
Cl	0.008	0.008	0.023	0.003	0.000	0.001
Total	12.625	12.523	12.556	12.562	12.539	12.545
Tet Al	1.297	1.238	1.260	1.266	1.251	1.252
Oct Al	1.362	1.334	1.323	1.331	1.326	1.344
Total Al	2.659	2.572	2.583	2.597	2.577	2.597

Table D2: Electron microprobe results: chlorite atomic proportions

Element	385367.2.45.2	385367.2.45.3	385367.2.45.4	385367.2.46.1	385367.2.46.2	385367.2.46.3
Si (IV)	2.733	2.731	2.713	2.734	2.708	2.720
Al (IV)	1.267	1.269	1.287	1.266	1.292	1.280
Al (VI)	1.341	1.319	1.350	1.336	1.334	1.325
Al (total)	2.607	2.588	2.638	2.602	2.626	2.605
FeO	2.536	2.458	2.454	2.484	2.498	2.525
MgO	2.036	2.142	2.108	2.101	2.097	2.069
MnO	0.023	0.023	0.024	0.023	0.024	0.024
CaO	0.000	0.001	0.001	0.001	0.001	0.002
Na₂O	0.001	0.006	0.002	0.005	0.003	0.004
K₂O	0.003	0.001	0.001	0.001	0.000	0.000
TiO₂	0.009	0.009	0.009	0.004	0.006	0.009
Cr₂O₃	0.000	0.000	0.001	0.001	0.001	0.000
ZnO	0.002	0.005	0.005	0.004	0.002	0.004
V₂O₃	0.002	0.001	0.001	0.001	0.002	0.002
BaO	0.001	0.001	0.000	0.001	0.002	0.000
SrO	0.001	0.003	0.001	0.001	0.000	0.001
F	0.000	0.000	0.000	0.000	0.000	0.000
Cl	0.001	0.002	0.003	0.001	0.004	0.005
Total	12.563	12.558	12.598	12.565	12.600	12.576
Tet Al	1.267	1.269	1.287	1.266	1.292	1.280
Oct Al	1.341	1.319	1.350	1.336	1.334	1.325
Total Al	2.607	2.588	2.638	2.602	2.626	2.605

Table D2: Electron microprobe results: chlorite atomic proportions

Element	385367.2.46.4	385367.2.47.1	385367.2.47.2	385367.2.47.3	385367.2.47.4	385367.2.48.1
Si (IV)	2.735	2.712	2.710	2.699	2.688	2.733
Al (IV)	1.265	1.288	1.290	1.301	1.312	1.267
Al (VI)	1.321	1.375	1.351	1.363	1.365	1.337
Al (total)	2.586	2.663	2.641	2.664	2.677	2.604
FeO	2.492	2.385	2.428	2.339	2.351	2.502
MgO	2.108	2.138	2.125	2.208	2.190	2.052
MnO	0.025	0.024	0.025	0.026	0.025	0.025
CaO	0.001	0.002	0.001	0.002	0.002	0.003
Na₂O	0.000	0.002	0.011	0.004	0.013	0.005
K₂O	0.002	0.005	0.003	0.006	0.009	0.012
TiO₂	0.005	0.006	0.007	0.005	0.005	0.005
Cr₂O₃	0.001	0.002	0.002	0.001	0.003	0.005
ZnO	0.006	0.006	0.008	0.005	0.004	0.004
V₂O₃	0.002	0.002	0.001	0.001	0.002	0.003
BaO	0.000	0.001	0.000	0.000	0.000	0.001
SrO	0.000	0.000	0.001	0.000	0.001	0.000
F	0.000	0.000	0.000	0.000	0.000	0.000
Cl	0.005	0.004	0.006	0.009	0.007	0.012
Total	12.554	12.616	12.610	12.634	12.656	12.571
Tet Al	1.265	1.288	1.290	1.301	1.312	1.267
Oct Al	1.321	1.375	1.351	1.363	1.365	1.337
Total Al	2.586	2.663	2.641	2.664	2.677	2.604

Table D2: Electron microprobe results: chlorite atomic proportions

Element	385367.2.48.2	385367.2.48.3	385367.2.49.1	385367.2.49.2	385367.2.49.3	385367.2.49.4
Si (IV)	2.773	2.722	2.666	2.662	2.658	2.659
Al (IV)	1.227	1.278	1.334	1.338	1.342	1.341
Al (VI)	1.346	1.317	1.378	1.348	1.397	1.381
Al (total)	2.573	2.595	2.712	2.686	2.739	2.722
FeO	2.536	2.400	2.203	2.257	2.215	2.231
MgO	1.989	2.206	2.338	2.317	2.297	2.310
MnO	0.024	0.023	0.034	0.032	0.033	0.033
CaO	0.003	0.001	0.001	0.000	0.000	0.000
Na₂O	0.001	0.003	0.004	0.008	0.005	0.005
K₂O	0.006	0.005	0.001	0.001	0.000	0.002
TiO₂	0.004	0.005	0.007	0.011	0.007	0.006
Cr₂O₃	0.008	0.004	0.000	0.000	0.001	0.001
ZnO	0.008	0.005	0.004	0.005	0.005	0.002
V₂O₃	0.001	0.000	0.001	0.005	0.001	0.001
BaO	0.000	0.002	0.000	0.001	0.001	0.001
SrO	0.003	0.000	0.001	0.001	0.000	0.001
F	0.000	0.000	0.000	0.000	0.000	0.000
Cl	0.007	0.007	0.000	0.002	0.004	0.001
Total	12.510	12.574	12.685	12.672	12.706	12.698
Tet Al	1.227	1.278	1.334	1.338	1.342	1.341
Oct Al	1.346	1.317	1.378	1.348	1.397	1.381
Total Al	2.573	2.595	2.712	2.686	2.739	2.722

Table D2: Electron microprobe results: chlorite atomic proportions

Element	385367.2.50.1	385367.2.50.2	385367.2.50.3	385367.2.50.4	385210.62.1	385210.62.2
Si (IV)	2.703	2.669	2.668	2.672	2.586	2.601
Al (IV)	1.297	1.331	1.332	1.328	1.414	1.399
Al (VI)	1.360	1.386	1.368	1.405	1.453	1.439
Al (total)	2.657	2.717	2.700	2.732	2.867	2.838
FeO	2.391	2.288	2.312	2.250	2.572	2.556
MgO	2.161	2.229	2.240	2.234	1.903	1.929
MnO	0.026	0.031	0.029	0.031	0.029	0.030
CaO	0.001	0.001	0.002	0.001	0.001	0.002
Na₂O	0.002	0.007	0.011	0.010	0.004	0.005
K₂O	0.002	0.002	0.002	0.003	0.001	0.000
TiO₂	0.007	0.009	0.006	0.008	0.004	0.004
Cr₂O₃	0.001	0.001	0.000	0.001	0.001	0.000
ZnO	0.003	0.007	0.005	0.007	0.004	0.006
V₂O₃	0.001	0.002	0.001	0.001	0.001	0.001
BaO	0.002	0.001	0.000	0.000	0.001	0.000
SrO	0.000	0.000	0.000	0.001	0.001	0.001
F	0.000	0.000	0.000	0.000	0.000	0.000
Cl	0.006	0.004	0.008	0.009	0.006	0.003
Total	12.620	12.685	12.684	12.693	12.848	12.816
Tet Al	1.297	1.331	1.332	1.328	1.414	1.399
Oct Al	1.360	1.386	1.368	1.405	1.453	1.439
Total Al	2.657	2.717	2.700	2.732	2.867	2.838

Table D2: Electron microprobe results: chlorite atomic proportions

Element	385210.62.3	385210.63.1	385210.63.2	385210.63.3	385210.64.1	385210.64.2	385210.64.3
Si (IV)	2.605	2.640	2.670	2.701	2.684	2.683	2.675
Al (IV)	1.395	1.360	1.330	1.299	1.316	1.317	1.325
Al (VI)	1.411	1.421	1.380	1.358	1.353	1.361	1.346
Al (total)	2.806	2.782	2.710	2.658	2.670	2.678	2.671
FeO	2.558	2.506	2.534	2.482	2.503	2.506	2.532
MgO	1.971	1.993	2.007	2.070	2.072	2.055	2.055
MnO	0.030	0.029	0.033	0.032	0.028	0.027	0.030
CaO	0.002	0.000	0.001	0.001	0.001	0.001	0.001
Na2O	0.004	0.005	0.005	0.001	0.001	0.004	0.001
K2O	0.001	0.001	0.000	0.002	0.000	0.001	0.000
TiO2	0.004	0.002	0.003	0.006	0.005	0.005	0.005
Cr2O3	0.000	0.001	0.000	0.000	0.002	0.002	0.000
ZnO	0.005	0.008	0.002	0.006	0.005	0.007	0.006
V2O3	0.001	0.001	0.001	0.001	0.001	0.001	0.002
BaO	0.001	0.001	0.000	0.001	0.001	0.001	0.001
SrO	0.000	0.001	0.001	0.001	0.001	0.001	0.001
F	0.000	0.000	0.000	0.000	0.000	0.000	0.000
Cl	0.003	0.001	0.006	0.006	0.004	0.004	0.005
Total	12.796	12.751	12.685	12.625	12.648	12.653	12.656
Tet Al	1.395	1.360	1.330	1.299	1.316	1.317	1.325
Oct Al	1.411	1.421	1.380	1.358	1.353	1.361	1.346
Total Al	2.806	2.782	2.710	2.658	2.670	2.678	2.671

Table D2: Electron microprobe results: chlorite atomic proportions

Element	385210.65.1	385210.65.2	385210.66.1	385210.66.2	385210.66.3	385210.66.4	385210.67.1
Si (IV)	2.696	2.705	2.793	2.721	2.767	2.696	2.685
Al (IV)	1.304	1.295	1.207	1.279	1.233	1.304	1.315
Al (VI)	1.354	1.338	1.357	1.349	1.426	1.374	1.364
Al (total)	2.659	2.633	2.564	2.628	2.659	2.679	2.679
FeO	2.494	2.509	2.508	2.453	2.478	2.464	2.481
MgO	2.062	2.071	1.979	2.103	1.921	2.066	2.075
MnO	0.025	0.029	0.042	0.027	0.039	0.026	0.026
CaO	0.002	0.002	0.009	0.003	0.007	0.002	0.001
Na2O	0.005	0.003	0.004	0.000	0.004	0.004	0.006
K2O	0.012	0.008	0.006	0.006	0.003	0.008	0.001
TiO2	0.006	0.005	0.005	0.005	0.007	0.005	0.006
Cr2O3	0.000	0.001	0.000	0.000	0.001	0.001	0.000
ZnO	0.011	0.007	0.011	0.008	0.008	0.008	0.008
V2O3	0.002	0.000	0.000	0.001	0.001	0.001	0.000
BaO	0.000	0.000	0.001	0.001	0.000	0.001	0.001
SrO	0.000	0.001	0.000	0.002	0.001	0.000	0.001
F	0.000	0.000	0.000	0.000	0.000	0.000	0.000
Cl	0.005	0.006	0.007	0.004	0.005	0.004	0.003
Total	12.637	12.613	12.490	12.592	12.560	12.645	12.652
Tet Al	1.304	1.295	1.207	1.279	1.233	1.304	1.315
Oct Al	1.354	1.338	1.357	1.349	1.426	1.374	1.364
Total Al	2.659	2.633	2.564	2.628	2.659	2.679	2.679

Table D2: Electron microprobe results: chlorite atomic proportions

Element	385210.67.2	385210.67.3	385210.67.4	385210.70.1	385210.70.2	385210.70.3	385210.70.4
Si (IV)	2.717	2.669	2.614	2.693	2.591	2.596	2.576
Al (IV)	1.283	1.331	1.386	1.307	1.409	1.404	1.424
Al (VI)	1.361	1.372	1.423	1.336	1.425	1.425	1.423
Al (total)	2.644	2.703	2.809	2.643	2.834	2.829	2.846
FeO	2.469	2.524	2.509	2.509	2.584	2.576	2.608
MgO	2.079	2.030	1.993	2.082	1.922	1.929	1.912
MnO	0.031	0.028	0.031	0.027	0.027	0.027	0.028
CaO	0.003	0.002	0.001	0.002	0.004	0.002	0.003
Na2O	0.001	0.001	0.001	0.001	0.003	0.001	0.004
K2O	0.003	0.001	0.004	0.000	0.000	0.001	0.001
TiO2	0.004	0.006	0.005	0.006	0.005	0.006	0.006
Cr2O3	0.000	0.001	0.000	0.001	0.000	0.000	0.000
ZnO	0.004	0.006	0.005	0.008	0.007	0.006	0.006
V2O3	0.001	0.001	0.002	0.001	0.003	0.003	0.002
BaO	0.000	0.001	0.001	0.000	0.002	0.001	0.001
SrO	0.000	0.000	0.002	0.001	0.001	0.001	0.001
F	0.000	0.000	0.000	0.000	0.000	0.000	0.000
Cl	0.004	0.003	0.002	0.005	0.005	0.004	0.002
Total	12.604	12.678	12.788	12.623	12.822	12.812	12.842
Tet Al	1.283	1.331	1.386	1.307	1.409	1.404	1.424
Oct Al	1.361	1.372	1.423	1.336	1.425	1.425	1.423
Total Al	2.644	2.703	2.809	2.643	2.834	2.829	2.846

Table D2: Electron microprobe results: chlorite atomic proportions

Element	385210.71.1	385210.71.2	385210.73.1	385210.73.2	385210.73.3	385210.75.1	385210.75.2
Si (IV)	2.592	2.635	2.685	2.687	2.688	2.684	2.694
Al (IV)	1.408	1.365	1.315	1.313	1.312	1.316	1.306
Al (VI)	1.445	1.400	1.360	1.363	1.370	1.366	1.365
Al (total)	2.853	2.765	2.675	2.676	2.682	2.682	2.671
FeO	2.552	2.571	2.645	2.653	2.629	2.504	2.487
MgO	1.919	1.938	1.898	1.884	1.909	2.052	2.062
MnO	0.029	0.032	0.026	0.028	0.028	0.025	0.027
CaO	0.003	0.004	0.006	0.006	0.004	0.000	0.002
Na2O	0.004	0.005	0.005	0.004	0.003	0.003	0.005
K2O	0.004	0.003	0.002	0.003	0.001	0.001	0.001
TiO2	0.006	0.007	0.008	0.008	0.005	0.008	0.004
Cr2O3	0.001	0.001	0.000	0.000	0.001	0.001	0.000
ZnO	0.005	0.010	0.010	0.008	0.006	0.005	0.005
V2O3	0.003	0.001	0.004	0.004	0.005	0.000	0.002
BaO	0.001	0.000	0.000	0.000	0.001	0.000	0.000
SrO	0.001	0.001	0.000	0.001	0.000	0.000	0.001
F	0.000	0.000	0.000	0.000	0.000	0.000	0.000
Cl	0.005	0.008	0.007	0.010	0.003	0.003	0.007
Total	12.832	12.746	12.647	12.647	12.647	12.651	12.641
Tet Al	1.408	1.365	1.315	1.313	1.312	1.316	1.306
Oct Al	1.445	1.400	1.360	1.363	1.370	1.366	1.365
Total Al	2.853	2.765	2.675	2.676	2.682	2.682	2.671

Table D2: Electron microprobe results: chlorite atomic proportions

Element	385210.75.3	385210.75.4	385210.76.1	385210.76.2	385210.76.3	385210.76.4	385210.77.1
Si (IV)	2.677	2.666	2.716	2.676	2.688	2.707	2.710
Al (IV)	1.323	1.334	1.284	1.324	1.312	1.293	1.290
Al (VI)	1.365	1.353	1.329	1.341	1.342	1.337	1.349
Al (total)	2.688	2.687	2.613	2.665	2.654	2.631	2.639
FeO	2.509	2.540	2.496	2.500	2.502	2.494	2.490
MgO	2.062	2.037	2.099	2.085	2.077	2.081	2.071
MnO	0.027	0.025	0.025	0.025	0.027	0.030	0.026
CaO	0.001	0.002	0.002	0.003	0.002	0.002	0.003
Na2O	0.004	0.003	0.000	0.009	0.003	0.004	0.005
K2O	0.002	0.001	0.002	0.001	0.003	0.002	0.004
TiO2	0.002	0.009	0.004	0.006	0.006	0.006	0.005
Cr2O3	0.000	0.000	0.001	0.001	0.001	0.000	0.001
ZnO	0.002	0.006	0.008	0.004	0.007	0.008	0.005
V2O3	0.002	0.001	0.002	0.001	0.001	0.002	0.003
BaO	0.000	0.000	0.000	0.002	0.000	0.001	0.000
SrO	0.000	0.001	0.001	0.000	0.001	0.001	0.001
F	0.000	0.000	0.000	0.000	0.000	0.000	0.000
Cl	0.002	0.007	0.006	0.014	0.010	0.009	0.009
Total	12.668	12.671	12.587	12.657	12.637	12.606	12.610
Tet Al	1.323	1.334	1.284	1.324	1.312	1.293	1.290
Oct Al	1.365	1.353	1.329	1.341	1.342	1.337	1.349
Total Al	2.688	2.687	2.613	2.665	2.654	2.631	2.639

Table D2: Electron microprobe results: chlorite atomic proportions

Element	385210.77.2	385210.77.3	385210.78.1	385210.78.2	385210.78.3	385210.78.4	385210.79.1
Si (IV)	2.694	2.704	2.602	2.608	2.634	2.596	2.650
Al (IV)	1.306	1.296	1.398	1.392	1.366	1.404	1.350
Al (VI)	1.339	1.356	1.435	1.420	1.414	1.421	1.383
Al (total)	2.645	2.652	2.833	2.811	2.780	2.825	2.733
FeO	2.511	2.450	2.553	2.517	2.589	2.547	2.541
MgO	2.077	2.115	1.911	1.981	1.891	1.940	1.986
MnO	0.027	0.024	0.029	0.028	0.034	0.029	0.028
CaO	0.003	0.001	0.010	0.007	0.007	0.012	0.002
Na2O	0.001	0.001	0.007	0.003	0.007	0.006	0.007
K2O	0.002	0.002	0.002	0.000	0.000	0.001	0.001
TiO2	0.007	0.006	0.007	0.005	0.009	0.006	0.011
Cr2O3	0.000	0.001	0.000	0.001	0.001	0.000	0.001
ZnO	0.005	0.002	0.010	0.008	0.006	0.006	0.007
V2O3	0.001	0.002	0.001	0.001	0.002	0.000	0.002
BaO	0.001	0.000	0.000	0.000	0.002	0.001	0.002
SrO	0.000	0.000	0.000	0.002	0.000	0.000	0.000
F	0.000	0.000	0.000	0.000	0.000	0.000	0.000
Cl	0.004	0.004	0.017	0.014	0.011	0.024	0.005
Total	12.624	12.617	12.815	12.797	12.752	12.819	12.709
Tet Al	1.306	1.296	1.398	1.392	1.366	1.404	1.350
Oct Al	1.339	1.356	1.435	1.420	1.414	1.421	1.383
Total Al	2.645	2.652	2.833	2.811	2.780	2.825	2.733

Table D2: Electron microprobe results: chlorite atomic proportions

Element	385210.79.2	385210.79.4	385210.82.1	385210.82.2	385210.82.3	385210.82.4
Si (IV)	2.643	2.574	2.677	2.586	2.675	2.618
Al (IV)	1.357	1.426	1.323	1.414	1.325	1.382
Al (VI)	1.405	1.426	1.387	1.447	1.370	1.433
Al (total)	2.762	2.852	2.710	2.860	2.695	2.814
FeO	2.509	2.590	2.480	2.579	2.498	2.541
MgO	1.991	1.924	2.042	1.895	2.036	1.926
MnO	0.026	0.028	0.027	0.030	0.034	0.028
CaO	0.002	0.004	0.001	0.000	0.003	0.002
Na2O	0.007	0.003	0.007	0.007	0.011	0.006
K2O	0.002	0.001	0.002	0.001	0.002	0.002
TiO2	0.009	0.008	0.007	0.007	0.008	0.013
Cr2O3	0.000	0.000	0.001	0.001	0.001	0.000
ZnO	0.008	0.005	0.003	0.005	0.008	0.008
V2O3	0.003	0.001	0.003	0.003	0.001	0.002
BaO	0.002	0.001	0.001	0.000	0.000	0.002
SrO	0.001	0.000	0.001	0.000	0.000	0.001
F	0.000	0.000	0.000	0.000	0.000	0.000
Cl	0.007	0.004	0.004	0.002	0.004	0.004
Total	12.734	12.846	12.675	12.839	12.671	12.780
Tet Al	1.357	1.426	1.323	1.414	1.325	1.382
Oct Al	1.405	1.426	1.387	1.447	1.370	1.433
Total Al	2.762	2.852	2.710	2.860	2.695	2.814

Table D2: Electron microprobe results: chlorite atomic proportions

Element	385347.2.88.1	385347.2.88.2	385347.2.88.3	385347.2.88.4	385347.2.89.1	385347.2.89.2
Si (IV)	2.717	2.865	2.727	2.690	2.623	2.673
Al (IV)	1.283	1.135	1.273	1.310	1.377	1.327
Al (VI)	1.322	1.299	1.339	1.324	1.390	1.394
Al (total)	2.605	2.434	2.612	2.634	2.767	2.721
FeO	2.492	2.521	2.561	2.510	2.497	2.468
MgO	2.092	1.995	1.992	2.092	2.020	2.039
MnO	0.033	0.056	0.037	0.028	0.044	0.037
CaO	0.004	0.014	0.010	0.002	0.002	0.002
Na₂O	0.007	0.000	0.001	0.000	0.004	0.003
K₂O	0.001	0.002	0.003	0.002	0.000	0.001
TiO₂	0.007	0.008	0.004	0.008	0.006	0.005
Cr₂O₃	0.002	0.000	0.003	0.001	0.001	0.000
ZnO	0.003	0.004	0.004	0.005	0.009	0.005
V₂O₃	0.003	0.005	0.004	0.005	0.005	0.002
BaO	0.000	0.001	0.001	0.002	0.001	0.001
SrO	0.001	0.001	0.000	0.002	0.000	0.002
F	0.000	0.000	0.000	0.000	0.000	0.000
Cl	0.008	0.003	0.003	0.003	0.005	0.004
Total	12.581	12.343	12.573	12.618	12.753	12.685
Tet Al	1.283	1.135	1.273	1.310	1.377	1.327
Oct Al	1.322	1.299	1.339	1.324	1.390	1.394
Total Al	2.605	2.434	2.612	2.634	2.767	2.721

Table D2: Electron microprobe results: chlorite atomic proportions

Element	385347.2.89.3	385347.2.89.4	385347.2.89.5	385347.2.89.6	385347.2.90.1	385347.2.90.2
Si (IV)	2.638	2.629	2.591	2.631	2.644	2.615
Al (IV)	1.362	1.371	1.409	1.369	1.356	1.385
Al (VI)	1.377	1.395	1.376	1.403	1.401	1.413
Al (total)	2.739	2.765	2.786	2.771	2.757	2.798
FeO	2.506	2.533	2.524	2.541	2.540	2.529
MgO	2.046	1.988	2.045	1.976	1.979	1.979
MnO	0.036	0.042	0.043	0.036	0.027	0.036
CaO	0.003	0.001	0.000	0.001	0.000	0.000
Na₂O	0.001	0.008	0.001	0.006	0.005	0.004
K₂O	0.001	0.001	0.001	0.000	0.000	0.001
TiO₂	0.004	0.005	0.005	0.005	0.005	0.004
Cr₂O₃	0.001	0.000	0.000	0.000	0.000	0.000
ZnO	0.008	0.007	0.009	0.007	0.007	0.007
V₂O₃	0.002	0.002	0.002	0.004	0.006	0.004
BaO	0.000	0.000	0.002	0.000	0.001	0.000
SrO	0.002	0.001	0.000	0.000	0.001	0.001
F	0.000	0.000	0.000	0.000	0.000	0.000
Cl	0.001	0.003	0.003	0.001	0.000	0.003
Total	12.728	12.752	12.798	12.750	12.730	12.782
Tet Al	1.362	1.371	1.409	1.369	1.356	1.385
Oct Al	1.377	1.395	1.376	1.403	1.401	1.413
Total Al	2.739	2.765	2.786	2.771	2.757	2.798

Table D2: Electron microprobe results: chlorite atomic proportions

Element	385347.2.90.3	385347.2.90.4	385347.2.90.5	385347.2.90.6	385347.2.91.2	385347.2.91.3
Si (IV)	2.607	2.617	2.607	2.667	2.615	2.607
Al (IV)	1.393	1.383	1.393	1.333	1.385	1.393
Al (VI)	1.398	1.417	1.395	1.371	1.379	1.391
Al (total)	2.791	2.800	2.788	2.704	2.764	2.784
FeO	2.531	2.544	2.550	2.547	2.578	2.567
MgO	2.003	1.956	1.979	1.980	1.970	1.972
MnO	0.038	0.034	0.035	0.039	0.039	0.037
CaO	0.001	0.003	0.013	0.017	0.003	0.001
Na₂O	0.004	0.007	0.005	0.004	0.004	0.002
K₂O	0.001	0.002	0.001	0.000	0.002	0.000
TiO₂	0.005	0.004	0.006	0.007	0.005	0.004
Cr₂O₃	0.000	0.001	0.001	0.001	0.001	0.001
ZnO	0.005	0.010	0.004	0.003	0.006	0.011
V₂O₃	0.002	0.004	0.003	0.003	0.005	0.004
BaO	0.001	0.001	0.000	0.000	0.000	0.001
SrO	0.001	0.001	0.001	0.001	0.000	0.001
F	0.000	0.000	0.000	0.000	0.000	0.000
Cl	0.002	0.000	0.003	0.001	0.006	0.004
Total	12.785	12.781	12.783	12.679	12.763	12.780
Tet Al	1.393	1.383	1.393	1.333	1.385	1.393
Oct Al	1.398	1.417	1.395	1.371	1.379	1.391
Total Al	2.791	2.800	2.788	2.704	2.764	2.784

Table D2: Electron microprobe results: chlorite atomic proportions

Element	385347.2.91.4	385347.2.91.5	385347.2.91.6	385347.2.91.7	385347.2.91.8	385347.2.91.9
Si (IV)	2.597	2.604	2.605	2.635	2.619	2.624
Al (IV)	1.403	1.396	1.395	1.365	1.381	1.376
Al (VI)	1.389	1.397	1.375	1.385	1.395	1.405
Al (total)	2.792	2.794	2.770	2.750	2.775	2.781
FeO	2.552	2.557	2.541	2.540	2.562	2.520
MgO	1.993	1.980	2.026	2.008	1.972	1.990
MnO	0.039	0.037	0.039	0.037	0.037	0.043
CaO	0.002	0.000	0.001	0.000	0.000	0.000
Na₂O	0.003	0.002	0.007	0.000	0.000	0.001
K₂O	0.002	0.000	0.001	0.000	0.000	0.000
TiO₂	0.006	0.004	0.004	0.003	0.005	0.006
Cr₂O₃	0.001	0.000	0.000	0.001	0.001	0.001
ZnO	0.008	0.007	0.010	0.007	0.006	0.009
V₂O₃	0.005	0.005	0.003	0.001	0.004	0.002
BaO	0.000	0.001	0.000	0.001	0.001	0.001
SrO	0.001	0.002	0.001	0.000	0.001	0.000
F	0.000	0.000	0.000	0.000	0.000	0.000
Cl	0.001	0.001	0.002	0.002	0.001	0.002
Total	12.793	12.788	12.780	12.737	12.762	12.760
Tet Al	1.403	1.396	1.395	1.365	1.381	1.376
Oct Al	1.389	1.397	1.375	1.385	1.395	1.405
Total Al	2.792	2.794	2.770	2.750	2.775	2.781

Table D2: Electron microprobe results: chlorite atomic proportions

Element	385347.2.91.10	385347.2.91.11	385347.2.91.12	385011.92.1	385011.92.2	385011.92.3
Si (IV)	2.619	2.624	2.640	2.736	2.738	3.134
Al (IV)	1.381	1.376	1.360	1.264	1.262	0.866
Al (VI)	1.377	1.371	1.371	1.321	1.307	1.414
Al (total)	2.758	2.747	2.731	2.586	2.569	2.280
FeO	2.613	2.524	2.588	2.262	2.273	1.942
MgO	1.957	2.038	1.978	2.272	2.288	1.896
MnO	0.030	0.038	0.028	0.061	0.061	0.046
CaO	0.000	0.000	0.000	0.009	0.007	0.006
Na2O	0.002	0.004	0.003	0.025	0.016	0.025
K2O	0.000	0.001	0.000	0.010	0.004	0.491
TiO2	0.004	0.006	0.005	0.005	0.006	0.070
Cr2O3	0.000	0.002	0.000	0.000	0.001	0.001
ZnO	0.007	0.008	0.008	0.007	0.007	0.004
V2O3	0.003	0.003	0.002	0.000	0.000	0.002
BaO	0.001	0.000	0.003	0.000	0.001	0.003
SrO	0.001	0.001	0.001	0.000	0.000	0.001
F	0.000	0.000	0.000	0.000	0.000	0.000
Cl	0.002	0.002	0.004	0.015	0.012	0.014
Total	12.756	12.745	12.722	12.573	12.553	12.196
Tet Al	1.381	1.376	1.360	1.264	1.262	0.866
Oct Al	1.377	1.371	1.371	1.321	1.307	1.414
Total Al	2.758	2.747	2.731	2.586	2.569	2.280

Table D2: Electron microprobe results: chlorite atomic proportions

Element	385011.92.4	385011.103.1	385011.103.2	385011.103.3	385011.103.4	385011.109.1
Si (IV)	2.746	2.787	2.728	2.718	2.784	2.734
Al (IV)	1.254	1.213	1.272	1.282	1.216	1.266
Al (VI)	1.311	1.309	1.314	1.320	1.309	1.324
Al (total)	2.566	2.522	2.586	2.602	2.525	2.590
FeO	2.267	2.367	2.454	2.383	2.415	2.516
MgO	2.261	2.130	2.091	2.169	2.119	2.032
MnO	0.061	0.048	0.052	0.050	0.051	0.051
CaO	0.011	0.022	0.016	0.010	0.020	0.004
Na₂O	0.025	0.036	0.022	0.026	0.016	0.008
K₂O	0.023	0.025	0.005	0.004	0.003	0.000
TiO₂	0.007	0.011	0.010	0.008	0.008	0.013
Cr₂O₃	0.000	0.001	0.001	0.000	0.001	0.000
ZnO	0.006	0.007	0.005	0.005	0.006	0.004
V₂O₃	0.001	0.000	0.003	0.002	0.001	0.002
BaO	0.001	0.000	0.001	0.001	0.000	0.000
SrO	0.001	0.001	0.001	0.001	0.001	0.003
F	0.000	0.000	0.000	0.000	0.000	0.000
Cl	0.014	0.018	0.011	0.007	0.007	0.003
Total	12.557	12.497	12.570	12.591	12.481	12.551
Tet Al	1.254	1.213	1.272	1.282	1.216	1.266
Oct Al	1.311	1.309	1.314	1.320	1.309	1.324
Total Al	2.566	2.522	2.586	2.602	2.525	2.590

Table D2: Electron microprobe results: chlorite atomic proportions

Element	385011.109.2	385011.109.4	385025.121.1	385025.121.2	385025.121.4	385025.122.1
Si (IV)	2.731	2.816	2.698	2.701	2.722	2.725
Al (IV)	1.269	1.184	1.302	1.299	1.278	1.275
Al (VI)	1.288	1.300	1.348	1.343	1.360	1.364
Al (total)	2.557	2.484	2.649	2.642	2.638	2.639
FeO	2.571	2.474	2.387	2.390	2.384	2.455
MgO	2.026	2.040	2.159	2.149	2.123	2.049
MnO	0.055	0.050	0.052	0.054	0.053	0.053
CaO	0.003	0.025	0.003	0.003	0.002	0.006
Na ₂ O	0.002	0.019	0.003	0.009	0.009	0.006
K ₂ O	0.001	0.004	0.001	0.003	0.005	0.005
TiO ₂	0.017	0.011	0.006	0.009	0.008	0.005
Cr ₂ O ₃	0.000	0.000	0.001	0.000	0.000	0.000
ZnO	0.005	0.005	0.004	0.006	0.007	0.004
V ₂ O ₃	0.001	0.002	0.002	0.000	0.001	0.001
BaO	0.002	0.001	0.001	0.001	0.001	0.001
SrO	0.001	0.001	0.000	0.001	0.001	0.002
F	0.000	0.000	0.000	0.000	0.000	0.000
Cl	0.001	0.013	0.004	0.008	0.003	0.006
Total	12.532	12.429	12.622	12.619	12.596	12.596
Tet Al	1.269	1.184	1.302	1.299	1.278	1.275
Oct Al	1.288	1.300	1.348	1.343	1.360	1.364
Total Al	2.557	2.484	2.649	2.642	2.638	2.639

Table D2: Electron microprobe results: chlorite atomic proportions

Element	385025.122.3	385025.122.4	385025.135.1	385025.135.2	385025.135.3	385025.136.1
Si (IV)	2.723	2.708	2.720	2.746	2.739	2.795
Al (IV)	1.277	1.292	1.280	1.254	1.261	1.205
Al (VI)	1.320	1.338	1.341	1.364	1.357	1.065
Al (total)	2.597	2.630	2.622	2.618	2.618	2.270
FeO	2.339	2.396	2.310	2.350	2.327	2.050
MgO	2.226	2.142	2.241	2.170	2.202	1.809
MnO	0.052	0.053	0.044	0.036	0.034	0.039
CaO	0.003	0.005	0.002	0.002	0.002	0.440
Na₂O	0.008	0.013	0.001	0.003	0.004	0.008
K₂O	0.006	0.006	0.000	0.002	0.002	0.005
TiO₂	0.009	0.008	0.010	0.006	0.008	0.315
Cr₂O₃	0.000	0.001	0.000	0.000	0.001	0.000
ZnO	0.004	0.006	0.005	0.002	0.003	0.004
V₂O₃	0.001	0.002	0.001	0.001	0.000	0.003
BaO	0.000	0.000	0.002	0.000	0.002	0.018
SrO	0.003	0.001	0.000	0.001	0.000	0.002
F	0.000	0.000	0.000	0.000	0.000	0.000
Cl	0.007	0.010	0.002	0.002	0.007	0.002
Total	12.574	12.609	12.582	12.559	12.566	12.030
Tet Al	1.277	1.292	1.280	1.254	1.261	1.205
Oct Al	1.320	1.338	1.341	1.364	1.357	1.065
Total Al	2.597	2.630	2.622	2.618	2.618	2.270

Table D2: Electron microprobe results: chlorite atomic proportions

Element	385025.136.2	385025.136.3	385199.154.1	385199.154.2	385199.154.3	385199.154.4
Si (IV)	2.816	3.272	2.635	2.638	2.629	2.640
Al (IV)	1.184	0.728	1.365	1.362	1.371	1.360
Al (VI)	1.316	1.457	1.377	1.378	1.382	1.392
Al (total)	2.500	2.185	2.741	2.740	2.753	2.752
FeO	2.464	2.030	2.531	2.507	2.565	2.548
MgO	2.081	1.605	2.026	2.050	1.980	1.989
MnO	0.041	0.030	0.024	0.023	0.023	0.022
CaO	0.001	0.048	0.000	0.001	0.003	0.001
Na ₂ O	0.002	0.008	0.002	0.002	0.002	0.006
K ₂ O	0.006	0.638	0.001	0.005	0.002	0.003
TiO ₂	0.009	0.066	0.013	0.010	0.008	0.009
Cr ₂ O ₃	0.000	0.000	0.001	0.002	0.001	0.000
ZnO	0.003	0.005	0.004	0.002	0.006	0.007
V ₂ O ₃	0.002	0.000	0.000	0.002	0.003	0.000
BaO	0.000	0.003	0.001	0.001	0.002	0.000
SrO	0.000	0.000	0.001	0.001	0.001	0.000
F	0.000	0.000	0.000	0.000	0.000	0.000
Cl	0.001	0.002	0.001	0.001	0.013	0.001
Total	12.428	12.078	12.724	12.724	12.744	12.731
Tet Al	1.184	0.728	1.365	1.362	1.371	1.360
Oct Al	1.316	1.457	1.377	1.378	1.382	1.392
Total Al	2.500	2.185	2.741	2.740	2.753	2.752

Table D2: Electron microprobe results: chlorite atomic proportions

Element	385199.155.1	385199.155.2	385199.155.3	385199.155.4	385336.2.156.1	385336.2.156.2
Si (IV)	2.601	2.618	2.605	2.632	2.723	2.747
Al (IV)	1.399	1.382	1.395	1.368	1.277	1.253
Al (VI)	1.388	1.386	1.400	1.361	1.331	1.317
Al (total)	2.787	2.768	2.795	2.729	2.608	2.571
FeO	2.503	2.551	2.525	2.569	2.061	2.051
MgO	2.058	1.980	2.020	2.016	2.508	2.524
MnO	0.024	0.025	0.022	0.024	0.035	0.038
CaO	0.001	0.001	0.001	0.000	0.005	0.003
Na2O	0.003	0.016	0.008	0.002	0.000	0.007
K2O	0.003	0.008	0.001	0.003	0.002	0.001
TiO2	0.006	0.006	0.008	0.007	0.004	0.007
Cr2O3	0.004	0.001	0.001	0.001	0.001	0.001
ZnO	0.005	0.006	0.004	0.003	0.010	0.006
V2O3	0.002	0.001	0.001	0.002	0.004	0.002
BaO	0.000	0.002	0.001	0.001	0.001	0.000
SrO	0.001	0.001	0.000	0.001	0.000	0.001
F	0.000	0.000	0.000	0.000	0.000	0.000
Cl	0.005	0.022	0.001	0.009	0.009	0.006
Total	12.788	12.776	12.789	12.729	12.578	12.537
Tet Al	1.399	1.382	1.395	1.368	1.277	1.253
Oct Al	1.388	1.386	1.400	1.361	1.331	1.317
Total Al	2.787	2.768	2.795	2.729	2.608	2.571

Table D2: Electron microprobe results: chlorite atomic proportions

Element	385336.2.156.3	385336.2.156.4	385336.2.157.1	385336.2.157.2	385336.2.157.3
Si (IV)	2.748	2.706	2.760	2.709	2.729
Al (IV)	1.252	1.294	1.240	1.291	1.271
Al (VI)	1.315	1.337	1.273	1.302	1.289
Al (total)	2.567	2.631	2.513	2.592	2.560
FeO	2.079	2.026	2.130	2.224	2.212
MgO	2.496	2.525	2.511	2.388	2.401
MnO	0.036	0.043	0.032	0.033	0.034
CaO	0.004	0.006	0.002	0.002	0.002
Na ₂ O	0.011	0.016	0.000	0.005	0.008
K ₂ O	0.001	0.004	0.000	0.003	0.001
TiO ₂	0.005	0.004	0.005	0.006	0.005
Cr ₂ O ₃	0.001	0.001	0.005	0.003	0.011
ZnO	0.007	0.005	0.004	0.006	0.005
V ₂ O ₃	0.004	0.005	0.006	0.006	0.006
BaO	0.000	0.000	0.001	0.001	0.001
SrO	0.001	0.000	0.001	0.000	0.000
F	0.000	0.000	0.000	0.000	0.000
Cl	0.011	0.013	0.003	0.011	0.010
Total	12.537	12.615	12.486	12.583	12.544
Tet Al	1.252	1.294	1.240	1.291	1.271
Oct Al	1.315	1.337	1.273	1.302	1.289
Total Al	2.567	2.631	2.513	2.592	2.560

Table D2: Electron microprobe results: chlorite atomic proportions

Element	385336.2.157.4	385336.2.159.1	385336.2.159.2	385336.2.159.3	385336.2.159.4
Si (IV)	2.705	2.748	2.782	2.800	2.733
Al (IV)	1.295	1.252	1.218	1.200	1.267
Al (VI)	1.303	1.311	1.274	1.293	1.285
Al (total)	2.598	2.563	2.493	2.493	2.552
FeO	2.165	2.182	2.185	2.086	2.220
MgO	2.439	2.399	2.433	2.483	2.404
MnO	0.033	0.031	0.036	0.033	0.032
CaO	0.002	0.001	0.002	0.004	0.002
Na₂O	0.016	0.004	0.009	0.007	0.006
K₂O	0.001	0.001	0.001	0.001	0.000
TiO₂	0.005	0.008	0.005	0.006	0.005
Cr₂O₃	0.007	0.007	0.005	0.006	0.008
ZnO	0.006	0.007	0.004	0.006	0.005
V₂O₃	0.008	0.006	0.005	0.007	0.006
BaO	0.001	0.001	0.001	0.001	0.002
SrO	0.001	0.001	0.001	0.002	0.002
F	0.000	0.000	0.000	0.000	0.000
Cl	0.010	0.001	0.009	0.012	0.005
Total	12.593	12.522	12.462	12.441	12.534
Tet Al	1.295	1.252	1.218	1.200	1.267
Oct Al	1.303	1.311	1.274	1.293	1.285
Total Al	2.598	2.563	2.493	2.493	2.552

Table D2: Electron microprobe results: chlorite atomic proportions

Element	385336.2.160.1	385336.2.160.2	385336.2.160.3	385336.2.160.4	385336.2.161.1
Si (IV)	2.745	2.720	2.741	2.731	2.711
Al (IV)	1.255	1.280	1.259	1.269	1.289
Al (VI)	1.284	1.332	1.319	1.308	1.277
Al (total)	2.539	2.612	2.578	2.577	2.567
FeO	2.211	2.198	2.180	2.227	2.257
MgO	2.411	2.362	2.386	2.358	2.399
MnO	0.031	0.032	0.029	0.034	0.035
CaO	0.003	0.002	0.002	0.002	0.003
Na₂O	0.005	0.007	0.011	0.009	0.004
K₂O	0.000	0.002	0.002	0.002	0.002
TiO₂	0.005	0.004	0.004	0.007	0.005
Cr₂O₃	0.003	0.004	0.003	0.003	0.001
ZnO	0.009	0.009	0.009	0.006	0.004
V₂O₃	0.006	0.008	0.006	0.007	0.005
BaO	0.001	0.001	0.000	0.001	0.002
SrO	0.001	0.000	0.000	0.001	0.000
F	0.000	0.000	0.000	0.000	0.000
Cl	0.011	0.008	0.017	0.013	0.009
Total	12.520	12.582	12.550	12.554	12.570
Tet Al	1.255	1.280	1.259	1.269	1.289
Oct Al	1.284	1.332	1.319	1.308	1.277
Total Al	2.539	2.612	2.578	2.577	2.567

Table D2: Electron microprobe results: chlorite atomic proportions

Element	385336.2.161.2	385336.2.161.3	385336.2.161.4	385336.2.162.1	385336.2.162.2
Si (IV)	2.721	2.725	2.726	2.739	2.703
Al (IV)	1.279	1.275	1.274	1.261	1.297
Al (VI)	1.308	1.297	1.307	1.306	1.305
Al (total)	2.587	2.572	2.581	2.566	2.603
FeO	2.144	2.184	2.132	2.184	2.132
MgO	2.469	2.428	2.482	2.429	2.483
MnO	0.035	0.035	0.032	0.032	0.036
CaO	0.001	0.003	0.001	0.002	0.002
Na₂O	0.001	0.012	0.006	0.003	0.006
K₂O	0.001	0.000	0.000	0.000	0.002
TiO₂	0.005	0.005	0.007	0.004	0.006
Cr₂O₃	0.001	0.001	0.000	0.001	0.000
ZnO	0.002	0.007	0.002	0.003	0.004
V₂O₃	0.005	0.006	0.004	0.004	0.006
BaO	0.000	0.000	0.000	0.000	0.000
SrO	0.001	0.000	0.000	0.001	0.001
F	0.000	0.000	0.000	0.000	0.000
Cl	0.007	0.016	0.006	0.006	0.011
Total	12.566	12.563	12.560	12.540	12.596
Tet Al	1.279	1.275	1.274	1.261	1.297
Oct Al	1.308	1.297	1.307	1.306	1.305
Total Al	2.587	2.572	2.581	2.566	2.603

Table D2: Electron microprobe results: chlorite atomic proportions

Element	385336.2.162.4	385336.2.163.1	385336.2.163.2	385336.2.163.3	385336.2.163.4
Si (IV)	2.723	2.740	2.691	2.707	2.707
Al (IV)	1.277	1.260	1.309	1.293	1.293
Al (VI)	1.301	1.278	1.296	1.305	1.315
Al (total)	2.578	2.538	2.605	2.597	2.608
FeO	2.117	2.074	2.147	2.062	2.123
MgO	2.492	2.553	2.476	2.546	2.474
MnO	0.036	0.039	0.040	0.039	0.036
CaO	0.001	0.001	0.001	0.002	0.002
Na ₂ O	0.004	0.005	0.002	0.000	0.000
K ₂ O	0.002	0.002	0.000	0.000	0.000
TiO ₂	0.008	0.003	0.005	0.005	0.004
Cr ₂ O ₃	0.001	0.006	0.008	0.007	0.007
ZnO	0.006	0.007	0.009	0.005	0.008
V ₂ O ₃	0.006	0.004	0.006	0.005	0.006
BaO	0.000	0.001	0.001	0.000	0.000
SrO	0.002	0.003	0.000	0.000	0.000
F	0.000	0.000	0.000	0.000	0.000
Cl	0.005	0.013	0.004	0.008	0.005
Total	12.559	12.528	12.602	12.582	12.588
Tet Al	1.277	1.260	1.309	1.293	1.293
Oct Al	1.301	1.278	1.296	1.305	1.315
Total Al	2.578	2.538	2.605	2.597	2.608

Table D2: Electron microprobe results: chlorite atomic proportions

Element	385336.2.164.1	385336.2.164.2	385336.2.164.3	385336.2.164.4	385336.2.166.1
Si (IV)	2.733	2.743	2.725	2.714	2.703
Al (IV)	1.267	1.257	1.275	1.286	1.297
Al (VI)	1.302	1.271	1.287	1.295	1.295
Al (total)	2.569	2.528	2.561	2.582	2.592
FeO	2.094	2.055	2.114	2.082	2.087
MgO	2.498	2.569	2.510	2.519	2.519
MnO	0.041	0.040	0.037	0.040	0.039
CaO	0.002	0.002	0.002	0.003	0.003
Na₂O	0.002	0.005	0.003	0.004	0.010
K₂O	0.002	0.001	0.000	0.000	0.001
TiO₂	0.005	0.005	0.005	0.006	0.004
Cr₂O₃	0.009	0.011	0.009	0.012	0.008
ZnO	0.006	0.004	0.004	0.010	0.006
V₂O₃	0.006	0.007	0.006	0.006	0.007
BaO	0.000	0.001	0.000	0.000	0.000
SrO	0.000	0.000	0.001	0.001	0.000
F	0.000	0.000	0.000	0.000	0.000
Cl	0.007	0.015	0.009	0.007	0.021
Total	12.542	12.513	12.547	12.566	12.592
Tet Al	1.267	1.257	1.275	1.286	1.297
Oct Al	1.302	1.271	1.287	1.295	1.295
Total Al	2.569	2.528	2.561	2.582	2.592

Table D2: Electron microprobe results: chlorite atomic proportions

Element	385336.2.166.2	385336.2.166.3	385336.2.166.4
Si (IV)	2.741	2.724	2.750
Al (IV)	1.259	1.276	1.250
Al (VI)	1.283	1.289	1.285
Al (total)	2.542	2.565	2.535
FeO	2.063	2.075	2.026
MgO	2.546	2.523	2.581
MnO	0.037	0.040	0.041
CaO	0.003	0.004	0.002
Na₂O	0.003	0.012	0.001
K₂O	0.000	0.002	0.000
TiO₂	0.005	0.004	0.005
Cr₂O₃	0.014	0.012	0.010
ZnO	0.008	0.008	0.008
V₂O₃	0.005	0.006	0.005
BaO	0.000	0.001	0.000
SrO	0.001	0.000	0.000
F	0.000	0.000	0.000
Cl	0.007	0.015	0.008
Total	12.518	12.556	12.508
Tet Al	1.259	1.276	1.250
Oct Al	1.283	1.289	1.285
Total Al	2.542	2.565	2.535

Table D3: Electron microprobe results: biotite atomic proportions

Element	385230.1.1	385230.1.2	385230.1.3	385230.1.4	385230.2.1	385230.2.2	385230.2.3
Si (IV)	2.701	2.733	2.695	2.679	3.229	3.242	3.241
Al (IV)	1.299	1.267	1.305	1.321	0.771	0.758	0.759
Al (VI)	0.417	0.476	0.438	0.416	1.780	1.777	1.691
Al (total)	1.716	1.743	1.743	1.738	2.551	2.535	2.450
FeO	1.267	1.266	1.298	1.337	0.117	0.131	0.178
MgO	1.034	0.962	1.064	1.096	0.140	0.162	0.224
MnO	0.017	0.016	0.022	0.021	0.001	0.001	0.003
CaO	0.001	0.000	0.001	0.002	0.001	0.000	0.000
Na₂O	0.011	0.010	0.010	0.012	0.042	0.044	0.040
K₂O	0.912	0.927	0.861	0.826	0.696	0.692	0.687
TiO₂	0.093	0.103	0.085	0.080	0.041	0.021	0.035
ZnO	0.004	0.000	0.004	0.001	0.000	0.000	0.000
BaO	0.000	0.000	0.000	0.000	0.006	0.006	0.005
SrO	0.001	0.001	0.001	0.000	0.001	0.000	0.000
F	0.104	0.000	0.000	0.000	0.000	0.000	0.000
Cl	0.001	0.001	0.003	0.002	0.001	0.001	0.001
Total	9.578	9.504	9.528	9.530	9.376	9.373	9.313
Tet Al	1.299	1.267	1.305	1.321	0.771	0.758	0.759
Oct Al	0.417	0.476	0.438	0.416	1.780	1.777	1.691
Total Al	1.716	1.743	1.743	1.738	2.551	2.535	2.450

Table D3: Electron microprobe results: biotite atomic proportions

Element	385230.2.4	385230.4.1	385230.4.2	385230.4.3	385230.4.4	385230.5.1	385230.5.2
Si (IV)	3.271	2.687	2.712	2.742	2.718	2.732	2.716
Al (IV)	0.729	1.313	1.288	1.258	1.282	1.268	1.284
Al (VI)	1.724	0.373	0.400	0.416	0.359	0.443	0.449
Al (total)	2.453	1.686	1.688	1.674	1.641	1.711	1.733
FeO	0.139	1.376	1.342	1.318	1.348	1.301	1.296
MgO	0.192	1.087	1.028	1.036	0.988	1.042	1.043
MnO	0.002	0.019	0.017	0.017	0.017	0.018	0.018
CaO	0.000	0.003	0.002	0.000	0.001	0.001	0.001
Na₂O	0.039	0.010	0.010	0.013	0.007	0.011	0.010
K₂O	0.664	0.806	0.866	0.888	0.903	0.889	0.891
TiO₂	0.043	0.100	0.105	0.089	0.121	0.075	0.078
ZnO	0.000	0.001	0.005	0.003	0.003	0.003	0.002
BaO	0.007	0.000	0.000	0.000	0.000	0.000	0.000
SrO	0.001	0.001	0.002	0.000	0.001	0.002	0.000
F	0.000	0.000	0.000	0.000	0.095	0.000	0.000
Cl	0.002	0.003	0.001	0.002	0.002	0.003	0.002
Total	9.264	9.465	9.466	9.458	9.485	9.500	9.523
Tet Al	0.729	1.313	1.288	1.258	1.282	1.268	1.284
Oct Al	1.724	0.373	0.400	0.416	0.359	0.443	0.449
Total Al	2.453	1.686	1.688	1.674	1.641	1.711	1.733

Table D3: Electron microprobe results: biotite atomic proportions

Element	385230.5.3	385230.5.4	385230.6.1	385230.6.2	385230.6.3	385230.6.4	385230.7.1
Si (IV)	2.722	2.763	2.747	2.731	2.762	2.760	2.736
Al (IV)	1.278	1.237	1.253	1.269	1.238	1.240	1.264
Al (VI)	0.462	0.431	0.456	0.424	0.449	0.455	0.450
Al (total)	1.739	1.667	1.709	1.692	1.687	1.695	1.714
FeO	1.307	1.286	1.278	1.260	1.274	1.267	1.306
MgO	1.005	1.041	1.026	1.054	1.021	1.029	1.025
MnO	0.018	0.018	0.017	0.017	0.017	0.017	0.017
CaO	0.001	0.002	0.000	0.000	0.000	0.018	0.000
Na₂O	0.006	0.010	0.007	0.010	0.015	0.021	0.010
K₂O	0.921	0.908	0.922	0.883	0.922	0.860	0.903
TiO₂	0.074	0.081	0.076	0.076	0.081	0.078	0.075
ZnO	0.003	0.003	0.003	0.002	0.002	0.006	0.002
BaO	0.000	0.000	0.000	0.000	0.000	0.000	0.000
SrO	0.001	0.001	0.001	0.002	0.001	0.001	0.000
F	0.000	0.000	0.000	0.129	0.000	0.000	0.000
Cl	0.001	0.001	0.000	0.000	0.002	0.008	0.001
Total	9.537	9.448	9.496	9.549	9.470	9.454	9.503
Tet Al	1.278	1.237	1.253	1.269	1.238	1.240	1.264
Oct Al	0.462	0.431	0.456	0.424	0.449	0.455	0.450
Total Al	1.739	1.667	1.709	1.692	1.687	1.695	1.714

Table D3: Electron microprobe results: biotite atomic proportions

Element	385230.7.2	385230.7.3	385230.7.4	385230.8.1	385230.8.2	385230.8.3	385230.8.4
Si (IV)	2.731	2.734	2.723	2.770	2.754	2.754	2.757
Al (IV)	1.269	1.266	1.277	1.230	1.246	1.246	1.243
Al (VI)	0.430	0.460	0.437	0.454	0.418	0.441	0.446
Al (total)	1.699	1.726	1.714	1.684	1.663	1.688	1.689
FeO	1.267	1.284	1.278	1.271	1.288	1.280	1.286
MgO	1.041	1.014	1.021	1.046	1.010	1.036	1.052
MnO	0.016	0.016	0.016	0.017	0.017	0.015	0.016
CaO	0.000	0.000	0.000	0.002	0.001	0.001	0.001
Na2O	0.014	0.008	0.009	0.011	0.013	0.013	0.011
K2O	0.912	0.934	0.922	0.896	0.895	0.886	0.887
TiO2	0.075	0.077	0.076	0.070	0.086	0.067	0.073
ZnO	0.001	0.002	0.003	0.002	0.003	0.003	0.002
BaO	0.000	0.000	0.000	0.000	0.000	0.000	0.000
SrO	0.000	0.001	0.000	0.000	0.001	0.000	0.001
F	0.101	0.000	0.092	0.000	0.100	0.085	0.000
Cl	0.001	0.002	0.000	0.004	0.001	0.000	0.001
Total	9.556	9.525	9.570	9.457	9.497	9.515	9.464
Tet Al	1.269	1.266	1.277	1.230	1.246	1.246	1.243
Oct Al	0.430	0.460	0.437	0.454	0.418	0.441	0.446
Total Al	1.699	1.726	1.714	1.684	1.663	1.688	1.689

Table D3: Electron microprobe results: biotite atomic proportions

Element	385230.10.1	385230.10.2	385230.10.3	385230.10.4	385230.11.1	385230.11.2	385230.11.3
Si (IV)	2.720	2.720	2.727	2.720	2.717	2.717	2.714
Al (IV)	1.280	1.280	1.273	1.280	1.283	1.283	1.286
Al (VI)	0.419	0.418	0.414	0.450	0.431	0.435	0.425
Al (total)	1.699	1.698	1.686	1.730	1.713	1.718	1.710
FeO	1.349	1.346	1.353	1.305	1.301	1.322	1.307
MgO	0.991	1.011	0.994	1.005	1.030	1.011	1.035
MnO	0.018	0.017	0.018	0.018	0.016	0.017	0.016
CaO	0.001	0.002	0.001	0.003	0.004	0.004	0.004
Na2O	0.016	0.007	0.008	0.015	0.016	0.007	0.021
K2O	0.934	0.910	0.923	0.903	0.898	0.907	0.891
TiO2	0.087	0.088	0.090	0.086	0.092	0.087	0.091
ZnO	0.002	0.001	0.003	0.001	0.002	0.003	0.002
BaO	0.000	0.000	0.000	0.001	0.000	0.000	0.000
SrO	0.002	0.001	0.000	0.000	0.000	0.000	0.001
F	0.000	0.000	0.000	0.000	0.000	0.000	0.000
Cl	0.001	0.002	0.000	0.002	0.002	0.000	0.002
Total	9.518	9.500	9.492	9.520	9.505	9.512	9.506
Tet Al	1.280	1.280	1.273	1.280	1.283	1.283	1.286
Oct Al	0.419	0.418	0.414	0.450	0.431	0.435	0.425
Total Al	1.699	1.698	1.686	1.730	1.713	1.718	1.710

Table D3: Electron microprobe results: biotite atomic proportions

Element	385230.11.4	385230.12.1	385230.12.2	385230.12.3	385230.12.4	385230.13.1	385230.13.2
Si (IV)	2.791	2.700	2.695	2.699	2.644	2.684	2.748
Al (IV)	1.209	1.300	1.305	1.301	1.356	1.316	1.252
Al (VI)	0.463	0.422	0.409	0.391	0.363	0.419	0.436
Al (total)	1.673	1.722	1.714	1.692	1.719	1.735	1.689
FeO	1.259	1.344	1.355	1.385	1.451	1.380	1.295
MgO	0.992	1.002	1.038	1.021	1.104	1.083	1.069
MnO	0.015	0.018	0.016	0.016	0.020	0.024	0.017
CaO	0.005	0.003	0.002	0.001	0.002	0.001	0.002
Na₂O	0.015	0.009	0.011	0.010	0.013	0.009	0.021
K₂O	0.905	0.934	0.865	0.891	0.746	0.833	0.887
TiO₂	0.087	0.088	0.095	0.093	0.088	0.060	0.064
ZnO	0.002	0.001	0.000	0.001	0.000	0.001	0.003
BaO	0.000	0.000	0.000	0.000	0.000	0.000	0.001
SrO	0.001	0.001	0.000	0.001	0.000	0.001	0.000
F	0.000	0.000	0.000	0.000	0.000	0.000	0.000
Cl	0.001	0.002	0.001	0.002	0.001	0.000	0.003
Total	9.419	9.546	9.506	9.505	9.507	9.545	9.488
Tet Al	1.209	1.300	1.305	1.301	1.356	1.316	1.252
Oct Al	0.463	0.422	0.409	0.391	0.363	0.419	0.436
Total Al	1.673	1.722	1.714	1.692	1.719	1.735	1.689

Table D3: Electron microprobe results: biotite atomic proportions

Element	385230.13.3	385230.13.4	385230.14.1	385230.14.2	385230.14.3	385230.14.4	385230.15.1
Si (IV)	2.733	2.741	2.701	2.634	2.666	2.667	2.677
Al (IV)	1.267	1.259	1.299	1.366	1.334	1.333	1.323
Al (VI)	0.457	0.423	0.421	0.383	0.414	0.409	0.378
Al (total)	1.724	1.683	1.720	1.749	1.748	1.741	1.701
FeO	1.302	1.312	1.346	1.418	1.373	1.391	1.384
MgO	1.052	1.085	1.025	1.141	1.066	1.063	1.101
MnO	0.016	0.017	0.017	0.025	0.022	0.020	0.018
CaO	0.001	0.000	0.000	0.004	0.002	0.001	0.003
Na2O	0.007	0.015	0.013	0.014	0.008	0.006	0.010
K2O	0.908	0.910	0.890	0.721	0.822	0.838	0.814
TiO2	0.059	0.058	0.087	0.075	0.082	0.076	0.059
ZnO	0.000	0.001	0.003	0.000	0.003	0.003	0.000
BaO	0.000	0.000	0.000	0.000	0.000	0.000	0.000
SrO	0.000	0.000	0.002	0.001	0.001	0.000	0.000
F	0.000	0.000	0.000	0.000	0.000	0.000	0.118
Cl	0.002	0.003	0.001	0.003	0.001	0.002	0.001
Total	9.528	9.507	9.523	9.534	9.541	9.550	9.587
Tet Al	1.267	1.259	1.299	1.366	1.334	1.333	1.323
Oct Al	0.457	0.423	0.421	0.383	0.414	0.409	0.378
Total Al	1.724	1.683	1.720	1.749	1.748	1.741	1.701

Table D3: Electron microprobe results: biotite atomic proportions

Element	385230.15.2	385230.15.3	385230.15.4	385253.1.16.1	385253.1.16.2	385253.1.16.3
Si (IV)	2.801	2.776	2.684	2.720	2.736	2.718
Al (IV)	1.199	1.224	1.316	1.280	1.264	1.282
Al (VI)	0.436	0.443	0.402	0.323	0.337	0.324
Al (total)	1.635	1.667	1.718	1.603	1.602	1.606
FeO	1.250	1.272	1.361	1.341	1.284	1.319
MgO	1.090	1.071	1.120	1.033	1.065	1.052
MnO	0.015	0.016	0.021	0.019	0.017	0.020
CaO	0.005	0.001	0.004	0.001	0.002	0.004
Na₂O	0.016	0.007	0.010	0.004	0.048	0.023
K₂O	0.909	0.912	0.809	0.959	0.948	0.949
TiO₂	0.060	0.062	0.067	0.138	0.124	0.134
ZnO	0.003	0.002	0.004	0.002	0.003	0.002
BaO	0.000	0.000	0.000	0.000	0.000	0.000
SrO	0.000	0.000	0.000	0.000	0.000	0.000
F	0.000	0.000	0.000	0.000	0.000	0.000
Cl	0.001	0.001	0.001	0.001	0.021	0.009
Total	9.420	9.455	9.517	9.425	9.450	9.442
Tet Al	1.199	1.224	1.316	1.280	1.264	1.282
Oct Al	0.436	0.443	0.402	0.323	0.337	0.324
Total Al	1.635	1.667	1.718	1.603	1.602	1.606

Table D3: Electron microprobe results: biotite atomic proportions

Element	385253.1.16.4	385253.1.17.1	385253.1.17.2	385253.1.17.3	385253.1.17.4	385253.1.18.1
Si (IV)	2.695	2.722	2.737	2.723	2.722	2.701
Al (IV)	1.305	1.278	1.263	1.277	1.278	1.299
Al (VI)	0.314	0.325	0.340	0.319	0.306	0.320
Al (total)	1.619	1.603	1.602	1.596	1.584	1.619
FeO	1.330	1.333	1.324	1.332	1.324	1.324
MgO	1.025	1.032	1.077	1.040	1.053	1.040
MnO	0.019	0.018	0.016	0.018	0.017	0.016
CaO	0.001	0.000	0.001	0.001	0.001	0.000
Na₂O	0.012	0.007	0.003	0.012	0.044	0.008
K₂O	0.948	0.960	0.917	0.950	0.943	0.938
TiO₂	0.136	0.141	0.120	0.143	0.141	0.129
ZnO	0.002	0.001	0.002	0.003	0.001	0.001
BaO	0.000	0.000	0.000	0.000	0.000	0.000
SrO	0.000	0.000	0.000	0.000	0.000	0.002
F	0.101	0.000	0.000	0.000	0.000	0.112
Cl	0.000	0.001	0.002	0.001	0.017	0.001
Total	9.509	9.422	9.405	9.414	9.431	9.509
Tet Al	1.305	1.278	1.263	1.277	1.278	1.299
Oct Al	0.314	0.325	0.340	0.319	0.306	0.320
Total Al	1.619	1.603	1.602	1.596	1.584	1.619

Table D3: Electron microprobe results: biotite atomic proportions

Element	385253.1.18.2	385253.1.18.3	385253.1.18.4	385253.1.19.1	385253.1.19.2	385253.1.19.3
Si (IV)	2.721	2.728	2.711	2.718	2.746	2.746
Al (IV)	1.279	1.272	1.289	1.282	1.254	1.254
Al (VI)	0.303	0.337	0.332	0.340	0.334	0.336
Al (total)	1.581	1.609	1.622	1.622	1.588	1.590
FeO	1.320	1.330	1.311	1.321	1.307	1.314
MgO	1.046	1.045	1.061	1.075	1.077	1.071
MnO	0.017	0.016	0.015	0.017	0.017	0.015
CaO	0.002	0.001	0.002	0.000	0.000	0.000
Na₂O	0.013	0.006	0.017	0.011	0.003	0.008
K₂O	0.937	0.944	0.933	0.943	0.959	0.949
TiO₂	0.133	0.130	0.113	0.118	0.120	0.121
ZnO	0.000	0.003	0.002	0.003	0.002	0.001
BaO	0.000	0.000	0.000	0.000	0.000	0.000
SrO	0.002	0.000	0.000	0.000	0.000	0.002
F	0.102	0.000	0.105	0.000	0.000	0.000
Cl	0.011	0.001	0.003	0.003	0.001	0.000
Total	9.468	9.422	9.516	9.454	9.408	9.407
Tet Al	1.279	1.272	1.289	1.282	1.254	1.254
Oct Al	0.303	0.337	0.332	0.340	0.334	0.336
Total Al	1.581	1.609	1.622	1.622	1.588	1.590

Table D3: Electron microprobe results: biotite atomic proportions

Element	385253.1.19.4	385253.1.20.1	385253.1.20.2	385253.1.20.3	385253.1.20.4	385253.1.21.1
Si (IV)	2.722	2.714	2.691	2.715	2.733	2.722
Al (IV)	1.278	1.286	1.309	1.285	1.267	1.278
Al (VI)	0.345	0.341	0.303	0.326	0.344	0.344
Al (total)	1.622	1.626	1.612	1.611	1.610	1.622
FeO	1.338	1.323	1.330	1.334	1.309	1.324
MgO	1.053	1.013	1.029	1.031	1.025	1.027
MnO	0.018	0.019	0.019	0.018	0.019	0.018
CaO	0.001	0.001	0.003	0.003	0.004	0.001
Na₂O	0.006	0.015	0.013	0.011	0.014	0.009
K₂O	0.932	0.941	0.914	0.940	0.916	0.968
TiO₂	0.120	0.148	0.146	0.144	0.146	0.131
ZnO	0.003	0.001	0.004	0.003	0.003	0.004
BaO	0.000	0.000	0.000	0.000	0.000	0.000
SrO	0.000	0.000	0.000	0.000	0.000	0.000
F	0.000	0.000	0.114	0.000	0.000	0.000
Cl	0.002	0.000	0.003	0.001	0.003	0.001
Total	9.439	9.429	9.490	9.422	9.392	9.447
Tet Al	1.278	1.286	1.309	1.285	1.267	1.278
Oct Al	0.345	0.341	0.303	0.326	0.344	0.344
Total Al	1.622	1.626	1.612	1.611	1.610	1.622

Table D3: Electron microprobe results: biotite atomic proportions

Element	385253.1.21.2	385253.1.21.3	385253.1.21.4	385253.1.22.1	385253.1.22.2	385253.1.22.3
Si (IV)	2.715	2.722	2.740	2.701	2.743	2.747
Al (IV)	1.285	1.278	1.260	1.299	1.257	1.253
Al (VI)	0.333	0.347	0.331	0.329	0.328	0.325
Al (total)	1.618	1.625	1.591	1.628	1.584	1.577
FeO	1.343	1.322	1.312	1.309	1.319	1.310
MgO	1.038	1.017	1.043	1.026	1.049	1.050
MnO	0.018	0.018	0.018	0.017	0.018	0.017
CaO	0.001	0.001	0.002	0.001	0.002	0.001
Na₂O	0.006	0.011	0.006	0.012	0.011	0.013
K₂O	0.951	0.958	0.953	0.964	0.940	0.945
TiO₂	0.131	0.137	0.139	0.132	0.136	0.141
ZnO	0.002	0.001	0.000	0.001	0.001	0.001
BaO	0.000	0.000	0.000	0.000	0.000	0.000
SrO	0.000	0.001	0.001	0.000	0.001	0.000
F	0.000	0.000	0.000	0.096	0.000	0.000
Cl	0.001	0.000	0.000	0.001	0.000	0.000
Total	9.442	9.438	9.397	9.517	9.389	9.380
Tet Al	1.285	1.278	1.260	1.299	1.257	1.253
Oct Al	0.333	0.347	0.331	0.329	0.328	0.325
Total Al	1.618	1.625	1.591	1.628	1.584	1.577

Table D3: Electron microprobe results: biotite atomic proportions

Element	385253.1.22.4	385253.1.24.1	385253.1.24.2	385253.1.24.3	385253.1.25.1	385253.1.25.2
Si (IV)	2.700	2.729	2.733	2.747	2.745	2.728
Al (IV)	1.300	1.271	1.267	1.253	1.255	1.272
Al (VI)	0.318	0.321	0.339	0.337	0.341	0.349
Al (total)	1.618	1.592	1.606	1.590	1.596	1.621
FeO	1.330	1.361	1.332	1.291	1.311	1.309
MgO	1.066	1.085	1.069	1.063	1.098	1.094
MnO	0.018	0.018	0.018	0.017	0.019	0.019
CaO	0.003	0.001	0.000	0.000	0.000	0.002
Na₂O	0.013	0.006	0.008	0.009	0.015	0.013
K₂O	0.895	0.906	0.947	0.950	0.919	0.933
TiO₂	0.122	0.116	0.112	0.111	0.108	0.106
ZnO	0.000	0.000	0.002	0.000	0.003	0.003
BaO	0.000	0.000	0.000	0.000	0.000	0.000
SrO	0.000	0.000	0.001	0.000	0.001	0.000
F	0.113	0.000	0.000	0.100	0.000	0.000
Cl	0.002	0.001	0.002	0.000	0.002	0.001
Total	9.498	9.408	9.437	9.466	9.413	9.450
Tet Al	1.300	1.271	1.267	1.253	1.255	1.272
Oct Al	0.318	0.321	0.339	0.337	0.341	0.349
Total Al	1.618	1.592	1.606	1.590	1.596	1.621

Table D3: Electron microprobe results: biotite atomic proportions

Element	385253.1.25.3	385253.1.27.1	385253.1.27.2	385253.1.27.3	385253.1.27.4	385253.1.28.1
Si (IV)	2.778	2.745	2.757	2.733	2.731	2.807
Al (IV)	1.222	1.255	1.243	1.267	1.269	1.193
Al (VI)	0.345	0.388	0.369	0.385	0.369	0.392
Al (total)	1.567	1.643	1.612	1.652	1.639	1.585
FeO	1.289	1.272	1.278	1.284	1.274	1.232
MgO	1.088	1.102	1.104	1.106	1.112	1.112
MnO	0.017	0.019	0.017	0.018	0.018	0.018
CaO	0.000	0.001	0.001	0.000	0.004	0.000
Na₂O	0.013	0.010	0.012	0.013	0.024	0.015
K₂O	0.935	0.921	0.939	0.927	0.922	0.857
TiO₂	0.111	0.091	0.094	0.087	0.096	0.103
ZnO	0.002	0.002	0.002	0.002	0.004	0.003
BaO	0.000	0.000	0.000	0.000	0.000	0.000
SrO	0.001	0.001	0.001	0.000	0.000	0.001
F	0.000	0.000	0.000	0.000	0.000	0.000
Cl	0.000	0.001	0.002	0.001	0.004	0.000
Total	9.368	9.452	9.431	9.477	9.468	9.319
Tet Al	1.222	1.255	1.243	1.267	1.269	1.193
Oct Al	0.345	0.388	0.369	0.385	0.369	0.392
Total Al	1.567	1.643	1.612	1.652	1.639	1.585

Table D3: Electron microprobe results: biotite atomic proportions

Element	385253.1.28.2	385253.1.28.3	385253.1.28.4	385253.1.29.1	385253.1.29.2	385253.1.29.3
Si (IV)	2.787	2.785	2.764	2.744	2.756	2.749
Al (IV)	1.213	1.215	1.236	1.256	1.244	1.251
Al (VI)	0.404	0.413	0.393	0.379	0.385	0.368
Al (total)	1.617	1.628	1.628	1.635	1.629	1.619
FeO	1.245	1.230	1.237	1.269	1.268	1.279
MgO	1.099	1.104	1.088	1.088	1.075	1.088
MnO	0.018	0.018	0.017	0.017	0.016	0.018
CaO	0.001	0.000	0.000	0.000	0.000	0.000
Na₂O	0.016	0.018	0.008	0.011	0.007	0.016
K₂O	0.864	0.870	0.848	0.953	0.946	0.945
TiO₂	0.098	0.094	0.098	0.100	0.102	0.103
ZnO	0.003	0.003	0.000	0.002	0.002	0.002
BaO	0.000	0.000	0.000	0.000	0.000	0.000
SrO	0.000	0.000	0.000	0.001	0.001	0.000
F	0.000	0.000	0.122	0.000	0.000	0.000
Cl	0.001	0.001	0.001	0.001	0.002	0.001
Total	9.364	9.380	9.441	9.456	9.434	9.439
Tet Al	1.213	1.215	1.236	1.256	1.244	1.251
Oct Al	0.404	0.413	0.393	0.379	0.385	0.368
Total Al	1.617	1.628	1.628	1.635	1.629	1.619

Table D3: Electron microprobe results: biotite atomic proportions

Element	385253.1.29.4	385253.1.30.1	385253.1.30.2	385253.1.30.3	385253.1.30.4	385253.1.31.1
Si (IV)	2.734	2.714	2.720	2.750	2.723	2.775
Al (IV)	1.266	1.286	1.280	1.250	1.277	1.225
Al (VI)	0.336	0.367	0.340	0.330	0.369	0.346
Al (total)	1.602	1.653	1.619	1.581	1.646	1.571
FeO	1.278	1.305	1.291	1.307	1.310	1.295
MgO	1.081	1.036	1.032	1.056	1.030	1.044
MnO	0.017	0.020	0.019	0.018	0.019	0.016
CaO	0.000	0.003	0.001	0.001	0.002	0.003
Na₂O	0.011	0.015	0.012	0.013	0.010	0.008
K₂O	0.949	0.940	0.944	0.952	0.928	0.936
TiO₂	0.105	0.124	0.128	0.131	0.126	0.130
ZnO	0.004	0.003	0.001	0.002	0.003	0.002
BaO	0.000	0.000	0.000	0.000	0.000	0.000
SrO	0.000	0.001	0.002	0.000	0.000	0.001
F	0.119	0.000	0.101	0.000	0.000	0.000
Cl	0.001	0.001	0.001	0.001	0.001	0.001
Total	9.502	9.467	9.491	9.393	9.444	9.353
Tet Al	1.266	1.286	1.280	1.250	1.277	1.225
Oct Al	0.336	0.367	0.340	0.330	0.369	0.346
Total Al	1.602	1.653	1.619	1.581	1.646	1.571

Table D3: Electron microprobe results: biotite atomic proportions

Element	385253.1.31.2	385253.1.31.3	385253.1.31.4	385367.2.40.2	385367.2.41.1	385367.2.41.2
Si (IV)	2.758	2.737	2.742	3.171	3.273	3.133
Al (IV)	1.242	1.263	1.258	0.829	0.727	0.867
Al (VI)	0.375	0.347	0.370	1.882	1.801	1.869
Al (total)	1.618	1.610	1.628	2.711	2.529	2.736
FeO	1.294	1.341	1.300	0.097	0.123	0.110
MgO	1.060	1.053	1.038	0.075	0.137	0.109
MnO	0.016	0.016	0.017	0.000	0.002	0.000
CaO	0.001	0.002	0.002	0.000	0.000	0.000
Na₂O	0.013	0.005	0.014	0.092	0.062	0.088
K₂O	0.948	0.908	0.953	0.681	0.629	0.679
TiO₂	0.102	0.120	0.115	0.011	0.022	0.009
ZnO	0.001	0.002	0.001	0.000	0.000	0.000
BaO	0.000	0.000	0.000	0.008	0.008	0.007
SrO	0.001	0.001	0.003	0.001	0.001	0.001
F	0.000	0.000	0.000	0.000	0.000	0.000
Cl	0.001	0.001	0.000	0.001	0.001	0.001
Total	9.430	9.405	9.440	9.560	9.316	9.610
Tet Al	1.242	1.263	1.258	0.829	0.727	0.867
Oct Al	0.375	0.347	0.370	1.882	1.801	1.869
Total Al	1.618	1.610	1.628	2.711	2.529	2.736

Table D3: Electron microprobe results: biotite atomic proportions

Element	385367.2.42.1	385367.2.42.2	385367.2.42.3	385381.51.1	385381.51.2	385381.51.3
Si (IV)	3.288	3.226	3.196	2.754	2.799	2.708
Al (IV)	0.712	0.774	0.804	1.246	1.201	1.292
Al (VI)	1.774	1.815	1.839	0.324	0.305	0.292
Al (total)	2.485	2.589	2.642	1.571	1.506	1.585
FeO	0.102	0.101	0.088	1.213	1.187	1.236
MgO	0.159	0.128	0.104	1.153	1.183	1.190
MnO	0.001	0.000	0.001	0.025	0.023	0.026
CaO	0.000	0.001	0.000	0.000	0.000	0.001
Na₂O	0.036	0.051	0.059	0.010	0.009	0.008
K₂O	0.623	0.642	0.735	0.940	0.931	0.887
TiO₂	0.050	0.041	0.022	0.135	0.139	0.129
ZnO	0.000	0.000	0.000	0.000	0.001	0.003
BaO	0.003	0.006	0.007	0.000	0.000	0.000
SrO	0.000	0.000	0.001	0.000	0.001	0.000
F	0.000	0.000	0.003	0.000	0.000	0.094
Cl	0.002	0.000	0.000	0.003	0.000	0.000
Total	9.235	9.374	9.501	9.373	9.285	9.450
Tet Al	0.712	0.774	0.804	1.246	1.201	1.292
Oct Al	1.774	1.815	1.839	0.324	0.305	0.292
Total Al	2.485	2.589	2.642	1.571	1.506	1.585

Table D3: Electron microprobe results: biotite atomic proportions

Element	385381.52.1	385381.52.2	385381.52.3	385381.52.4	385381.53.1	385381.53.2	385381.53.3
Si (IV)	2.741	2.723	2.747	2.759	3.351	3.327	3.246
Al (IV)	1.259	1.277	1.253	1.241	0.649	0.673	0.754
Al (VI)	0.308	0.285	0.310	0.325	1.741	1.783	1.536
Al (total)	1.566	1.562	1.563	1.565	2.390	2.457	2.290
FeO	1.223	1.203	1.206	1.190	0.111	0.114	0.327
MgO	1.182	1.202	1.181	1.176	0.235	0.200	0.405
MnO	0.023	0.022	0.022	0.022	0.002	0.002	0.008
CaO	0.000	0.003	0.001	0.001	0.001	0.001	0.002
Na₂O	0.008	0.018	0.011	0.004	0.026	0.035	0.023
K₂O	0.934	0.895	0.937	0.928	0.609	0.574	0.576
TiO₂	0.133	0.134	0.136	0.137	0.022	0.017	0.014
ZnO	0.003	0.004	0.004	0.004	0.000	0.000	0.000
BaO	0.000	0.000	0.000	0.000	0.003	0.004	0.002
SrO	0.000	0.000	0.001	0.000	0.000	0.001	0.001
F	0.000	0.098	0.000	0.000	0.000	0.000	0.000
Cl	0.001	0.003	0.001	0.001	0.002	0.002	0.002
Total	9.380	9.430	9.373	9.353	9.140	9.191	9.185
Tet Al	1.259	1.277	1.253	1.241	0.649	0.673	0.754
Oct Al	0.308	0.285	0.310	0.325	1.741	1.783	1.536
Total Al	1.566	1.562	1.563	1.565	2.390	2.457	2.290

Table D3: Electron microprobe results: biotite atomic proportions

Element	385381.54.1	385381.54.2	385381.54.3	385381.55.1	385381.55.2	385381.56.1	385381.56.2
Si (IV)	2.763	2.766	2.762	3.317	3.330	3.284	3.340
Al (IV)	1.237	1.234	1.238	0.683	0.670	0.716	0.660
Al (VI)	0.325	0.343	0.333	1.797	1.762	1.831	1.742
Al (total)	1.562	1.577	1.571	2.481	2.432	2.547	2.402
FeO	1.212	1.177	1.202	0.106	0.104	0.113	0.127
MgO	1.170	1.175	1.225	0.181	0.193	0.157	0.208
MnO	0.025	0.023	0.020	0.003	0.002	0.002	0.002
CaO	0.002	0.002	0.003	0.000	0.000	0.000	0.001
Na₂O	0.019	0.014	0.019	0.028	0.025	0.032	0.033
K₂O	0.877	0.887	0.851	0.616	0.644	0.599	0.609
TiO₂	0.132	0.134	0.115	0.014	0.027	0.010	0.025
ZnO	0.006	0.005	0.001	0.002	0.000	0.001	0.003
BaO	0.000	0.000	0.000	0.003	0.003	0.003	0.004
SrO	0.001	0.002	0.001	0.001	0.000	0.001	0.001
F	0.000	0.000	0.000	0.000	0.000	0.000	0.000
Cl	0.005	0.001	0.008	0.000	0.001	0.000	0.001
Total	9.337	9.340	9.348	9.232	9.194	9.295	9.158
Tet Al	1.237	1.234	1.238	0.683	0.670	0.716	0.660
Oct Al	0.325	0.343	0.333	1.797	1.762	1.831	1.742
Total Al	1.562	1.577	1.571	2.481	2.432	2.547	2.402

Table D3: Electron microprobe results: biotite atomic proportions

Element	385381.56.3	385381.57.1	385381.57.2	385381.57.3	385381.57.4	385381.58.1	385381.58.2
Si (IV)	3.328	2.818	2.788	2.771	2.777	2.805	2.756
Al (IV)	0.672	1.182	1.212	1.229	1.223	1.195	1.244
Al (VI)	1.924	0.290	0.322	0.311	0.305	0.332	0.337
Al (total)	2.595	1.472	1.534	1.540	1.528	1.527	1.581
FeO	0.111	1.169	1.181	1.198	1.156	1.170	1.188
MgO	0.153	1.232	1.212	1.214	1.199	1.190	1.213
MnO	0.001	0.020	0.021	0.021	0.020	0.022	0.021
CaO	0.000	0.000	0.001	0.001	0.001	0.001	0.001
Na₂O	0.010	0.012	0.011	0.005	0.003	0.015	0.013
K₂O	0.296	0.913	0.902	0.903	0.911	0.899	0.910
TiO₂	0.012	0.134	0.125	0.129	0.131	0.127	0.113
ZnO	0.002	0.003	0.002	0.001	0.002	0.003	0.004
BaO	0.004	0.000	0.000	0.000	0.000	0.000	0.000
SrO	0.000	0.001	0.000	0.000	0.000	0.000	0.000
F	0.000	0.000	0.000	0.000	0.110	0.000	0.000
Cl	0.001	0.001	0.001	0.001	0.001	0.002	0.004
Total	9.111	9.247	9.311	9.324	9.369	9.290	9.386
Tet Al	0.672	1.182	1.212	1.229	1.223	1.195	1.244
Oct Al	1.924	0.290	0.322	0.311	0.305	0.332	0.337
Total Al	2.595	1.472	1.534	1.540	1.528	1.527	1.581

Table D3: Electron microprobe results: biotite atomic proportions

Element	385381.58.3	385381.58.4	385381.59.1	385381.59.2	385381.59.3	385381.59.4	385381.60.1
Si (IV)	2.808	2.737	2.795	2.782	2.808	2.767	2.777
Al (IV)	1.192	1.263	1.205	1.218	1.192	1.233	1.223
Al (VI)	0.344	0.291	0.426	0.421	0.433	0.418	0.381
Al (total)	1.536	1.554	1.631	1.638	1.625	1.651	1.604
FeO	1.155	1.208	1.092	1.116	1.066	1.105	1.095
MgO	1.201	1.209	1.281	1.279	1.286	1.280	1.270
MnO	0.021	0.024	0.021	0.021	0.022	0.022	0.022
CaO	0.001	0.004	0.000	0.004	0.000	0.000	0.000
Na₂O	0.012	0.010	0.007	0.012	0.014	0.014	0.008
K₂O	0.861	0.850	0.919	0.880	0.920	0.934	0.932
TiO₂	0.132	0.129	0.050	0.054	0.051	0.052	0.065
ZnO	0.002	0.003	0.004	0.002	0.004	0.003	0.004
BaO	0.000	0.000	0.000	0.000	0.000	0.000	0.000
SrO	0.000	0.000	0.001	0.001	0.000	0.001	0.001
F	0.000	0.118	0.000	0.000	0.000	0.000	0.096
Cl	0.000	0.002	0.001	0.002	0.001	0.002	0.000
Total	9.264	9.402	9.435	9.430	9.422	9.482	9.478
Tet Al	1.192	1.263	1.205	1.218	1.192	1.233	1.223
Oct Al	0.344	0.291	0.426	0.421	0.433	0.418	0.381
Total Al	1.536	1.554	1.631	1.638	1.625	1.651	1.604

Table D3: Electron microprobe results: biotite atomic proportions

Element	385381.60.2	385381.60.3	385381.60.4	385381.61.1	385381.61.2	385210.68.1	385210.68.2
Si (IV)	2.781	2.786	2.763	2.877	2.782	2.750	2.717
Al (IV)	1.219	1.214	1.237	1.123	1.218	1.250	1.283
Al (VI)	0.394	0.408	0.388	0.415	0.445	0.462	0.440
Al (total)	1.613	1.621	1.625	1.539	1.663	1.712	1.723
FeO	1.106	1.124	1.123	1.028	1.080	1.350	1.399
MgO	1.246	1.252	1.255	1.314	1.246	0.966	0.963
MnO	0.021	0.023	0.023	0.019	0.022	0.010	0.012
CaO	0.000	0.000	0.000	0.000	0.000	0.004	0.005
Na₂O	0.011	0.008	0.006	0.009	0.007	0.006	0.009
K₂O	0.938	0.921	0.925	0.904	0.946	0.886	0.838
TiO₂	0.064	0.064	0.062	0.059	0.057	0.075	0.086
ZnO	0.003	0.003	0.004	0.002	0.002	0.006	0.003
BaO	0.000	0.000	0.000	0.000	0.000	0.000	0.000
SrO	0.000	0.001	0.000	0.000	0.000	0.000	0.002
F	0.078	0.000	0.085	0.000	0.000	0.000	0.000
Cl	0.001	0.000	0.000	0.001	0.002	0.002	0.002
Total	9.475	9.425	9.495	9.290	9.470	9.478	9.483
Tet Al	1.219	1.214	1.237	1.123	1.218	1.250	1.283
Oct Al	0.394	0.408	0.388	0.415	0.445	0.462	0.440
Total Al	1.613	1.621	1.625	1.539	1.663	1.712	1.723

Table D3: Electron microprobe results: biotite atomic proportions

Element	385210.68.3	385210.68.4	385210.69.1	385210.69.2	385210.69.3	385210.69.4	385210.72.1
Si (IV)	2.754	2.733	2.759	2.703	2.751	2.684	2.770
Al (IV)	1.246	1.267	1.241	1.297	1.249	1.316	1.230
Al (VI)	0.459	0.438	0.443	0.426	0.441	0.435	0.476
Al (total)	1.706	1.706	1.683	1.722	1.690	1.750	1.706
FeO	1.343	1.390	1.369	1.425	1.362	1.426	1.341
MgO	0.972	0.960	0.945	0.953	0.963	1.014	0.983
MnO	0.012	0.010	0.010	0.011	0.012	0.014	0.009
CaO	0.002	0.002	0.000	0.001	0.001	0.004	0.005
Na2O	0.010	0.008	0.008	0.010	0.011	0.006	0.016
K2O	0.884	0.879	0.867	0.843	0.850	0.745	0.850
TiO2	0.077	0.083	0.096	0.094	0.096	0.084	0.064
ZnO	0.004	0.003	0.003	0.004	0.001	0.002	0.002
BaO	0.000	0.000	0.000	0.000	0.000	0.000	0.000
SrO	0.001	0.000	0.001	0.001	0.001	0.000	0.001
F	0.000	0.000	0.000	0.000	0.000	0.000	0.000
Cl	0.001	0.003	0.000	0.001	0.001	0.002	0.001
Total	9.470	9.482	9.425	9.490	9.430	9.483	9.452
Tet Al	1.246	1.267	1.241	1.297	1.249	1.316	1.230
Oct Al	0.459	0.438	0.443	0.426	0.441	0.435	0.476
Total Al	1.706	1.706	1.683	1.722	1.690	1.750	1.706

Table D3: Electron microprobe results: biotite atomic proportions

Element	385210.72.2	385210.72.3	385210.72.4	385210.74.1	385210.74.2	385210.74.3	385210.74.4
Si (IV)	2.718	2.737	2.748	2.758	2.740	2.764	2.730
Al (IV)	1.282	1.263	1.252	1.242	1.260	1.236	1.270
Al (VI)	0.452	0.490	0.482	0.418	0.419	0.447	0.454
Al (total)	1.734	1.753	1.734	1.661	1.678	1.683	1.724
FeO	1.359	1.350	1.358	1.395	1.404	1.359	1.391
MgO	0.965	0.957	0.975	0.979	0.974	0.974	0.949
MnO	0.011	0.011	0.011	0.010	0.009	0.011	0.011
CaO	0.011	0.005	0.006	0.001	0.000	0.000	0.001
Na₂O	0.027	0.037	0.025	0.008	0.011	0.007	0.008
K₂O	0.843	0.846	0.853	0.917	0.919	0.928	0.905
TiO₂	0.060	0.063	0.055	0.071	0.073	0.066	0.071
ZnO	0.008	0.003	0.003	0.003	0.002	0.004	0.003
BaO	0.000	0.000	0.000	0.000	0.000	0.000	0.000
SrO	0.000	0.001	0.000	0.000	0.001	0.000	0.001
F	0.108	0.000	0.000	0.000	0.000	0.000	0.000
Cl	0.001	0.002	0.001	0.001	0.002	0.001	0.000
Total	9.578	9.519	9.504	9.465	9.492	9.480	9.517
Tet Al	1.282	1.263	1.252	1.242	1.260	1.236	1.270
Oct Al	0.452	0.490	0.482	0.418	0.419	0.447	0.454
Total Al	1.734	1.753	1.734	1.661	1.678	1.683	1.724

Table D3: Electron microprobe results: biotite atomic proportions

Element	385210.80.1	385210.80.2	385210.80.3	385210.80.4	385210.81.1	385210.81.2	385210.81.3
Si (IV)	2.706	2.693	2.698	2.681	2.690	2.715	2.693
Al (IV)	1.294	1.307	1.302	1.319	1.310	1.285	1.307
Al (VI)	0.412	0.409	0.420	0.385	0.432	0.456	0.419
Al (total)	1.707	1.716	1.722	1.703	1.743	1.742	1.726
FeO	1.404	1.428	1.432	1.423	1.413	1.360	1.380
MgO	0.949	0.940	0.924	0.969	0.963	0.944	0.943
MnO	0.012	0.012	0.011	0.012	0.012	0.010	0.012
CaO	0.002	0.004	0.002	0.001	0.005	0.002	0.002
Na2O	0.009	0.007	0.010	0.014	0.015	0.012	0.009
K2O	0.922	0.864	0.887	0.863	0.847	0.905	0.899
TiO2	0.096	0.108	0.101	0.091	0.089	0.091	0.085
ZnO	0.002	0.003	0.002	0.002	0.003	0.001	0.004
BaO	0.000	0.000	0.000	0.000	0.001	0.000	0.000
SrO	0.001	0.000	0.000	0.000	0.000	0.002	0.001
F	0.000	0.000	0.000	0.108	0.000	0.000	0.116
Cl	0.002	0.001	0.002	0.001	0.002	0.002	0.002
Total	9.519	9.493	9.512	9.572	9.524	9.525	9.597
Tet Al	1.294	1.307	1.302	1.319	1.310	1.285	1.307
Oct Al	0.412	0.409	0.420	0.385	0.432	0.456	0.419
Total Al	1.707	1.716	1.722	1.703	1.743	1.742	1.726

Table D3: Electron microprobe results: biotite atomic proportions

Element	385210.81.4	385210.83.1	385210.83.2	385210.83.3	385210.84.1	385210.84.2	385210.84.3
Si (IV)	2.680	2.729	2.738	2.739	2.760	2.632	2.728
Al (IV)	1.320	1.271	1.262	1.261	1.240	1.368	1.272
Al (VI)	0.426	0.478	0.483	0.484	0.435	0.426	0.461
Al (total)	1.746	1.749	1.745	1.745	1.675	1.794	1.732
FeO	1.418	1.363	1.353	1.368	1.351	1.472	1.358
MgO	0.981	0.948	0.950	0.956	0.983	1.070	0.983
MnO	0.013	0.012	0.010	0.011	0.010	0.016	0.011
CaO	0.006	0.010	0.008	0.008	0.002	0.012	0.005
Na2O	0.015	0.007	0.009	0.007	0.010	0.003	0.012
K2O	0.840	0.878	0.856	0.821	0.904	0.668	0.872
TiO2	0.087	0.070	0.074	0.072	0.080	0.068	0.071
ZnO	0.000	0.003	0.006	0.004	0.004	0.002	0.003
BaO	0.000	0.000	0.000	0.000	0.000	0.000	0.000
SrO	0.000	0.000	0.000	0.000	0.000	0.000	0.002
F	0.000	0.000	0.000	0.000	0.000	0.000	0.000
Cl	0.002	0.001	0.000	0.000	0.001	0.002	0.000
Total	9.535	9.519	9.493	9.476	9.455	9.533	9.509
Tet Al	1.320	1.271	1.262	1.261	1.240	1.368	1.272
Oct Al	0.426	0.478	0.483	0.484	0.435	0.426	0.461
Total Al	1.746	1.749	1.745	1.745	1.675	1.794	1.732

Table D3: Electron microprobe results: biotite atomic proportions

Element	385210.84.4	385210.85.1	385210.85.2	385210.85.3	385210.85.4	385347.2.86.1
Si (IV)	2.740	2.758	2.739	2.771	2.753	2.752
Al (IV)	1.260	1.242	1.261	1.229	1.247	1.248
Al (VI)	0.434	0.458	0.460	0.471	0.462	0.431
Al (total)	1.694	1.701	1.721	1.700	1.709	1.679
FeO	1.388	1.342	1.351	1.323	1.347	1.308
MgO	0.988	0.965	0.958	0.959	0.936	1.050
MnO	0.010	0.011	0.012	0.010	0.013	0.012
CaO	0.003	0.004	0.004	0.003	0.004	0.003
Na₂O	0.010	0.017	0.015	0.019	0.015	0.012
K₂O	0.864	0.866	0.852	0.874	0.890	0.808
TiO₂	0.072	0.082	0.086	0.082	0.084	0.096
ZnO	0.005	0.006	0.007	0.002	0.007	0.002
BaO	0.000	0.000	0.000	0.000	0.000	0.000
SrO	0.001	0.001	0.002	0.000	0.001	0.002
F	0.000	0.000	0.000	0.000	0.000	0.000
Cl	0.001	0.000	0.001	0.001	0.003	0.000
Total	9.472	9.452	9.470	9.443	9.472	9.402
Tet Al	1.260	1.242	1.261	1.229	1.247	1.248
Oct Al	0.434	0.458	0.460	0.471	0.462	0.431
Total Al	1.694	1.701	1.721	1.700	1.709	1.679

Table D3: Electron microprobe results: biotite atomic proportions

Element	385347.2.86.2	385347.2.86.3	385347.2.86.4	385347.2.7.1	385347.2.7.2	385347.2.7.3
Si (IV)	2.680	2.626	2.744	2.755	2.830	2.724
Al (IV)	1.320	1.374	1.256	1.245	1.170	1.276
Al (VI)	0.394	0.401	0.426	0.457	0.464	0.425
Al (total)	1.714	1.775	1.682	1.702	1.634	1.701
FeO	1.385	1.407	1.348	1.303	1.281	1.325
MgO	1.124	1.173	0.976	1.022	1.003	1.018
MnO	0.011	0.016	0.008	0.009	0.009	0.010
CaO	0.003	0.005	0.002	0.002	0.003	0.002
Na₂O	0.010	0.014	0.012	0.011	0.006	0.012
K₂O	0.735	0.616	0.871	0.836	0.852	0.836
TiO₂	0.086	0.084	0.106	0.086	0.080	0.078
ZnO	0.002	0.002	0.001	0.004	0.003	0.002
BaO	0.000	0.000	0.000	0.000	0.000	0.000
SrO	0.001	0.000	0.000	0.000	0.000	0.001
F	0.000	0.000	0.000	0.000	0.000	0.126
Cl	0.000	0.002	0.000	0.001	0.001	0.000
Total	9.464	9.494	9.433	9.433	9.337	9.536
Tet Al	1.320	1.374	1.256	1.245	1.170	1.276
Oct Al	0.394	0.401	0.426	0.457	0.464	0.425
Total Al	1.714	1.775	1.682	1.702	1.634	1.701

Table D3: Electron microprobe results: biotite atomic proportions

Element	385347.2.7.4	385011.93.1	385011.93.2	385011.93.3	385011.93.4	385011.94.1
Si (IV)	2.753	2.915	2.851	2.682	2.881	2.757
Al (IV)	1.247	1.085	1.149	1.318	1.119	1.243
Al (VI)	0.472	0.457	0.448	0.414	0.462	0.445
Al (total)	1.719	1.541	1.597	1.731	1.581	1.688
FeO	1.299	1.143	1.191	1.380	1.148	1.278
MgO	1.030	1.212	1.186	1.230	1.191	1.146
MnO	0.009	0.021	0.022	0.031	0.023	0.026
CaO	0.001	0.001	0.002	0.003	0.008	0.000
Na₂O	0.009	0.014	0.010	0.016	0.032	0.009
K₂O	0.844	0.842	0.877	0.673	0.830	0.897
TiO₂	0.073	0.023	0.027	0.023	0.028	0.023
ZnO	0.004	0.005	0.004	0.001	0.005	0.003
BaO	0.000	0.000	0.000	0.000	0.000	0.000
SrO	0.000	0.000	0.000	0.000	0.001	0.002
F	0.000	0.000	0.000	0.000	0.000	0.000
Cl	0.000	0.001	0.000	0.003	0.006	0.002
Total	9.460	9.260	9.364	9.506	9.316	9.518
Tet Al	1.247	1.085	1.149	1.318	1.119	1.243
Oct Al	0.472	0.457	0.448	0.414	0.462	0.445
Total Al	1.719	1.541	1.597	1.731	1.581	1.688

Table D3: Electron microprobe results: biotite atomic proportions

Element	385011.94.2	385011.94.3	385011.94.4	385011.95.1	385011.95.2	385011.95.3	385011.95.4
Si (IV)	2.734	2.797	2.760	2.716	2.687	2.584	2.704
Al (IV)	1.266	1.203	1.240	1.284	1.313	1.416	1.296
Al (VI)	0.437	0.434	0.457	0.411	0.387	0.392	0.423
Al (total)	1.703	1.637	1.697	1.695	1.700	1.808	1.719
FeO	1.285	1.242	1.259	1.318	1.349	1.463	1.334
MgO	1.171	1.129	1.155	1.081	1.100	1.214	1.073
MnO	0.027	0.023	0.025	0.025	0.027	0.032	0.027
CaO	0.001	0.009	0.002	0.002	0.001	0.003	0.001
Na₂O	0.013	0.039	0.010	0.047	0.013	0.006	0.015
K₂O	0.878	0.821	0.883	0.869	0.840	0.579	0.880
TiO₂	0.021	0.055	0.020	0.065	0.063	0.055	0.064
ZnO	0.003	0.002	0.003	0.003	0.002	0.002	0.004
BaO	0.002	0.000	0.002	0.000	0.000	0.000	0.000
SrO	0.001	0.000	0.001	0.001	0.000	0.001	0.000
F	0.000	0.000	0.000	0.000	0.086	0.000	0.000
Cl	0.000	0.008	0.000	0.014	0.000	0.002	0.001
Total	9.542	9.400	9.515	9.532	9.571	9.558	9.540
Tet Al	1.266	1.203	1.240	1.284	1.313	1.416	1.296
Oct Al	0.437	0.434	0.457	0.411	0.387	0.392	0.423
Total Al	1.703	1.637	1.697	1.695	1.700	1.808	1.719

Table D3: Electron microprobe results: biotite atomic proportions

Element	385011.96.1	385011.96.2	385011.96.3	385011.96.4	385011.97.1	385011.97.2	385011.97.3
Si (IV)	2.763	2.718	2.739	2.721	2.727	2.721	2.700
Al (IV)	1.237	1.282	1.261	1.279	1.273	1.279	1.300
Al (VI)	0.397	0.424	0.432	0.436	0.371	0.370	0.370
Al (total)	1.634	1.706	1.693	1.715	1.644	1.649	1.670
FeO	1.282	1.306	1.288	1.314	1.414	1.407	1.436
MgO	1.087	1.075	1.083	1.086	0.977	0.974	0.992
MnO	0.026	0.024	0.025	0.023	0.021	0.021	0.020
CaO	0.003	0.004	0.004	0.004	0.003	0.002	0.001
Na₂O	0.012	0.014	0.012	0.018	0.018	0.013	0.015
K₂O	0.888	0.920	0.896	0.870	0.890	0.910	0.884
TiO₂	0.062	0.062	0.062	0.055	0.103	0.107	0.096
ZnO	0.000	0.003	0.004	0.002	0.003	0.001	0.002
BaO	0.000	0.001	0.001	0.002	0.000	0.000	0.000
SrO	0.001	0.000	0.000	0.000	0.001	0.002	0.000
F	0.100	0.000	0.000	0.000	0.000	0.000	0.000
Cl	0.000	0.000	0.001	0.002	0.002	0.000	0.002
Total	9.493	9.540	9.500	9.527	9.446	9.458	9.489
Tet Al	1.237	1.282	1.261	1.279	1.273	1.279	1.300
Oct Al	0.397	0.424	0.432	0.436	0.371	0.370	0.370
Total Al	1.634	1.706	1.693	1.715	1.644	1.649	1.670

Table D3: Electron microprobe results: biotite atomic proportions

Element	385011.97.4	385011.98.1	385011.98.2	385011.98.3	385011.98.4	385011.99.1	385011.99.2
Si (IV)	2.706	2.726	2.722	2.722	2.719	2.743	2.719
Al (IV)	1.294	1.274	1.278	1.278	1.281	1.257	1.281
Al (VI)	0.379	0.373	0.371	0.391	0.379	0.377	0.395
Al (total)	1.673	1.647	1.650	1.670	1.660	1.634	1.676
FeO	1.424	1.417	1.401	1.414	1.417	1.389	1.397
MgO	0.973	1.001	1.002	0.979	0.999	1.005	0.987
MnO	0.021	0.021	0.021	0.020	0.022	0.022	0.020
CaO	0.002	0.001	0.001	0.002	0.003	0.003	0.002
Na2O	0.008	0.009	0.011	0.004	0.012	0.011	0.013
K2O	0.891	0.889	0.909	0.910	0.874	0.906	0.908
TiO2	0.103	0.093	0.097	0.090	0.092	0.092	0.089
ZnO	0.002	0.003	0.003	0.000	0.002	0.001	0.001
BaO	0.000	0.000	0.000	0.000	0.000	0.000	0.000
SrO	0.002	-0.001	0.001	0.000	0.001	-0.001	0.001
F	0.000	0.000	0.000	0.000	0.000	0.000	0.000
Cl	-0.001	0.001	-0.001	0.001	0.001	0.002	0.002
Total	9.477	9.454	9.466	9.481	9.463	9.441	9.491
Tet Al	1.294	1.274	1.278	1.278	1.281	1.257	1.281
Oct Al	0.379	0.373	0.371	0.391	0.379	0.377	0.395
Total Al	1.673	1.647	1.650	1.670	1.660	1.634	1.676

Table D3: Electron microprobe results: biotite atomic proportions

Element	385011.99.3	385011.100.1	385011.100.2	385011.100.3	385011.101.1	385011.101.2
Si (IV)	2.726	2.673	2.686	2.677	2.712	2.719
Al (IV)	1.274	1.327	1.314	1.323	1.288	1.281
Al (VI)	0.402	0.366	0.358	0.358	0.375	0.388
Al (total)	1.676	1.693	1.672	1.680	1.663	1.669
FeO	1.383	1.446	1.454	1.425	1.421	1.406
MgO	0.985	1.047	1.036	1.034	0.976	0.970
MnO	0.021	0.027	0.027	0.025	0.021	0.019
CaO	0.002	0.003	0.002	0.002	0.012	0.015
Na₂O	0.006	0.020	0.010	0.011	0.054	0.034
K₂O	0.913	0.804	0.816	0.817	0.878	0.895
TiO₂	0.091	0.089	0.091	0.088	0.090	0.091
ZnO	0.003	0.002	0.004	0.003	0.001	0.000
BaO	0.000	0.000	0.000	0.000	0.000	0.000
SrO	0.000	0.000	0.002	0.000	0.001	0.000
F	0.000	0.000	0.000	0.089	0.000	0.000
Cl	0.000	0.001	0.002	0.001	0.005	0.003
Total	9.481	9.497	9.473	9.534	9.497	9.490
Tet Al	1.274	1.327	1.314	1.323	1.288	1.281
Oct Al	0.402	0.366	0.358	0.358	0.375	0.388
Total Al	1.676	1.693	1.672	1.680	1.663	1.669

Table D3: Electron microprobe results: biotite atomic proportions

Element	385011.101.3	385011.101.4	385011.102.1	385011.102.2	385011.102.3	385011.102.4
Si (IV)	2.704	2.715	2.655	2.666	2.640	2.658
Al (IV)	1.296	1.285	1.345	1.334	1.360	1.342
Al (VI)	0.399	0.389	0.324	0.373	0.362	0.357
Al (total)	1.695	1.674	1.669	1.706	1.722	1.699
FeO	1.402	1.394	1.501	1.463	1.492	1.454
MgO	1.001	0.987	1.129	1.010	1.039	0.997
MnO	0.022	0.022	0.026	0.024	0.023	0.023
CaO	0.010	0.013	0.004	0.003	0.003	0.003
Na₂O	0.039	0.029	0.011	0.010	0.004	0.006
K₂O	0.849	0.884	0.737	0.833	0.820	0.857
TiO₂	0.084	0.091	0.075	0.092	0.082	0.083
ZnO	0.001	0.002	0.002	0.001	0.003	0.004
BaO	0.000	0.000	0.000	0.000	0.000	0.000
SrO	0.000	0.000	0.001	0.000	0.001	0.000
F	0.000	0.000	0.000	0.000	0.000	0.110
Cl	0.004	0.002	0.001	0.002	0.001	0.000
Total	9.505	9.488	9.478	9.517	9.551	9.595
Tet Al	1.296	1.285	1.345	1.334	1.360	1.342
Oct Al	0.399	0.389	0.324	0.373	0.362	0.357
Total Al	1.695	1.674	1.669	1.706	1.722	1.699

Table D3: Electron microprobe results: biotite atomic proportions

Element	385011.104.1	385011.104.2	385011.104.3	385011.105.1	385011.105.2	385011.105.3
Si (IV)	2.724	2.677	2.722	2.739	2.704	2.729
Al (IV)	1.276	1.323	1.278	1.261	1.296	1.271
Al (VI)	0.380	0.362	0.385	0.391	0.387	0.380
Al (total)	1.656	1.685	1.663	1.652	1.684	1.651
FeO	1.397	1.403	1.394	1.391	1.412	1.406
MgO	0.997	0.995	0.989	0.980	0.983	0.986
MnO	0.020	0.019	0.020	0.020	0.021	0.020
CaO	0.001	0.003	0.001	0.002	0.001	0.001
Na₂O	0.010	0.009	0.014	0.009	0.010	0.009
K₂O	0.912	0.879	0.915	0.883	0.907	0.890
TiO₂	0.095	0.098	0.095	0.100	0.093	0.100
ZnO	0.002	0.003	0.002	0.004	0.002	0.001
BaO	0.000	0.000	0.000	0.000	0.000	0.000
SrO	0.001	0.000	0.000	0.001	0.002	0.001
F	0.000	0.112	0.000	0.000	0.000	0.000
Cl	0.000	0.001	0.001	0.000	0.001	0.001
Total	9.471	9.568	9.480	9.433	9.503	9.445
Tet Al	1.276	1.323	1.278	1.261	1.296	1.271
Oct Al	0.380	0.362	0.385	0.391	0.387	0.380
Total Al	1.656	1.685	1.663	1.652	1.684	1.651

Table D3: Electron microprobe results: biotite atomic proportions

Element	385011.105.4	385011.106.1	385011.106.2	385011.106.3	385011.106.4	385011.107.1
Si (IV)	2.711	2.733	2.717	2.714	2.518	2.723
Al (IV)	1.289	1.267	1.283	1.286	1.482	1.277
Al (VI)	0.391	0.444	0.447	0.427	0.344	0.425
Al (total)	1.680	1.711	1.730	1.713	1.826	1.702
FeO	1.422	1.377	1.395	1.415	1.619	1.419
MgO	0.969	1.045	1.033	1.048	1.228	1.080
MnO	0.021	0.021	0.021	0.022	0.029	0.022
CaO	0.001	0.000	0.000	0.002	0.002	0.002
Na₂O	0.008	0.011	0.005	0.009	0.007	0.004
K₂O	0.901	0.911	0.895	0.882	0.590	0.825
TiO₂	0.094	0.031	0.032	0.033	0.023	0.030
ZnO	0.002	0.002	0.005	0.001	0.002	0.001
BaO	0.000	0.000	0.002	0.000	0.000	0.000
SrO	0.001	0.001	0.000	0.001	0.000	0.000
F	0.000	0.000	0.000	0.000	0.000	0.000
Cl	0.001	0.000	0.000	0.003	0.003	0.002
Total	9.490	9.553	9.566	9.557	9.671	9.514
Tet Al	1.289	1.267	1.283	1.286	1.482	1.277
Oct Al	0.391	0.444	0.447	0.427	0.344	0.425
Total Al	1.680	1.711	1.730	1.713	1.826	1.702

Table D3: Electron microprobe results: biotite atomic proportions

Element	385011.107.2	385011.107.3	385011.107.4	385011.108.1	385011.108.2	385011.108.3
Si (IV)	2.699	2.746	2.724	2.740	2.738	4.119
Al (IV)	1.301	1.254	1.276	1.260	1.262	-0.119
Al (VI)	0.447	0.437	0.440	0.439	0.444	0.958
Al (total)	1.749	1.692	1.716	1.699	1.706	0.840
FeO	1.392	1.377	1.394	1.372	1.375	0.723
MgO	1.039	1.050	1.037	1.043	1.038	0.546
MnO	0.020	0.020	0.020	0.020	0.020	0.013
CaO	0.001	0.001	0.002	0.001	0.000	0.007
Na₂O	0.008	0.007	0.011	0.009	0.011	0.004
K₂O	0.918	0.909	0.906	0.922	0.910	0.350
TiO₂	0.030	0.031	0.031	0.033	0.035	0.018
ZnO	0.003	0.001	0.004	0.002	0.002	0.000
BaO	0.002	0.001	0.000	0.000	0.000	0.000
SrO	0.001	0.002	0.000	0.000	0.001	0.001
F	0.000	0.000	0.000	0.000	0.000	0.000
Cl	0.001	0.000	0.003	0.000	0.000	0.001
Total	9.610	9.528	9.563	9.542	9.541	7.461
Tet Al	1.301	1.254	1.276	1.260	1.262	-0.119
Oct Al	0.447	0.437	0.440	0.439	0.444	0.958
Total Al	1.749	1.692	1.716	1.699	1.706	0.840

Table D3: Electron microprobe results: biotite atomic proportions

Element	385011.108.4	385011.110.1	385011.110.2	385011.110.3	385011.111.1	385011.111.2
Si (IV)	2.744	2.728	2.723	2.697	2.705	2.714
Al (IV)	1.256	1.272	1.277	1.303	1.295	1.286
Al (VI)	0.453	0.394	0.394	0.371	0.380	0.411
Al (total)	1.709	1.666	1.671	1.674	1.675	1.697
FeO	1.361	1.398	1.414	1.408	1.411	1.407
MgO	1.036	0.984	0.954	0.956	0.942	0.954
MnO	0.020	0.023	0.022	0.020	0.022	0.023
CaO	0.001	0.003	0.002	0.002	0.003	0.005
Na₂O	0.011	0.011	0.012	0.015	0.006	0.003
K₂O	0.905	0.894	0.914	0.922	0.911	0.905
TiO₂	0.034	0.092	0.094	0.092	0.092	0.091
ZnO	0.003	0.001	0.004	0.002	0.002	0.003
BaO	0.000	0.000	0.000	0.000	0.000	0.000
SrO	0.002	0.000	0.000	0.001	0.000	0.000
F	0.000	0.000	0.000	0.102	0.110	0.000
Cl	0.000	0.000	0.002	0.000	0.000	0.001
Total	9.535	9.465	9.483	9.567	9.554	9.499
Tet Al	1.256	1.272	1.277	1.303	1.295	1.286
Oct Al	0.453	0.394	0.394	0.371	0.380	0.411
Total Al	1.709	1.666	1.671	1.674	1.675	1.697

Table D3: Electron microprobe results: biotite atomic proportions

Element	385011.111.3	385011.111.4	385011.112.1	385011.112.2	385011.112.3	385011.112.4
Si (IV)	2.704	2.719	2.738	2.687	2.735	2.758
Al (IV)	1.296	1.281	1.262	1.313	1.265	1.242
Al (VI)	0.396	0.398	0.375	0.327	0.372	0.395
Al (total)	1.692	1.680	1.637	1.640	1.638	1.637
FeO	1.430	1.404	1.408	1.431	1.421	1.369
MgO	0.954	0.955	0.949	1.042	0.954	0.963
MnO	0.022	0.021	0.022	0.021	0.022	0.022
CaO	0.003	0.005	0.002	0.002	0.002	0.011
Na₂O	0.010	0.016	0.011	0.010	0.008	0.017
K₂O	0.912	0.909	0.899	0.797	0.891	0.864
TiO₂	0.091	0.097	0.114	0.106	0.110	0.110
ZnO	0.001	0.001	0.002	0.002	0.004	0.003
BaO	0.000	0.000	0.000	0.000	0.000	0.000
SrO	0.001	0.000	0.000	0.001	0.001	0.001
F	0.000	0.000	0.000	0.100	0.000	0.000
Cl	0.000	0.003	0.003	0.002	0.003	0.000
Total	9.512	9.489	9.423	9.482	9.425	9.392
Tet Al	1.296	1.281	1.262	1.313	1.265	1.242
Oct Al	0.396	0.398	0.375	0.327	0.372	0.395
Total Al	1.692	1.680	1.637	1.640	1.638	1.637

Table D3: Electron microprobe results: biotite atomic proportions

Element	385011.113.1	385011.113.2	385011.113.3	385011.113.4	385011.114.1	385011.114.2
Si (IV)	2.750	2.718	3.366	2.713	2.682	2.717
Al (IV)	1.250	1.282	0.634	1.287	1.318	1.283
Al (VI)	0.370	0.374	1.487	0.373	0.311	0.378
Al (total)	1.620	1.655	2.121	1.660	1.629	1.661
FeO	1.394	1.428	0.016	1.420	1.520	1.425
MgO	0.959	0.926	0.002	0.931	0.981	0.942
MnO	0.022	0.023	0.001	0.023	0.024	0.022
CaO	0.001	0.003	0.738	0.002	0.001	0.003
Na₂O	0.012	0.016	0.622	0.012	0.002	0.013
K₂O	0.905	0.921	0.029	0.916	0.863	0.894
TiO₂	0.116	0.115	0.000	0.121	0.116	0.113
ZnO	0.002	0.003	0.000	0.002	0.002	0.001
BaO	0.000	0.000	0.000	0.000	0.000	0.000
SrO	0.001	0.000	0.005	0.001	0.000	0.002
F	0.000	0.000	0.000	0.000	0.000	0.000
Cl	0.000	0.000	0.000	0.001	0.001	0.002
Total	9.403	9.463	9.020	9.460	9.450	9.455
Tet Al	1.250	1.282	0.634	1.287	1.318	1.283
Oct Al	0.370	0.374	1.487	0.373	0.311	0.378
Total Al	1.620	1.655	2.121	1.660	1.629	1.661

Table D3: Electron microprobe results: biotite atomic proportions

Element	385011.114.3	385011.114.4	385011.115.1	385011.115.2	385011.115.3	385011.115.4
Si (IV)	2.665	2.726	2.737	2.683	2.747	2.719
Al (IV)	1.335	1.274	1.263	1.317	1.253	1.281
Al (VI)	0.346	0.370	0.430	0.383	0.408	0.419
Al (total)	1.681	1.644	1.693	1.700	1.661	1.700
FeO	1.472	1.430	1.382	1.433	1.392	1.402
MgO	1.011	0.947	1.017	1.130	1.041	1.026
MnO	0.023	0.023	0.022	0.023	0.021	0.022
CaO	0.002	0.002	0.007	0.004	0.003	0.005
Na₂O	0.013	0.004	0.012	0.007	0.011	0.020
K₂O	0.820	0.887	0.865	0.753	0.861	0.863
TiO₂	0.111	0.116	0.058	0.054	0.058	0.057
ZnO	0.002	0.001	0.001	0.003	0.002	0.000
BaO	0.000	0.000	0.000	0.000	0.000	0.000
SrO	0.000	0.000	0.001	0.000	0.002	0.000
F	0.000	0.000	0.000	0.000	0.000	0.000
Cl	0.000	0.001	0.003	0.001	0.001	0.003
Total	9.482	9.426	9.490	9.494	9.462	9.517
Tet Al	1.335	1.274	1.263	1.317	1.253	1.281
Oct Al	0.346	0.370	0.430	0.383	0.408	0.419
Total Al	1.681	1.644	1.693	1.700	1.661	1.700

Table D3: Electron microprobe results: biotite atomic proportions

Element	385011.116.1	385011.116.2	385011.116.3	385011.116.4	385011.117.1	385011.117.2
Si (IV)	2.709	2.718	2.728	2.731	2.765	2.715
Al (IV)	1.291	1.282	1.272	1.269	1.235	1.285
Al (VI)	0.359	0.389	0.408	0.400	0.436	0.422
Al (total)	1.650	1.671	1.680	1.669	1.671	1.707
FeO	1.433	1.438	1.410	1.391	1.316	1.409
MgO	1.032	1.016	1.012	0.993	1.043	0.998
MnO	0.022	0.022	0.021	0.021	0.018	0.019
CaO	0.000	0.001	0.001	0.000	0.003	0.000
Na₂O	0.006	0.009	0.009	0.009	0.005	0.009
K₂O	0.857	0.888	0.911	0.911	0.908	0.907
TiO₂	0.067	0.063	0.058	0.058	0.062	0.060
ZnO	0.003	0.003	0.004	0.002	0.003	0.004
BaO	0.000	0.000	0.000	0.000	0.000	0.000
SrO	0.001	0.001	0.000	0.000	0.000	0.001
F	0.104	0.000	0.000	0.101	0.000	0.000
Cl	0.000	0.000	0.000	0.001	0.000	0.001
Total	9.534	9.503	9.514	9.556	9.465	9.536
Tet Al	1.291	1.282	1.272	1.269	1.235	1.285
Oct Al	0.359	0.389	0.408	0.400	0.436	0.422
Total Al	1.650	1.671	1.680	1.669	1.671	1.707

Table D3: Electron microprobe results: biotite atomic proportions

Element	385011.117.3	385011.117.4	385011.118.1	385011.118.2	385011.118.3	385011.119.1
Si (IV)	2.721	2.775	2.798	2.750	2.790	2.286
Al (IV)	1.279	1.225	1.202	1.250	1.210	1.714
Al (VI)	0.417	0.404	0.239	0.230	0.176	0.071
Al (total)	1.696	1.630	1.441	1.480	1.386	1.785
FeO	1.399	1.372	1.188	1.241	1.204	1.356
MgO	1.005	1.025	1.652	1.602	1.786	2.346
MnO	0.019	0.019	0.011	0.010	0.010	0.013
CaO	0.001	0.001	0.004	0.002	0.002	0.010
Na₂O	0.013	0.005	0.008	0.004	0.005	0.008
K₂O	0.922	0.918	0.705	0.690	0.622	0.013
TiO₂	0.059	0.062	0.013	0.017	0.011	0.005
ZnO	0.002	0.002	0.004	0.003	0.003	0.003
BaO	0.000	0.000	0.000	0.000	0.000	0.000
SrO	0.002	0.000	0.000	0.001	0.000	0.001
F	0.000	0.000	0.000	0.082	0.000	0.000
Cl	0.001	0.002	0.002	0.000	0.001	0.003
Total	9.536	9.441	9.266	9.361	9.206	9.613
Tet Al	1.279	1.225	1.202	1.250	1.210	1.714
Oct Al	0.417	0.404	0.239	0.230	0.176	0.071
Total Al	1.696	1.630	1.441	1.480	1.386	1.785

Table D3: Electron microprobe results: biotite atomic proportions

Element	385011.119.2	385011.119.3	385011.119.4	385011.120.1	385011.120.2	385011.120.3
Si (IV)	2.826	2.690	2.823	2.566	2.781	2.721
Al (IV)	1.174	1.310	1.177	1.434	1.219	1.279
Al (VI)	0.109	0.068	0.118	0.013	0.356	0.317
Al (total)	1.283	1.378	1.295	1.447	1.576	1.596
FeO	1.096	1.213	1.111	1.282	1.360	1.431
MgO	1.911	2.070	1.952	0.962	1.053	1.076
MnO	0.010	0.014	0.011	0.019	0.013	0.016
CaO	0.020	0.015	0.016	0.359	0.001	0.006
Na₂O	0.039	0.015	0.027	0.010	0.010	0.006
K₂O	0.586	0.392	0.564	0.533	0.890	0.826
TiO₂	0.014	0.018	0.011	0.381	0.097	0.107
ZnO	0.000	0.000	0.003	0.002	0.003	0.002
BaO	0.000	0.000	0.000	0.000	0.000	0.000
SrO	0.002	0.001	0.000	0.000	0.000	0.001
F	0.081	0.000	0.000	0.078	0.000	0.000
Cl	0.007	0.003	0.003	0.001	0.000	0.001
Total	9.158	9.187	9.111	9.086	9.360	9.387
Tet Al	1.174	1.310	1.177	1.434	1.219	1.279
Oct Al	0.109	0.068	0.118	0.013	0.356	0.317
Total Al	1.283	1.378	1.295	1.447	1.576	1.596

Table D3: Electron microprobe results: biotite atomic proportions

Element	385011.120.4	385011.123.1	385011.123.2	385011.123.3	385011.123.4	385011.124.1
Si (IV)	2.705	2.728	2.734	2.733	2.723	2.728
Al (IV)	1.295	1.272	1.266	1.267	1.277	1.272
Al (VI)	0.360	0.336	0.347	0.324	0.321	0.346
Al (total)	1.655	1.608	1.613	1.591	1.598	1.618
FeO	1.412	1.336	1.343	1.359	1.323	1.312
MgO	1.024	1.077	1.037	1.071	1.057	1.067
MnO	0.016	0.020	0.019	0.018	0.018	0.018
CaO	0.002	0.000	0.001	0.001	0.000	0.000
Na₂O	0.008	0.014	0.011	0.012	0.010	0.012
K₂O	0.878	0.922	0.934	0.890	0.934	0.940
TiO₂	0.104	0.115	0.119	0.122	0.117	0.120
ZnO	0.002	0.001	0.002	0.004	0.001	0.002
BaO	0.000	0.000	0.000	0.000	0.000	0.000
SrO	0.000	0.000	0.001	0.000	0.000	0.001
F	0.000	0.000	0.000	0.000	0.104	0.000
Cl	0.001	0.001	0.000	0.001	0.000	0.000
Total	9.462	9.429	9.426	9.392	9.483	9.437
Tet Al	1.295	1.272	1.266	1.267	1.277	1.272
Oct Al	0.360	0.336	0.347	0.324	0.321	0.346
Total Al	1.655	1.608	1.613	1.591	1.598	1.618

Table D3: Electron microprobe results: biotite atomic proportions

Element	385011.124.2	385011.124.3	385011.124.4	385011.125.1	385011.125.2	385011.125.3
Si (IV)	3.309	2.805	2.720	2.725	2.740	2.720
Al (IV)	0.691	1.195	1.280	1.275	1.260	1.280
Al (VI)	1.779	0.527	0.319	0.331	0.348	0.375
Al (total)	2.470	1.723	1.599	1.606	1.608	1.655
FeO	0.101	1.191	1.266	1.339	1.310	1.282
MgO	0.164	0.918	1.088	1.079	1.059	1.095
MnO	0.002	0.017	0.018	0.018	0.019	0.018
CaO	0.003	0.001	0.048	0.001	0.001	0.001
Na₂O	0.055	0.017	0.006	0.006	0.017	0.011
K₂O	0.655	0.914	0.868	0.917	0.931	0.883
TiO₂	0.025	0.107	0.152	0.120	0.120	0.117
ZnO	0.000	0.000	0.002	0.002	0.002	0.000
BaO	0.000	0.000	0.000	0.000	0.000	0.000
SrO	0.001	0.001	0.001	0.001	0.002	0.000
F	0.000	0.000	0.000	0.000	0.000	0.000
Cl	0.001	0.001	0.000	0.000	0.002	0.000
Total	9.257	9.417	9.365	9.420	9.419	9.437
Tet Al	0.691	1.195	1.280	1.275	1.260	1.280
Oct Al	1.779	0.527	0.319	0.331	0.348	0.375
Total Al	2.470	1.723	1.599	1.606	1.608	1.655

Table D3: Electron microprobe results: biotite atomic proportions

Element	385011.126.1	385011.126.2	385011.126.3	385011.126.4	385011.127.1	385011.127.2
Si (IV)	2.730	2.732	2.721	2.730	2.721	2.728
Al (IV)	1.270	1.268	1.279	1.270	1.279	1.272
Al (VI)	0.331	0.338	0.343	0.319	0.338	0.324
Al (total)	1.601	1.606	1.621	1.589	1.617	1.596
FeO	1.336	1.308	1.325	1.360	1.332	1.341
MgO	1.062	1.073	1.053	1.073	1.059	1.075
MnO	0.020	0.020	0.019	0.017	0.021	0.017
CaO	0.000	0.000	0.002	0.001	0.001	0.000
Na₂O	0.012	0.013	0.014	0.022	0.009	0.010
K₂O	0.935	0.934	0.916	0.883	0.941	0.943
TiO₂	0.121	0.124	0.129	0.124	0.121	0.119
ZnO	0.003	0.002	0.003	0.002	0.001	0.002
BaO	0.000	0.000	0.000	0.000	0.000	0.000
SrO	0.002	0.002	0.000	0.000	0.001	0.000
F	0.000	0.000	0.000	0.000	0.000	0.000
Cl	0.000	0.001	0.002	0.007	0.000	0.001
Total	9.424	9.421	9.427	9.397	9.442	9.428
Tet Al	1.270	1.268	1.279	1.270	1.279	1.272
Oct Al	0.331	0.338	0.343	0.319	0.338	0.324
Total Al	1.601	1.606	1.621	1.589	1.617	1.596

Table D3: Electron microprobe results: biotite atomic proportions

Element	385011.127.3	385011.127.4	385011.128.1	385011.128.2	385011.128.3	385011.128.4
Si (IV)	2.720	2.702	2.728	2.714	2.722	2.864
Al (IV)	1.280	1.298	1.272	1.286	1.278	1.136
Al (VI)	0.324	0.301	0.340	0.326	0.328	0.377
Al (total)	1.603	1.599	1.612	1.612	1.606	1.512
FeO	1.334	1.340	1.332	1.345	1.350	1.267
MgO	1.083	1.056	1.045	1.050	1.045	1.040
MnO	0.019	0.019	0.019	0.020	0.017	0.018
CaO	0.001	0.000	0.001	0.001	0.000	0.001
Na₂O	0.006	0.010	0.010	0.013	0.008	0.011
K₂O	0.942	0.917	0.919	0.931	0.935	0.866
TiO₂	0.121	0.128	0.131	0.132	0.129	0.117
ZnO	0.001	0.001	0.001	0.002	0.003	0.003
BaO	0.000	0.000	0.000	0.000	0.000	0.000
SrO	0.000	0.001	0.001	0.001	0.001	0.000
F	0.000	0.119	0.000	0.000	0.000	0.000
Cl	0.000	0.001	0.001	0.001	0.002	0.001
Total	9.434	9.493	9.412	9.432	9.424	9.214
Tet Al	1.280	1.298	1.272	1.286	1.278	1.136
Oct Al	0.324	0.301	0.340	0.326	0.328	0.377
Total Al	1.603	1.599	1.612	1.612	1.606	1.512

Table D3: Electron microprobe results: biotite atomic proportions

Element	385011.129.1	385011.129.2	385011.129.3	385011.129.4	385011.130.1	385011.130.2
Si (IV)	2.716	2.704	2.722	2.737	2.682	2.702
Al (IV)	1.284	1.296	1.278	1.263	1.318	1.298
Al (VI)	0.353	0.343	0.350	0.346	0.322	0.332
Al (total)	1.637	1.639	1.628	1.610	1.640	1.630
FeO	1.329	1.347	1.328	1.320	1.394	1.364
MgO	1.055	1.066	1.063	1.078	1.061	1.065
MnO	0.019	0.020	0.020	0.019	0.022	0.020
CaO	0.001	0.001	0.001	0.002	0.002	0.002
Na₂O	0.014	0.011	0.016	0.013	0.009	0.004
K₂O	0.925	0.906	0.915	0.894	0.880	0.900
TiO₂	0.117	0.118	0.118	0.119	0.125	0.121
ZnO	0.002	0.002	0.000	0.000	0.003	0.004
BaO	0.000	0.000	0.000	0.000	0.000	0.000
SrO	0.001	0.001	0.001	0.001	0.000	0.001
F	0.000	0.000	0.000	0.000	0.000	0.000
Cl	0.006	0.006	0.002	0.001	0.000	0.000
Total	9.458	9.459	9.440	9.403	9.457	9.444
Tet Al	1.284	1.296	1.278	1.263	1.318	1.298
Oct Al	0.353	0.343	0.350	0.346	0.322	0.332
Total Al	1.637	1.639	1.628	1.610	1.640	1.630

Table D3: Electron microprobe results: biotite atomic proportions

Element	385011.131.1	385011.131.2	385011.131.3	385011.131.4	385011.132.1	385011.132.2
Si (IV)	2.732	2.725	2.719	2.730	2.733	2.726
Al (IV)	1.268	1.275	1.281	1.270	1.267	1.274
Al (VI)	0.359	0.357	0.346	0.369	0.333	0.343
Al (total)	1.627	1.633	1.626	1.639	1.600	1.617
FeO	1.313	1.314	1.290	1.307	1.329	1.329
MgO	1.048	1.058	1.052	1.041	1.070	1.075
MnO	0.020	0.019	0.018	0.020	0.020	0.018
CaO	0.001	0.001	0.001	0.001	0.001	0.003
Na₂O	0.017	0.013	0.013	0.017	0.012	0.009
K₂O	0.899	0.911	0.896	0.915	0.901	0.903
TiO₂	0.126	0.123	0.124	0.122	0.126	0.120
ZnO	0.003	0.003	0.003	0.002	0.003	0.001
BaO	0.000	0.000	0.000	0.000	0.000	0.000
SrO	0.000	0.000	0.001	0.001	0.001	0.001
F	0.000	0.000	0.109	0.000	0.000	0.000
Cl	0.001	0.000	0.002	0.001	0.001	0.000
Total	9.414	9.431	9.480	9.434	9.398	9.419
Tet Al	1.268	1.275	1.281	1.270	1.267	1.274
Oct Al	0.359	0.357	0.346	0.369	0.333	0.343
Total Al	1.627	1.633	1.626	1.639	1.600	1.617

Table D3: Electron microprobe results: biotite atomic proportions

Element	385011.132.3	385011.132.4	385011.133.1	385011.133.2	385011.133.3	385011.133.4
Si (IV)	2.732	2.726	2.721	2.701	2.719	2.760
Al (IV)	1.268	1.274	1.279	1.299	1.281	1.240
Al (VI)	0.325	0.315	0.333	0.324	0.372	0.309
Al (total)	1.594	1.589	1.613	1.624	1.653	1.549
FeO	1.314	1.346	1.316	1.347	1.316	1.327
MgO	1.088	1.076	1.075	1.081	1.028	1.101
MnO	0.018	0.020	0.018	0.019	0.019	0.021
CaO	0.002	0.002	0.001	0.001	0.001	0.002
Na₂O	0.013	0.011	0.009	0.009	0.005	0.013
K₂O	0.920	0.908	0.939	0.903	0.908	0.888
TiO₂	0.128	0.129	0.125	0.128	0.129	0.126
ZnO	0.001	0.002	0.004	0.002	0.002	0.002
BaO	0.000	0.000	0.000	0.000	0.000	0.000
SrO	0.000	0.001	0.000	0.001	0.000	0.000
F	0.000	0.000	0.000	0.000	0.000	0.000
Cl	0.000	0.001	0.001	0.000	0.001	0.003
Total	9.404	9.399	9.434	9.439	9.435	9.340
Tet Al	1.268	1.274	1.279	1.299	1.281	1.240
Oct Al	0.325	0.315	0.333	0.324	0.372	0.309
Total Al	1.594	1.589	1.613	1.624	1.653	1.549

Table D3: Electron microprobe results: biotite atomic proportions

Element	385011.134.1	385011.134.2	385011.134.3	385011.134.4	385011.135.1	385011.135.2
Si (IV)	2.724	2.701	2.733	2.710	2.734	2.694
Al (IV)	1.276	1.299	1.267	1.290	1.266	1.306
Al (VI)	0.356	0.340	0.360	0.333	0.372	0.343
Al (total)	1.632	1.639	1.627	1.622	1.638	1.649
FeO	1.306	1.334	1.308	1.303	1.305	1.337
MgO	1.059	1.069	1.061	1.060	1.077	1.137
MnO	0.019	0.020	0.019	0.019	0.018	0.020
CaO	0.001	0.003	0.002	0.002	0.002	0.002
Na₂O	0.015	0.014	0.009	0.015	0.008	0.012
K₂O	0.924	0.912	0.903	0.908	0.889	0.816
TiO₂	0.123	0.124	0.124	0.124	0.110	0.113
ZnO	0.003	0.002	0.001	0.003	0.004	0.002
BaO	0.000	0.000	0.000	0.000	0.000	0.000
SrO	0.000	0.000	0.000	0.001	0.001	0.000
F	0.000	0.000	0.000	0.093	0.000	0.000
Cl	0.000	0.001	0.001	0.002	0.002	0.000
Total	9.439	9.458	9.414	9.485	9.425	9.432
Tet Al	1.276	1.299	1.267	1.290	1.266	1.306
Oct Al	0.356	0.340	0.360	0.333	0.372	0.343
Total Al	1.632	1.639	1.627	1.622	1.638	1.649

Table D3: Electron microprobe results: biotite atomic proportions

Element	385011.135.3	385011.136.1	385011.136.2	385011.136.3	385011.136.4	385011.137.1
Si (IV)	2.715	2.718	2.730	2.728	2.707	2.757
Al (IV)	1.285	1.282	1.270	1.272	1.293	1.243
Al (VI)	0.355	0.299	0.350	0.330	0.329	0.364
Al (total)	1.640	1.582	1.620	1.602	1.622	1.607
FeO	1.315	1.347	1.335	1.328	1.330	1.285
MgO	1.108	1.056	1.058	1.096	1.062	1.089
MnO	0.020	0.018	0.019	0.017	0.018	0.018
CaO	0.002	0.001	0.001	0.001	0.001	0.001
Na₂O	0.015	0.002	0.008	0.002	0.013	0.011
K₂O	0.859	0.904	0.937	0.913	0.929	0.897
TiO₂	0.111	0.131	0.112	0.119	0.111	0.111
ZnO	0.002	0.002	0.001	0.003	0.002	0.002
BaO	0.000	0.000	0.000	0.000	0.000	0.000
SrO	0.002	0.001	0.000	0.000	0.000	0.002
F	0.000	0.099	0.000	0.000	0.093	0.000
Cl	0.001	0.001	0.001	0.001	0.000	0.001
Total	9.431	9.445	9.441	9.413	9.511	9.390
Tet Al	1.285	1.282	1.270	1.272	1.293	1.243
Oct Al	0.355	0.299	0.350	0.330	0.329	0.364
Total Al	1.640	1.582	1.620	1.602	1.622	1.607

Table D3: Electron microprobe results: biotite atomic proportions

Element	385011.137.2	385011.137.3	385011.137.4	385199.140.1	385199.140.2	385199.140.3
Si (IV)	2.731	2.761	2.713	2.709	2.706	2.712
Al (IV)	1.269	1.239	1.287	1.291	1.294	1.288
Al (VI)	0.355	0.390	0.317	0.414	0.391	0.411
Al (total)	1.624	1.629	1.603	1.706	1.685	1.698
FeO	1.310	1.257	1.326	1.362	1.352	1.367
MgO	1.105	1.084	1.155	0.978	0.973	0.984
MnO	0.019	0.018	0.020	0.010	0.010	0.010
CaO	0.001	0.002	0.016	0.000	0.001	0.000
Na₂O	0.008	0.015	0.009	0.007	0.013	0.011
K₂O	0.869	0.889	0.785	0.942	0.936	0.935
TiO₂	0.114	0.111	0.125	0.098	0.096	0.095
ZnO	0.000	0.000	0.002	0.002	0.001	0.002
BaO	0.000	0.000	0.000	0.000	0.000	0.000
SrO	0.001	0.000	0.001	0.001	0.000	0.000
F	0.000	0.000	0.000	0.000	0.113	0.000
Cl	0.000	0.000	0.001	0.000	0.000	0.002
Total	9.406	9.395	9.361	9.521	9.571	9.516
Tet Al	1.269	1.239	1.287	1.291	1.294	1.288
Oct Al	0.355	0.390	0.317	0.414	0.391	0.411
Total Al	1.624	1.629	1.603	1.706	1.685	1.698

Table D3: Electron microprobe results: biotite atomic proportions

Element	385199.140.4	385199.141.1	385199.141.2	385199.141.3	385199.141.4	385199.142.1
Si (IV)	2.719	2.713	2.693	2.696	2.714	2.222
Al (IV)	1.281	1.287	1.307	1.304	1.286	1.778
Al (VI)	0.418	0.416	0.387	0.387	0.406	0.206
Al (total)	1.699	1.703	1.694	1.691	1.692	1.983
FeO	1.384	1.390	1.391	1.382	1.381	1.842
MgO	0.958	0.965	0.966	0.965	0.974	1.499
MnO	0.009	0.011	0.010	0.010	0.010	0.018
CaO	0.000	0.000	0.001	0.001	0.000	0.003
Na₂O	0.012	0.004	0.013	0.010	0.017	0.009
K₂O	0.919	0.926	0.923	0.928	0.933	0.169
TiO₂	0.096	0.093	0.094	0.096	0.095	0.062
ZnO	0.005	0.002	0.002	0.004	0.002	0.003
BaO	0.000	0.000	0.000	0.000	0.000	0.000
SrO	0.001	0.001	0.000	0.000	0.001	0.001
F	0.000	0.000	0.095	0.095	0.000	0.000
Cl	0.000	0.000	0.000	0.001	0.002	0.004
Total	9.500	9.511	9.576	9.571	9.513	9.798
Tet Al	1.281	1.287	1.307	1.304	1.286	1.778
Oct Al	0.418	0.416	0.387	0.387	0.406	0.206
Total Al	1.699	1.703	1.694	1.691	1.692	1.983

Table D3: Electron microprobe results: biotite atomic proportions

Element	385199.142.2	385199.142.3	385199.142.4	385199.143.1	385199.143.2	385199.143.3
Si (IV)	2.736	2.245	2.276	2.713	2.718	2.727
Al (IV)	1.264	1.755	1.724	1.287	1.282	1.273
Al (VI)	0.389	0.217	0.197	0.425	0.410	0.417
Al (total)	1.654	1.972	1.921	1.712	1.692	1.690
FeO	1.387	1.783	1.789	1.370	1.389	1.364
MgO	0.980	1.505	1.499	0.970	0.965	0.974
MnO	0.012	0.018	0.017	0.010	0.012	0.010
CaO	0.002	0.002	0.002	0.001	0.002	0.001
Na₂O	0.025	0.007	0.008	0.024	0.022	0.028
K₂O	0.894	0.195	0.223	0.908	0.907	0.911
TiO₂	0.101	0.068	0.069	0.091	0.093	0.091
ZnO	0.004	0.004	0.003	0.004	0.005	0.004
BaO	0.000	0.000	0.000	0.000	0.000	0.000
SrO	0.000	0.000	0.000	0.000	0.001	0.001
F	0.000	0.000	0.000	0.000	0.000	0.000
Cl	0.002	0.003	0.005	0.003	0.002	0.012
Total	9.450	9.775	9.733	9.520	9.499	9.502
Tet Al	1.264	1.755	1.724	1.287	1.282	1.273
Oct Al	0.389	0.217	0.197	0.425	0.410	0.417
Total Al	1.654	1.972	1.921	1.712	1.692	1.690

Table D3: Electron microprobe results: biotite atomic proportions

Element	385199.143.4	385199.144.1	385199.144.2	385199.144.3	385199.144.4	385199.145.1
Si (IV)	2.713	2.710	2.724	2.724	2.719	2.704
Al (IV)	1.287	1.290	1.276	1.276	1.281	1.296
Al (VI)	0.389	0.403	0.422	0.421	0.418	0.383
Al (total)	1.676	1.692	1.698	1.697	1.699	1.679
FeO	1.408	1.402	1.388	1.370	1.382	1.381
MgO	0.974	0.961	0.955	0.959	0.963	0.967
MnO	0.011	0.010	0.011	0.011	0.009	0.009
CaO	0.001	0.002	0.002	0.002	0.001	0.001
Na₂O	0.020	0.021	0.022	0.019	0.016	0.017
K₂O	0.883	0.917	0.911	0.908	0.913	0.911
TiO₂	0.106	0.097	0.091	0.098	0.093	0.094
ZnO	0.002	0.003	0.001	0.003	0.003	0.002
BaO	0.000	0.000	0.000	0.000	0.000	0.000
SrO	0.000	0.000	0.000	0.001	0.000	0.000
F	0.000	0.000	0.000	0.000	0.000	0.120
Cl	0.002	0.002	0.002	0.001	0.004	0.001
Total	9.472	9.509	9.501	9.491	9.504	9.566
Tet Al	1.287	1.290	1.276	1.276	1.281	1.296
Oct Al	0.389	0.403	0.422	0.421	0.418	0.383
Total Al	1.676	1.692	1.698	1.697	1.699	1.679

Table D3: Electron microprobe results: biotite atomic proportions

Element	385199.145.2	385199.145.3	385199.145.4	385199.146.1	385199.146.2	385199.146.3
Si (IV)	2.722	2.690	2.722	2.712	2.511	2.727
Al (IV)	1.278	1.310	1.278	1.288	1.489	1.273
Al (VI)	0.411	0.395	0.379	0.420	0.295	0.420
Al (total)	1.689	1.705	1.657	1.708	1.785	1.694
FeO	1.381	1.367	1.400	1.363	1.610	1.364
MgO	0.968	0.932	1.005	0.965	1.233	0.966
MnO	0.010	0.008	0.010	0.011	0.015	0.011
CaO	0.000	0.000	0.001	0.003	0.004	0.003
Na₂O	0.011	0.008	0.013	0.028	0.007	0.025
K₂O	0.935	0.922	0.908	0.913	0.525	0.902
TiO₂	0.092	0.113	0.096	0.097	0.084	0.097
ZnO	0.003	0.002	0.003	0.005	0.003	0.002
BaO	0.000	0.000	0.000	0.000	0.000	0.000
SrO	0.002	0.000	0.001	0.001	0.002	0.001
F	0.000	0.123	0.000	0.000	0.000	0.000
Cl	0.000	0.002	0.001	0.004	0.005	0.004
Total	9.504	9.578	9.471	9.518	9.566	9.489
Tet Al	1.278	1.310	1.278	1.288	1.489	1.273
Oct Al	0.411	0.395	0.379	0.420	0.295	0.420
Total Al	1.689	1.705	1.657	1.708	1.785	1.694

Table D3: Electron microprobe results: biotite atomic proportions

Element	385199.146.4	385199.147.1	385199.147.2	385199.147.3	385199.147.4	385199.148.1
Si (IV)	2.707	2.573	2.635	2.623	2.715	2.700
Al (IV)	1.293	1.427	1.365	1.377	1.285	1.300
Al (VI)	0.397	0.260	0.296	0.303	0.414	0.390
Al (total)	1.689	1.687	1.661	1.681	1.700	1.690
FeO	1.399	1.604	1.549	1.542	1.395	1.382
MgO	0.980	1.173	1.071	1.101	0.958	0.954
MnO	0.010	0.010	0.011	0.010	0.008	0.010
CaO	0.003	0.001	0.001	0.001	0.001	0.000
Na₂O	0.021	0.011	0.012	0.008	0.016	0.016
K₂O	0.896	0.675	0.805	0.769	0.909	0.920
TiO₂	0.099	0.093	0.097	0.093	0.096	0.094
ZnO	0.002	0.003	0.002	0.004	0.003	0.003
BaO	0.000	0.000	0.000	0.000	0.000	0.000
SrO	0.001	0.002	0.000	0.000	0.001	0.000
F	0.000	0.000	0.000	0.000	0.000	0.118
Cl	0.001	0.001	0.001	0.001	0.002	0.002
Total	9.498	9.521	9.507	9.513	9.503	9.579
Tet Al	1.293	1.427	1.365	1.377	1.285	1.300
Oct Al	0.397	0.260	0.296	0.303	0.414	0.390
Total Al	1.689	1.687	1.661	1.681	1.700	1.690

Table D3: Electron microprobe results: biotite atomic proportions

Element	385199.148.2	385199.148.3	385199.148.4	385199.149.1	385199.149.2	385199.149.3
Si (IV)	2.686	2.703	2.694	2.706	2.711	2.730
Al (IV)	1.314	1.297	1.306	1.294	1.289	1.270
Al (VI)	0.387	0.420	0.389	0.424	0.413	0.454
Al (total)	1.701	1.717	1.695	1.718	1.702	1.724
FeO	1.398	1.391	1.382	1.383	1.397	1.338
MgO	0.950	0.963	0.968	0.960	0.951	0.945
MnO	0.011	0.010	0.011	0.009	0.008	0.010
CaO	0.000	0.001	0.001	0.001	0.000	0.001
Na₂O	0.010	0.014	0.012	0.017	0.014	0.017
K₂O	0.927	0.927	0.906	0.911	0.927	0.916
TiO₂	0.096	0.091	0.092	0.094	0.096	0.095
ZnO	0.002	0.001	0.001	0.003	0.004	0.002
BaO	0.000	0.000	0.000	0.000	0.000	0.000
SrO	0.000	0.000	0.001	0.001	0.001	0.000
F	0.109	0.000	0.124	0.000	0.000	0.000
Cl	0.000	0.001	0.000	0.002	0.001	0.002
Total	9.592	9.535	9.581	9.524	9.515	9.505
Tet Al	1.314	1.297	1.306	1.294	1.289	1.270
Oct Al	0.387	0.420	0.389	0.424	0.413	0.454
Total Al	1.701	1.717	1.695	1.718	1.702	1.724

Table D3: Electron microprobe results: biotite atomic proportions

Element	385199.149.4	385199.150.1	385199.150.2	385199.150.3	385199.150.4	385199.151.1
Si (IV)	2.681	2.728	2.733	2.725	2.704	2.643
Al (IV)	1.319	1.272	1.267	1.275	1.296	1.357
Al (VI)	0.377	0.413	0.420	0.423	0.404	0.337
Al (total)	1.696	1.685	1.687	1.698	1.701	1.694
FeO	1.406	1.376	1.368	1.366	1.414	1.543
MgO	0.968	0.963	0.967	0.965	0.955	1.070
MnO	0.011	0.009	0.008	0.009	0.008	0.010
CaO	0.001	0.001	0.000	0.000	0.002	0.001
Na₂O	0.015	0.008	0.012	0.011	0.011	0.005
K₂O	0.902	0.926	0.932	0.932	0.915	0.771
TiO₂	0.097	0.099	0.091	0.095	0.098	0.079
ZnO	0.002	0.002	0.004	0.001	0.004	0.003
BaO	0.000	0.000	0.000	0.000	0.000	0.000
SrO	0.000	0.001	0.001	0.000	0.000	0.000
F	0.109	0.000	0.000	0.000	0.000	0.000
Cl	0.001	0.001	0.001	0.000	0.000	0.001
Total	9.583	9.482	9.492	9.500	9.512	9.514
Tet Al	1.319	1.272	1.267	1.275	1.296	1.357
Oct Al	0.377	0.413	0.420	0.423	0.404	0.337
Total Al	1.696	1.685	1.687	1.698	1.701	1.694

Table D3: Electron microprobe results: biotite atomic proportions

Element	385199.151.2	385199.151.3	385199.151.4	385199.152.1	385199.152.2	385199.152.3
Si (IV)	2.697	2.715	2.708	2.739	2.730	2.728
Al (IV)	1.303	1.285	1.292	1.261	1.270	1.272
Al (VI)	0.429	0.411	0.408	0.427	0.433	0.433
Al (total)	1.732	1.696	1.700	1.688	1.703	1.705
FeO	1.400	1.423	1.437	1.356	1.379	1.373
MgO	0.963	0.963	0.941	0.991	0.953	0.987
MnO	0.010	0.009	0.008	0.008	0.009	0.008
CaO	0.001	0.000	0.000	0.000	0.001	0.000
Na₂O	0.011	0.008	0.010	0.023	0.016	0.011
K₂O	0.928	0.908	0.926	0.893	0.911	0.884
TiO₂	0.080	0.085	0.088	0.087	0.088	0.085
ZnO	0.003	0.002	0.003	0.002	0.003	0.001
BaO	0.000	0.000	0.000	0.000	0.000	0.000
SrO	0.000	0.000	0.000	0.000	0.000	0.001
F	0.000	0.000	0.000	0.000	0.000	0.000
Cl	0.002	0.001	0.002	0.001	0.004	0.002
Total	9.558	9.507	9.523	9.477	9.500	9.488
Tet Al	1.303	1.285	1.292	1.261	1.270	1.272
Oct Al	0.429	0.411	0.408	0.427	0.433	0.433
Total Al	1.732	1.696	1.700	1.688	1.703	1.705

Table D3: Electron microprobe results: biotite atomic proportions

Element	385199.152.4	385199.153.1	385199.153.2	385199.153.3	385199.153.4	385336.2.158.1
Si (IV)	2.723	2.710	2.695	2.709	2.725	3.308
Al (IV)	1.277	1.290	1.305	1.291	1.275	0.692
Al (VI)	0.445	0.414	0.408	0.408	0.386	1.633
Al (total)	1.722	1.704	1.713	1.699	1.661	2.325
FeO	1.354	1.401	1.398	1.403	1.400	0.188
MgO	0.967	0.952	0.966	0.955	0.976	0.306
MnO	0.008	0.008	0.008	0.009	0.009	0.002
CaO	0.000	0.000	0.000	0.000	0.000	0.004
Na₂O	0.011	0.016	0.017	0.011	0.011	0.036
K₂O	0.915	0.932	0.934	0.941	0.922	0.586
TiO₂	0.086	0.092	0.097	0.093	0.102	0.039
ZnO	0.005	0.006	0.001	0.005	0.002	0.001
BaO	0.000	0.000	0.000	0.000	0.000	0.002
SrO	0.001	0.000	0.000	0.000	0.000	0.001
F	0.000	0.000	0.000	0.000	0.000	0.000
Cl	0.003	0.001	0.000	0.000	0.001	0.003
Total	9.516	9.524	9.541	9.524	9.471	9.128
Tet Al	1.277	1.290	1.305	1.291	1.275	0.692
Oct Al	0.445	0.414	0.408	0.408	0.386	1.633
Total Al	1.722	1.704	1.713	1.699	1.661	2.325

Table D3: Electron microprobe results: biotite atomic proportions

Element	385336.2.158.2	385336.2.158.3	385156.1.1	385156.1.2	385156.2.1	385156.2.2
Si (IV)	3.252	3.271	2.741	2.743	2.737	2.704
Al (IV)	0.748	0.729	1.259	1.257	1.263	1.296
Al (VI)	1.540	1.627	0.382	0.384	0.385	0.330
Al (total)	2.288	2.355	1.641	1.641	1.647	1.626
FeO	0.276	0.178	1.416	1.408	1.398	1.409
MgO	0.401	0.267	0.985	0.986	0.972	0.967
MnO	0.003	0.002	0.013	0.014	0.013	0.015
CaO	0.003	0.003	0.001	0.001	0.000	0.000
Na₂O	0.029	0.034	0.005	0.003	0.011	0.008
K₂O	0.568	0.631	0.924	0.924	0.932	0.921
TiO₂	0.039	0.069	0.109	0.112	0.123	0.118
ZnO	0.000	0.000	0.001	0.002	0.001	0.004
BaO	0.002	0.002	0.002	0.003	0.002	0.002
SrO	0.001	0.001	-0.001	0.000	0.001	0.000
F	0.000	0.000	-0.091	-0.100	-0.101	0.111
Cl	0.003	0.003	0.003	0.002	0.000	0.000
Total	9.152	9.172	9.390	9.380	9.384	9.511
Tet Al	0.748	0.729	1.259	1.257	1.263	1.296
Oct Al	1.540	1.627	0.382	0.384	0.385	0.330
Total Al	2.288	2.355	1.641	1.641	1.647	1.626

Table D3: Electron microprobe results: biotite atomic proportions

Element	385156.3.1	385156.3.2	385156.4.1	385156.4.2	385156.5.1	385156.5.2	385156.6.1
Si (IV)	2.791	2.823	2.746	3.514	2.733	2.737	2.731
Al (IV)	1.209	1.177	1.254	0.486	1.267	1.263	1.269
Al (VI)	0.467	0.497	0.370	0.662	0.398	0.398	0.368
Al (total)	1.676	1.674	1.624	1.148	1.665	1.661	1.637
FeO	1.420	1.454	1.396	1.056	1.383	1.396	1.400
MgO	1.008	0.996	0.979	0.721	0.974	0.963	0.978
MnO	0.013	0.016	0.015	0.010	0.014	0.014	0.013
CaO	0.000	0.001	0.000	0.001	0.000	0.001	0.000
Na₂O	0.011	0.007	0.006	0.005	0.008	0.011	0.010
K₂O	0.359	0.362	0.921	0.648	0.915	0.901	0.940
TiO₂	0.115	0.115	0.130	0.089	0.123	0.124	0.128
ZnO	0.003	0.002	0.001	0.002	0.002	0.001	-0.001
BaO	0.003	0.003	0.003	0.001	0.003	0.002	0.001
SrO	0.000	0.000	0.001	0.001	-0.001	0.002	-0.001
F	0.081	-0.091	-0.093	-0.092	-0.094	-0.097	-0.085
Cl	0.001	0.000	0.001	0.000	0.001	0.000	0.003
Total	9.158	9.038	9.354	8.252	9.391	9.378	9.394
Tet Al	1.209	1.177	1.254	0.486	1.267	1.263	1.269
Oct Al	0.467	0.497	0.370	0.662	0.398	0.398	0.368
Total Al	1.676	1.674	1.624	1.148	1.665	1.661	1.637

Table D3: Electron microprobe results: biotite atomic proportions

Element	385156.6.2	385156.7.1	385156.7.2	385156.8.1	385156.8.2	385156.9.1	385156.9.2
Si (IV)	2.734	2.743	2.748	2.756	2.746	2.742	2.734
Al (IV)	1.266	1.257	1.252	1.244	1.254	1.258	1.266
Al (VI)	0.385	0.376	0.376	0.388	0.396	0.382	0.385
Al (total)	1.651	1.632	1.628	1.632	1.650	1.640	1.652
FeO	1.397	1.387	1.376	1.367	1.368	1.394	1.407
MgO	0.970	0.982	0.981	0.984	0.973	0.985	0.960
MnO	0.014	0.015	0.014	0.015	0.014	0.015	0.014
CaO	0.001	0.001	0.001	0.000	0.000	0.000	0.001
Na2O	0.010	0.004	0.009	0.009	0.015	0.008	0.010
K2O	0.938	0.932	0.936	0.928	0.928	0.922	0.931
TiO2	0.124	0.126	0.128	0.126	0.121	0.124	0.125
ZnO	0.000	0.001	0.004	0.000	0.003	0.001	0.001
BaO	0.002	0.003	0.003	0.003	0.002	0.003	0.003
SrO	0.000	0.000	0.000	0.000	0.000	0.000	0.000
F	-0.103	-0.087	-0.093	-0.101	-0.084	-0.111	-0.104
Cl	0.001	0.000	0.001	0.001	0.002	0.001	0.000
Total	9.390	9.372	9.364	9.352	9.389	9.364	9.385
Tet Al	1.266	1.257	1.252	1.244	1.254	1.258	1.266
Oct Al	0.385	0.376	0.376	0.388	0.396	0.382	0.385
Total Al	1.651	1.632	1.628	1.632	1.650	1.640	1.652

Table D3: Electron microprobe results: biotite atomic proportions

Element	385156.10.1	385156.10.2	385156.11.1	385156.11.2	385156.12.1	385156.12.2	385156.13.1
Si (IV)	2.722	2.763	2.755	2.479	2.744	2.728	2.736
Al (IV)	1.278	1.237	1.245	1.521	1.256	1.272	1.264
Al (VI)	0.381	0.413	0.376	0.255	0.364	0.375	0.381
Al (total)	1.659	1.649	1.621	1.776	1.620	1.647	1.645
FeO	1.410	1.351	1.383	1.624	1.405	1.423	1.403
MgO	0.987	0.997	0.989	1.355	0.991	0.973	0.975
MnO	0.015	0.020	0.014	0.017	0.014	0.015	0.015
CaO	0.000	0.001	0.001	0.000	0.000	0.000	0.000
Na2O	0.011	0.008	0.017	-0.001	0.008	0.009	0.008
K2O	0.898	0.883	0.926	0.527	0.920	0.925	0.932
TiO2	0.120	0.114	0.120	0.096	0.125	0.122	0.122
ZnO	0.003	0.002	0.000	0.000	0.001	0.002	0.003
BaO	0.002	0.003	0.002	0.003	0.002	0.001	0.002
SrO	-0.001	0.002	0.001	0.000	0.001	0.000	0.001
F	-0.087	-0.102	-0.087	-0.149	-0.089	-0.103	-0.109
Cl	0.000	0.002	0.000	0.001	-0.001	0.000	0.000
Total	9.398	9.342	9.363	9.503	9.359	9.390	9.380
Tet Al	1.278	1.237	1.245	1.521	1.256	1.272	1.264
Oct Al	0.381	0.413	0.376	0.255	0.364	0.375	0.381
Total Al	1.659	1.649	1.621	1.776	1.620	1.647	1.645

Table D3: Electron microprobe results: biotite atomic proportions

Element	385156.13.2	385156.13.3	385156.13.4	385156.14.1	385156.14.2	385156.14.3	385156.15.1
Si (IV)	2.723	3.231	2.728	2.748	2.738	2.599	2.725
Al (IV)	1.277	0.769	1.272	1.252	1.262	1.401	1.275
Al (VI)	0.371	0.519	0.391	0.409	0.400	0.307	0.354
Al (total)	1.648	1.288	1.663	1.662	1.662	1.708	1.629
FeO	1.434	0.092	1.393	1.356	1.377	1.540	1.370
MgO	0.997	0.091	0.983	0.985	0.995	1.223	0.981
MnO	0.013	0.003	0.014	0.014	0.014	0.015	0.014
CaO	0.001	2.009	0.000	0.002	0.001	0.001	0.004
Na₂O	0.009	0.025	0.009	0.009	0.009	0.011	0.012
K₂O	0.907	0.413	0.935	0.913	0.917	0.668	0.871
TiO₂	0.113	0.013	0.119	0.118	0.115	0.094	0.111
ZnO	0.003	-0.001	0.001	0.001	0.002	0.003	0.011
BaO	0.004	0.005	0.002	0.003	0.002	0.002	0.003
SrO	0.001	0.001	0.001	0.002	0.000	0.000	0.000
F	-0.108	0.318	-0.109	-0.096	-0.105	-0.148	0.120
Cl	0.000	0.002	0.000	0.002	0.000	0.002	0.002
Total	9.392	8.779	9.402	9.379	9.389	9.427	9.482
Tet Al	1.277	0.769	1.272	1.252	1.262	1.401	1.275
Oct Al	0.371	0.519	0.391	0.409	0.400	0.307	0.354
Total Al	1.648	1.288	1.663	1.662	1.662	1.708	1.629

Table D3: Electron microprobe results: biotite atomic proportions

Element	385156.15.2	385156.15.3	385156.16.1	385156.16.2	385156.17.1	385156.17.2	385156.17.3
Si (IV)	2.721	2.718	2.750	2.733	2.735	2.733	2.738
Al (IV)	1.279	1.282	1.250	1.267	1.265	1.267	1.262
Al (VI)	0.395	0.368	0.398	0.394	0.402	0.388	0.381
Al (total)	1.674	1.650	1.648	1.661	1.668	1.655	1.643
FeO	1.391	1.363	1.357	1.371	1.375	1.390	1.398
MgO	0.989	0.973	0.989	0.990	0.974	0.983	0.977
MnO	0.014	0.013	0.014	0.014	0.014	0.014	0.013
CaO	0.001	0.001	0.002	0.002	0.000	0.001	0.002
Na₂O	0.008	0.014	0.030	0.036	0.005	0.008	0.007
K₂O	0.929	0.903	0.882	0.891	0.936	0.943	0.936
TiO₂	0.115	0.113	0.121	0.119	0.121	0.118	0.120
ZnO	0.000	0.003	0.003	0.004	0.003	0.000	0.001
BaO	0.002	0.003	0.002	0.002	0.003	0.005	0.002
SrO	0.000	0.001	0.002	0.000	0.001	0.000	0.000
F	-0.100	0.092	-0.078	-0.090	-0.107	-0.111	-0.095
Cl	0.001	0.002	0.004	0.003	0.000	0.003	-0.001
Total	9.420	9.500	9.372	9.399	9.395	9.398	9.387
Tet Al	1.279	1.282	1.250	1.267	1.265	1.267	1.262
Oct Al	0.395	0.368	0.398	0.394	0.402	0.388	0.381
Total Al	1.674	1.650	1.648	1.661	1.668	1.655	1.643

Table D3: Electron microprobe results: biotite atomic proportions

Element	385156.18.1	385156.18.2	385156.18.3	385156.18.4
Si (IV)	2.740	2.704	2.727	2.744
Al (IV)	1.260	1.296	1.273	1.256
Al (VI)	0.361	0.323	0.368	0.388
Al (total)	1.621	1.619	1.641	1.644
FeO	1.405	1.412	1.389	1.386
MgO	1.008	0.964	0.991	0.992
MnO	0.012	0.013	0.013	0.013
CaO	0.001	0.002	0.003	0.001
Na₂O	0.015	0.018	0.044	0.016
K₂O	0.905	0.901	0.905	0.914
TiO₂	0.122	0.119	0.119	0.118
ZnO	0.004	0.015	0.008	0.002
BaO	0.002	0.002	0.003	0.002
SrO	0.000	0.001	0.000	-0.001
F	-0.098	0.110	-0.083	-0.101
Cl	0.002	0.006	0.012	0.002
Total	9.361	9.504	9.414	9.376
Tet Al	1.260	1.296	1.273	1.256
Oct Al	0.361	0.323	0.368	0.388
Total Al	1.621	1.619	1.641	1.644

Table D4: Secondary standard compilation: chlorite

Element	Asttimex chlorite				
F wt%	-0.14	-0.21	-1.46	-0.20	-0.16
FeO wt%	3.10	3.18	3.14	3.17	2.98
V2O3 wt%	0.02	0.04	0.03	0.04	0.02
TiO2 wt%	0.01	-0.01	0.01	-0.01	0.01
BaO wt%	-0.01	-0.03	0.00	-0.03	-0.02
Cl wt%	0.01	0.01	0.00	0.00	0.00
K2O wt%	0.01	0.00	0.01	0.00	0.01
CaO wt%	0.00	0.00	0.00	0.00	0.00
SrO wt%	0.02	0.02	0.05	0.03	0.01
Na2O wt%	0.00	-0.01	0.01	-0.04	0.00
Al2O3 wt%	17.66	17.58	17.55	17.56	17.51
SiO2 wt%	29.98	30.01	30.16	30.07	29.93
MgO wt%	32.42	32.29	32.09	32.18	31.95
Cr2O3 wt%	1.79	1.80	1.71	1.80	1.77
MnO wt%	0.00	0.02	0.02	0.01	0.01
ZnO wt%	0.01	0.00	0.02	0.00	-0.01
Total wt%	84.95	84.79	83.96	84.67	84.08

Table D4: Secondary standard compilation: chlorite

Element	Asttimex chlorite				
F wt%	-0.21	-0.14	-0.17	-0.20	-0.28
FeO wt%	3.34	3.09	3.15	3.13	3.13
V2O3 wt%	0.05	0.04	0.03	0.04	0.01
TiO2 wt%	0.00	0.01	0.00	0.00	0.01
BaO wt%	0.01	0.00	0.01	-0.01	0.00
Cl wt%	0.00	0.00	0.00	0.00	0.00
K2O wt%	0.00	0.00	0.01	0.01	0.00
CaO wt%	0.00	0.01	0.01	0.01	0.00
SrO wt%	0.01	0.02	0.02	0.03	0.00
Na2O wt%	0.02	0.01	0.00	-0.01	-0.01
Al2O3 wt%	17.88	17.51	17.53	17.52	17.31
SiO2 wt%	30.54	30.00	29.89	30.06	29.93
MgO wt%	32.83	32.02	31.87	32.26	31.91
Cr2O3 wt%	1.86	1.73	1.72	1.80	1.79
MnO wt%	0.02	0.02	0.03	0.02	0.02
ZnO wt%	0.00	0.01	-0.01	0.01	-0.01
Total wt%	86.43	84.38	84.15	84.75	83.92

Table D4: Secondary standard compilation: chlorite

Element	Asttimex chlorite				
F wt%	-0.37	-0.23	-0.17	-0.17	-0.25
FeO wt%	3.12	3.13	3.12	3.27	3.12
V2O3 wt%	0.02	0.03	0.04	0.02	0.02
TiO2 wt%	0.01	0.03	0.00	0.00	0.00
BaO wt%	0.02	-0.04	0.01	0.00	-0.01
Cl wt%	0.00	0.01	0.01	0.00	0.01
K2O wt%	0.00	0.00	0.00	0.00	0.00
CaO wt%	0.00	0.00	0.01	0.00	0.00
SrO wt%	0.03	0.05	0.02	0.06	0.02
Na2O wt%	-0.01	0.01	0.00	0.00	-0.03
Al2O3 wt%	17.77	17.76	17.58	17.95	17.52
SiO2 wt%	29.81	30.20	30.02	30.50	29.74
MgO wt%	32.15	32.58	32.17	32.98	31.99
Cr2O3 wt%	1.80	1.80	1.67	1.83	1.78
MnO wt%	0.01	0.01	0.01	0.01	0.02
ZnO wt%	0.04	0.02	-0.02	-0.03	0.02
Total wt%	84.56	85.45	84.56	86.52	84.05

Table D4: Secondary standard compilation: chlorite

Element	Asttimex chlorite				
F wt%	-0.16	-0.17	-0.15	-0.19	-0.21
FeO wt%	2.94	3.19	3.14	3.21	3.25
V2O3 wt%	0.03	0.04	0.02	0.02	0.03
TiO2 wt%	0.00	0.02	0.02	0.02	0.00
BaO wt%	0.01	0.01	0.03	0.00	-0.02
Cl wt%	0.01	0.00	0.01	0.00	0.00
K2O wt%	-0.01	0.01	0.00	0.01	0.00
CaO wt%	0.00	0.00	0.00	0.01	0.00
SrO wt%	0.04	0.02	0.00	0.02	0.02
Na2O wt%	0.01	0.01	-0.02	-0.01	0.00
Al2O3 wt%	17.56	17.59	17.63	17.33	17.70
SiO2 wt%	30.09	30.04	29.85	29.72	30.15
MgO wt%	32.00	32.41	32.14	32.01	32.39
Cr2O3 wt%	1.73	1.82	1.77	1.77	1.82
MnO wt%	0.01	0.01	0.01	0.01	0.03
ZnO wt%	0.00	-0.02	0.02	-0.02	-0.01
Total wt%	84.32	85.06	84.53	83.98	85.26

Table D4: Secondary standard compilation: chlorite

Element	Asttimex chlorite				
F wt%	-1.07	-0.96	-0.13	-0.28	-0.17
FeO wt%	3.15	3.22	3.28	3.18	3.17
V2O3 wt%	0.03	0.03	0.04	0.03	0.02
TiO2 wt%	0.01	0.02	0.01	0.00	0.04
BaO wt%	0.02	-0.02	-0.04	0.05	0.00
Cl wt%	0.00	0.01	0.00	0.00	0.01
K2O wt%	0.00	0.00	0.00	0.00	0.00
CaO wt%	0.01	0.00	0.00	0.00	0.01
SrO wt%	0.04	0.01	0.03	0.03	-0.01
Na2O wt%	-0.01	0.02	-0.02	0.00	0.00
Al2O3 wt%	17.41	17.40	17.87	17.43	17.61
SiO2 wt%	29.91	29.89	30.48	29.93	30.12
MgO wt%	31.89	31.67	33.02	32.12	32.09
Cr2O3 wt%	1.81	1.77	1.75	1.78	1.77
MnO wt%	0.02	0.02	0.02	0.02	0.03
ZnO wt%	0.00	0.01	0.00	-0.02	0.04
Total wt%	83.66	83.48	86.36	84.40	84.80

Table D4: Secondary standard compilation: chlorite

Element	Asttimex chlorite				
F wt%	-0.14	-0.14	-0.17	-0.17	-0.12
FeO wt%	3.09	3.03	2.96	3.42	3.23
V2O3 wt%	0.03	0.02	0.05	0.05	0.04
TiO2 wt%	0.03	0.00	0.02	0.00	0.01
BaO wt%	0.01	0.02	-0.01	0.00	0.00
Cl wt%	0.00	-0.01	0.01	0.00	-0.01
K2O wt%	0.01	0.00	-0.01	0.01	0.01
CaO wt%	0.00	0.00	0.00	0.00	0.01
SrO wt%	0.02	0.05	0.00	0.01	0.02
Na2O wt%	0.00	0.01	0.00	-0.01	-0.01
Al2O3 wt%	17.89	17.60	17.50	18.88	17.59
SiO2 wt%	30.11	29.84	29.97	31.96	29.92
MgO wt%	32.58	32.14	32.17	33.78	32.15
Cr2O3 wt%	1.78	1.78	1.74	1.96	1.84
MnO wt%	0.04	0.03	0.03	0.02	0.02
ZnO wt%	0.00	0.00	-0.01	0.05	0.02
Total wt%	85.50	84.44	84.31	90.02	84.78

Table D4: Secondary standard compilation: chlorite

<u>Element</u>	<u>Astimex chlorite</u>
F wt%	-0.13
FeO wt%	3.08
V2O3 wt%	0.03
TiO2 wt%	0.01
BaO wt%	0.00
Cl wt%	0.00
K2O wt%	0.01
CaO wt%	0.00
SrO wt%	0.05
Na2O wt%	0.00
Al2O3 wt%	17.56
SiO2 wt%	30.12
MgO wt%	32.38
Cr2O3 wt%	1.79
MnO wt%	0.02
ZnO wt%	-0.03
Total wt%	84.92

Table D5: Secondary standard compilation: biotite

Element	Astimex biotite					
F wt%	0.20	0.29	-0.46	-0.06	-0.25	-0.19
FeO wt%	9.70	12.94	13.11	9.84	13.33	9.74
TiO2 wt%	1.54	2.03	1.63	1.44	2.01	1.49
BaO wt%	0.02	0.01	0.05	0.02	0.07	0.03
Cl wt%	0.02	0.03	0.02	0.01	0.01	0.01
K2O wt%	9.35	9.34	8.43	6.74	8.69	9.22
CaO wt%	0.11	0.14	0.07	0.24	0.17	0.14
SrO wt%	0.04	0.01	0.01	0.04	-0.01	0.02
Na2O wt%	0.10	0.08	0.06	0.10	0.08	0.06
Al2O3 wt%	14.84	14.87	16.29	15.30	15.71	15.14
SiO2 wt%	37.94	36.91	39.37	39.60	38.55	38.67
MgO wt%	19.53	16.39	18.08	20.60	17.18	20.21
MnO wt%	0.10	0.22	0.25	0.12	0.23	0.09
ZnO wt%	0.01	0.02	0.04	0.03	0.07	0.01
Total wt%	93.41	93.13	97.15	94.02	95.93	94.73

Table D5: Secondary standard compilation: biotite

Element	Astimex biotite					
F wt%	-0.20	-0.52	-0.45	0.08	0.14	0.34
FeO wt%	12.75	9.70	13.23	9.72	13.08	12.86
TiO2 wt%	1.96	1.51	1.92	1.51	1.96	1.64
BaO wt%	0.03	0.04	0.05	0.04	0.03	0.06
Cl wt%	0.03	0.01	0.01	0.00	0.02	0.01
K2O wt%	9.35	9.32	9.78	8.50	8.76	9.59
CaO wt%	0.23	0.20	0.17	0.22	0.23	0.15
SrO wt%	0.01	0.00	0.01	0.01	0.00	0.02
Na2O wt%	0.09	0.14	0.10	0.10	0.08	0.06
Al2O3 wt%	14.84	14.72	15.35	15.09	15.01	14.23
SiO2 wt%	36.46	38.09	37.61	38.84	36.89	35.25
MgO wt%	16.33	19.59	16.90	20.17	16.34	15.90
MnO wt%	0.22	0.12	0.23	0.13	0.22	0.23
ZnO wt%	0.02	0.02	0.00	0.02	0.01	0.02
Total wt%	92.18	93.15	95.10	94.40	92.70	90.21

Table D5: Secondary standard compilation: biotite

Element	Astimex biotite					
F wt%	-0.39	0.07	-0.37	-0.19	-0.27	-0.30
FeO wt%	9.52	13.26	13.14	9.39	13.14	9.61
TiO2 wt%	1.50	2.05	1.62	1.43	1.88	1.58
BaO wt%	0.05	-0.03	0.03	0.00	0.00	0.01
Cl wt%	0.01	0.02	0.03	0.02	0.02	0.01
K2O wt%	9.72	8.24	9.56	8.53	9.74	9.45
CaO wt%	0.19	0.15	0.17	0.27	0.13	0.20
SrO wt%	0.02	0.06	0.01	0.00	0.00	0.05
Na2O wt%	0.11	0.07	0.09	0.09	0.08	0.10
Al2O3 wt%	14.92	15.23	15.40	14.35	15.80	14.35
SiO2 wt%	38.51	37.64	38.04	37.08	37.11	37.18
MgO wt%	20.01	16.61	17.09	19.00	16.53	19.14
MnO wt%	0.11	0.23	0.24	0.13	0.22	0.13
ZnO wt%	0.03	0.01	0.06	0.03	0.05	0.04
Total wt%	94.46	93.57	95.25	90.21	94.53	91.67

Table D5: Secondary standard compilation: biotite

Element	Astimex biotite					
F wt%	-0.04	0.05	-0.05	-0.14	-0.42	-0.45
FeO wt%	9.60	13.01	9.68	13.27	13.05	10.17
TiO₂ wt%	1.51	1.92	1.67	2.08	1.79	1.72
BaO wt%	-0.01	0.05	0.10	-0.01	0.06	0.08
Cl wt%	0.00	0.02	0.03	0.01	0.01	0.01
K₂O wt%	7.03	9.58	8.53	8.95	9.77	6.57
CaO wt%	0.28	0.15	0.21	0.16	0.17	0.08
SrO wt%	0.03	0.00	0.05	0.04	0.04	0.03
Na₂O wt%	0.04	0.08	0.12	0.06	0.11	0.04
Al₂O₃ wt%	14.53	15.02	14.95	15.91	15.00	16.02
SiO₂ wt%	37.53	36.76	38.42	39.10	36.97	40.25
MgO wt%	19.05	16.44	19.53	17.53	16.63	21.06
MnO wt%	0.11	0.24	0.11	0.24	0.22	0.09
ZnO wt%	0.04	0.02	0.00	0.02	0.07	0.04
Total wt%	89.74	93.31	93.36	97.29	93.62	95.91

Table D5: Secondary standard compilation: biotite

Element	Astimex biotite					
F wt%	-0.42	0.08	-0.21	0.11	-0.28	-0.70
FeO wt%	9.27	2.96	9.73	9.59	13.19	9.80
TiO2 wt%	1.53	0.47	1.52	1.50	2.03	1.62
BaO wt%	0.01	0.00	0.05	-0.01	-0.02	0.01
Cl wt%	0.01	0.25	0.00	0.01	0.02	0.01
K2O wt%	9.66	2.80	7.91	8.58	9.56	8.69
CaO wt%	0.10	0.09	0.17	0.16	0.16	0.09
SrO wt%	0.01	0.03	-0.01	0.02	0.03	0.01
Na2O wt%	0.06	0.02	0.09	0.09	0.08	0.11
Al2O3 wt%	15.10	12.83	15.26	15.32	14.88	15.15
SiO2 wt%	38.51	11.18	38.97	39.10	36.23	38.41
MgO wt%	20.31	5.45	20.45	20.49	16.11	20.15
MnO wt%	0.10	0.02	0.11	0.11	0.24	0.10
ZnO wt%	0.05	0.02	0.00	0.00	0.02	0.03
Total wt%	94.48	36.11	94.14	95.02	92.36	93.76

Table D5: Secondary standard compilation: biotite

Element	Astimex biotite					
F wt%	-0.38	-0.30	-0.25	-0.08	-0.30	-0.50
FeO wt%	9.39	0.11	9.43	13.54	12.93	9.52
TiO2 wt%	1.41	0.01	1.44	2.09	1.75	1.54
BaO wt%	0.06	0.00	0.00	0.06	0.08	0.02
Cl wt%	0.02	0.31	0.02	0.02	0.02	0.01
K2O wt%	9.42	0.04	9.69	7.91	9.63	9.75
CaO wt%	0.13	0.01	0.19	0.13	0.16	0.14
SrO wt%	0.02	-0.01	0.00	0.03	0.02	0.05
Na2O wt%	0.12	0.00	0.12	0.07	0.11	0.12
Al2O3 wt%	14.71	0.01	14.91	15.05	15.12	14.39
SiO2 wt%	38.13	0.02	38.48	37.52	37.21	36.80
MgO wt%	19.90	0.00	20.04	16.58	16.65	19.21
MnO wt%	0.09	0.00	0.11	0.22	0.24	0.12
ZnO wt%	0.02	-0.01	0.00	0.02	0.02	0.03
Total wt%	93.18	0.24	94.29	93.19	93.78	91.41

Table D5: Secondary standard compilation: biotite

Element	Astimex biotite					
F wt%	-0.48	-0.26	-0.43	-0.29	-0.42	-0.36
FeO wt%	9.71	13.50	9.65	9.56	9.63	9.27
TiO₂ wt%	1.27	1.90	1.30	1.46	1.61	1.47
BaO wt%	0.07	0.00	0.03	0.02	0.08	0.14
Cl wt%	0.02	0.02	0.01	0.01	0.03	0.01
K₂O wt%	9.06	8.07	9.61	8.30	9.65	9.36
CaO wt%	0.17	0.10	0.16	0.17	0.12	0.13
SrO wt%	0.04	0.03	0.01	0.03	0.00	0.00
Na₂O wt%	0.09	0.05	0.11	0.11	0.07	0.10
Al₂O₃ wt%	15.47	14.56	15.17	14.60	14.54	14.28
SiO₂ wt%	38.80	35.81	38.09	37.38	37.39	37.12
MgO wt%	20.39	15.79	20.22	19.52	19.55	19.27
MnO wt%	0.11	0.25	0.10	0.10	0.11	0.10
ZnO wt%	0.02	0.03	0.02	0.04	0.01	0.04
Total wt%	94.94	89.94	94.23	91.12	92.54	91.10

Element	Astimex biotite				
F wt%	-0.44	-0.46	-0.40	-0.01	-0.28
FeO wt%	9.77	9.59	9.86	10.04	13.23
TiO₂ wt%	1.60	1.72	1.61	1.66	2.03
BaO wt%	0.26	0.20	0.27	0.20	0.23
Cl wt%	0.02	0.02	0.02	0.01	0.02
K₂O wt%	8.57	9.19	8.41	7.33	9.20
CaO wt%	0.11	0.10	0.14	0.09	0.15
SrO wt%	0.01	0.02	0.03	-0.01	0.01
Na₂O wt%	0.07	0.10	0.05	0.06	0.08
Al₂O₃ wt%	15.26	14.30	15.05	15.69	14.58
SiO₂ wt%	38.78	37.80	38.53	39.47	36.12
MgO wt%	20.31	19.30	19.80	20.53	15.82
MnO wt%	0.09	0.10	0.11	0.11	0.23
ZnO wt%	0.03	0.01	0.01	0.02	0.14
Total wt%	94.61	92.18	93.64	95.19	91.67

Appendix E: Chlorite Geothermometry

Table E1: Chlorite geothermometric results

Sample	Cathelineau (1988)	Kranidiotis and MacLean (1987)	Zang and Fyfe (1995)	Xie (1997)
	T (°C)	T (°C)	T (°C)	T (°C)
385230.9.1	386.823	110.12	50.46	-236.81
385230.9.2	357.417	112.25	53.62	-226.34
385230.9.3	377.998	108.96	50.78	-234.55
385230.9.4	356.518	108.83	50.44	-235.78
385230.23.1	330.940	204.88	147.98	61.09
385230.23.2	349.300	195.50	137.90	29.93
385230.23.3	344.703	201.67	145.45	54.00
385230.23.4	319.612	194.51	138.47	33.01
385230.26.1	359.751	185.41	130.90	11.41
385230.26.2	366.639	191.16	137.32	31.44
385230.26.3	359.842	189.45	136.06	27.98
385230.26.4	359.119	181.02	127.99	3.85
385230.32.1	350.002	195.07	140.18	39.20
385230.32.2	350.900	196.69	143.26	49.80
385230.32.4	361.993	194.83	140.55	40.84
385230.33.1	358.582	194.69	140.18	39.52
385230.33.2	344.611	192.52	136.13	25.63
385230.33.3	356.460	192.28	137.11	29.63
385230.33.4	362.275	196.28	140.32	38.67
385367.2.34.1	344.298	194.35	140.22	39.96
385367.2.34.2	348.105	190.09	135.18	24.02
385367.2.34.3	345.313	194.02	139.05	35.68
385367.2.34.4	344.824	196.10	140.76	40.54
385367.2.35.1	354.420	192.69	131.67	8.09
385367.2.35.2	356.771	193.68	133.26	13.43
385367.2.35.3	359.575	193.31	131.64	7.46
385367.2.35.4	355.306	193.13	131.51	7.07
385367.2.36.1	348.191	193.35	138.37	33.63
385367.2.36.2	351.258	193.61	139.80	38.98
385367.2.37.1	343.306	195.55	139.44	35.90
385367.2.37.2	340.769	194.18	137.99	31.42
385367.2.38.1	350.280	191.97	135.47	23.52
385367.2.38.2	352.126	193.38	135.99	24.30
385367.2.38.3	340.205	192.03	131.77	9.05
385367.2.38.4	351.618	190.82	131.39	8.63
385367.2.39.1	366.665	194.00	134.48	17.91
385367.2.39.2	364.356	196.17	133.12	10.71
385367.2.39.3	360.700	191.06	130.67	5.62
385367.2.39.4	364.950	194.70	134.59	17.72
385367.2.43.1	347.772	196.65	143.33	50.09
385367.2.43.2	359.061	196.13	142.28	46.43
385367.2.43.3	355.767	195.14	140.80	41.52
385367.2.44.1	336.596	196.63	142.08	45.25
385367.2.44.2	343.902	190.32	137.24	31.83
385367.2.44.3	345.567	194.03	140.97	43.18
385367.2.44.4	340.763	193.51	139.17	36.60
385367.2.45.1	341.255	188.98	130.61	7.16
385367.2.45.2	345.987	191.48	132.91	13.96
385367.2.45.3	346.778	191.96	133.53	15.98
385367.2.45.4	352.542	189.78	132.71	14.65
385367.2.46.1	345.857	191.76	130.58	4.67

Table E1: Chlorite geothermometric results

Sample	Cathelineau (1988)	Kranidiotis and MacLean (1987)	Zang and Fyfe (1995)	Xie (1997)
	T (°C)	T (°C)	T (°C)	T (°C)
385367.2.46.2	354.113	193.45	131.97	8.62
385367.2.46.3	350.276	192.20	134.14	18.12
385367.2.46.4	345.409	194.36	135.70	22.34
385367.2.47.1	352.804	192.44	133.14	14.05
385367.2.47.2	353.350	195.30	135.69	21.49
385367.2.47.3	356.959	194.49	133.86	15.07
385367.2.47.4	360.474	192.30	133.00	13.60
385367.2.48.1	345.995	193.65	136.79	27.20
385367.2.48.2	333.104	194.28	136.41	25.20
385367.2.48.3	349.586	194.07	139.36	36.87
385367.2.49.1	367.485	195.47	140.22	38.98
385367.2.49.2	369.008	193.06	132.47	10.89
385367.2.49.3	370.168	189.63	127.19	-6.71
385367.2.49.4	369.769	192.14	136.31	26.64
385367.2.50.1	355.617	195.36	145.57	59.93
385367.2.50.2	366.613	196.48	145.30	57.89
385367.2.50.3	366.985	196.67	145.92	60.16
385367.2.50.4	365.627	196.57	145.75	59.59
385210.62.1	393.446	194.43	137.91	30.88
385210.62.2	388.439	196.67	143.28	49.87
385210.62.3	387.378	196.89	143.28	49.68
385210.63.1	376.086	195.99	143.40	50.92
385210.63.2	366.297	210.56	145.76	47.52
385210.63.3	356.392	208.55	144.56	44.60
385210.64.1	361.956	207.82	144.69	45.73
385210.64.2	362.193	203.52	141.70	37.78
385210.64.3	364.551	200.38	138.36	27.50
385210.65.1	358.051	196.18	136.29	23.06
385210.65.2	355.059	198.14	137.95	27.84
385210.66.1	326.632	198.39	137.81	27.08
385210.66.2	349.950	199.36	138.35	28.35
385210.66.3	335.063	196.88	136.63	23.80
385210.66.4	358.017	195.92	135.62	20.67
385210.67.1	361.399	187.39	125.19	-12.56
385210.67.2	351.295	193.54	134.81	19.57
385210.67.3	366.692	190.50	127.56	-6.01
385210.67.4	384.497	196.61	136.95	25.28
385210.70.1	358.752	197.77	138.01	28.39
385210.70.2	391.626	194.32	134.83	18.99
385210.70.3	390.055	200.23	138.85	29.55
385210.70.4	396.419	206.32	144.44	46.03
385210.71.1	391.505	197.04	136.95	24.89
385210.71.2	377.630	209.87	145.27	46.22
385210.73.1	361.507	209.22	144.92	45.40
385210.73.2	360.843	211.71	146.52	49.49
385210.73.3	360.524	209.63	145.49	47.26
385210.75.1	361.890	205.02	140.96	33.63
385210.75.2	358.591	200.59	134.53	12.40
385210.75.3	364.124	200.57	134.07	10.62
385210.75.4	367.482	200.06	134.47	12.60
385210.76.1	351.563	198.31	137.69	26.69

Table E1: Chlorite geothermometric results

Sample	Cathelineau (1988)	Kranidiotis and MacLean (1987)	Zang and Fyfe (1995)	Xie (1997)
	T (°C)	T (°C)	T (°C)	T (°C)
385210.76.2	364.221	197.01	136.88	24.64
385210.76.3	360.400	198.99	138.50	29.25
385210.76.4	354.418	200.55	139.04	30.00
385210.77.1	353.587	194.43	134.89	19.14
385210.77.2	358.589	198.75	138.87	30.89
385210.77.3	355.365	197.58	137.50	26.59
385210.78.1	388.180	195.51	135.66	21.19
385210.78.2	386.146	195.29	135.31	20.02
385210.78.3	377.830	197.05	136.82	24.38
385210.78.4	389.985	195.20	136.75	25.70
385210.79.1	372.627	208.61	144.29	43.46
385210.79.2	375.087	207.03	144.77	46.73
385210.79.4	397.231	205.66	140.31	30.52
385210.82.1	364.160	208.89	145.29	47.12
385210.82.2	393.224	202.70	140.15	32.48
385210.82.3	364.825	203.24	141.31	36.53
385210.82.4	382.919	211.74	147.09	51.69
385347.2.88.1	351.139	198.97	138.56	29.48
385347.2.88.2	303.429	210.61	145.52	46.56
385347.2.88.3	347.872	199.37	138.55	29.10
385347.2.88.4	359.859	206.66	142.83	39.50
385347.2.89.1	381.322	194.32	134.71	18.52
385347.2.89.2	365.359	179.70	117.60	-35.47
385347.2.89.3	376.631	194.64	131.88	7.21
385347.2.89.4	379.407	197.32	137.42	26.50
385347.2.89.5	391.851	204.94	143.81	44.79
385347.2.89.6	378.734	199.30	139.02	31.01
385347.2.90.1	374.817	203.22	142.48	41.09
385347.2.90.2	384.169	204.86	142.48	39.68
385347.2.90.3	386.604	208.38	147.32	55.48
385347.2.90.4	383.389	204.81	142.04	38.01
385347.2.90.5	386.586	203.48	140.80	34.33
385347.2.90.6	367.344	206.49	143.98	44.11
385347.2.91.2	384.049	207.08	145.04	47.73
385347.2.91.3	386.517	206.55	143.32	41.49
385347.2.91.4	389.830	207.43	144.59	45.67
385347.2.91.5	387.724	201.07	138.28	26.57
385347.2.91.6	387.268	206.88	143.39	41.46
385347.2.91.7	377.666	207.60	144.33	44.51
385347.2.91.8	382.587	208.39	145.80	49.55
385347.2.91.9	381.115	207.85	144.91	46.56
385347.2.91.10	382.792	207.16	145.43	49.18
385347.2.91.11	381.172	204.16	142.07	38.68
385347.2.91.12	376.089	206.27	143.08	40.79
385011.92.1	345.186	205.32	143.18	42.00
385011.92.2	344.494	206.83	142.52	38.11
385011.92.4	341.991	204.92	143.72	44.46
385011.103.1	328.623	204.25	140.78	33.57
385011.103.2	347.653	189.05	136.92	31.71
385011.103.3	350.784	188.77	136.75	31.28
385011.103.4	329.451	188.12	135.72	27.81

Table E1: Chlorite geothermometric results

Sample	Cathelineau (1988)	Kranidiotis and MacLean (1987)	Zang and Fyfe (1995)	Xie (1997)
	T (°C)	T (°C)	T (°C)	T (°C)
385011.109.1	345.634	185.63	128.90	3.41
385011.109.2	346.616	192.89	133.92	16.66
385011.109.4	319.369	192.71	136.48	26.80
385025.121.1	357.196	186.37	128.58	1.53
385025.121.2	356.420	193.22	132.00	8.92
385025.121.4	349.446	193.99	131.76	7.30
385025.122.1	348.579	184.19	123.82	-15.13
385025.122.3	349.223	194.94	138.44	32.51
385025.122.4	354.092	194.79	138.05	31.13
385025.135.1	350.297	192.67	135.53	23.12
385025.135.2	341.813	193.59	133.73	15.34
385025.135.3	344.208	191.37	137.00	30.00
385199.154.1	377.442	194.14	137.14	28.17
385199.154.2	376.563	191.37	137.80	33.11
385199.154.3	379.654	189.49	133.85	19.35
385199.154.4	376.021	189.83	135.21	24.35
385199.155.1	388.581	203.85	142.29	39.81
385199.155.2	382.945	203.18	142.49	41.15
385199.155.3	387.206	205.24	142.18	38.19
385199.155.4	378.659	203.85	141.23	35.69
385336.2.156.1	349.115	207.03	146.58	53.75
385336.2.156.2	341.673	206.23	143.39	42.04
385336.2.156.3	341.077	207.08	145.49	49.47
385336.2.156.4	354.760	204.61	142.24	38.94
385336.2.157.1	337.352	186.78	142.70	56.17
385336.2.157.2	353.725	184.13	140.49	49.87
385336.2.157.3	347.290	184.39	139.72	46.64
385336.2.157.4	355.125	188.21	145.11	64.31
385336.2.159.1	341.091	183.50	138.08	40.99
385336.2.159.2	330.402	190.61	141.31	47.44
385336.2.159.3	324.388	188.29	139.44	42.15
385336.2.159.4	346.007	190.18	142.89	53.96
385336.2.160.1	342.151	186.02	137.69	37.32
385336.2.160.2	350.313	182.27	134.46	27.96
385336.2.160.3	343.468	179.06	134.02	29.03
385336.2.160.4	346.782	187.92	138.95	40.59
385336.2.161.1	353.233	186.52	137.84	37.46
385336.2.161.2	349.751	189.48	140.19	44.08
385336.2.161.3	348.637	186.89	138.36	39.16
385336.2.161.4	348.290	188.59	138.68	38.94
385336.2.162.1	344.034	190.64	140.91	45.85
385336.2.162.2	355.800	188.01	141.63	50.95
385336.2.162.4	349.264	188.30	140.44	46.04
385336.2.163.1	343.867	187.33	141.39	50.59
385336.2.163.2	359.538	186.77	138.93	41.49
385336.2.163.3	354.315	189.79	143.89	58.20
385336.2.163.4	354.500	187.45	141.98	52.77
385336.2.164.1	345.940	184.85	141.23	52.13
385336.2.164.2	342.654	191.21	144.88	60.85
385336.2.164.3	348.467	188.23	144.75	62.89
385336.2.164.4	352.237	189.35	143.47	56.95

Table E1: Chlorite geothermometric results

Sample	Cathelineau (1988)	Kranidiotis and MacLean (1987)	Zang and Fyfe (1995)	Xie (1997)
	T (°C)	T (°C)	T (°C)	T (°C)
385336.2.166.1	355.688	186.11	141.19	50.87
385336.2.166.2	343.374	184.16	141.19	52.54
385336.2.166.3	348.983	187.03	141.90	52.84
385336.2.166.4	340.700	187.93	143.58	58.61